QUANTITATIVE ANALYSIS OF CARBONATE SANDBODIES: OUTCROP ANALOG STUDY FROM AN EPICONTINENTAL BASIN (TRIASSIC GERMANY)

Dissertation
zur Erlangung des Grades eines Doktors der Naturwissenschaften

der Geowissenschaftlichen Fakultät
der Eberhard-Karls-Universität Tübingen

vorgelegt von
Sascha Braun
aus Ostfildern / Ruit

2003

Tag der mündlichen Prüfung: 17. November 2003

Dekan: Prof. Dr. Dr. h.c. Muharrem Satir

1. Berichterstatter: Prof. Dr. Thomas Aigner

2. Berichterstatter: Prof. Dr. Hans-Peter Luterbacher

Contents

Ia List of Figures

Ib List of Plates

Atlas of lithofacies types and their petrophysical properties:

Ic List of Enclosures

II Abstract

Scope

This outcrop analog study aims to provide quantitative data concerning dimensions, spatial distribution, internal structure and poro-perm characteristics of carbonate shoal bodies on a carbonate ramp system. Shelly-oolitic carbonate bodies of the SW-German Upper Muschelkalk represent excellent outcrop analogs for hydrocarbon reservoirs in epeiric carbonate systems of the Middle East (e.g. Khuff, Hanifa, Arab).

Methods & data

Sampling of a few thousand polished slabs and detailed sedimentological logging in 21 outcrops plus outcrop gamma-ray measurements constitute the data basis for facies & genetic stratigraphic analysis. The reservoir quality of carbonate shoal bodies was quantified by more than 650 poro-perm samples. Thin section investigations analyzed diagenetic effects on Φ / k using cathodoluminescence microscopy. Regional high resolution sequence stratigraphic correlations highlight the architecture and geometry of carbonate shoals while facies- and poro-perm maps show the continuity, distribution and potential of reservoir bodies.

Results (* = Average values)

- The best reservoir quality occurs in (1) shell hash grainstones (Φ* = 15 %, k* = 45 mD) and (2) poorly sorted, bioclastic grainstones (Φ* = 13 %, k* = 82 mD) on wind-sheltered leeward sides of the shoals, where primary porosity is preserved in addition to moldic porosity.
- Stratigraphically, shoals occur in the top parts of meter-scale shallowing upward cycles. These stack vertically in large-scale transgressive and regressive trends, building multiple reservoir storeys.
- In the course of the larger-scale regression, shoal reservoir bodies systematically increase in abundance, size and thickness and decrease during larger-scale transgression.
- Length / thickness plots of shoal bodies show scattering, but also rough trends. Individual shoal reservoir bodies are up to 18 km x 8 km in extend and up to 2 m thick.
- The best reservoir quality occurs during large-scale transgression due to the predominance of highly permeable shelly shoals in contrast to lower permeability of oolite shoal facies.
- Shoal bodies preferentially occur on paleotectonic highs. These shallow-water areas were sites (1) of enhanced primary grain accumulation and (2) of secondary meteoric leaching

during diagenesis. Shapes and elongations of the shoal bodies follow both predominant structural and paleocurrent patterns.

- The most prominent porous and permeable shoals are situated on local, subtle present-day anticlines, separated by synclines. The prediction of shoal reservoir bodies may thus be possible by integration of detailed structural data.

Conclusion

The present outcrop analog study demonstrates that the distribution, dimension and reservoir potential of investigated shoal bodies follows systematic stratigraphic / diagenetic and paleotectonic trends. The quantitative data are useful for both predicting the reservoir architecture in productive hydrocarbon provinces of the storm-dominated carbonate ramp type and for building static reservoir models.

II Kurzfassung

Der Rahmen

Ziel dieser Aufschluß-Analog Studie war die Erforschung quantitativer Daten, wie Größe, räumliche Verteilung, innerer Aufbau und Poro-Perm Eigenschaften von Karbonat-Shoal-Körpern entlang einer Karbonatrampe. Die aus Schalen und Ooiden aufgebauten Karbonatkörper des Südwestdeutschen Oberen Muschelkalks sind hervorragend geeignete Aufschluß-Analog Beispiele für Kohlenwasserstoffspeicher in epeirischen Karbonat-Systemen des Mittleren Ostens (z.B. Khuff, Hanifa, Arab).

Methoden & Datenbasis

Die Beprobung einiger tausend Anschliffe, sowie die ausführliche sedimentologische Aufnahme von 21 Aufschlüssen einschließlich ihrer Gamma-Ray Vermessung bilden die Datenbasis zur Fazies- und genetisch-stratigraphischen Analyse. Die Reservoirqualität der Karbonat-Shoal-Körper wurde anhand von mehr als 650 Poro-Perm Proben bestimmt. Der Einfluß der Diagenese auf Porosität (Φ) und Permeabilität (k) wurde in Dünnschliff-untersuchungen, mit Hilfe der Kathodenlumineszenz-Mikroskopie analysiert. Regional hochauflösende sequenzstratigraphische Korrelationen verdeutlichen die Architektur und Geometrie der Karbonat-Shoals, während Fazies und Poro-Perm Karten Kontinuität, Verteilung und Potential der Reservoirkörper veranschaulichen.

Ergebnisse (* = Durchschnittswerte)

- Die besten Reservoirqualitäten sind in (1) shell hash grainstones (Φ* = 15 %, k* = 45 mD) und (2) schlecht sortierten, bioklastischen grainstones (Φ* = 13 %, k* = 82 mD) an den windabgewandten, leewärtigen Seiten der Shoals zu finden. Dort bleibt primäre Porosität zusätzlich zur Lösungsporosität erhalten.
- Stratigraphisch treten Shoals in den oberen Bereichen von Meter-maßstäblichen Verflachungszyklen auf. Diese stapeln sich vertikal und zeigen großmaßstäblich trangressive oder regressive Tendenzen, wobei mehrfache Reservoirstockwerke aufgebaut werden können.
- Während einer großmaßstäblichen Regression nehmen Shoal-Reservoirkörper systematisch an Häufigkeit, Größe und Mächtigkeit zu, während sie im Laufe einer großmaßstäblichen Transgression abnehmen.
- Länge- / Mächtigkeits-Verhältnisse von Shoal-Körpern streuen, dennoch sind grobe Trends erkennbar. Einzelne Shoal-Reservoirkörper erstrecken sich bis zu 18 km x 8 km und werden bis zu 2 m mächtig.
- Die beste Reservoirqualität tritt während einer großmaßstäblichen Transgression auf. Dann überwiegen hochdurchlässige, aus Schalen aufgebauten Shoals, im Gegensatz zu einer oolitischen Shoal-Fazies mit niedriger Permeabilität.
- Shoal-Körper sind bevorzugt an paläotektonisch erhöhten Positionen zu finden. Diese Flachwasser Bereiche sind Orte (1) erhöhter primärer Sedimentanhäufung und (2) erhöhter sekundärer, meteorischer Lösung während der Diagenese.
  Form und Ausdehnung der Shoal-Körper folgen überwiegend tektonischen Strukturen wie Paläoströmungsmustern.
- Die porösesten und permeabelsten Shoals liegen auf lokalen, gegenwärtigen Antiklinalen und sind durch Synklinalen voneinander getrennt. Die Vorhersage von Shoal-Reservoirkörpern scheint somit durch Integration genauer tektonischer Daten möglich zu sein.

Zusammenfassung

Die vorliegende Aufschluß-Analog Studie zeigt, daß Verteilung, Größe und Reservoirpotential der untersuchten Shoal-Körper systematisch stratigraphischen / diagenetischen und paläotektonischen Mustern folgt. Die quantitativen Daten sind sowohl zur Vorhersage der Reservoir-Architektur in produzierenden Kohlenwasserstoffgebieten des sturm-dominierten Karbonatrampen-Typs verwendbar, sowie zum Aufbau von Reservoir-Modellen nützlich.

1. Introduction

1.1 Aims of the study

The value of outcrop analogs is widely acknowledged for modelling the geometry of siliciclastic reservoirs (e.g. FLINT & BRYANT, 1993). By contrast, quantitative data of carbonate bodies on the reservoir scale are very scare. The purpose of this PhD-thesis was to undertake a detailed study on the architecture, sedimentology and petrophysics of carbonate sandbodies in outcrop analogs of Middle Triassic Upper Muschelkalk.
The Upper Muschelkalk represents the gently inclined carbonate ramp, filling an epicontinental basin, and therefore represents an analog to an important type of „non-reefal" skeletal and oolitic carbonate sand reservoirs, especially in the Middle East (e.g. Khuff, Hanifa, Arab).
Numerous studies of the Upper Muschelkalk in the South German Basin provide a well-established regional stratigraphy. However process-oriented and high resolution sequence stratigraphic investigations with an emphasis of reservoir potential have only rarely been carried out (e.g. SCHAUER & AIGNER, 1997). This is the approach of the present study by further developing concepts of „Dynamic Stratigraphy" originally presented by MATTHEWS (1984) and AIGNER (1985).

Exposures in many quarries and natural outcrops in Southern Germany preserve the geometries within shoalwater high-energy deposits along the margin of the Upper Muschelkalk Basin. This represents a unique opportunity to study, in two and three dimensions, the composition, internal structure, evolution and petrophysical characteristics of reservoir-sized carbonate sandbodies. Moreover, it offers the opportunity to directly map the distribution of porosity and permeability.

1.2 Geological and stratigraphic setting

1.2.1 Introduction

Rifting and disintegration of the Pangean supercontinent caused the western extension of the Tethys ocean during the Triassic (Fig. 1A). This regional crustal extension induced the subsidence of a complex network of grabens and troughs in Western and Central Europe (ZIEGLER, 1982) and formed the Triassic basins including the South German Muschelkalk basin, which is subject of this study.
The Muschelkalk was deposited during the Middle Triassic (~ 240 - 231 MA) in a cratonic, slowly subsiding basin. The depocenter was located in Northern Germany. The Muschelkalk Sea was separated from the Tethys by the Vindelician high and the Bohemian massif (Fig. 2). Connections existed through temporally shifting seaways. Carbonate production dominated during marine ingression, when huge areas were flooded rapidly, while evaporites were deposited during limited connections to the Tethys.
According to DERCOURT (1993) and ZIEGLER (1990), the German basin was located at about 30° north of the equator under subtropical climatic conditions. The paleolatitude of the Muschelkalk basin was within the „hurricane-dominated“ and „winter-storm“ zone (MARSAGLIA and KLEIN, 1983) in their paleo-storm model (see Fig 1A).

1.2.2 Facies of the Upper Muschelkalk in the study area

During Upper Muschelkalk times (Upper Anisian / Lower Ladinian) a connection with the Tethys through the Burgundian and the Silesian gate (see Fig. 2) facilitated shallow – open marine conditions (KOZUR, 1974) with carbonate production.
The following general facies distribution can be observed (Fig. 1C, AIGNER, 1985):

1. Siliciclastic coastal deposits around denudation areas
2. Dolomitic, muddy carbonates in lagoonal zones
3. Clean, massive limestones, mostly skeletal and oolitic carbonate sands towards the nearshore basin margin.
4. Argillaceous mudstones and marlstones offshore and in the basin center.

The Upper Muschelkalk was interpreted as a gently inclined carbonate ramp (AIGNER, 1985).

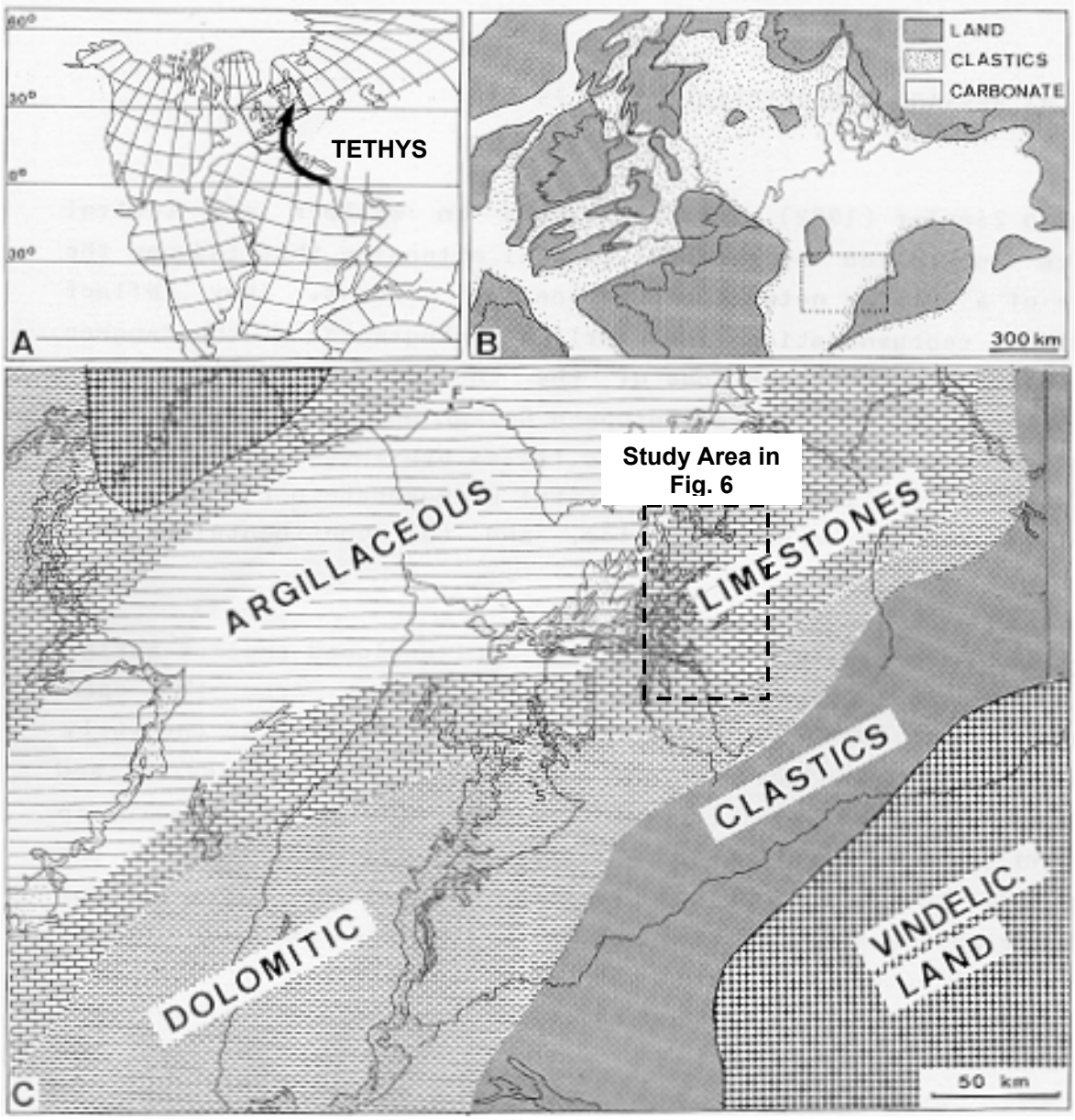

Fig. 1: Geological setting of the Upper Muschelkalk.

A) Plate tectonic situation of the Triassic during Anisian (after SMITH at al., 1981); arrow: Possible pathway of storms and hurricanes using paleo-storm model of MARSAGLIA & KLEIN (1983).

B) Paleogeography of the Muschelkalk (Anisian-Ladinian) in Central Europe (simplified after ZIEGLER, 1982).

C) Strongly generalized facies distribution in the South-German Basin during upper part of the Upper Muschelkalk; S = Stuttgart, F = Frankfurt. Complete figure from AIGNER (1985).

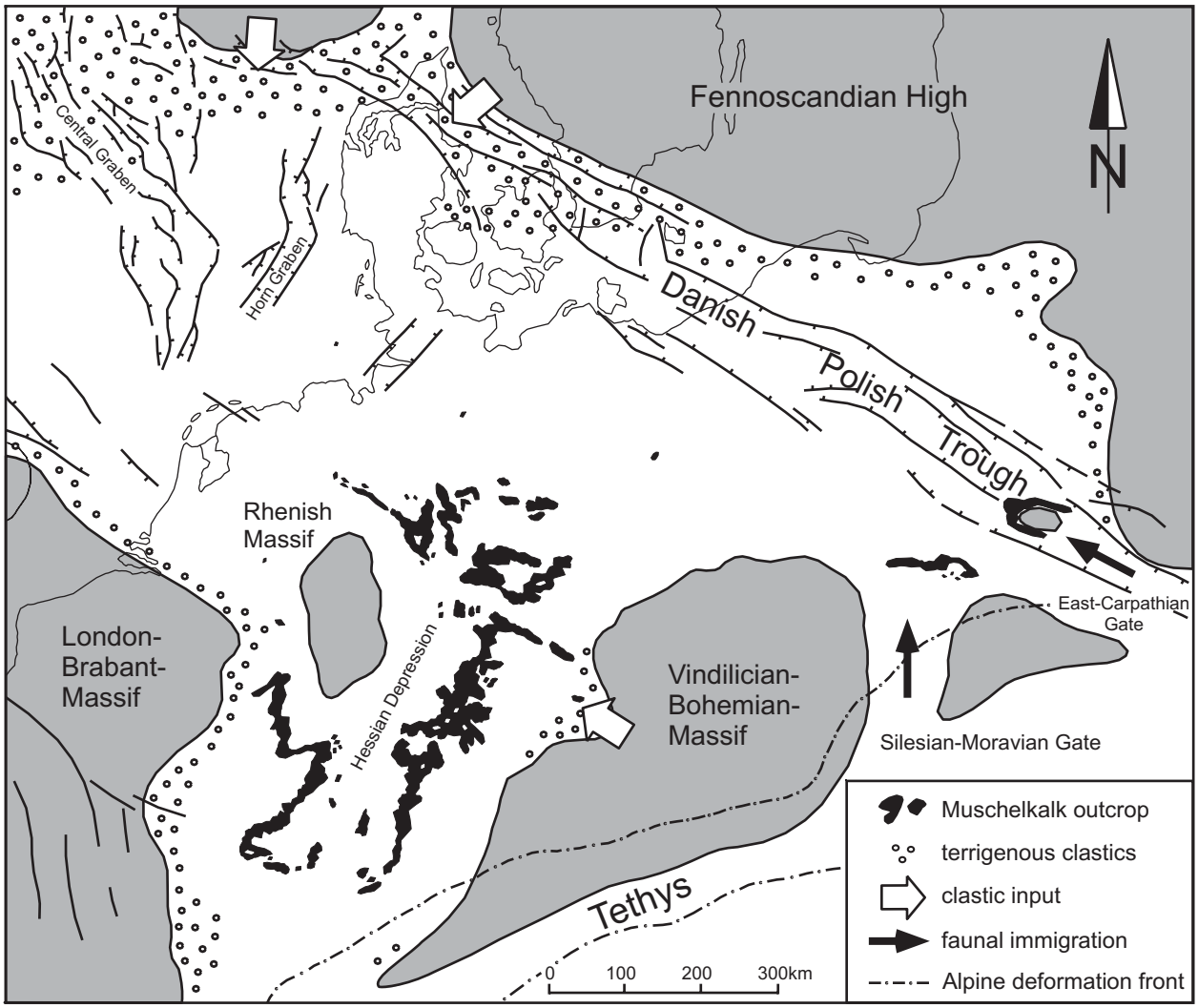

Fig. 2: Paleogeography and present outcrops of the Muschelkalk in Central Europe (modified after ZIEGLER, 1990).

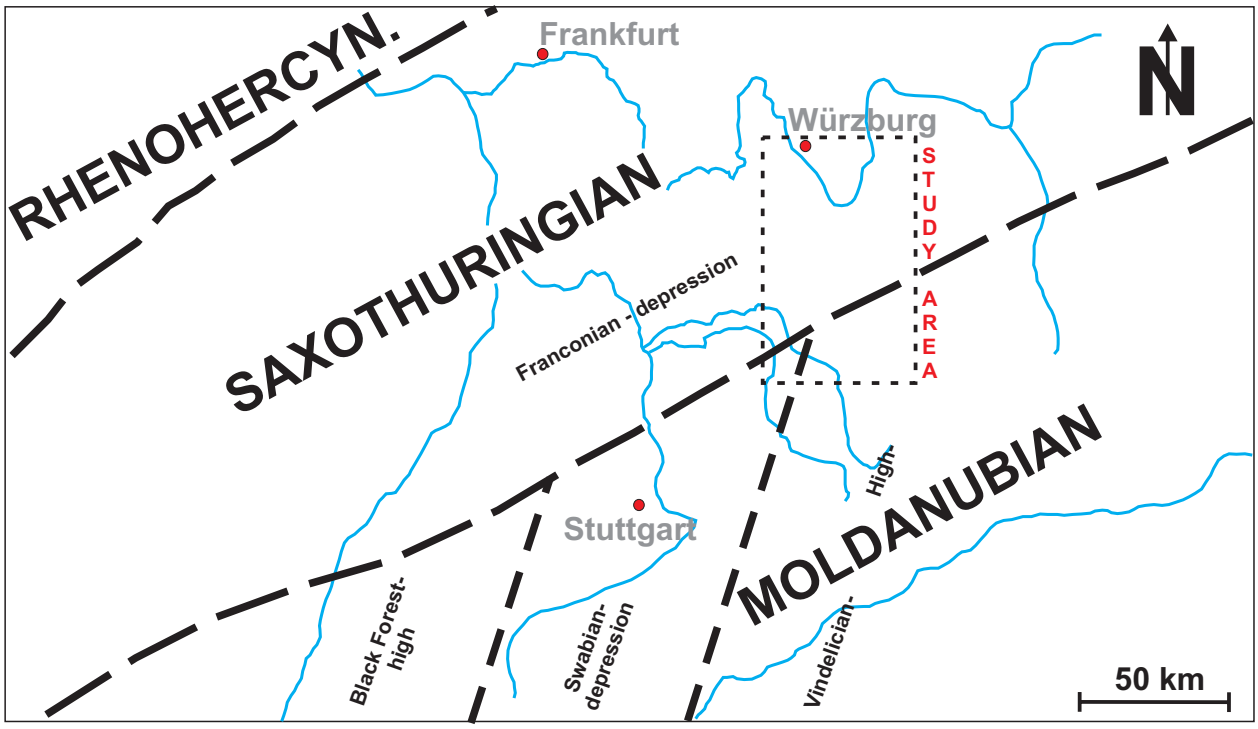

Fig. 3: The intercratonic Upper Muschelkalk Basin is influenced by differential subsidence of Variscan crustal blocks. Variscan paleotectonic zones with higher subsidence are the central Saxothuringian block, the Franconian- and the Swabian- depression. Map is modified from AIGNER (1985). Variscan Zones after BEHR ET AL. (1984) and KRIMMEL (1980).

The nearshore carbonate sandbodies, subject of this study, are regarded as submarine barrier bars on local paleohighs (e.g. „Gammesfeld-high“) according to RUTTE (1957) and WAGNER (1913) and as mobile nearshore shoal belts (VOLLRATH, 1955, HATZOLD, 1981).

1.2.3 Tectonics (Figs. 3 & 4)

South Germany and the area of investigation is indirectly influenced by the Variscan continental collision during the Carboniferous by reactivation of ancient plate margins. The Variscan orogenic belt in this area was WSW-ENE oriented, as is the Vindelician high, a denudation area during the entire Triassic (see figs. 1B & 2). This South German Basin is influenced by differential subsidence of Variscan crustal blocks. The Variscan paleotectonic zones are the Rhenohercynian block in the north, the Moldanubian block in the south and the most rapidly subsiding central basin zone, the Saxothuringian block (Fig. 3). Examples of other zones with higher subsidence are the Franconian- and the Swabian depression (see Fig. 3).
Four major fault systems are dominant within the study area (see Fig. 3 and 4):

1. The Hercynian, in SE-NW direction
2. The Rhenish, in SSW-NNE direction
3. The Erzgebirgish, SW-NE direction and
4. The Swabian, WSW-ENE direction.

These fault systems played an important role during the Variscan orogeny and seem to have become repeatedly reactivated up to the recent. Isopach-maps of different time-slices of the Upper Muschelkalk show temporally and spatially variable depocenters (VOLLRATH, 1955) clearly documenting zones of differential subsidence. Upper Muschelkalk isopachs show that the South German Basis axis follows the Variscan SW-NE direction. According to BEHR ET AL. (1984),Variscan zonal boundaries might be regarded as plate boundaries (sutures). Subsidence in the South German basin therefore seems to reflect the reactivation of ancient plate margin lineaments. Besides the mentioned major and extensive paleotectonic zones also small-scale paleotectonic elements (horst and graben structures) exist that considerably influence the facies distribution and even more the occurrence of reservoir bodies.
These elements were compiled in the tectonic map of Fig. 4. Presently known surface fault systems that could be traced over longer distances were extrapolated over the whole study area. The resulting networks of faults reflect three of the major fault systems that were originated during the Variscan orogeny (HAGDORN & SIMON, 1988). Intersecting structures form paleotectonic blocks of some km´s extension. These locations reflecting preferred evolution of shoal geobodies. Shoals clearly plot within such smaller-scale paleotectonic blocks. Moreover, it

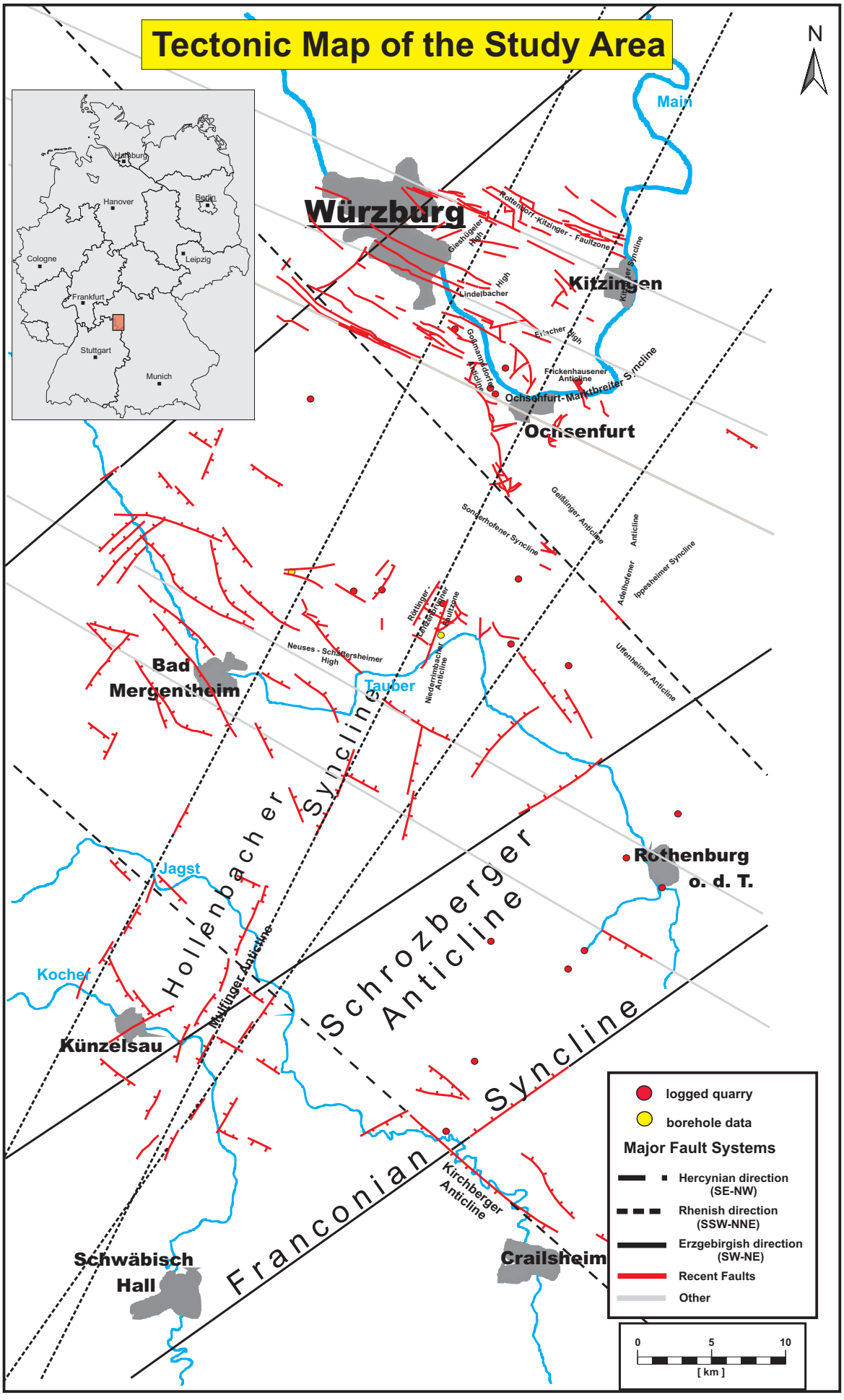

Fig. 4: Map of recent tectonic structures, marked with red and major (Variscan) fault systems (stippled lines) in the study area.

was observed that during the overall regression the lateral extension of shoal bodies ranges within the fault boundaries marking their paleotectonic blocks.

1.2.4 Stratigraphy of the upper part of the Upper Muschelkalk (Fig. 5)

A well-constrained litho- and biostratigraphic framework has been established for the Muschelkalk in SW-Germany (e.g. compilations of BACHMANN & GWINNER, 1971, GEYER & GWINNER, 1991, HAGDORN & SIMON, 1993), (see Fig. 5). Based on that, the Upper Muschelkalk is lithostratigraphically subdivided by marlstone layers (numbered) and bioclastic marker beds (named).

The focus of this study is the uppermost part of the Upper Muschelkalk starting with marlstone marker bed „Tonhorizont ε“ (Fig. 5), a more prominent one among the various marlstone marker beds and is further subdivided by thicker skeletal and oolitic units (with local / regional terminology such as „Kornsteinbänke“, „Schalentrümmerbänke“ and „Quaderkalkbänke“), thinner but more widespread brachiopod shell beds („Hauptterebratelbank“, „obere Terebratelbank“) and marlstone horizonts („Tonhorizonte ε and ξ“, „Dolomitische Mergelbänke“, „Gelbe Mergelbänke“). The prominent uppermost marker beds are a limestone layer with scattered glauconite minerals („Grenzglaukonitkalk“) and a thin bonebed layer („Grenzbonebed“), representing the Upper Muschelkalk-Lower Keuper boundary.

1.2.5 Study Area (Fig. 6)

The studied skeletal and oolitic carbonate sandbodies within the Upper Muschelkalk of Franconia are situated south of the city of Würzburg and occur in a ~ 60 km long, 30 km wide area.
The investigated quarries are located along a roughly N-S section approximately parallel to the paleo-coastline and connected SE-NW to E-W dip-lines across the gently inclined carbonate ramp.
The dense occurrence of outcrops allowed a lateral tracing of beds and mapping of lateral facies transitions (see stratigraphic cross section panels of chapter 5).

Upper Muschelkalk Stratigraphy

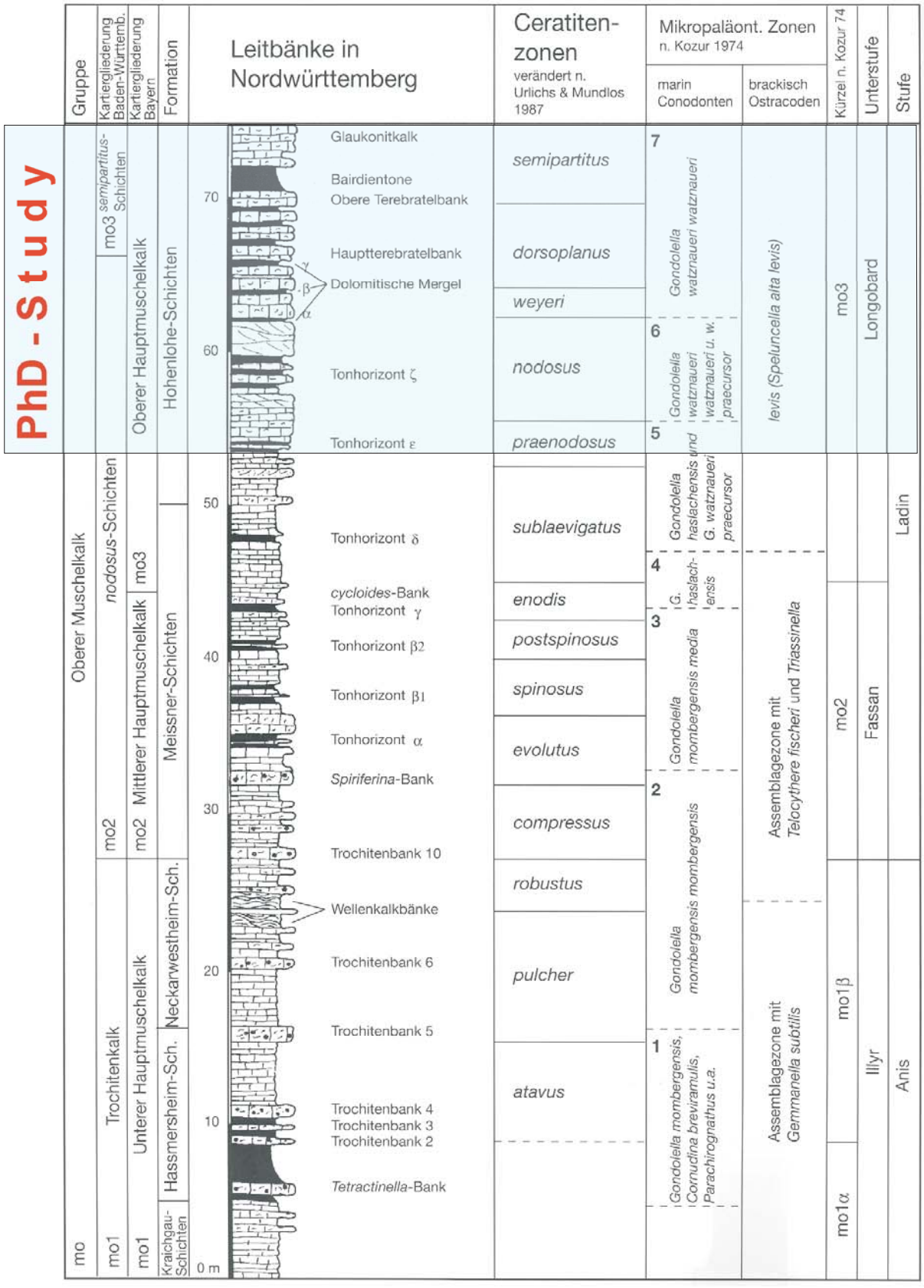

Fig. 5: Stratigraphy of the Upper Muschelkalk in Southern Germany (according to HAGDORN, 1991) and investigated succession in this PhD-study.

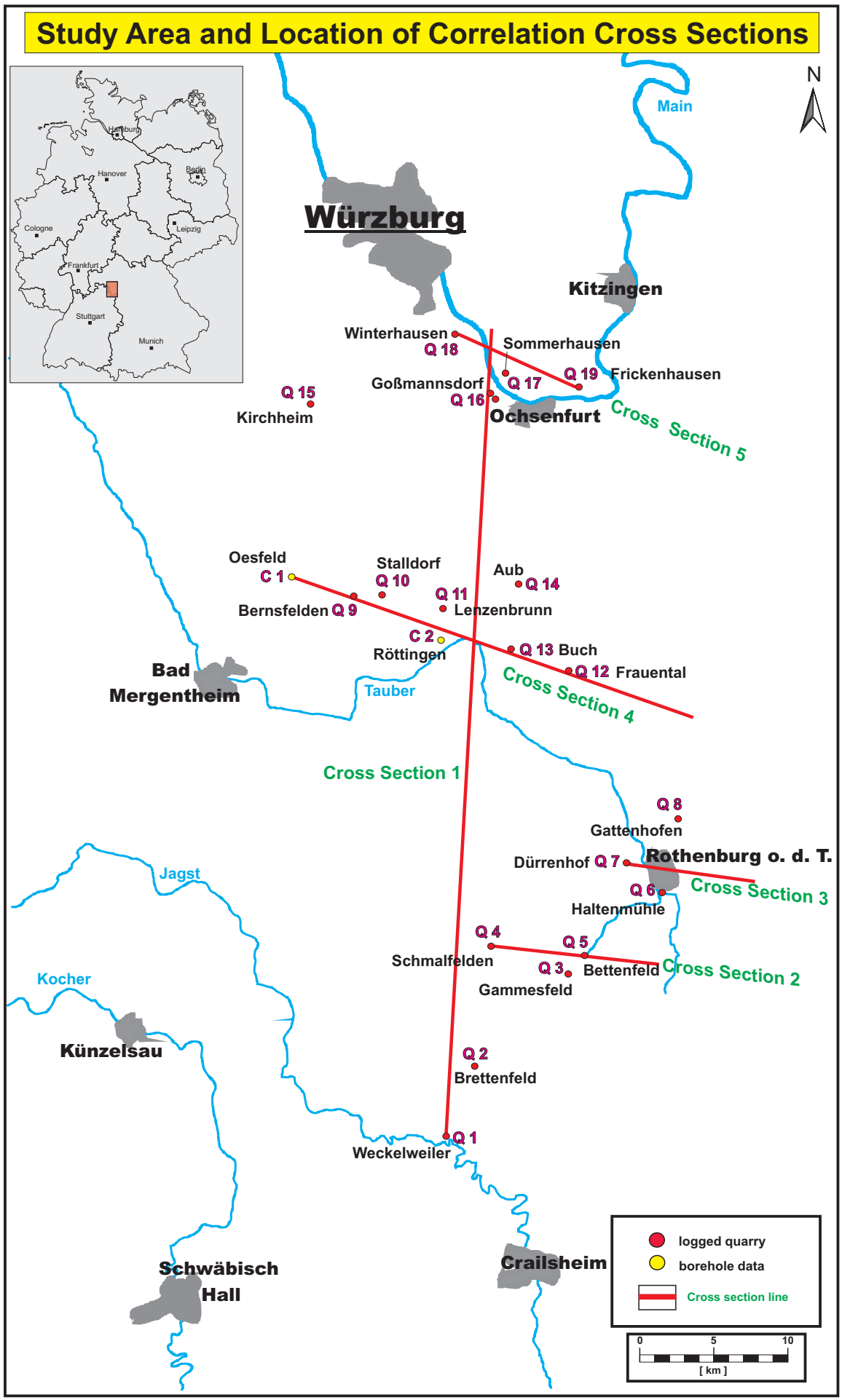

Fig. 6: Study area and location of correlation cross sections.

2. Methods

2.1 Sedimentological logging

2.1.1 Qualitative sedimentological logging

21 vertical sections were logged in quarries at the scale 1:25 and were graphically visualised as sedimentologic log with the program WellCAD 2.50 (scale 1:60), see logs in Appendix.
The logged properties were:

- **Textures** according to the DUNHAM (1962) classification.
- **Lithology**, limestone, marlstone and dolomite.
- **Particle size**, subdivided in clay / marl, calcilutite, calcisiltite, calcarenite and calcirudite, including intermediate sizes.
- **Grain components** separated in non-skeletal grains and skeletal grains.
  Main emphasis was put on ooids, shells with and without micritic envelopes, brachiopods and skeletal debris.
- **Sedimentary structures**, mainly syndepositional structures like different types of cross-bedding, lamination and grading (see chapter 3.1 and legend, in the Appendix), but also pre- and postdepositional structures and bioturbation.
- **Pore-types** according to the pore-type classification of CHOQUETTE and PRAY (1970).
- **Sediment color** and color of components (subjective description). During an initial overview the content of clay minerals and calcium carbonate can already visually be estimated by the color of the sediments.

2.1.2 Quantitative sedimentological logging

Two numeric codes were used:

1. The porosity was visually estimated in the field by an index from 0 to 6 (0 = no porosity, 2 = low porosity, 4 = medium, 6 = high porosity) with intermediate steps.
   The blue bars in the stratigraphic cross-section panels (Figs. 22 - 26) indicate porosity between 4 and 6.

2. The frequency of components and the degree of bioturbation was indexed from 0 – 3 (0 = not existing, 1 = rare, 2 = common, 3= very common) and translated graphically by three different sizes of symbols of the respective component-type (see legend in Appendix). The results were charted as graphic logs beside the sedimentological logs.

2.2 1-D Sequence stratigraphic analysis

1. Step: Description of lithofacies types

15 lithofacies types were distinguished, mainly based on the modified DUNHAM classification as proposed by LUCIA (1995) and on water-energy regime properties in order to reflect initial reservoir qualities.

2. Step: Vertical lithofacies succession

Within the lithofacies successions trends in lithofacies arrangement, stacking pattern and thickness of packages (lithofacies proportions) can commonly be recognized (e.g. Fig. 7, Fig. 21 and logs in Appendix).

3. Step: Interpretation of transgressive-regressive cycles

With help of the previous steps, sufficient indicators are available to interpret shallowing and deepening trends of the depositional environment for translation into (fundamental) transgressive-regressive cycles including their turn-around points. The cycles are discussed in detail in chapter 4.

4. Step: Establishment of a cycle hierarchy

The previously small-scale, fundamental cycles are examined terms of large-scale trends. Commonly several fundamental cycles show an overall regressive or transgressive trend.

5. Step: Cycle stacking pattern

Stacking pattern analysis examines a stratigraphic section for systematic upward changes in cycle thickness or composition with the aim to interpret accommodation trends (see Fig. 21).

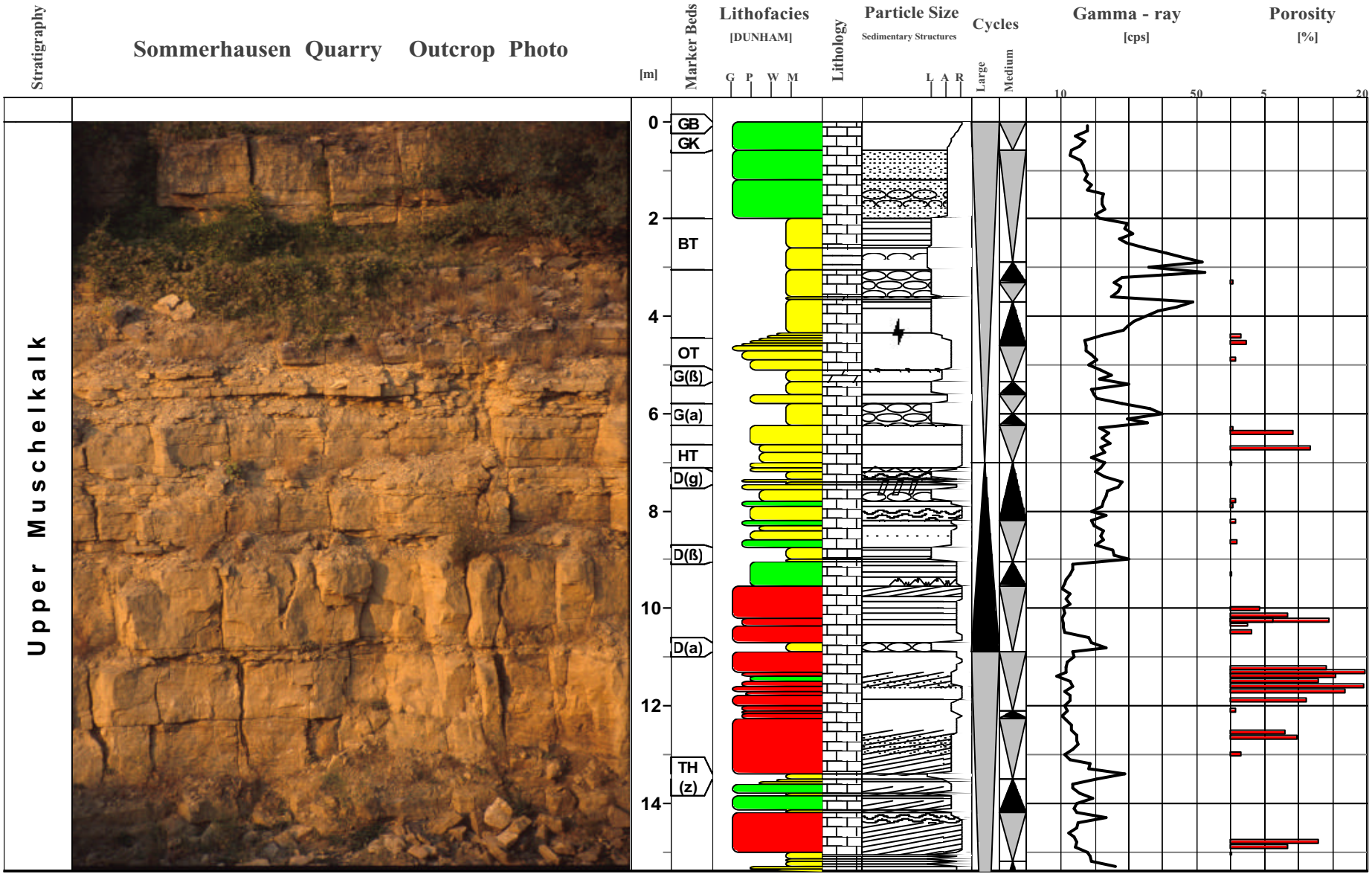

Fig. 7: Sedimentological logging and petrophysical analysis represented on Quarry Sommerhausen.

2.3 2-D Sequence stratigraphic correlation

The correlation is based on the interpretation of 21 sequence stratigraphic logs (1-D).
The goal of the correlation is to reconstruct the geometry, facies distribution and lateral facies changes of the original depositional environment. The steps were carried out as proposed by KERANS and TINKER (1997).

1. Step: Datum selection

The datum on which all logs were „hang on“ is the Upper Muschelkalk-Lower Keuper boundary.

2. Step: Cross section orientation

The cross sections run either approximately parallel (SSW-NNE, cross section 1) or perpendicular (WNW-ESE, cross sections 2 to 5) to the paleoslope of the carbonate ramp (see Fig. 6 for cross section orientation).
Data points that were not directly situated on one of these sections were projected onto the line of section. The distance between the quarries is therefore scaled along the cross section. This method ensures the authentic stratigraphic dip and allows the correct mapping of the depositional environment and the geometries of the sedimentary bodies.

3. Step: Correlation

Well-known and well-defined markers, commonly regional marker beds, are correlated first, for example prominent marl beds like „Tonhorizont ε“ and ξ, „gelbe Mergel α“, etc..
Cycle boundaries defined in the 1-D analysis, i.e. turn-around points like maximum flooding surfaces, are correlated next. Once these genetically defined surfaces are correlated, which commonly reflect the depositional topography, less prominent surfaces such as the fall / rise turnarounds are attempted to be correlated.

2.4. Petrophysical analysis

2.4.1 Field methods

Field gamma-ray measurements (total count gamma-ray)

The measurement of natural gamma radiation of outcrop walls was intended to relate the gamma-ray patterns to the sedimentary facies (see log of Sommerhausen quarry, Fig. 7) and to link outcrop gamma-ray and subsurface data.

The logging was carried out with portable scintillation counters of G.B.-H. Electronics and Geofyzika Co.. The spacing of measurements was generally 10 cm with a sampling interval of 10 seconds each. The results are displayed in counts per seconds [cps].

2.4.2 Laboratory methods

Macrofacies analysis

A few thousand hand specimens were cut and polished for macrofacies characterisation and further detailed analysis of sedimentary structures, sorting and composition.

Microfacies and cathodoluminescence microscopy

For microfacies characterisation, understanding of component – matrix composition as well as cementation and diagenesis, thin section have been examined by conventional transmission light microscopy and cathodoluminescence (CL) microscopy.

Porosity types, according to CHOQUETTE and PRAY (1970) and LUCIA (1983), their evolution as well as their destruction processes were analysed on both, thin sections and hand specimens.

Plug samples

About 650 plugs were drilled out of hand specimens and cores in order to measure porosity, permeability and grain density.

The goal of plug analysis is to evaluate the reservoir potential (poro-perm) of the carbonate sandbodies. Furthermore these data can also be used to guide stratigraphic interpretation and in an later step as input for 3-D geologic modelling.

Porosity measurements of plugs

The porosity was determined in two steps.

1. Measuring the plug in a helium pycnometer (Accupyc 1330 of Micromeritics Company) providing the net volume.
2. Measuring the plug in a powder pycnometer (Geopyc 1360 of Micromeritics Company) where the envelope volume was measured.

The calculated porosity is the proportion of pore space to net volume, calculated by the equation: (envelope volume – net volume) x 100 / envelope volume = porosity [%].

Permeability measurements of plugs

In order to determine the permeability of the plugs in two different spatial directions (horizontal and vertical) the measurements were carried out with the gas-minipermeameter FPP 300 of Edinburgh Petroleum Services.

Air is injected into the plug sample with known pressure by an injection head while the air flow rate is measured in [ml/s]. The permeability is calculated by input of the result into the Darcy equation. Under laboratory conditions that means by constant defined parameters of measurement (i.e. constant pressure of the injection head onto the sample etc.), the tool has proven its suitability for a fast record of permeability in different spatial directions by cross checks with a conventional column gas permeameter.

3. Facies and Petrophysical Analysis

3.1 Lithofacies analysis

Within the study area 15 lithofacies types were identified in the upper part of the Upper Muschelkalk. Some of them are further subdivided in A and B subtypes. The lithofacies types are based on a systematic analysis in the following order a) DUNHAM texture, b) sedimentary structures & bioturbation, c) sorting, d) components. The determination approach is illustrated in the flow chart of Fig. 8. The interpretation and a more detailed description of the lithofacies types is listed in Table 1. An integrated overview, including poro-perm properties, GR-log signature and photodocumentation of all lithofacies types is compiled in an atlas of lithofacies types and their petrophysical properties (see Appendix).

Sedimentary Structures (Plates 1 – 3)

Asymmetric ripples

In this study asymmetric ripples are restricted to arenitic carbonate sands of shoal-lithofacies types 9a, 10 and 13b. The ripples show a (high angle) cross-laminated internal structure and form cm-scale sets. This ripple type was observed most abundantly within large-scale sandwaves. Amalgamated sets cause dm-scale co-sets indicating ripple migration. The 3-D geometry of this ripples type is trough-like with a width of some dm´s.
Asymmetric ripples are formed generally by unidirectional currents. Their frequent appearance on large sandwaves indicates preferred occurrence and preservation during relatively lower energy periods.

Dune-scale cross-bedding (Plate 1)

Sanddunes are the most abundant bedforms within the shoal facies (9a, 10, 11, 13b). Trough cross-bedding in these arenitic- to medium-ruditic carbonate sands was frequently observed in 3-D outcrops (see Plate 1). Individual sets are dm-scale, commonly stack to several dm-thick co-sets. All sets show erosive bases and are also eroded at the top by the succeeding sets. While single sets wedge out laterally within a few meters, co-sets extend several 10´s to 100´s of meters.

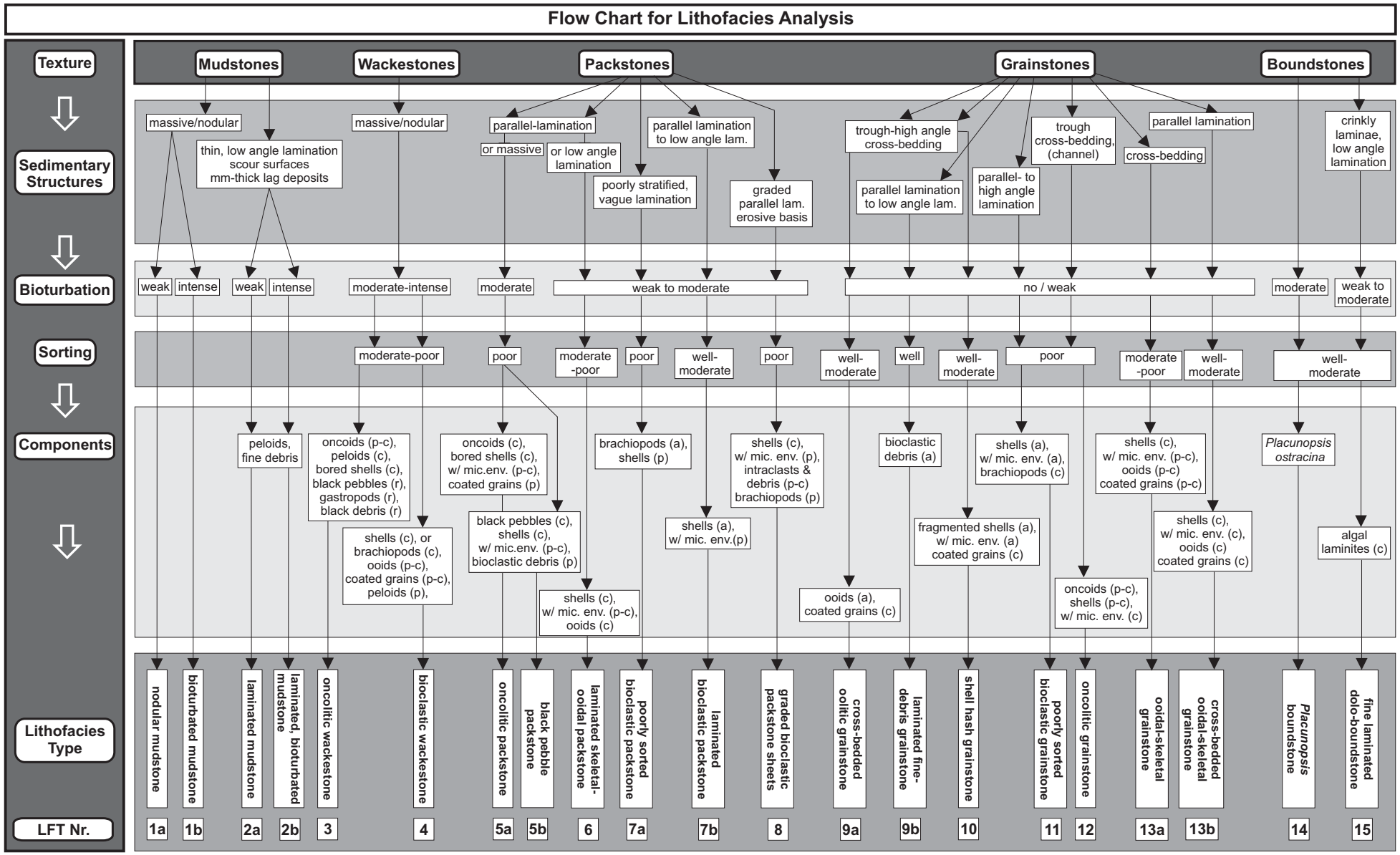

Fig. 8: Flow diagram for lithofacies analysis. (w/ = with)

LF Nr.	Texture [Dunham]	Lithology & rock-color	Sedimentary structures	Component grain size & sorting	Components & Frequency	Bed-thick-ness	Depositional environment & Interpretation
1a **1b**	mudstone & dolo-mudstone	argillaceous, marly & dolomitic limestone dark-medium grey & beige	a) nodular to massiv, weak biotubated b) nodular, intense bioturbated marly intercalations may present in both subtypes	lutite well-moderate	peloids (r-c)	cm–dm	Low energy environment, quiet water conditions a) deeper ramp, sub storm-wave-base, (partly anaerobic ?) b) sheltered backshoal, lagoonal setting
2a **2b**	mudstone & mud- to wackestone	limestone medium-light grey	a) low angle-, cm-scaled physical lamination of siltit grained laminae, scour surfaces, weak bioturbated b) scoured, intense bioturbated to unstratified	lutite & siltite well-moderate	peloids (p-c), fine siltitic-arenitic debris	cm-dm	a) shallow subtidal zone, distal, (aerobic) b) very shallow backshoal, lagoonal setting
3	wackestone	limestone medium-light grey	massive to nodular bedding, moderate to intense bioturbated	fine-medium rudite moderate-poor	oncoids (p-c), (bored) shells (c), peloids (c), black pebbles (r), gastropods (r), black debris (r), intraclasts (poorly rounded) (r), ophiure ossicles (r)	cm-dm	shallow, quiet lagoonal setting
4	wackestone wacke-to packstone	limestone medium-light grey	poorly stratified and massive to nodular bedded due to moderate to intense bioturbation	coarse arenite to fine rudite moderate-poor	shells (c), brachiopods (p-c), ooids (p-c), coated grains (p-c),	dm	distal mid ramp, transition zone shallow to deep ramp or sheltered backshoal, quiet laggonal setting
5a **5b**	packstone	limestone medium grey, light grey-beige	a) cruedly even-lamination or massiv b) parallel lamination or rarly low angle lamination both subtypes are moderate bioturbated	vc-arenite to medium rudite poor-very poor	a) oncoids (c), bored shells (c), micritic envelopes (p-c), coated grains (p), ooids (r), b) black pebbles (c), shells (c), bio-debris (p), peloids (p)	cm-dm	Low to medium energy setting within the shallow subtidal backshoal area a) oncolite channel b) event sheets
6	packstone	limestone light grey-beige	frequently parallel lamination by alignment of shells, low angle lamination possible, weak bioturbated	vc arenite to fine rudite moderate-poor	shells (c), micritic envelopes (p-c), ooids in various sizes, partly dolomitized (c), coated grains (r-p), peloids (p), brachiopods (r), intraclasts (r)	cm-dm	storm-generated proximal event-sheets fringing the shoal-complex area (transition zone to deeper ramp)
7a **7b**	packstone & wacke- to packstone	limestone/ dolo-limestone medium grey-beige	a) poorly stratified, vague lamination, weak- to moderately bioturbated b) frequently parallel to low angle lamination by aligned shells, weak-to moderately bioturbated	fine-medium rudite a) poor b) well-moderate	a) original preserved brachiopods (a), shells (p), micritic envelopes (r), bio- & intraclastic debris (p), peloids (r) b) fragmented shells (a), micritic envelopes (p), bio- & intraclastic debris (p), brachiopods (r), gastropods (r-p)	cm-dm	a) storm-generated distal offshoal event sheets b) storm-generated, shoal derived, proximal to medial flanking event sheets and / or spillover lobes (shallow to deeper ramp and backshoal)
8	packstone & wacke- to packstone	limestone medium grey	erosive base, graded, parallel lamination by aligned components, wave rippled top	fine arenite to medium rudite poor	shells (c), micritic envelopes (p), brachiopods (p), intraclasts and debris (p-c), peloids (p)	cm-dm	proximal- to distal tempestites in the transition zone shallow to deep ramp
9a **9b**	pack-grainstones + grainstones	limestone light grey-white, beige	a) trough & planar-tabular, high angle cross-bedding, even-lamination, partly massive, no/weak bioturbation b) parallel lamination to low angle cross bedding, partly massive, no/weak bioturbation	medium arenite to very coarse arenite well-(moderate)	a) ooids (a), coated grains (c), shells with micritic envelopes (p) b) bioclastic debris (a), micro-lithoclasts (p), siliciclastic debris /quartz (p), shells fragments (r)	dm-m	a) central shoal complex on the shallow ramp, accumulated as sanddunes and mega ripples b) wave-induced beach deposits and backshoal beach bars
10	pack-grainstones + grainstones	limestone light grey-white, beige	trough & tabular, high angle cross-bedding, rarely massive, no/weak bioturbation	very coarse arenite to fine rudite well to moderate	shells (a), micritic envelopes (a), coated grains (c), bioclastic detritus (p)	dm-m	proximal flank of the central shoal complex shallow ramp position)
11	pack-grainstones + grainstones	limestone light grey-white, beige	parallel laminated, massive sheets, faintly high angle cross-bedded, umbrella structures (c), no/weak bioturbation	very coarse arenite to medium rudite poor-very poor	shells and brachiopods (a), micritic envelopes (a), coated grains (p), ooids (p), intraclasts (r)	dm	storm induced event sheets without subsequent reworking, located at the landward flank of a shoal complex
12	pack-grainstones + grainstones	limestone light grey-white, beige	parallel lamination by aligned skeletal grains, trough cross-bedding, partly poorly stratified beds, channel geometries, no/weak bioturbation	fine-medium rudite poor	oncoids (p-c), fragmented shells (p-c), micritic envelopes (c), (dolomitized) ooids (p-c), coated grains (p), bored shells (p), fine bioclastic debris (p)	cm-dm	channel fills of- or from an shallow lagoonal environment (backshoal)
13a **13b**	pack-grainstones + grainstones	limestone medium-light grey	a) vague to faintly parallel laminated, alternating successions of ooids or shells, umbrella structures (p-c) b) parallel lamination and high angle, (trough) cross-bedding, alternating successions of ooids in all types bioturbation is weak or not present	a) very coarse arenite to medium rudite b) very coarse arenite a) moderate-poor b) moderate-well	a) shells (c), micritic envelopes (p-c), ooids (p-c), coated grains (p-c), intraclasts & debris (p), brachiopods (r) b) shells (c), micritic envelopes (c), (dolomitized) ooids (c), coated grains (c), intraclasts & debris (p)	cm-dm rarely several dm	a) storm induced event sheets/ spillover lobes besides the shoal complex b) transition of oolite to shell hash-dominated shoal
14	boundstone	limestone medium to light grey	nodular, cauliflower-like bioherms, patchy distribution, commonly bored (bioturbated)	fine-medium rudite well-medium	pure bivalve boundstone composed of oyster *Placunopsis ostracina*	dm-few m	„patch-bioherms“ on the seaward flank of a shallow ramp
15	boundstone	dolomite to dolo-limestone beige, yellow, grey	crinkly parallel laminated and wavy fine laminated, partly massive, weak- to moderate bioturbation	siltite well-moderate	algae (a), sparitic and siliciclastic debris (a)	cm-(dm)	algal laminites in a quite subtidal to intertidal setting (backshoal, shallow ramp position)

Table 1: Description and interpretation of main lithofacies types.

Photodocumentation Plate 1: Sedimentary structures

Dune-scale cross-bedding (2D view)

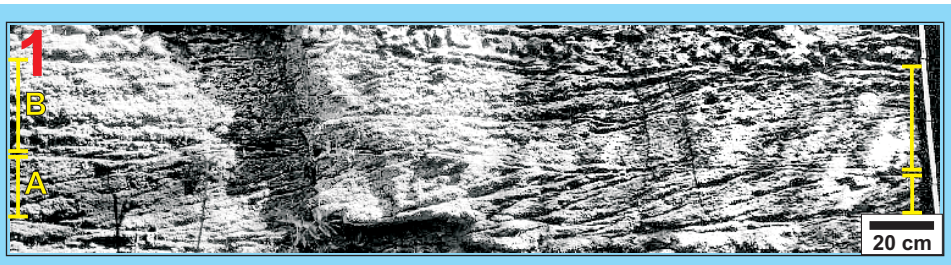

1) Shoal facies is accumulated most frequently in form of cross-bedded sanddunes.

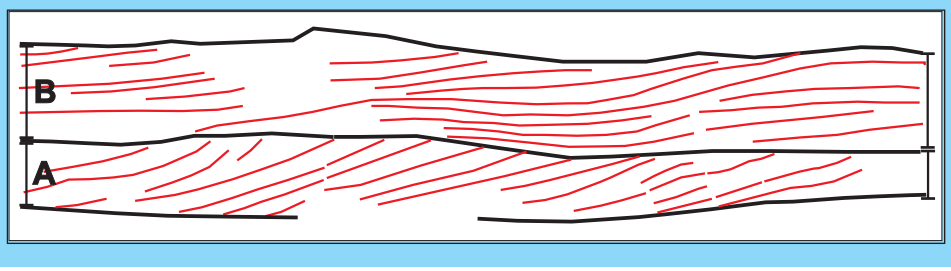

Foreset laminae are marked by red lines. Set tops are truncated by the succeeding sets. Black lines mark the set boundaries of the sets A and B.

Dune-scale trough cross-bedding (3D-view)

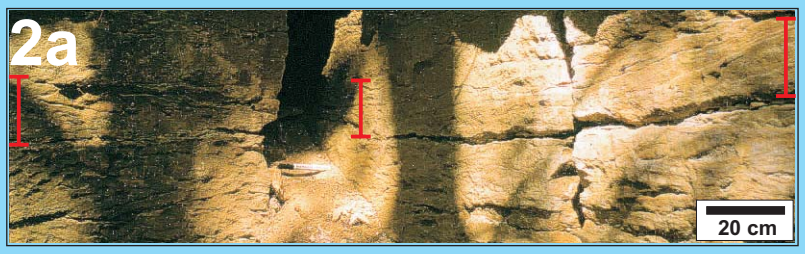

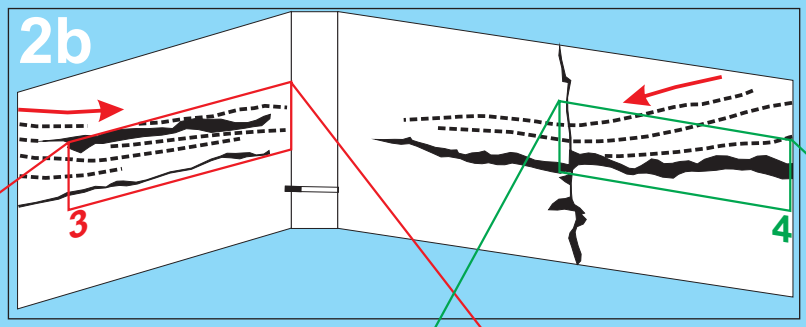

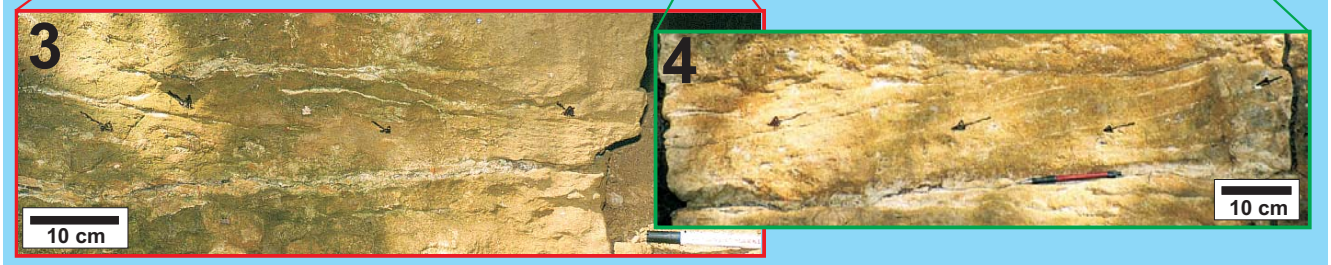

2a) Foresets within the red marked section forming a trough cross-bedded carbonate sanddune almost exclusively composed of oolitic grainstone (LFT 9a).
2b) The fence diagram of the quarry walls illustrates the 3D sectional view of the trough shaped sanddune, where the different dip directions of the individual foresets (stippled lines) are highlighted by arrows. The reconstructed total dip of the trough cross-bedded sanddune in north-eastern direction corresponds to the major storm induced wind and paleocurrent direction.
3 / 4) The detail photos show 30 - 45° dipping single foresets.

Sanddunes are formed by unidirectional flows under higher hydrodynamic conditions.

Symmetric ripples / wave ripples (Plate 2)

Symmetric ripples are more often observed in fine-grained (calcisiltitic / -arenitic) facies types, usually in offshoal settings, i.e. in LFT 8. Their morphology is frequently preserved on bedding planes, showing continuous, sinuous-like crests (Plate 2, Fig. 2). The occurrence of climbing ripples attests episodic high sediment supply (Plate 2, Fig. 1). According to KOSTIC (2001), several features point to a formation by oscillatory wave activity under shallow-water conditions.

Hummocky cross-stratification (HCS) (Plate 3)

Hummocky cross-stratification is restricted to siltitic- to fine-arenitic offshoal facies (LFT 2). A detailed description of hummocky cross-stratification is given in Plate 3. According to DOTT & BOURGEOIS (1982), HCS indicates combined flows caused by storms.

3.2 Facies associations

Lithofacies types were grouped into three facies associations composed of genetically related facies-types.

- Shoal facies association
- Shoal transition facies association
- Offshoal facies association, (where possible subdivided into fore- and backshoal facies).

The grouping of lithofacies types to one of these facies associations is based on DUNHAM texture, sedimentary structures, sorting and composition.
NOTE: In cases where lithofacies types 9a, 10, 11 and 13b were below a thickness of 0,5 m, they are grouped to the shoal transition facies association rather than to the shoal facies association.

These facies associations reflect the lateral facies succession, the various hydrodynamic conditions, and related to that, different reservoir potential from shoal to offshoal.
A detailed listing of all lithofacies types in relation to their facies association is shown in Table 2, including the reservoir potential of these facies associations, marked by individual color codes used in the sedimentary logs and figures elsewhere in this report.

Photodocumentation Plate 2: Sedimentary structures

Symmetric ripples / wave ripples (side view)

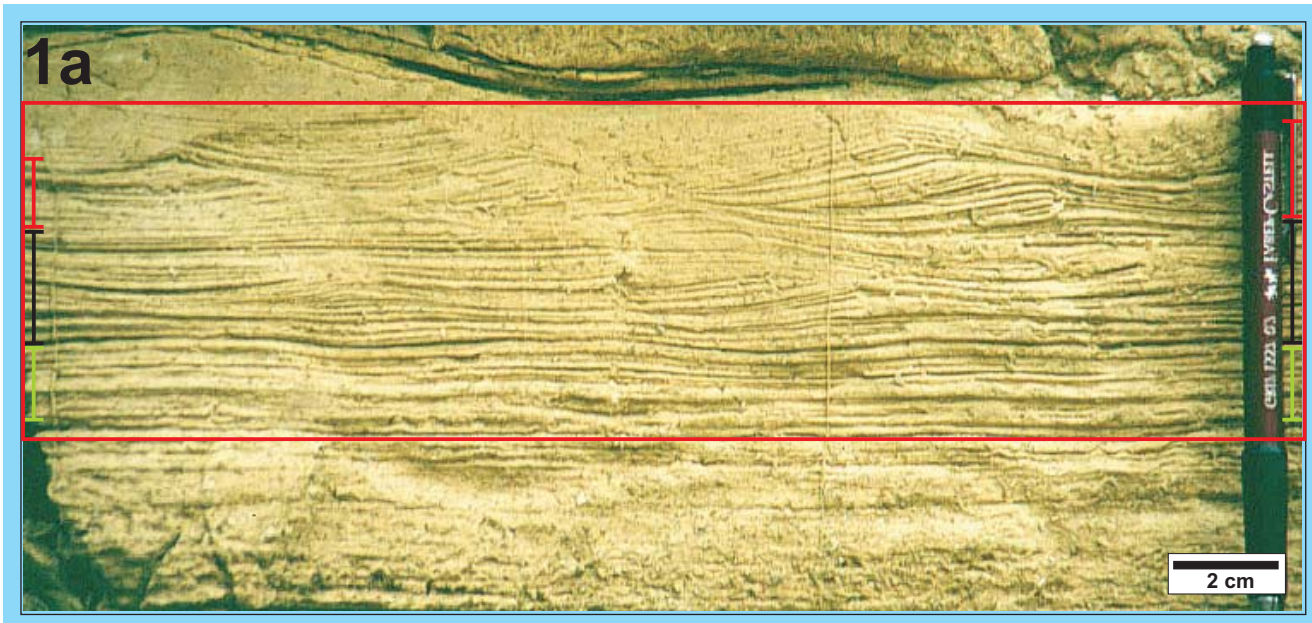

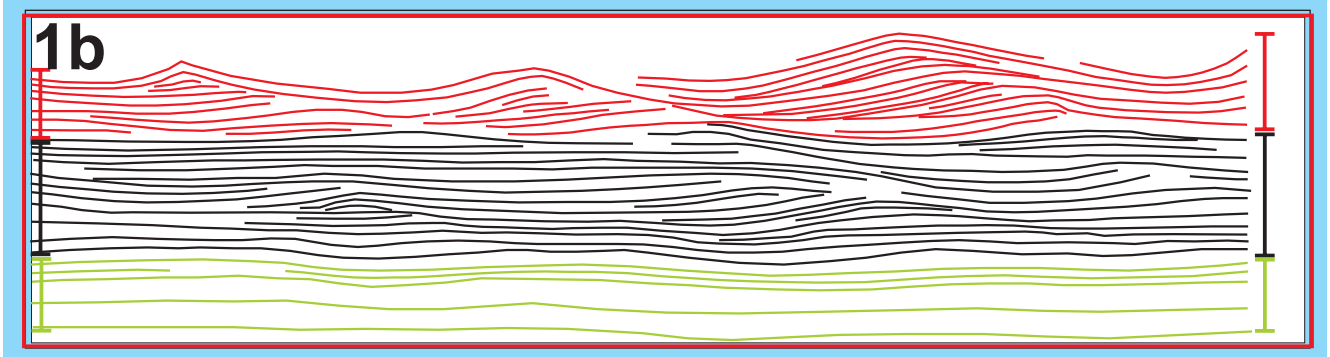

1a & b) The succession starts with parallel lamination (marked green), succeeded upwards by wavy lamination (marked black) which further upwards turns into ripple cross lamination (marked red). The ripples show a clear climbing trend (to the left).
Hydrodynamically the succession reflects initial high- energetic conditions (parallel lamination) which afterwards slowly decrease.

Symmetric ripples / wave ripples (top view)

2) Symmetric (wave-) ripples are preserved mainly under low hydro-energetic conditions, e.g. this mudstone bedding plane, showing continous sinuous-like crests (arrow). The occurrence of this ripple type attests oscillatory wave activity.

Photodocumentation Plate 3: Sedimentary structures

Hummocky cross-stratification (field-scale)

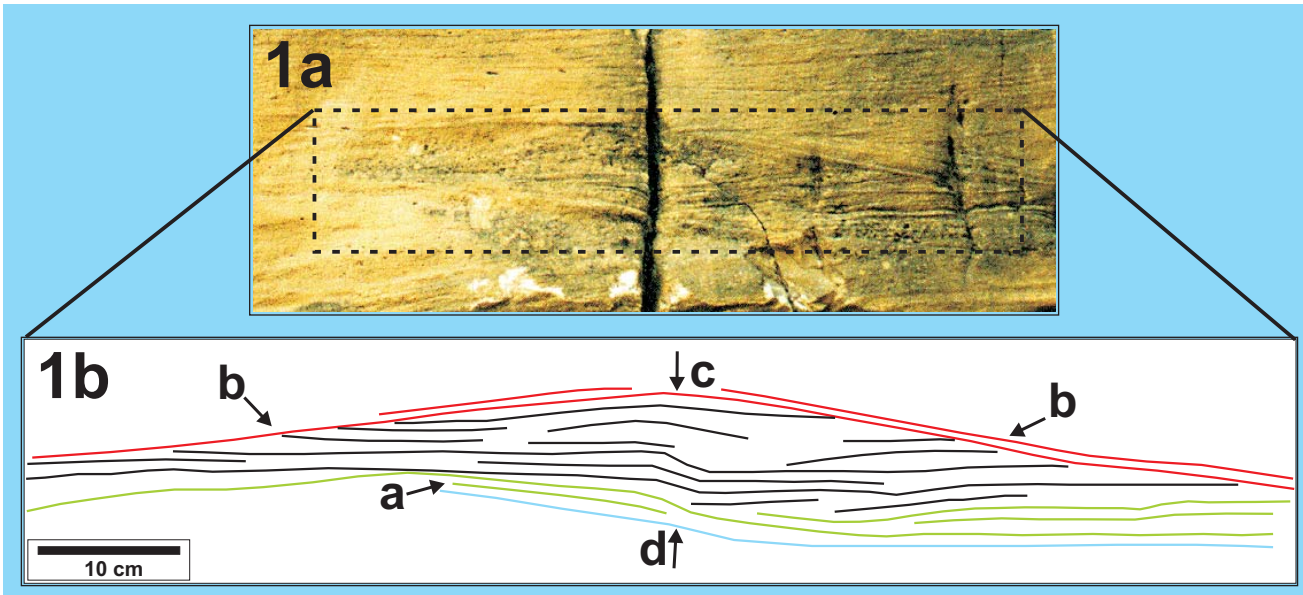

1b) The drawn stratification from photograph 1a illustrate all characteristic features of hummocky cross-stratification:
a) Slightly upward curvature of laminations (green lines).
b) Low angle curved lamina intersections (intersection of black & red lines) because of slight migration of hummocks and swales.
c) Hummocks are draped by lamina (red lines).
d) Sharp base (blue line).
e) Long wavelength (here ~1 m), low height (here ~10 cm) and lamina that dip less than 10°.

Hummocky cross-stratification indicate complex combined flows with a strong oscillatory component caused by storms and alongshore paleocurrents (see DOTT & BOURGEOIS, 1982).

Hummocky cross-stratification (slab-scale)

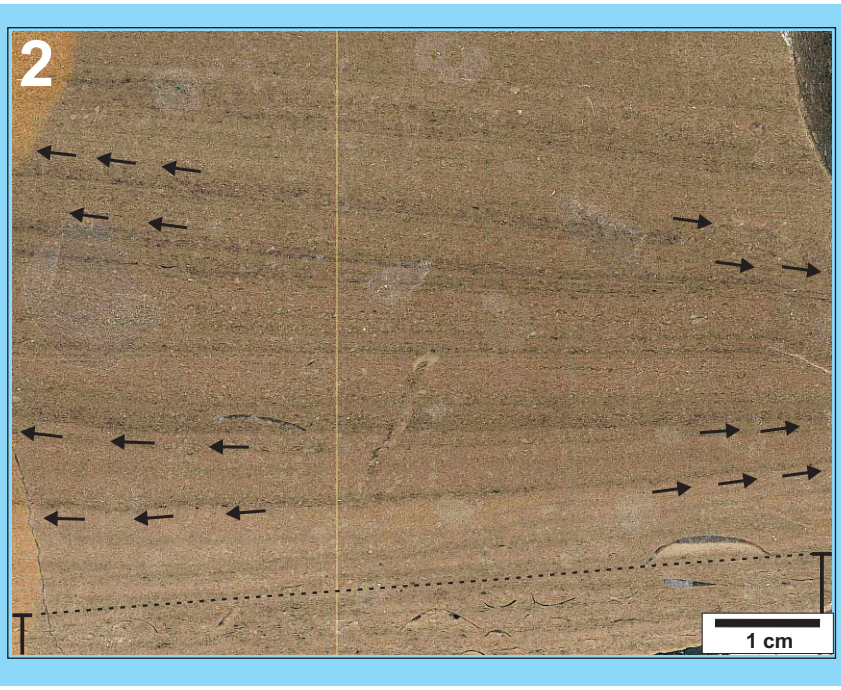

2) In slab-/ core-scale hummocky cross-stratification may be distinguished from other forms of (cross-) stratification by upward curved lamina (swales), see arrows in the lower part of this photo, while succeeded lamina are downward curved (hummocks), see arrows in the upper part.
Additionally low angle of lamination (>10°) and low height of cross stratified sets are indicative features. Hummocky cross-stratification is restricted to fine calcarenites & calcisiltites, most frequently preserved in the upper part of a tempestite succession (see plane laminated shelly bed, in brackets, which corresponds to the intermediate tempestite part).

Table 2: List of associated lithofacies types combined to facies associations and their reservoir quality.

Facies association	Lithofacies types associated	Reservoir quality	Color
shoal facies association	9a, 10, 11, 13b	good-excellent	red
shoal transition facies association	6, 7b, 9b, 13a	moderate	green
offshoal facies association (foreshoal)	1a, 2a, 4, 7a, 8, 14	poor	yellow
offshoal facies association (backshoal)	1b, 2b, 3, 4, 5, 12, 15	poor (sporadically good)	yellow

3.3 Depositional environment and lateral facies succession (Fig. 9)

The facies succession from backshoal to basinal environments follows previous work by WAGNER (1913), VOLLRATH (1955), HAGDORN (1982) and AIGNER (1985) extended by own observations and new field data.

Description:

The generally recognized lateral facies pattern is, that nearshore skeletal and oolitic carbonate sands form mappable „shoal“ bodies, often on well-known „paleotectonic highs“. These bodies are elongated in shape and concentrically arranged. The shoal centers consists of well sorted oolitic grainstones (LFT 9a), followed sea- and landwards by mixed skeletal-oolitic units (LFT 13b) and are replaced finally by pure, well sorted fragmented shell accumulations (shell hash, LFT 10). Commonly these facies types are characterized by cross-bedding and a grain-dominated fabric. In most proximal landward position of these „shoals“ or „barrier-banks“, ruditic, poorly sorted bioclastic units (pack-grainstones) were observed (LFT 11).

Near-shoal packstones are grain-dominated (LFT 13a) but turn to mud-dominated packstones further away (LFT 6 & 7b). Their main constituents are ooids and shells with micritic envelopes (LFT 13a & 6) decreasing in abundance towards all directions. Lithofacies type 7b finally consists of fragmented shells in a muddy matrix.

The 3 lithofacies types surrounding the shoal bodies (LFT 6, 7b and 13a) show frequently parallel-to low angle lamination by aligned shells and moderate to poor sorting. Sharp erosive bases of beds are also often observed.

Towards the basin, the abundance of skeletal particles as well as their grainsize decreases while the mud content increases. Graded bioclastic packstone sheets (LFT 8) pass basinwards into poorly sorted bioclastic wacke- to packstones (LFT 7a) and bioclastic wackestones (LFT 4),

Depositional Environment and Lateral Facies Succession

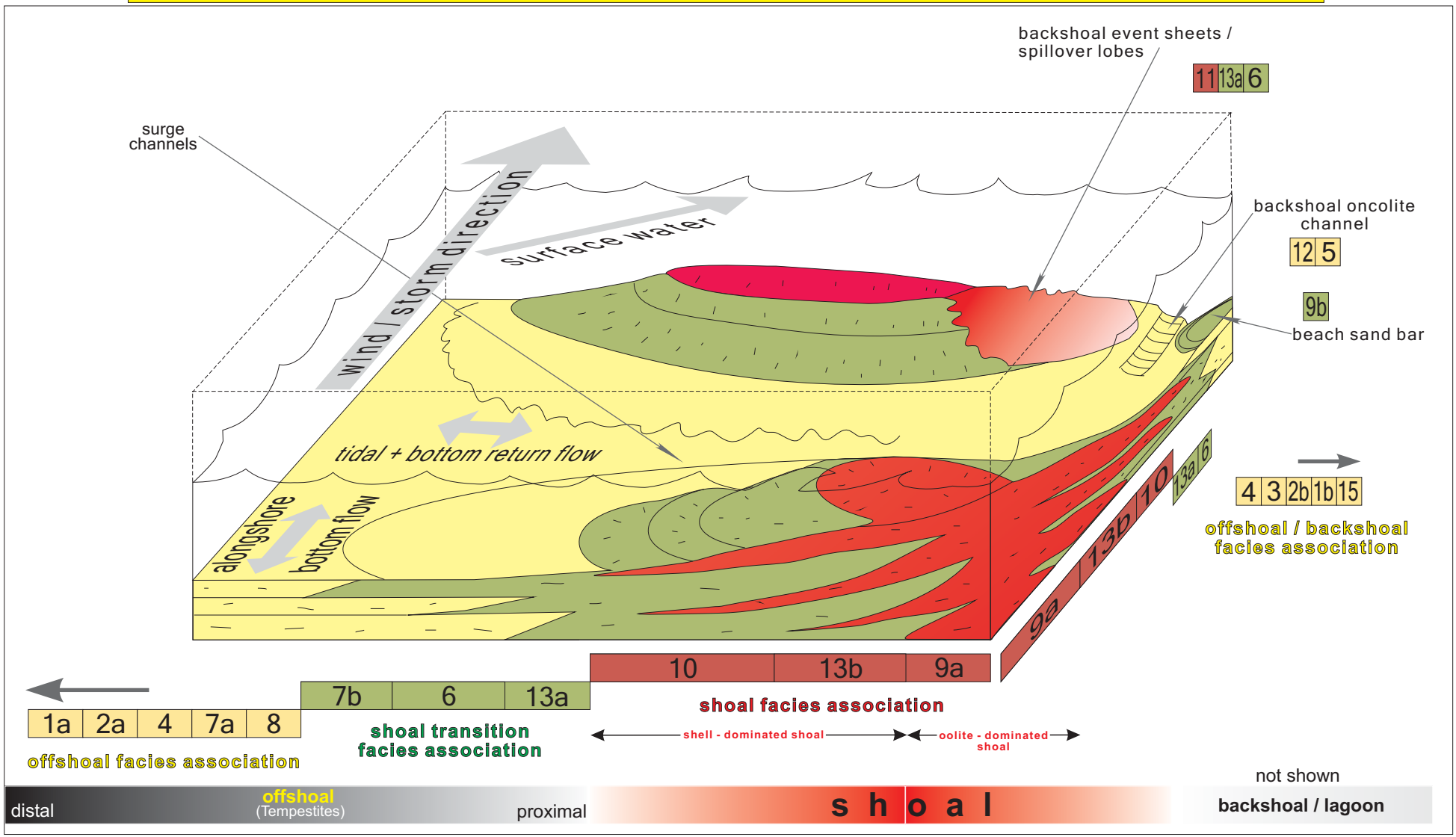

Fig. 9: Schematic facies model illustrating the depositional environment and lateral facies succession (lithofacies types & facies associations) of the Upper Muschelkalk in the studied area.

both brachiopod-dominated. Finally scoured, finely-laminated mud- to wackestones (2a) and nodular mud- to marlstone (1a) alternations occur.
In sheltered backshoal areas also mud-dominated facies predominate. In contrast to basinal mud-dominated facies, they are characterized by a high degree of bioturbation and abundant peloids (LFT 1b, 2b). Additionally oncolites (LFT 3), bored shells with micritic envelopes (LFT 4) and/or black pebbles may occur (LFT 5b).
Less abundant in this "backshoal"-setting are oncolite-dominated pack- and grainstones (LFT 5a & 12) and fine dolo-laminites (LFT 15). Restricted to near-coast settings are grain-dominated, well sorted, pure calcarenites (LFT 9b).

Interpretation:
The high-energy shelly / oolitic facies belt is interpreted as shallow shoal-water complex, similar to carbonate sand bodies in the Persian Gulf, while the backshoal zone is interpreted as lagoonal facies (cf. AIGNER, 1985). Laminated skeletal packstones surrounding the shoal are considered as shoal transitions. Graded, poorly sorted packstones and wackestones belong to the transition zone between shallow and deep ramp, while mud-and marlstones are part of the deep ramp facies.

3.4 Basic diagenetic analysis (Fig. 10, Plates 4 & 5)

In the framework of this study, only a basic diagenetic analysis using standard petrography and cathodoluminescence microscopy was carried out. No geochemical techniques have been applied.

The following general diagenetic succession (see Fig. 10) was frequently observed during petrographic analysis of more than 60 thin sections from different outcrop locations and stratigraphic horizons. This analysis essentially confirms the results of previous diagenetic investigations (i.e. BACHMANN, 1973).

1. **Early marine cementation phase:** All components are fringed by isopachous radial-fibrous cements (A_1-cement). Their morphology (bladed- and needle shaped calcite crystals) indicates marine phreatic precipitation.

- Effect on Φ/k: On the one hand this extensive cementation phase stabilizes the primary grain-framework and prevents extensive compaction, preserving interparticle porosity. On the other hand early A_1-cements partly occlude interparticle pore space, especially in fine-grained carbonate sands with small pore throats.

2. **Leaching:** Large portions of the shoal- and shoal transition facies are affected by selective solution of former aragonitic components, mainly ooids and bivalve shells. This large-scale dissolution process is generally considered to be caused either by subaerial exposure and / or fresh water influence under shallow water conditions (at shoal lithofacies types) or by undersaturated marine (pore-) waters with respect to aragonite (see TUCKER & WRIGHT, 1990).

- Effect on Φ/k: This phase is responsible for the abundant bio- and oo-moldic porosity observed in shoal lithofacies within the entire Upper Muschelkalk. This generation of separate-vug porosity results a large increase in porosity, particularly in usually low porosity mud-dominated facies types (i.e. shoal transition packstones). Permeabilities however are low in all lithofacies types with separate-vug porosity only.

3. **Second marine cementation phase:** On a minor scale, renewed isopachous fringe cement was observed exclusively inside of (large) dissolved skeletal components. This cement (named A_2) attests continuous marine phreatic precipitation after the large-scale dissolution phase. Crystal sizes are smaller compared to early A_1-cement fringes due to smaller intraparticle pore space.

Diagenetic sequence

Primary sediment

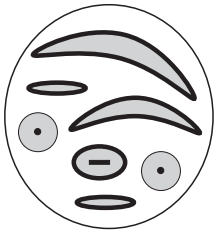

Early diagenesis

❶ First marine cementation phase

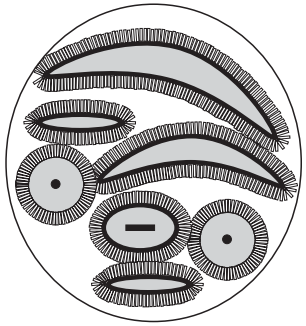

Cement:
Isopachous fringe cement (A_1-cement)

Environment:
Marine phreatic

Effect on Φ/k:
Prevents compaction, partly occludes small interparticle pore space

❷ Leaching

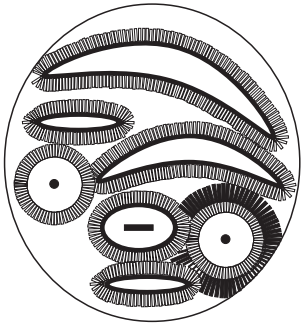

Dissolution:
Selective solution of former aragonitic components (ooids, bivalve shells)

Processes: Subaerial exposure/ fresh water dissolution, undersaturated marine (pore-) waters

Effect on Φ/k:
Generation of abundant moldic porosity

❸ Second marine cementation phase

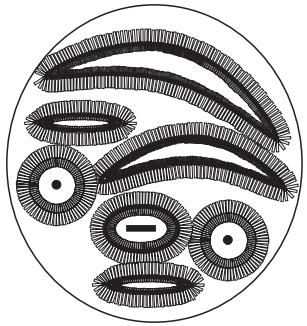

Cement:
Isopachous fringe cement (A_2-cement) visible only inside of dissolved components. Outside grown together with A_1-cement

Environment:
Marine phreatic

Effect on Φ/k:
Low to moderate decrease in separate-vug (moldic-) porosity

Late diagenesis

❹ Third marine cementation phase

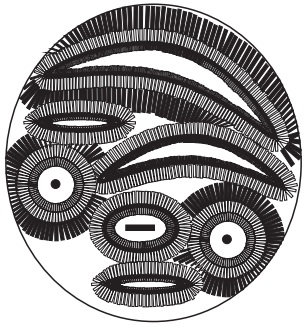

Cement:
Dog-tooth cement, (isopachous prismatic spar) (B_1-cement)

Environment:
Shallow burial

Effect on Φ/k:
Moderate decrease of interparticle- and separate-vug porosity

❺ Fourth marine cementation phase

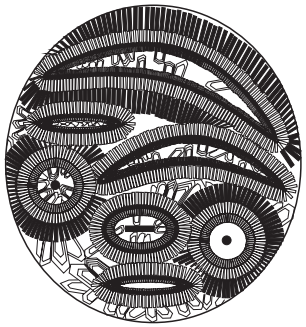

Cement:
Drusy, equant, blocky calcite spar (B_2-cement)

Environment:
Burial

Effect on Φ/k:
Generally strong reduction of interparticle- and moldic porosity and permeability

❻ Spotty dolomitization

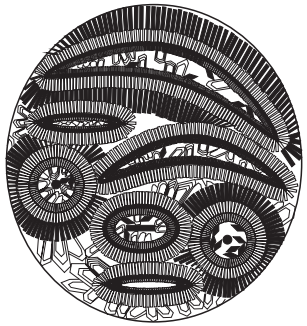

Cement:
Dolomite rhombs

Environment:
Burial

Effect on Φ/k:
Minor decrease of poro-perm properties

Fig. 10: This diagenetic sequence, based on thin section microscopy and cathodoluminescence studies illustrates the influence of diagenesis on reservoir quality.

Photodocumentation Plate 4: Diagenetic Analysis

Early Diagenesis: First and second marine cementation phases (A-cements)

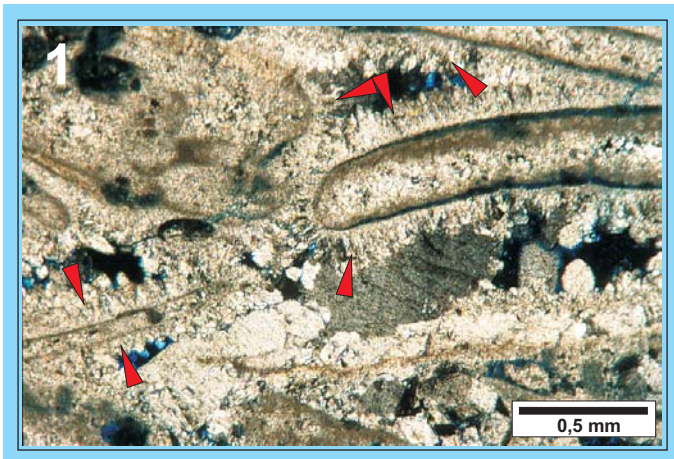

1) First marine cementation phase: Isopachous fringes of bladed and needle shaped calcite crystals indicate marine phreatic precipitation. This isopachous fringe cement (A_1-cement, marked by red arrows) precipitated before the large-scale leaching phase and therefore only occurs outside of the components.
Effect on Φ/ k: A_1-cement prevents compaction but also partly occludes interparticle pore space.

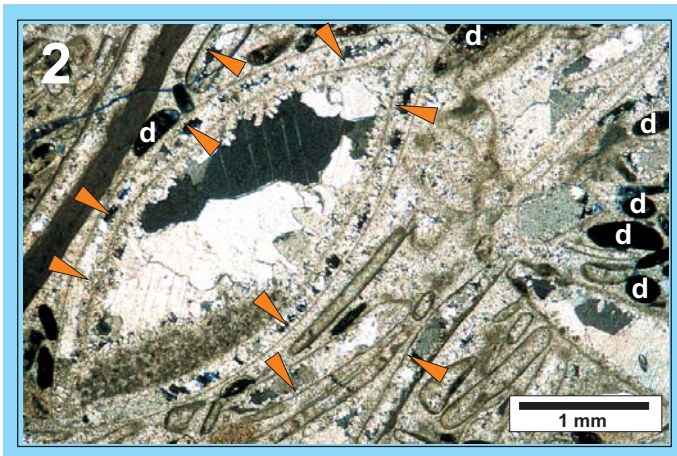

2) Second marine cementation phase: Isopachous fringe cement (A_2-cement, marked by orange arrows) precipitated **after** the large-scale dissolution phase (see remnants of dissolved components, marked by a "d") attesting continuous marine phreatic precipitation. Thus, A_2 -cement can be differentiated from A_1 -cement only on the inside of dissolved components. Crystal sizes are smaller compared to early A_1 -cement fringes due to smaller intraparticle pore space.
Effect on Φ/ k: Low- to moderate decrease in separate-vug (moldic) porosity.

Late Diagenesis: Third marine cementation phase (B_1-cements)

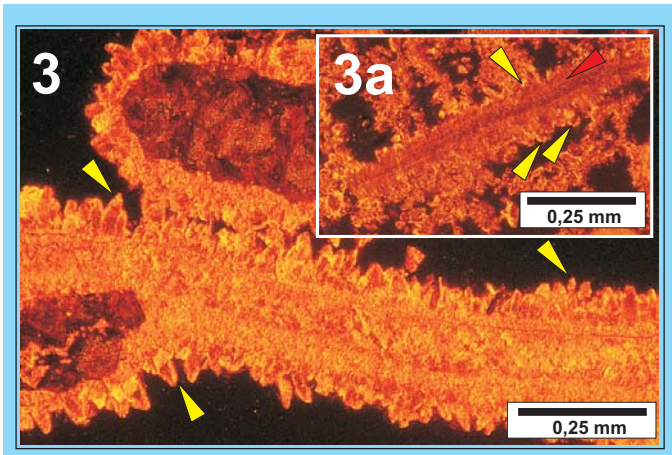

3) Third marine cementation phase: This dog-tooth cement forms rims of isopachous prismatic calcite crystals. Using cathodoluminescence this cement (B_1-cement, marked by yellow arrows) have a distinct luminescence pattern. The crystal cores show a dull inner zone and a brightly luminescing fringe. This pattern allows a clear differentiation of major isopachous fringe cement-types A (dull luminescing) and B_1 (see Fig. 3a). According to REINHOLD (1997) this dog-tooth cement represents an shallow-burial environment. Effect on Φ/ k: Moderate decrease of interparticle- and separate-vug porosity.

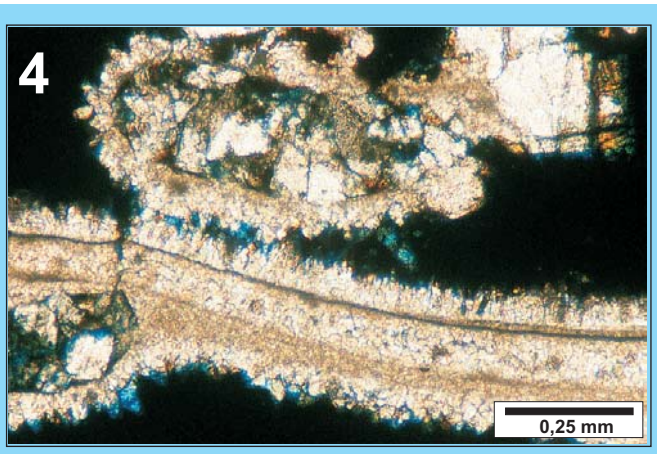

4) The same section as in Fig. 3 under the transmission light microscope (x-Nicols). With that it is more difficult to separate the both major isopachous fringe forming cement types A and B_1. The fine- to medium-sized crystals (50 - 150 µm) of the dog-tooth cement B_1 show prismatic shapes with equant crystal faces. These crystals are also wider and show a more irregular growth form than the radiaxial-fibrous A -cements with smaller, needle- to blade-shaped crystals.

- Effect on Φ/k: A low- to moderate decrease in separate-vug (moldic-) porosity is caused by this cementation phase. A negative influence concerning interparticle pore space was not observed.

1. **Third marine cementation phase:** This dog-tooth cement forms irregular isopachous rims of prismatic spar (B_1-cement). The fine- to medium sized crystals (50-150 µm) have euhedral, scalenohedral and rhombohedral crystal shapes with equant crystal faces. They grew on early A_1-/ A_2-cement fringes. As both major (A- and B_1-) cement-types form isopachous fringes are not distinguishable at the first glance. On closer examination however, these cement-types are easy to separate. Under the normal microscope the above described characteristical crystal shapes, the size and more irregular growth form of the dog-tooth type cement is apparent. Using cathodoluminescence, a characteristic luminescence pattern distinguishes B_1-cements clearly from dull luminescent A-cements. The crystal cores show no luminescence or are dull while the ends exhibit a thin, bright luminescent fringing zone. According to REINHOLD (1997) this dog-tooth cement type represents an oxic to suboxic shallow burial environment.

- Effect on Φ/k: A moderate decrease of interparticle and separate-vug pore space.

2. **Fourth marine cementation phase:** The drusy, equant calcite spar of this final cementation phase is very widespread (B_2-cement). According to BATHURST (1975), this B-cement type is known as precipitation in a burial environment. The presence of different growth zones as well as different cement generations is visible with cathodoluminescence. Growth zones and generations reflect changing calcite spar geochemistry with progressive burial and evolution of porewaters.

- Effect on Φ/k: Due to the increasing crystal size towards the cavity center as well as the competitive growth, B_2-cement is the most important pore-filling, porosity-destructive cement. Both primary (interparticle pores) as well as secondary (moldic pores) pore space is greatly reduced by coarse equant calcite spar.

3. **Spotty dolomitization:** Minor growth of dolomite-rhombs in remnant separate-vug pore space was observed. The precipitation of dolomite is assumed to have taken place during burial.

- Effect on Φ/k: The effect of dolomite rhombs decreasing Φ/k is probably rather low.

Neomorphism: Aggrading neomorphism, recrystallisation and calcitisation were occasionally, in selected samples commonly observed. As these processes have only minor influence on Φ/k they were not further evaluated.

Photodocumentation Plate 5: Diagenetic Analysis

Late Diagenesis: Fourth marine cementation phase (B_2-cements)

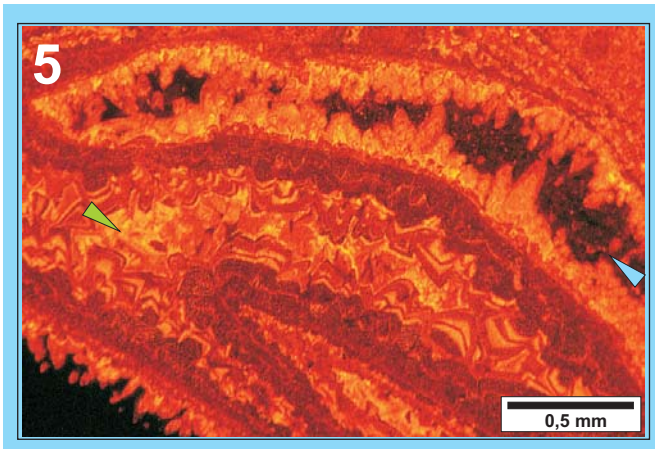

5) Fourth marine cementation phase: This drusy, equant calcite spar (B_2-cement) is indicative for calcite precipitation in a burial environment (BATHURST, 1975). By cathodoluminescence microscopy the presence of different growth zones as well as different cement generations, reducing original porosity, become apparent. Growth zones and generations reflect changing calcite spar geochemistry with progressive burial and evolution of pore waters.
Effect on Φ/ k: B_2-cement is the most important pore-filling, porosity-destructive cement, due to increasing crystal sizes towards the cavity center as well as the competitive growth.

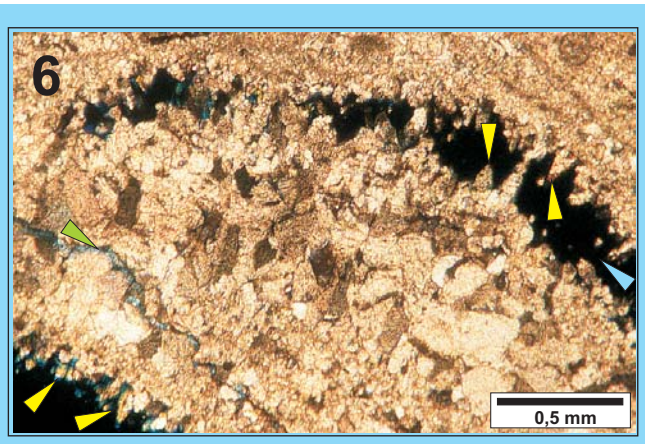

6) The same section as in Fig. 5 under the transmission light microscope (x-Nicols). The equant, blocky shapes of the B_2 -cement crystals are easy to distinguish from prismatic B_1 -cement crystals (yellow arrows). Their effect on porosity and permeability is visually comparable in this figure and Fig. 5. While the B_1 -cement decreases the present pore space in a moderate degree (blue arrow), the former pore space below was completely filled by B_2 -cement (green arrow). This illustrates the high amount of both, primary (interparticle-) as well as secondary (moldic-) pore space destroyed by coarse blocky calcite spar.

Dolomitization and general diagenetic succession

7) Dolomitization: Minor growth of dolomite-rhombs (indicated by pink arrows), fill remnant separate-vug (moldic-) pore space. The selective solution of former aragonitic components during the large-scale leaching phase cause a preferential dolomite occurrence in ooids, as can be seen here. The precipitation of dolomite is assumed to have taken place during burial.
Effect on Φ / k: Minor decrease of poro-perm properties.

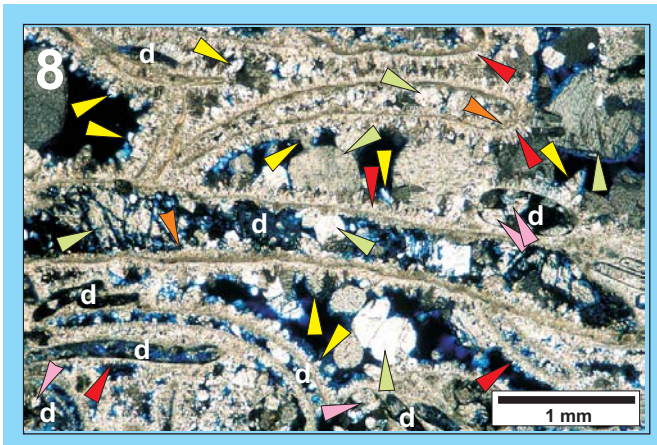

8) General diagenetic succession: 1) Radial-fibrous isopachous cement fringes all components (A_1-cement, see red arrows) 2) The large-scale dissolution phase of prefered former aragonitic components (marked by a “d”) generated abundant moldic porosity. 3) Isopachous fringe cement precipitates inside (& outside) of dissolved components (A_2 -cement, see orange arrows). 4) Dog-tooth cement (B_1 -cement, see yellow arrows) forms isopachous rims of prismatic calcite spar grown on early A -cements. 5) Drusy, equant, blocky calcite spar (B_2 -cement, see green arrows) fills largely remnant pore space. 6) The precipitation of dolomite (pink arrows) is the final porosity-destructive cementation phase.

3.5 Petrophysical Analysis

Over 650 plugs were drilled and analyzed for this study, focusing on detailed sampling (dm-spacing) of shoal lithofacies types with apparent reservoir character.
The aim was a poro-perm characterization of the different shoal facies types in order to estimate their reservoir potential and to determine fluid flow units. The results should enter in a 3-D reservoir simulation planned as follow-up study.
Only few samples from low energy, mud-dominated facies types (wackestones) as well as finely crystalline dolostones were measured.

3.5.1 Pore-types

Pore-types are classified according to the terminology of CHOQUETTE and PRAY (1970) and LUCIA (1983), while rock-fabric terminology is based on the modified DUNHAM classification as proposed by LUCIA (1995).
Most investigated porous samples belong to one of the following three (combined) major pore-types after LUCIA (1983):

1. Separate-vug pore-type (bio-/ oo-moldic porosity)
2. Separate-vug- and interparticle pore-type (moldic and intergranular porosity)
3. Separate-vug- and touching vug pore-type (moldic and fracture/ stylolitic porosity)

A few samples of macroscopically tight appearance do not fit to one of these classes. They are summarized as samples with „microporosity“ (see Fig. 11).
Interparticle or touching-vug porosity without additional separate-vug porosity was not observed.
The following general patterns appear of the porosity-permeability crossplot in Fig. 11:
Samples with

- microporosity (assumed) plot into a field below $\Phi = 5$ % and k(h) = 1 mD
- separate-vug porosity define a larger field between $\Phi = 2$ to 12 % and k(h) < 10 mD
- separate-vug and interparticle pores cluster in a distinct field from $\Phi = 7$ to 20 % and k(h) between 8 and 200 mD.

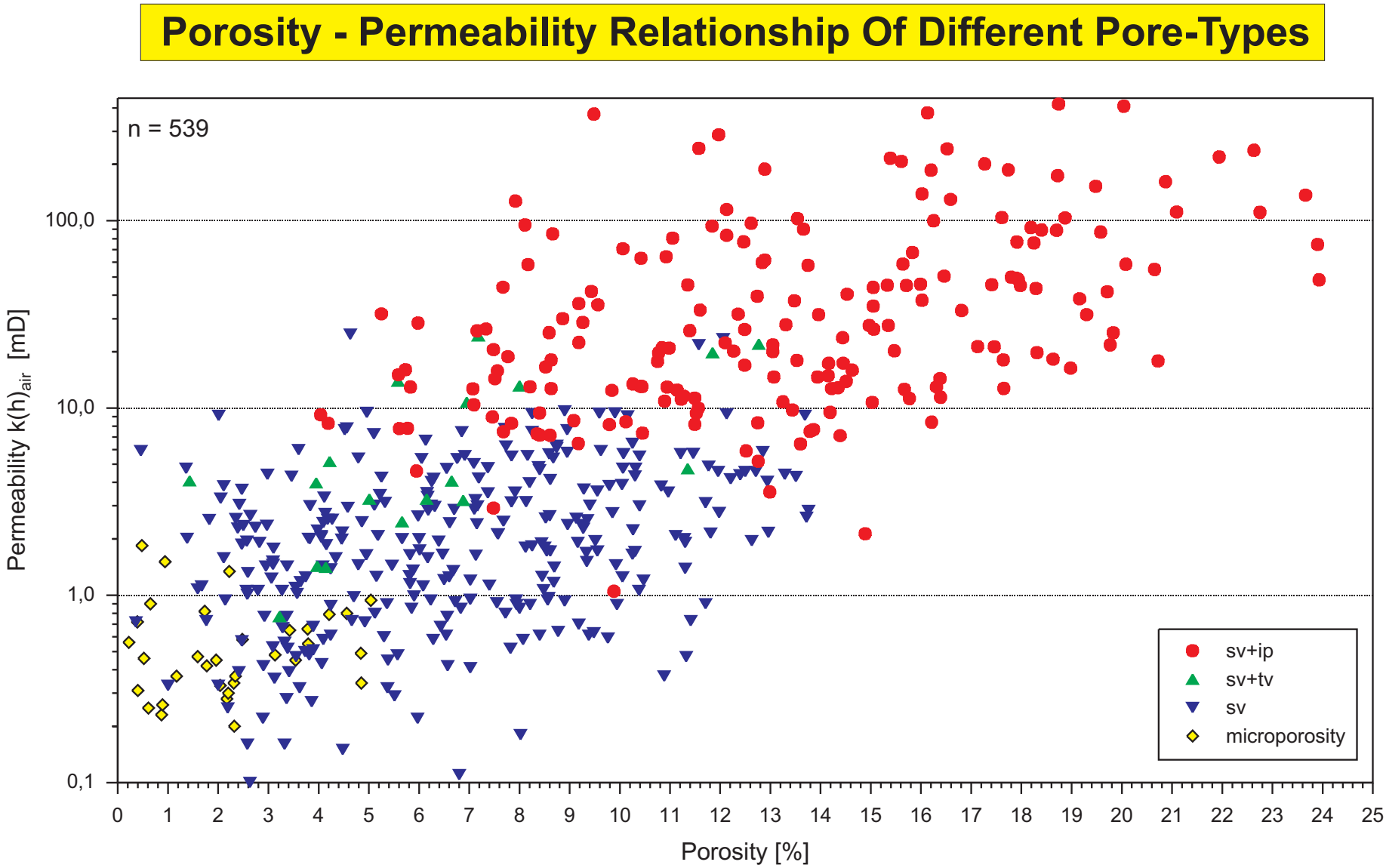

Fig. 11: This crossplot illustrates that reservoir quality is mainly controlled by the respective pore-type. Samples with separate-vug (moldic) and interparticle pores have the highest reservoir potential.

- separate-vug and touching-vug pores scatter in a poorly defined field of Φ = 3 to 7 % and k(h) = 1 to 20 mD. Thus, the values of this pore-type are located between the separate-vug pore-type and separate-vug plus interparticle pore fields.

Occurrence, formation and evaluation of different pore types

Each class has a different type of pore-size distribution, pore space volume and interconnection.

- 1.) **Separate-vug porosity**

  Occurrence: Most abundant pore-type class in this study. This type occurs in shoal facies types as well as in shoal transition- and offshoal deposits. Porosities in general decrease from shoal to basin.

  Formation: This type almost exclusively consists of bio- and oo-moldic pores. Separate-vugs are typically fabric-selective in their origin. This was frequently confirmed by selective dissolution of aragonitic particles (ooids, some bivalve shells) in comparison to mostly well preserved, calcitic brachiopod shells. The dissolution of skeletal grains and ooids in this study is explained either by subaerial exposure and / or fresh water influence under shallow-water conditions (at shoal lithofacies types) or dissolution by undersaturated marine (pore-) waters with respect to aragonite (see TUCKER & WRIGHT, 1990).

  Summary: Samples with only separate-vug pores have porosities roughly between 2 and 12 % and low permeabilities, i.e. poor to moderate reservoir properties.

- 2.) **Separate-vug and interparticle porosity**

  Occurrence: Second most frequent pore-type class in this study. This class is limited to distinct shoal, shoal transition and rarely backshoal lithofacies types (see chapter 3.5.2 for details).

  Formation: For development of separate-vug pores see discussion above.
  Interparticle pores represent the original, primary depositional porosity of the sediment. They are controlled by particle sizes and the packing fabric, best are grain-dominated fabrics. Interparticle pores are always linked to high-energy sediment accumulation processes, such as frequent storm events and permanent current action. These favour the formation of grain-dominated textures without interparticle mud. Moreover rapid sedimentation rates increase the chance to preserve interparticle pore space.

Evaluation: According to LUCIA (1995), the pore space volume and therefore the pore size distribution of interparticle pores depend on particle size and sorting. However, his data focus on particles below 500 µm. This is in contrast to the fragmented shells (mostly > 2 mm) as main constituents in the Upper Muschelkalk. Poro-perm measurements of this study showed increasing reservoir qualities in grainstones with increasing grainsize and decreasing level of sorting. In addition differential diagenesis played a role. In the present material it was observed that increasing sorting and decreasing grain size enhance the chance of porosity destruction by marine isopachous fringe cements.
Summary: Porosity is enormously increased when separate-vug and interparticle pores occur together (from about 7 to over 20 %). This class is limited to carbonates with grain-dominated fabric. Best porosities are observed in grainstones of rudite grainsize, with permeabilities between 22 and 82 mD.

- 3.) **Separate-vug and touching-vug porosity**
  Occurrence: This pore-type class is the least abundant in this study, although it may be present in almost all facies types.
  Formation: Touching-vug porosity is typically non-fabric selective. The most common types are solution-enlarged stylolithes (channel porosity) and fracture pores. Fractures result mainly from tectonic deformation and solution collapse associated with evaporite or limestone dissolution. Channel porosity is a product of dissolution and enlargement of present pathways by flow of undersaturated fluids. Vuggy and fenestral pores are only rarely observed. Vugs may represent superficial phenomena, as they were not recorded in cores. Vugs represent solution enhancement of previous intergranular or moldic pores, presumably by (recent?) CO_2- rich rain water. Fenestral pores are restricted to algal laminites (LFT 15).
  Summary: Samples with separate-vug and touching-vug porosity just show a slightly enhanced porosity compared to samples with separate-vug pores only (between 3 to 7 %). However their permeabilities may increase considerably.

- 4.) **Microporosity**
  Occurrence: This type was not investigated in detail and is restricted to dolomitic limestones and dolomites.
  Formation: Microporosity may be caused by dissolved dolomite or calcite crystals.
  Evaluation: Microporosity depends on mud- or dolomite crystal size, which controls volume and connecting pore size.

Summary: This class has very little reservoir potential (Φ = < 5 % and k(h) = < 1 mD) and was thus not investigated.

1.5.2 Rock-fabric types

The lithofacies types (see chapter 3.1) have no 1 : 1 relationship to their petrophysical properties. After the concept of LUCIA (1983), however a relation between rock-fabric (modified DUNHAM textures) of carbonates and pore size distribution exists. Thus, an important step is to link rock-fabric (of the lithofacies types) to the pore-type classes (described above), resulting in different rock-fabric types that display specific petrophysical properties. The evaluation of the different rock-fabric types allows a pragmatic means for evaluating reservoir quality (poor to good, main-reservoir, marginal reservoir, baffle etc.). The approach and workflow is illustrated in Fig. 12. In this study 19 rock-fabric types are distinguished, whereby 6 have good reservoir potential. The petrophysical properties and reservoir quality of every rock-fabric type is listed in Table 3, below.

Table 3: Rock-fabric types and their petrophysical properties (*average values)

Rock-Fabric-Type	Φ [%]*	$k(h)_{air}$ [mD]*	$k(v)_{air}$ [mD]*	Reservoir Quality
4-sv	2,96	0,80	0,81	poor
5a-sv	5,49	1,46	1,08	poor
5a-sv+ip	9,93	11,94	2,69	medium-good
6-sv	4,49	1,12	0,68	poor
7a-sv	3,99	2,02	1,29	poor
7b-sv	4,92	1,85	0,85	poor
7b-sv+tv	12,42	22,73	3,70	**good**
8-sv	3,14	2,24	0,68	poor
9a-sv	6,79	2,73	1,15	poor
9b-sv+ip	6,91	4,75	5,52	medium
10-sv	8,17	2,99	3,17	poor
10-sv+ip	15,05	45,41	43,63	**excellent**
11-sv+ip	12,92	82,12	84,51	**excellent**
12-sv+ip	11,52	21,98	21,23	**good**
13a-sv	5,76	2,80	2,40	poor
13a-sv+ip	9,26	28,30	24,82	**good**
13b-sv	6,65	2,28	1,81	poor
13b-sv+ip	9,08	60,35	12,54	**excellent**
15-ip	9,88	2,67	1,54	poor

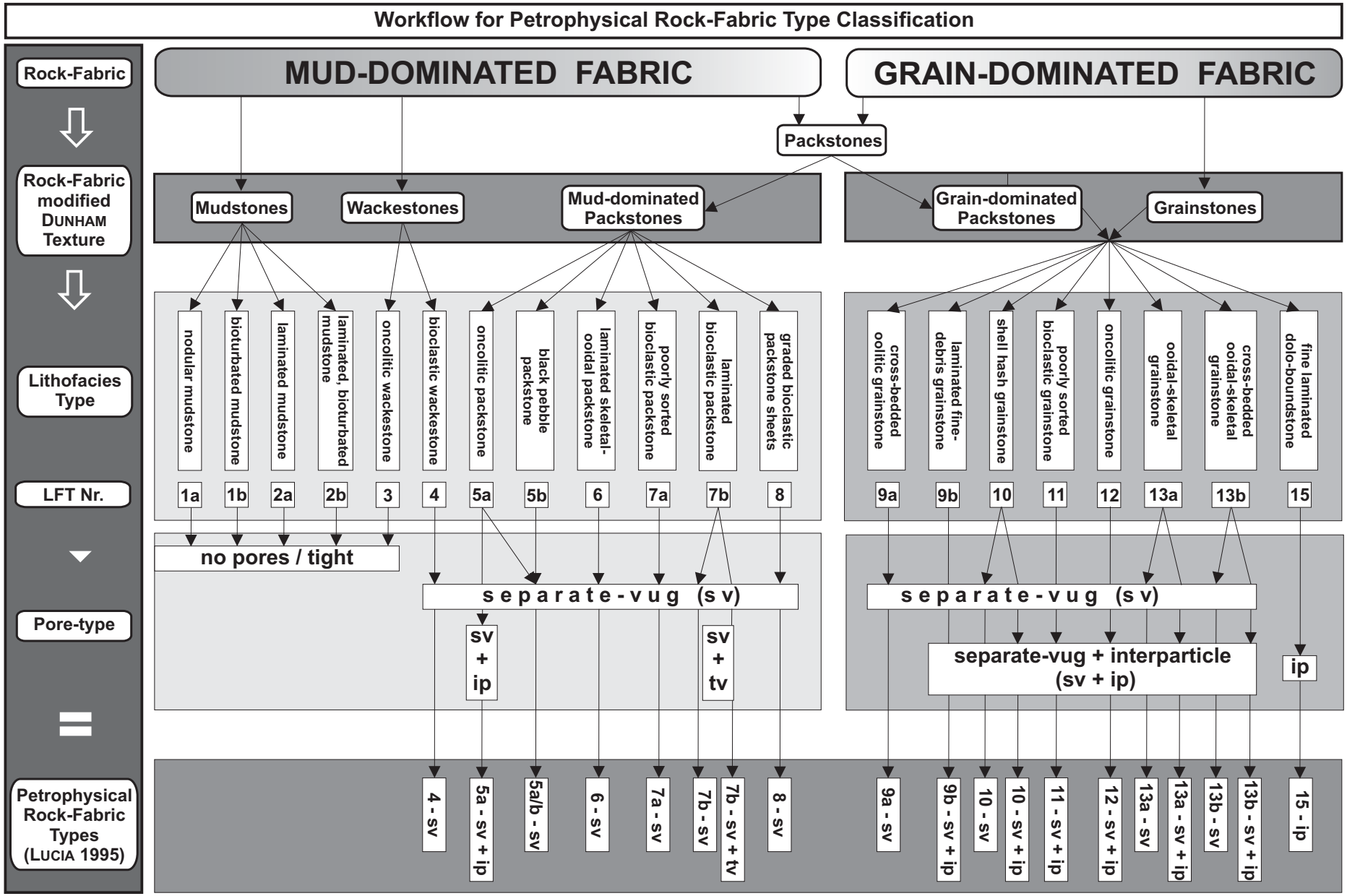

Fig. 12: In order to relate lithofacies types to their petrophysical properties, their rock-fabric was linked to the pore-types, resulting in petrophysical rock-fabric types (LUCIA, 1995) with distinct poro-perm properties reflecting their specific reservoir potential.

The relationship between rock-fabric types and porosity & permeability is shown in Fig. 13. Several rock-fabric types were grouped together (e.g. lithofacies with mud-dominated fabric, like LFT 4 to 8, + separate-vug pore-type = 4-8-sv).
Usually poro-perm crossplots of carbonate rocks show a wide scatter. As illustrated in the poro-perm crossplot related to pore-types only (Fig. 11), it is apparent that permeability is controlled by the dominant pore-type, resulting in separate poro-perm fields. On the rock-fabric types crossplot these fields can be further refined.
There are no apparent trends in rock-fabric types with separate-vug porosity only. In contrast, clear trends in rock-fabric types with separate-vug and interparticle porosity are observed. Shell hash grainstones with separate-vug and interparticle pores (RFT: 10-sv+ip) are confined to a field between 10 to 20 % porosity and between 10 and 200 mD permeability, while poorly sorted bioclastic grainstones with the same pore-types (RFT: 11-sv+ip) plot into a wider field between 7 to 20 % and 8 to more than 200 mD. The combined rock-fabric type 13a & b-sv+ip, clusters around 5 to 13 % porosity and above 10 and below 100 mD permeability.
Rock-fabric types with additional touching-vug porosity scatter very widely as expected, caused by their non-fabric selective nature.

Thus the petrophysical rock-fabric type approach of LUCIA (1995) allows to illustrate the controlling factors of poro-perm properties, namely pore-type and rock-fabric and to relate distinct poro-perm fields to specific lithofacies types.

3.5.3 Porosity-permeability relationship

According to LUCIA (1999), permeability is determined by the pore size distribution controlled by:

1. The rock-fabric, classified after the modified DUNHAM texture classification.
2. The pore-type (see pore-type classes in chapter 3.5.1).
3. Volume of pore space (in case of additional interparticle- and touching-vug porosity).
4. Particle size and sorting (in case of interparticle porosity only).
5. Diagenetic processes.
6. Alignment and form of components influencing vertical permeability.

In the following some of these properties, like DUNHAM texture (Fig. 14), grainsize (Fig. 15) and sorting (Fig. 16) are plotted in relation to porosity-permeability. All crossplots do not

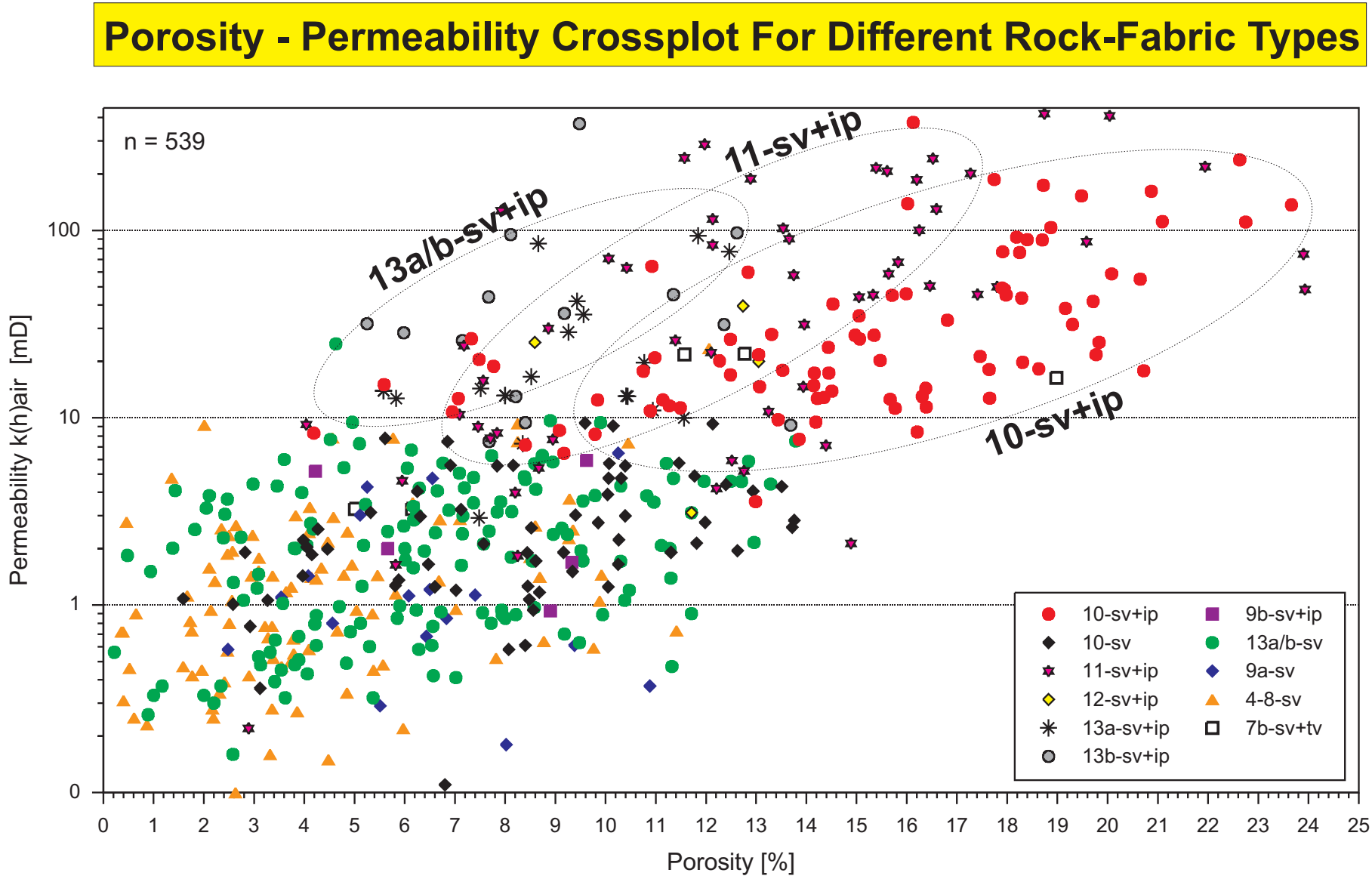

Fig. 13: The evaluation of different rock-fabric types (LUCIA, 1995) allows a pragmatic means for evaluating reservoir quality. Specific rock-fabric types relate to distinct poro-perm fields reflecting their respective reservoir potential.

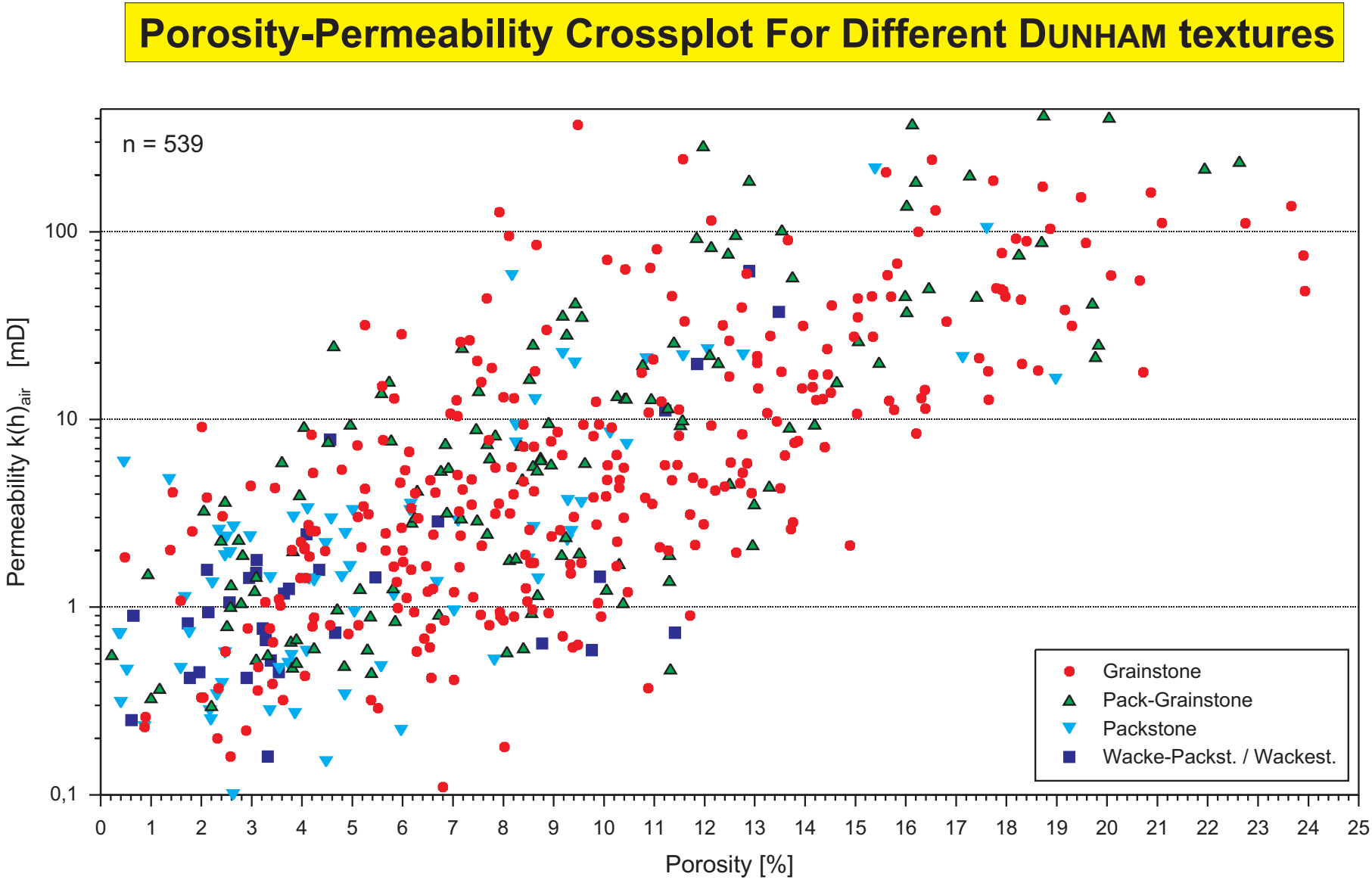

Fig. 14: DUNHAM texture in relation to porosity & permeability: No distinct poro-perm trends were observed.

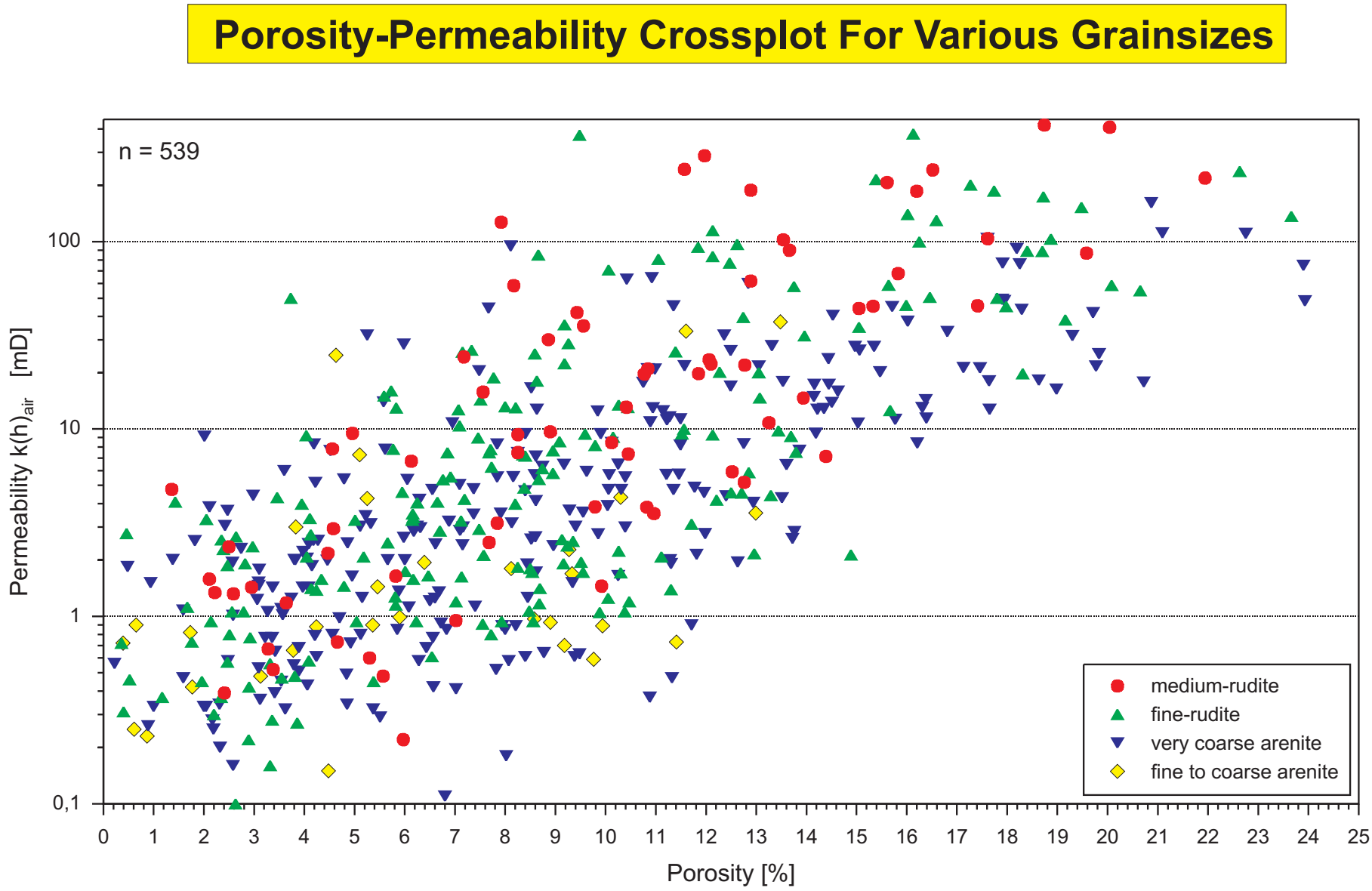

Fig. 15: Grainsize in relation to porosity & permeability: No distinct poro-perm trends were observed.

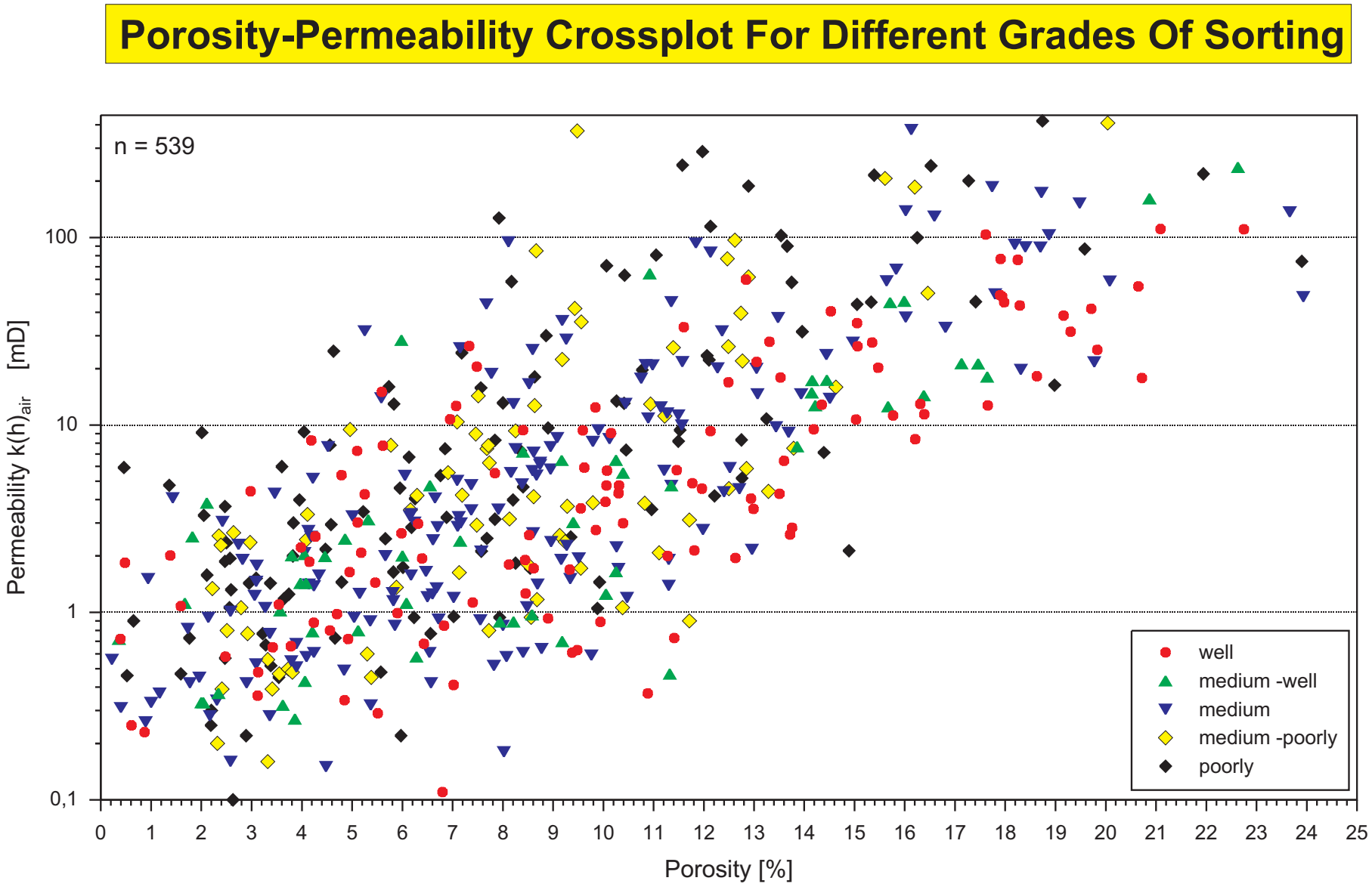

Fig. 16: Grade of sorting in relation to porosity & permeability: No distinct poro-perm trends were observed.

show distinct poro-perm trends. Previous studies by RUF (2001) and KOSTIC (2001) additionally presented poro-perm crossplots in relation to combined rock-fabric type and grainsize or sorting, but were also not able to further differentiate the data clouds.

This is apparently caused by differential diagenesis. The diagenetic influence to the pore-size distribution and therefore permeability is illustrated by the oolite-dominated shoal lithofacies type 9a, a pure, well sorted oolite grainstone with only separate-vug porosity and low permeability (RFT: 9a-sv). The primary interparticle pore space was cemented largely by early diagenetic marine fringe cements. Later dissolution of aragonitic oolites caused prevailing oo-moldic porosity. Still existing rather small interparticle pore space was finally cemented by later diagenetic dog-tooth and blocky spar cements.

As described in chapter 3.4 all grain-dominated lithofacies types are subject to diagenetic cementation. In spite of diagenetic changes, rock-fabric and grain size plays an important role: It was observed that grain-dominated lithofacies types, reflecting not only high hydrodynamic conditions but above all rapid sedimentation, show better poro-perm properties with increasing grainsize. This is probably caused by (1) the absence of interparticle mud due to very high water energy and (2) the fast accumulation of skeletal grains favoring preservation of large interparticle pore space. In this case porosity was also reduced by subsequent diagenetic cementation, but due to the high primary pore volume much more interparticle- and therefore interconnected pore space was preserved.

The best examples for this are the shell hash lithofacies type (LFT 10), the poorly sorted bioclastic lithofacies-type (LFT 11) and the cross-bedded ooidal-skeletal lithofacies-type (LFT 13b). They represent the best reservoir units in this study.

In general the values of horizontal permeability k(h) are in the same order of magnitude as the vertical permeability k(v). However, vertical permeability is mostly lower than horizontal permeability caused by often horizontally aligned skeletal grains. The connection between vertical and horizontal permeability to component-type and size, alignment and lithofacies type is illustrated in Fig. 17.

Thus horizontal permeability increases with increasing amounts of elongated components and better horizontal alignment. Such lithofacies types, like LFT 13b form typical high-k-streaks.

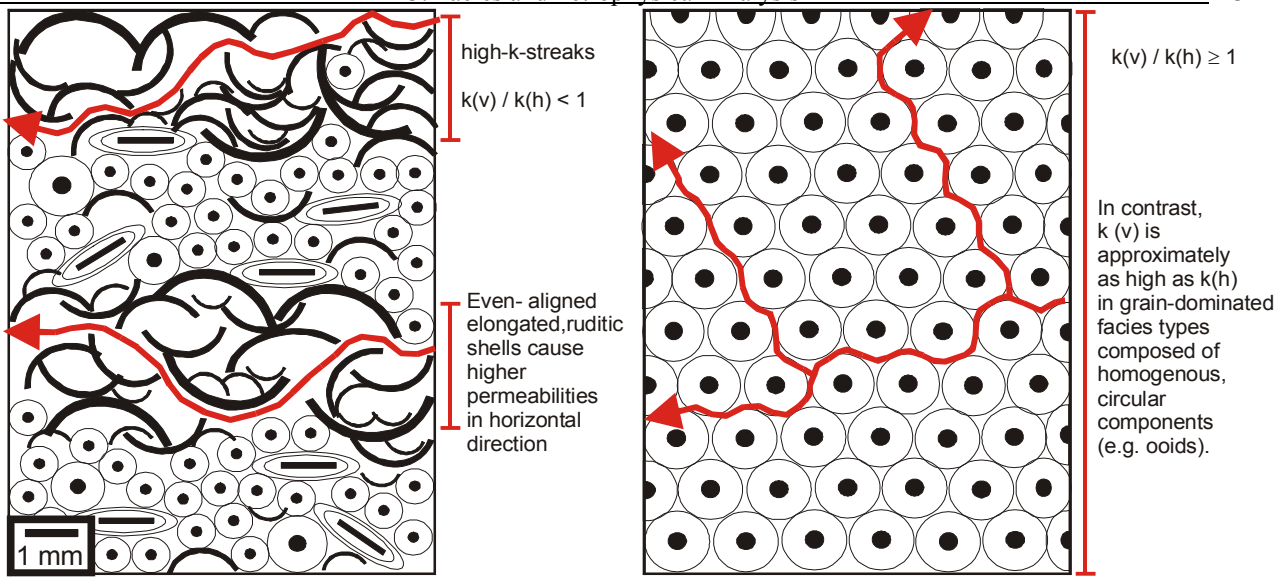

LFT 13b: "ooidal-skeletal pack-to grainstone"

LFT 9a: "cross-bedded oolitic grainstone"

Fig. 17: Illustrates the relationship between component-form, grainsize and alignment of particles to vertical and horizontal permeability.

Summary:

A) The following pore types were most important in this study:

1. separate-vug porosity (oo-and bio-moldic porosity)
2. separate-vug and interparticle porosity (moldic- and interparticle porosity)
3. separate-vug and touching-vug porosity (moldic- and fracture/ stylolitic porosity)

Fig. 11, shows a poro-perm crossplot keyed to these three pore-type classes, illustrating that reservoir quality is mainly controlled by the type of pores. The best reservoir properties are associated with separate-vug and interparticle pores.

B) Linking rock-fabric to pore-types resulted in rock-fabric types with distinct petrophysical properties (LUCIA, 1999). In poro-perm crossplot keyed to different rock-fabric types (Fig. 13), samples of grain-dominated fabric with separate-vug and interparticle pores cluster in particular fields reflecting their specific reservoir potential.

C) All grain-dominated lithofacies types in this study were subject to various diagenetic modifications, mainly decreasing their permeabilities.

D) In case of additional interparticle porosity, grainsize and form is an important factor (e.g. in LFT 9b, 10 and 11). The larger and more elongated the particles are, the better preserved is their interparticle pore space increasing reservoir properties.

E) Even-aligned, elongated skeletal grains cause highly permeable horizontal units (high-k-streaks), while vertical permeability is lower k(v) / k(h) < 1. This is restricted to episodic storm-generated, grain-dominated lithofacies. Generally k(h) and k(v) are in the same order of magnitude.

4. 1-D High-resolution sequence stratigraphy

4.1 Fundamental transgressive / regressive cycles

Meter-scale cycles are ubiquitous and can be recognized immediately at an initial inspection of quarry walls and lithofacies logs in the Upper Muschelkalk. They are therefore called fundamental cycles.

The cycle interpretation is based on the lithofacies succession. Each meter-scale fundamental cycle consists of a regressive and a transgressive hemi-cycle separated by turn-around points which represent the maximum trans- and regression. The total cycle thickness ranges from 0.7 m to 3.55 m. The average thickness is about 2 m.
Turn-around points are used as markers for stratigraphic correlation.
Three types of fundamental cycles were identified. The first two cycle-types only occur within the analyzed shoal- and shoal transition setting while the third cycle-type appears in the adjacent offshoal parts (except in backshoal areas). Due to their lithofacies composition they are subdivided in:
1. Oolite-dominated cycles
2. Shell-dominated cycles, and
3. Bioclastic-debris-dominated cycles.

4.1.1 Oolite-dominated fundamental cycle (Fig. 18)

a) Regressive hemi-cycle
Description:
The basal part of this cycle-type consists of dark grey lime mudstones with marly partings (LFT 1a or 2a), followed by brighter-colored wackestones. These bioturbated wackestones are typically poorly sorted and composed of fine-grained skeletal debris, peloids, filaments and larger bioclasts (LFT 4). Skeletal (oolitic-) packstones form the middle cycle part. The degree of sorting and the abundance of micritic envelopes around shells increases, while intercalated mud- and marlstone beds decrease (upward succession of LFT 8, 7b and 6).

a) In the upper pack-grainstone (LFT 13b) and grainstone part „crushing“ of components by increasing wave-action can be observed. Also an increase in coating of particles, from abundant micritic envelopes around shells to lenticular coated grains and finally ooids was recognized in cycles.

Fundamental Transgressive / Regressive Cycles

Fundamental Cycle Type 1

Oolite - dominated cycle

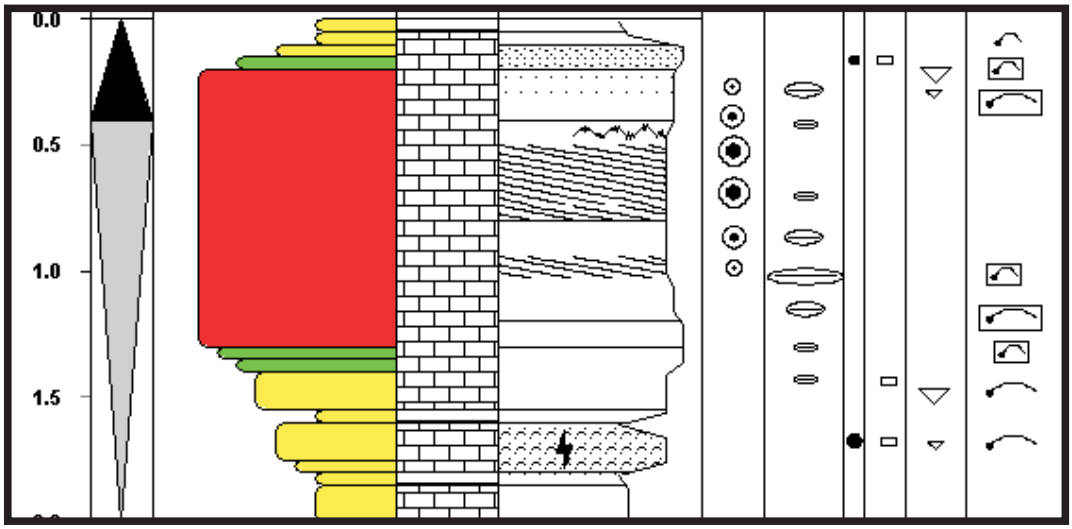

Fig. 18: This log represents an “idealized-succession” of an oolite-dominated cycle. This cycle type is described in detail in chapter 4.

Fundamental Cycle Type 2

Shell - dominated cycle

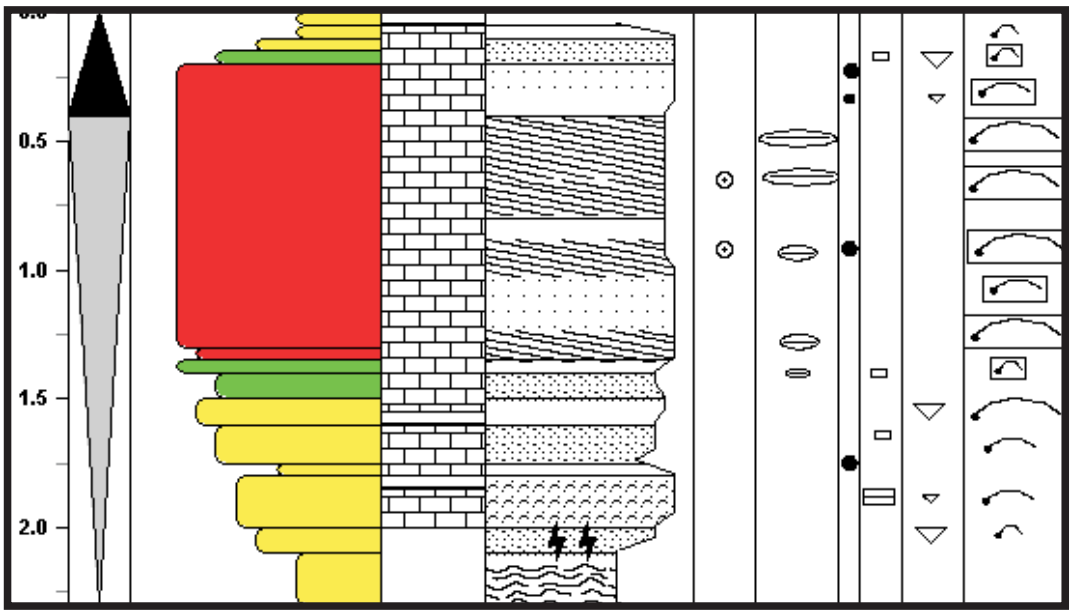

Fig. 19: This log represents an “idealized-succession” of an shell-dominated cycle. This cycle type is described in detail in chapter 4.

combination with an increasing level of sorting. These oolitic grainstone beds (LFT 9a) are usually thicker than 0.5 m, cross-bedded and occur in light grey to beige colors.

Interpretation:

The upward increase in bioclasts and ooids is interpreted as an increase in paleo-water energy and therefore as shallowing-up trend. This lithofacies succession reflects the oolite-dominated, central part of a carbonate sandbody.

b) Transgressive hemi-cycle

Description:

The upper part of the oolite grainstone is characterized by a decreasing level of sorting combined with a decrease in the abundance of ooids and micritic envelopes around shells. Thin bedded pack- and / or wackestones and finally marlstones commonly overlie the oolite grainstone. The grain spectrum ranges from coated grains, shells and scattered ooids (LFT 6) in the lower part of the hemi-cycle, to mixed bio- and intraclasts (LFT 7b) and finally shell debris (LFT 8, 4) and lime muds (LFT 1a/b) in the upper part of the hemi-cycle.

Interpretation:

This succession indicates a decrease in energy and is interpreted as deepening-up of the paleo-environment and therefore as a transgressive hemi-cycle. The point of highest clay content and smallest grain-size was presumed to be the maximum flooding-surface and is used for stratigraphic correlation.

4.1.2 Shell-dominated fundamental cycle (Fig. 19)

a) Regressive hemi-cycle

Description:

Within this cycle an upward change from a mudstone basis (mostly LFT 2a) to a variable succession of shelly arenitic to ruditic wacke- and packstones, with a high proportion of skeletal debris can be observed (LFT succession 4, 7a, 8, 7b). This is combined with an increasing proportion of micritic envelopes and a better sorting. A thick (1-2 m) grainstone bed composed of well sorted, shelly rudites, commonly cross-bedded (LFT 10, 13b), forms the top of the hemi-cycle. The shells are very commonly fragmented and preserved as „shell hash“ with abundant micritic envelopes and coated grains. This sequence is the most frequent cycle type observed within the studied logs. Paleogeographically it occurs on both sides of the oolite-dominated-cycle belt.

Interpretation:

This vertical succession is generally similar in its composition and trends (thickening-upwards of beds, increasing level of sorting and paleo-water energy etc.) as the oolite-dominated cycle. It is thus interpreted as a shallowing-upward succession. The lowermost mud- and marlstones representing deeper ramp conditions and the overlain wacke-pack- and grainstones are interpreted as proximal tempestites, channels and spillover lobes (event-sheets), depending on composition, grading and sorting.

b) Transgressive hemi-cycle

In the upper part of the shell grainstone the level of sorting as well as the abundance of micritic envelopes around shells decreases upwards. Sometimes, a change to thin pack- and / or wackestones (LFT 7b, 8, 4) and finally mudstones (LFT 1a/b) can be observed with the same characteristics as described in the oolite-dominated cycle.
This renewed decrease in water-energy indicates deepening of the ramp, i.e. a transgression.

Conclusion:

In both above described high-energy cycles the following characteristics document shallowing-up trends:

- Thickening-up of limestone beds
- Increasing level of sorting
- Increasing proportion of micritic envelopes around components
- Decreasing lime-mud and clay content
- Brighter colors of rocks
- Cleaning-up trend of carbonates
- Increasing number of ooids (oolite-dominated fundamental cycle) or shell hash (shell-dominated fundamental cycle).

The opposite is valid for deeping-up trends.

Note ! : The described cycle-types do not always occur in an „ideal“ succession.

4.1.3 Bioclastic-debris-dominated cycle (Fig. 20)

This cycle type occurs in a larger variability than all other cycle types depending on the position seawards (proximal to distal foreshoal) or landwards (proximal to distal backshoal) to the shoal. In general the following characteristics can be observed:

a) Regressive hemi-cycle

Description:

Thick dark-colored mudstones (LFT 1a), marlstones or alternations of both form the cycle basis. Interbedded mudstone layers decrease upward, also in thickness. The predominating wackestones (LFT 3 or 4) show intensive bioturbation and are poorly sorted. Main components are peloids and skeletal debris (LFT 4, foreshoal), as well as bivalve and brachiopod shells, or oncolites (LFT 3, backshoal).

Wacke-packstones (LFT 7a, 8) increase upwards in abundance and become better sorted and often graded. These are composed of shells, filaments, skeletal debris and micritic intraclast, especially on basal erosional surfaces of small channels and gutters.

The uppermost cycle-part is formed by pack- and pack-grainstones consisting of commonly bored or encrusted components as large shells, coated grains and scattered ooids (LFT 6, 13a) together with minor large brachiopods and / or intraclasts. These grain-dominated lithofacies occur in backshoal areas, in contrast to foreshoal zones mainly being composed of bored shells with thick micritic envelopes, oncolites (LFT 5a, 12) or black pebbles (LFT 5b).

Generally a coarsening-up trend of components can be observed.

Interpretation:

While thick mud- and marlstone beds on cycle basis reflect offshore deep ramp conditions, peloidal, debris-dominated wackestones were regarded as transitional deposits between shallow and deeper ramp and / or lagoonal setting.

Graded intra- and bioclastic wacke-packstones especially with channel-like geometries were interpreted as storm-induced flows (distal tempestites or backshoal spillover lobes). Pack- and pack-grainstones are interpreted as storm layers (proximal tempestites or backshoal oncolite channels) in shallow water areas.

Predominantly dark limestones, abundant black components and continuously strong bioturbation throughout the whole succession, are typical for the quiet, lower energetic backshoal-zone or (restricted?) lagoon. The described sequence represents a shallowing-upward trend and the regressive part of the cycle.

b) Transgressive hemi-cycle

The skeletal pack-grainstones are followed by mud-dominated lithofacies types (LFT 1 and 2) with decreasing bed thickness. The percentage of skeletal debris decreases again.

This cycle part expresses generally a decrease in water-energy and can be interpreted as renewed deepening.

Fundamental Transgressive / Regressive Cycles

Fundamental Cycle Type 3

Bioclastic - debris - dominated cycle

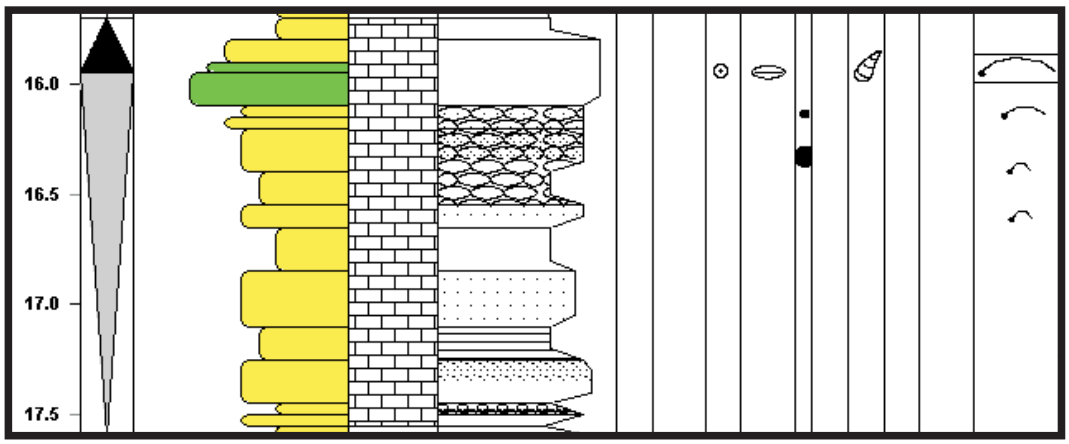

Fig. 20: Example of an bioclastic-debris-dominated cycle of quarry “Haltenmühle” (Q 6). For explanation see chapter 4.

4.2 Cycle Hierarchy (Fig. 21 & logs in Appendix)

In the studied part of the Upper Muschelkalk the above described fundamental transgressive-regressive cycles are arranged in larger-scale transgressive / regressive trends.
This cycle hierarchy probably corresponds to the 4th and 5th order cycles after the terminology of VAIL (1987) and GOLDHAMMER ET AL. (1991).
The first six fundamental cycles of the studied succession show a larger-scale regression. This trend is represented by a characteristic upward increase of pack- and grainstones and therefore an increase in reservoir facies, reflected clearly by decreasing gamma-ray values (see Fig. 21).
Cycles 7 and 8 reflect a larger-scale transgression. This trend can be recognized by increasing mud-dominated lithofacies types, higher gamma-ray values together with decreasing bed thicknesses. Thus reservoir potential decreases in the course of the larger-scale transgression (see Fig. 21).

4.3 Cycle stacking pattern and cycle symmetries (Fig. 21)

Nearly all fundamental cycles show various degrees of asymmetry (see Fig. 21 & logs in Appendix).

a) The larger-scale regressive hemi-cycle is formed by the first six fundamental cycles (cycles 1 to 6). In these, the regressive hemi-cycle parts predominate with only thin transgressive caps.
b) The larger-scale transgressive hemi-cycle is formed by fundamental cycles 7 and 8. In these, the transgression proportions are generally thicker leading to more symmetrical cycles.

Cycle stacking pattern and cycle symmetries

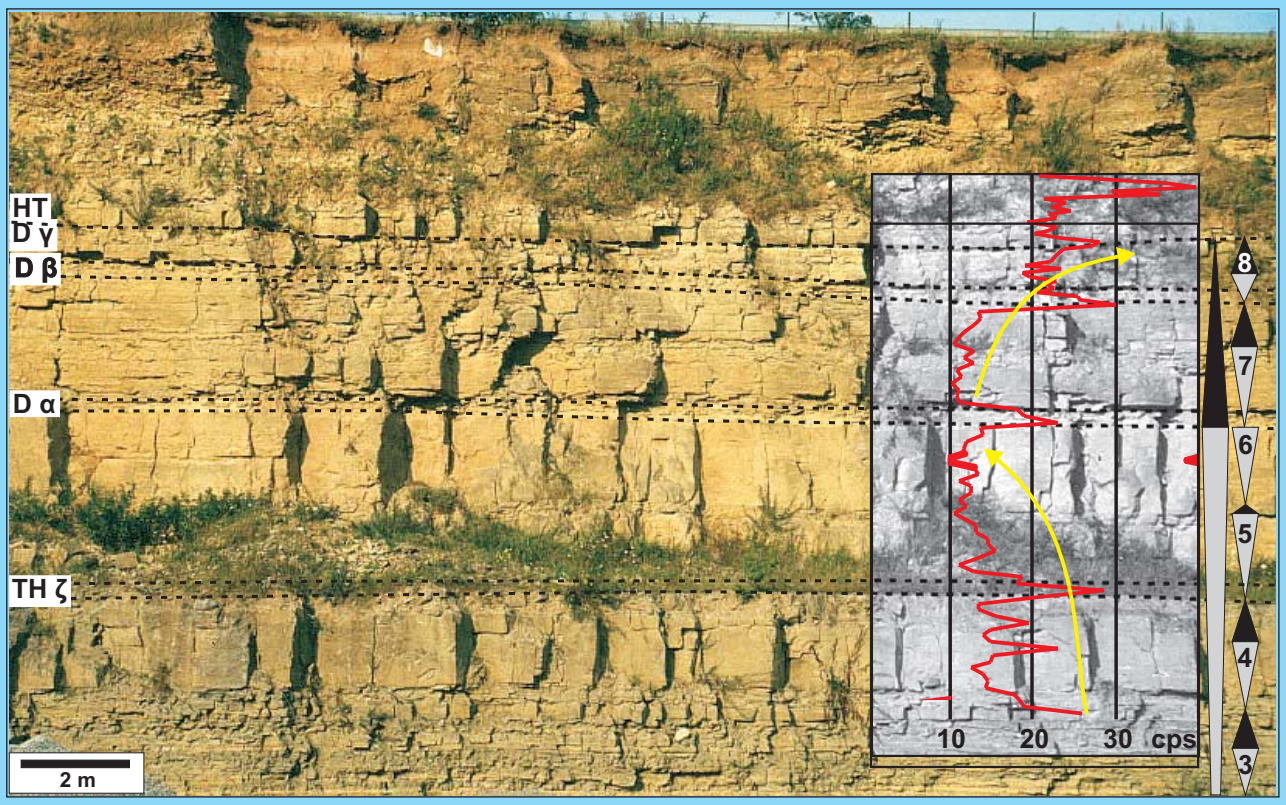

Fig. 21: The outcrop photo of quarry Sommerhausen illustrates the arrangement of small-scale fundamental cycles to larger-scale transgressive / regressive cycles.

Stacking pattern:
Fundamental cycles 3 to 6 stack to a larger-scale regression. This trend is represented by a characteristic upward increase in bed thickness and grainstones (= increase in potential reservoir facies), reflected by decreasing gamma-ray values (see lower yellow arrow).

Fundamental cycles 7 & 8 reflect a larger-scale transgression. This trend is indicated by decreasing bed thicknesses together with an increase in mud-dominated lithofacies types (= decrease in potential reservoir facies) and increasing gamma-ray values (see upper yellow arrow).

Marlstone marker beds (marked by stippled lines) can be recognized easily in the GR-log by wider peaks above 20 cps.

Cycle symmetries:
The systematic change in transgressive / regressive ratios of the fundamental cycles visualized by various degrees of cycle asymmetries additionally illustrate the overall transgressive / regressive trends.

The increasing asymmetry from fundamental cycle 3 to 6 by increasing regressive hemi-cycle parts indicates the larger-scale regressive trend.

The increasing transgressive proportions, leading to more symmetrical fundamental cycles 7 and 8, indicates the larger-scale transgressive trend.

5. 2-D Sequence Stratigraphic Correlation

21 stratigraphic logs (1-D) were correlated and are compiled into stratigraphic cross section panels (Fig. 22 to 26).

Discussion of datum selection

The datum should fulfill two criteria, as discussed in KERANS and TINKER (1997):

1. Easily traceable, prominent and therefore easy to correlate.
2. The datum should correspond to an approximately near horizontal original time-surface without much influence of local paleotopography.

The Upper Muschelkalk-Lower Keuper boundary is marked by the so-called „Grenzbonebed“, consisting of vertebrate relicts, phosphate pebbles, coprolites, skeletal fragments and sometimes glauconite minerals and is easy to recognize in the field. This bed can be traced over long distances in the whole study area in nearly all quarries, and has long been used as a lithostratigraphic marker bed.
Therefore the „Grenzbonebed“ was used as datum according to the first criterion.
The ramp topography of the uppermost Muschelkalk was nearly leveled out towards the beginning of the Lower Keuper, leading to an epeiric platform with a negligible morphologic gradient (0.2-0.002°) (PÖPPELREITER, 1999).
Thus the Upper Muschelkalk-Lower Keuper boundary also fulfils the second criterion of an excellent datum - a nearly horizontal time-surface.

Cross section orientation

The cross-section orientation is shown in Fig. 6. Cross section 1 runs approximately parallel, all other sections more or less perpendicular to the paleoslope of the carbonate ramp.
The 1-D logs were transferred in scaled distances onto the correlation panel (scale 1: 50.000). This method ensures the representation of the actual dip of the original depositional topography and facilitates the reconstruction of sedimentary geometries.

Analysis of correlation results

Every fundamental cycle was analyzed separately, in terms of:

a) Lateral and vertical changes of lithofacies. b) The dip of the cycle boundaries. c) Lateral variations in thickness.

Stratigraphic geometries became apparent when plotting the 2-D cycle thicknesses, reflecting the paleotopography of the depositional environment.

Main emphasis was put on cycles 1-6, forming one large-scale regression.

Cross Section 1 (Fig. 22)

Orientation S-N, Quarries: Weckelweiler (Q 1), Brettenfeld (Q 2), Schmalfelden (Q 4), Buch (Q 13), Aub (Q 14), Sommerhausen (Q 17), Goßmannsdorf (Q 16), Winterhausen (Q 18).

Main results:

- **Evolution and movement of shoal geobodies**
  This cross section documents the initial evolution of shoal geobodies at the start of a large-scale regression. During fundamental cycle 1, the shoal steps northwards (seawards), from the most southern position at Q 1 to Q 2 and Q 4 (fundamental cycle 2), increasing systematically in size and thickness. After a period of almost no shoal development (except in Q 17) during cycle 3 and 4, shoals increase in size and thickness during cycle 5 and further step seawards. Their maximum extension and most seaward positions are reached during cycle 6. This trend reflects a large-scale regression.
  The preferred shoal accumulation at locations Q 13 & 14 and Q 16 & 17 appears to be related to two separate paleotectonic highs.
  During cycles 7 and 8 an obvious decrease in shoal extensions and a trend towards solitary, backstepping carbonate sandbodies in southern (landward) direction can be observed.
  This trend reflects a large-scale transgression.
  The renewed seaward occurrence of shoals in Q 16 & 18 during cycle 11 reflects a renewed overall regressive trend.
- **Observed lateral facies succession and reservoir prediction**
  The observed seaward stepping and increase in shoal dimension during fundamental cycles 1 & 2 is also combined with an increase in reservoir quality. While in Q 1 low permeable oolite grainstones occur (LFT 9a), the shoals in Q 2 consists of mixed ooidal-skeletal- (LFT 13b) and in Q 4 of highly permeable shell hash grainstone (LFT 10).
  From fundamental cycle 5 to 6 a seaward stepping of the thickest shell hash grainstone units and thus highest reservoir volume, was observed (from Q 13 to Q 14 and Q 17 to Q 16).

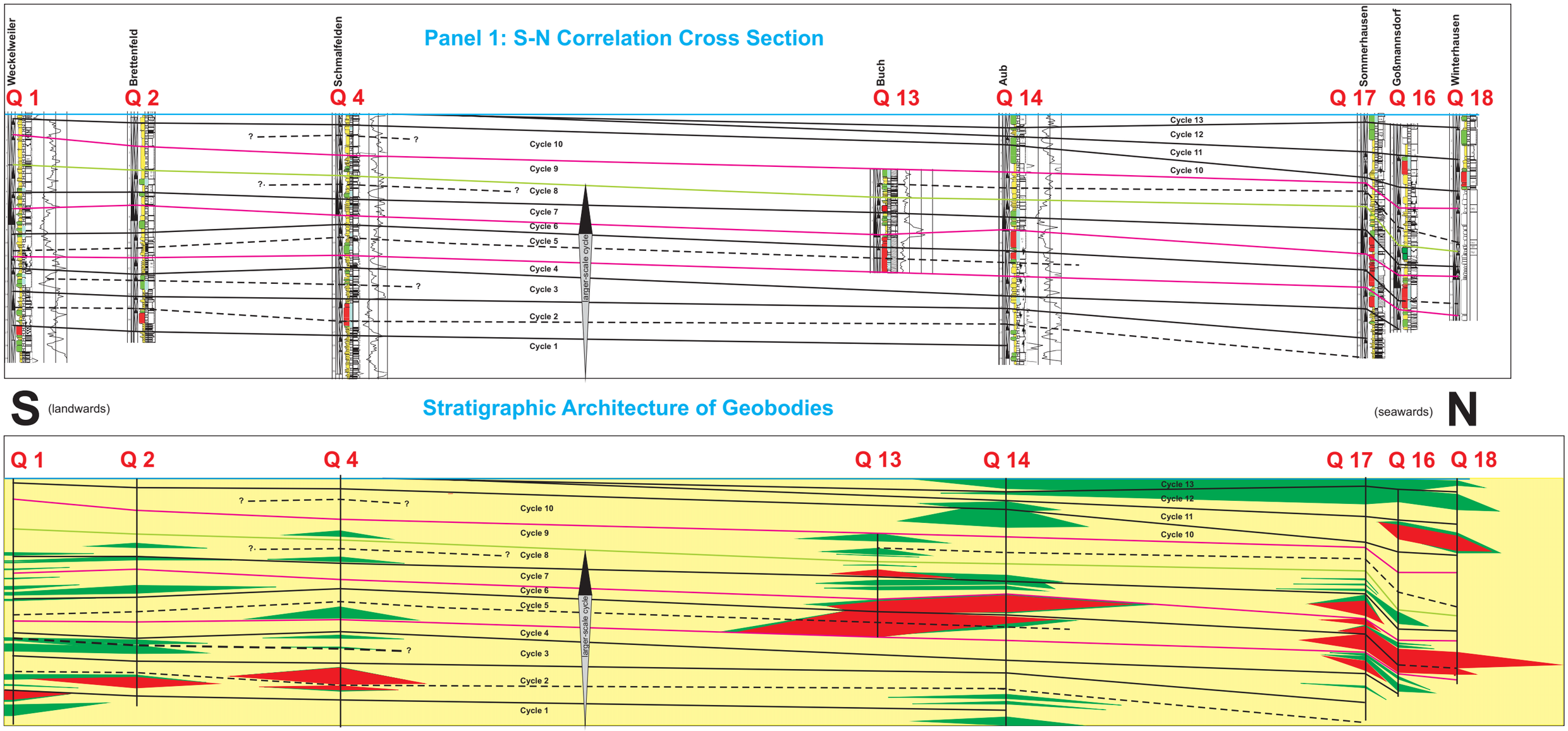

Fig. 22: Correlation cross-section 1 & stratigraphic architecture of geobodies.
Note seaward stepping of shoal reservoir bodies and the increase in shoal facies (red) towards the peak regression of the larger-scale cycle.

The isolated, small-scale shoal in Q 17 consists of shell hash grainstone (cycle 7). During cycles 7 and 8 shoal proportions apparently decrease, reflecting a large-scale transgression, however the poro-perm properties are constantly good (shell hash grainstone in Q 17 and ooidal-skeletal grainstones in Q 16).

During the renewed regression in cycles 11, the shoal consists of shell hash (LFT 10) to medium sorted ooidal-skeletal grainstones (LFT 13b).

Cross Section 2 (Fig. 23)

Orientation W-E, Quarries: Schmalfelden (Q 4), Gammesfeld (Q 3), Bettenfeld (Q 5), Haltenmühle (Q 6)

Main Results:

- **Evolution and movement of shoal geobodies**

  Notice: The abrupt wedge-out of geobodies in this cross section (i.e. in cycle 5) are often due to the orientation of the section, oblique to strike.

  The first shoal geobody appears in cycle 2 in the southern part of the study area. This reservoir unit pinches out towards the east (landwards). A slight backstepping of the shoal may occur in cycle 3 , while in cycle 4 no shoal facies was observed. This shifting may be interpreted as small-scale, possibly local transgressive pulse within the large-scale regression. In cycle 5 a shoal geobody was established once again in Q 3.

  Slightly prograding shoal bodies amalgamate to the thickest shoal in cycle 6.

  The apparent retrogradation of shoals in landward direction (Q 6) and formation of small-scale solitary shoals illustrates the large-scale transgressive trend during cycle 7 and 8.

  The preferred shoal evolution on Q 3 and Q 5 can be explained by the local paleotectonic high situation of both locations (well known from the literature as „Gammesfeld high“, i.e. WAGNER, 1913) leading to preferred shoal accumulation compared to the surrounded locations (Q 4 and Q 6).

- **Observed vertical and lateral facies changes and reservoir prediction**

  Within the large-scale regression (fundamental cycles 1-6), the best reservoir facies is developed in cycles 2, 5 and 6. In fundamental cycle 2, the shoal body consists of well sorted shell hash (LFT 10), intercalated by ruditic, poorly sorted, bioclastic grainstone sheets (LFT 11). The carbonate sandbodies in cycles 5 and 6 show a similar vertical facies succession at the beginning, starting with shellhash (LFT 10) or ruditic, bioclastic grainstones (LFT 11) in

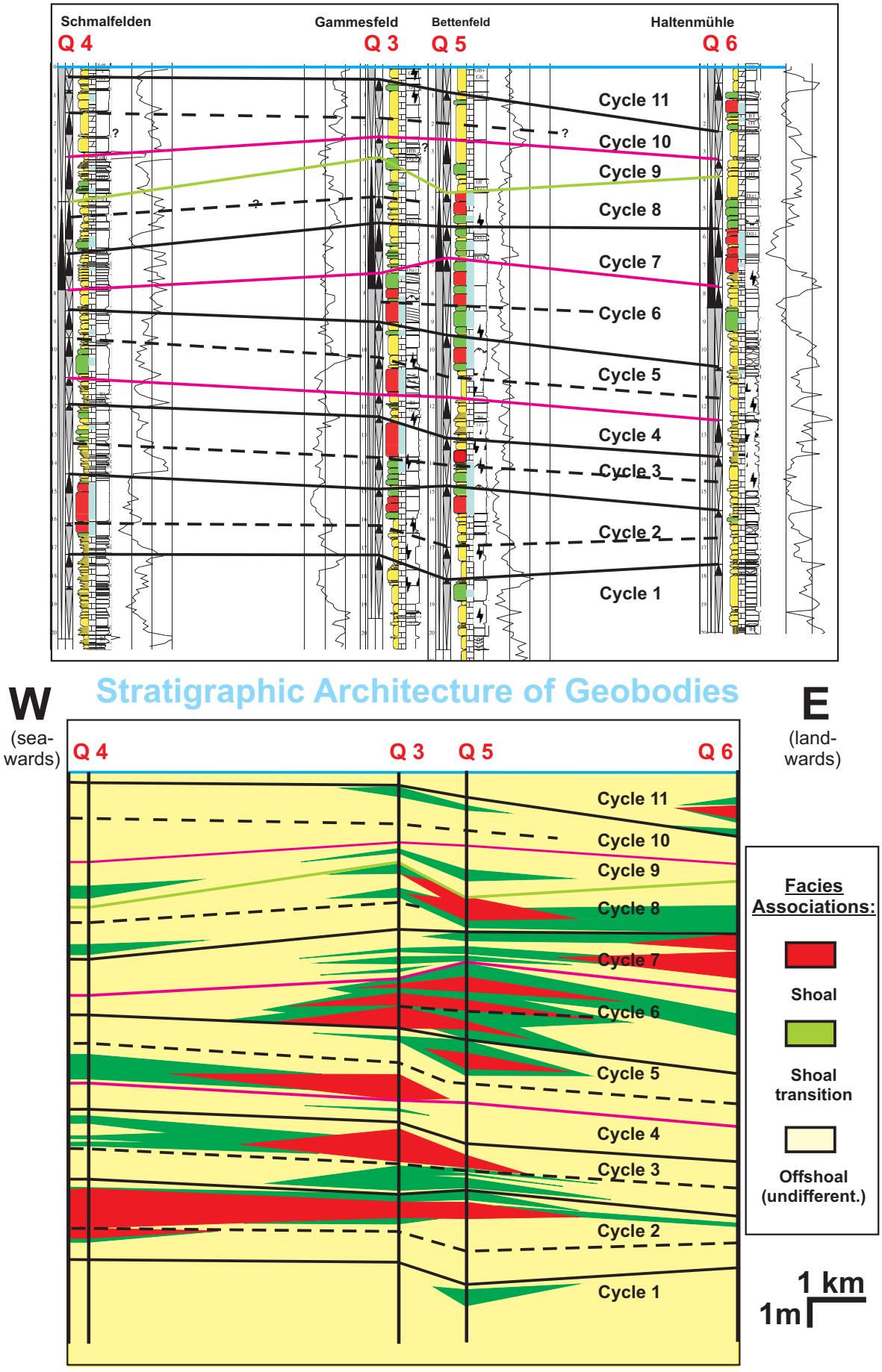

Fig. 23: Correlation cross section 2 & stratigraphic architecture of geobodies. The preferred shoal evolution on Q 3 & 5 can be explained by the local paleohigh situation of both locations (”Gammesfeld high”).

the lower part of the geobodies, but are succeeded by mixed ooidal-skeletal- (LFT 13b) and / or oolitic grainstones (LFT 9a) in the upper part.

In contrast the shoal body during cycle 3 exclusively consists of ooidal-skeletal grainstones (LFT 13b), succeeded by pure oolitic grainstones (LFT 9a).

Cross Section 3 (Fig. 24)

Orientation W-E, Quarries: Dürrenhof (Q 7), Gattenhofen (Q 8), Haltenmühle (Q 6).

Main Results

- **Evolution and movement of shoal geobodies**

  Shoals did not develop in this area during the large-scale regression (cycles 1 – 6). The first shoal geobodies appear in this section in cycle 7 and 8. The apparent backstepping of the shoal from cycle 7 to 8 reflects the large-scale transgressive trend.

  Small-scale solitary shoals appear again in cycles 11 and 12. This represents the beginning of a renewed large-scale regression.

- **Observed lateral facies succession and reservoir prediction**

  In cycle 6 a widespread facies belt consists of homogenous, sometimes laminated or low angle cross-bedded calcarenitic, well sorted pack- to grainstones (LFT 9b). These massive bars occur in this landward location in a 2 to 3 km distance to the seaward shoal bodies. They are interpreted as wave-induced beach deposits. Their reservoir properties are rather low.

  The lateral facies succession in cycle 7 shows cross-bedded, well to medium sorted shell hash grainstones (LFT 10), which pass further landwards to ruditic, poorly sorted bioclastic pack- to grainstone sheets (LFT 11). Both facies types form excellent reservoirs. The reservoir potential decreases further landwards where well sorted, pure calcarenites of the 9b LFT-type predominate. The shoal, mainly consisting of shell hash with good reservoir potential, retrogrades in cycle 8 to the most landward position observed in the study area.

Panel 3: Southern landward W-E Correlation Cross Section

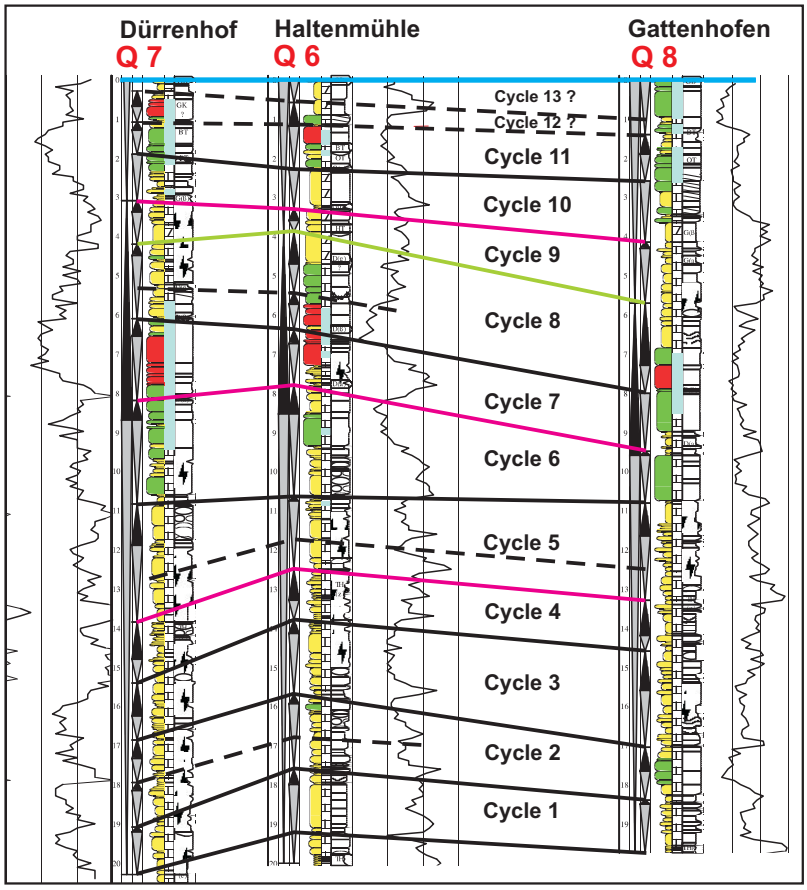

Stratigraphic Architecture of Geobodies

W (sea-wards)

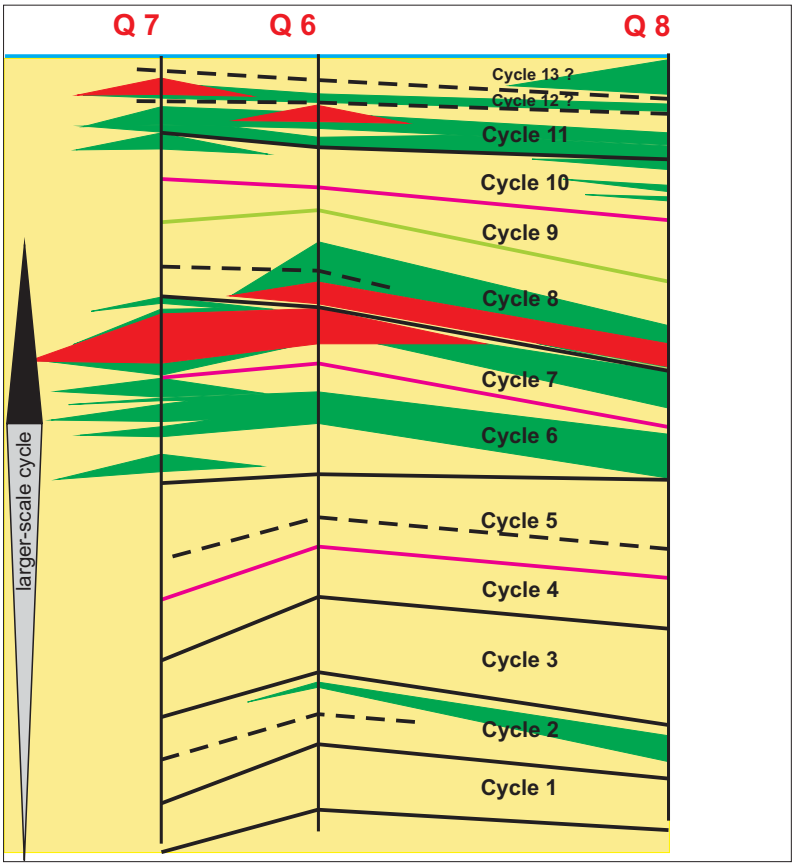

E (land-wards)

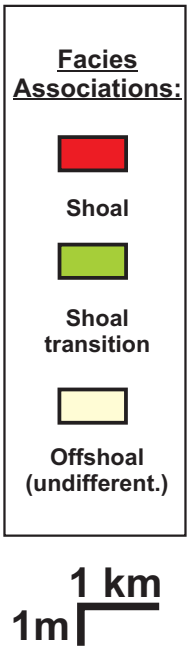

Fig. 24: Correlation cross section 3 & stratigraphic architecture of geobodies. Note the apparent backstepping of the shoal from cycle 7 to 8 to its most landward position in the study area. This reflects the large-scale transgressive trend.

Cross Section 4 (Fig. 25 & Appendix Tables A & B)

This cross section illustrates very well shoal body evolution, lateral and vertical facies distribution and movement of shoals in relation to large-scale regressive and transgressive trends and their relationship to reservoir potential. For this reason the results of a detailed evaluation of facies and reservoir characteristics for all fundamental cycles is listed in Tables A and B in the Appendix.

Orientation WNW-ESE, Quarries & Cores: Oesfeld (C 1), Bernsfelden (Q 9), Stalldorf (Q 10), Lenzenbrunn (Q 11), Röttingen (C 2), Buch (Q 13), Frauental (Q 12), Gattenhofen (Q 8).

Main Results:

- **Evolution and movement of shoal geobodies**
  Initial shoal geobodies appear in cycle 4. They extend and step seawards combined with an enormous increase in thickness during cycle 5. In cycle 6 the shoal body reaches its maximum extension and most seaward position.
  Stacked fundamental cycles 1 – 6 represent the larger-scale regressive cycle.
  In cycle 7 no shoals developed and also during cycle 8 just small-scaled carbonate sand bodies form solitary bodies (Q 9) in a landward position. This trend reflects a renewed large-scale transgression.
  A renewed large-scale regression explains the existence of larger shoals in the most seaward position observed in this study and reflects the overall shallowing-up and overall regressive trend respectively.
- **Observed lateral facies succession and reservoir prediction**
  The following lateral facies succession is preserved during cycles 5 and 10:
  Seaward cross-bedded, well sorted oolitic grainstones (LFT 9a) pass landwards to medium sorted ooidal-skeletal grainstones (LFT 13b) and are replaced by pure, well sorted shell hash (LFT 10), both commonly trough cross-bedded. In the most landward position ruditic, poorly sorted bioclastic grainstone sheets (LFT 11) were observed. This reflects a well developed lateral facies succession from the central oolite-dominated shoal (LFT 9a) to the fringing shell-dominated shoal (LFT 10) in landward direction. The apparent lateral lithofacies belts, as described above are not as distinct anymore during further regression (i.e. cycle 6). The extent of the mixed ooidal-skeletal facies belt is wider, while the pure oolitic- and shell hash grainstones are less wide spread. This reflects probably a shallowing and a smoother paleotopography.

Panel 4: Central NW-SE Correlation Cross Section

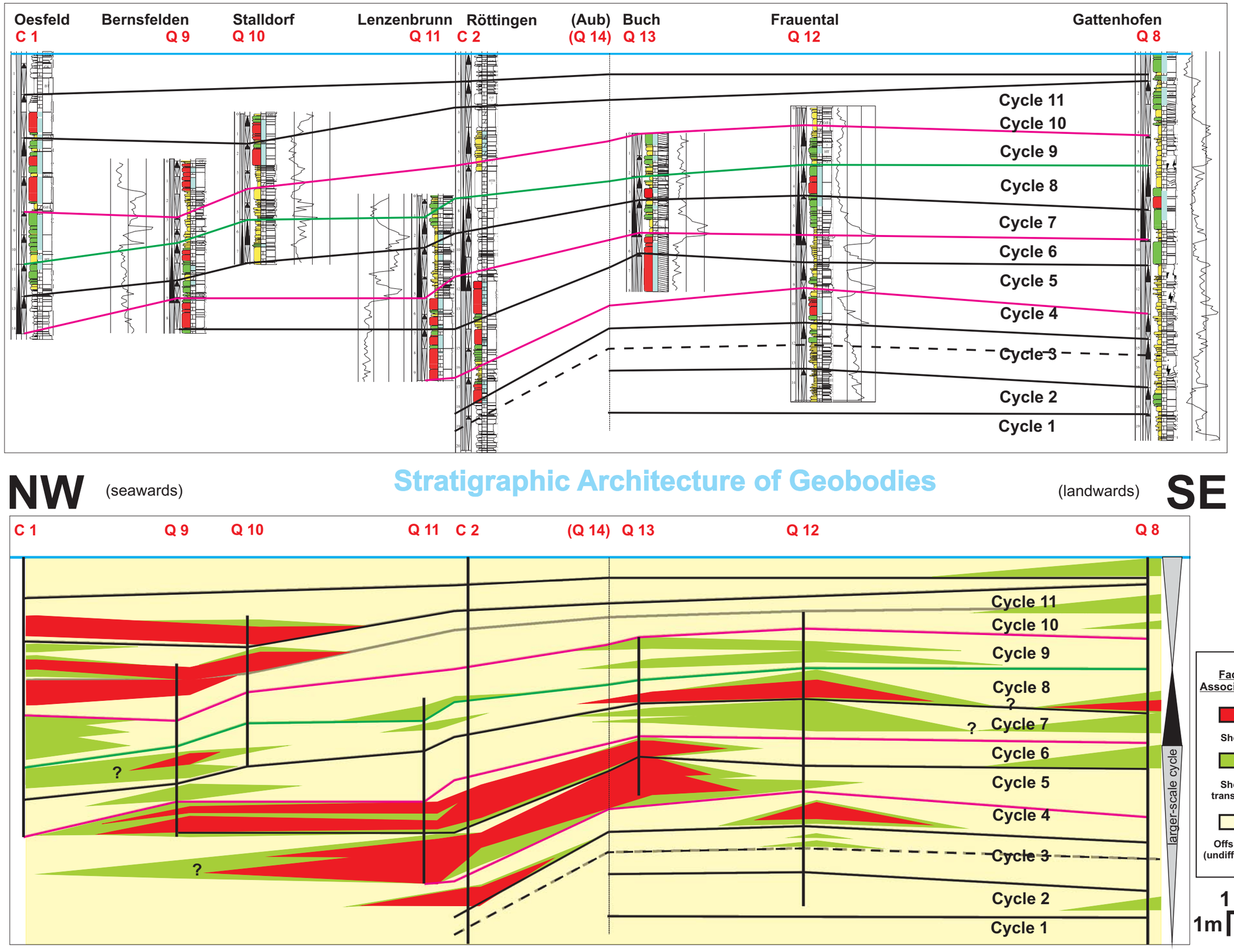

Fig. 25: Correlation cross section 4 & stratigraphic architecture of geobodies. The apparent seaward stepping of shoal bodies (red) and their increasing dimensions reflect the regressive trend of the larger-scale cycle (peak regression in fundamental cycle 6). Landward stepping plus decreasing shoal facies illustrates the overall transgressive trend.

An independed facies belt, restricted to near-coast position, is represented by laminated to low angle cross-bedded, well sorted, pure calcarenites (pack- to grainstones, LFT 9b). These massive bars represent possibly deposition of wave-induced beach deposits.
Behind the shoals commonly low energy sediments accumulated. Intense bioturbation, components like abundant peloids and black pebbles point to quiet conditions of lagoons and sheltered backshoal settings.

Cross Section 5 (Fig. 26)

Orientation WNW-ESE, Quarries: Kirchheim (Q 15), Winterhausen (Q 18), Goßmannsdorf (Q 16), Sommerhausen (Q 17), Frickenhausen (Q 19).

Main Results:

- **Evolution and movement of shoal geobodies**
  Initial shoals develop in cycle 4. In the succeeding cycle, the shoal increases in lateral extent and thickness, while in cycle 6 the maximum seaward step and thickness was observed. The stacking pattern of the fundamental cycles represents a larger-scale regressive trend.
  Backstepping of the carbonate sandbody in landward direction occurs in cycle 7, where only a solitary shoal with limited extent remains. This trend reflects the large-scale transgression.
  While in cycles 9 no shoals occur, a new shoal starts during cycle 10 in a landward position (Q 19) which steps further basinwards in cycle 11.
  This trend reflects a renewed large-scale regression.
  The unusual steep time lines between Q 17 and Q 16 as well as the relatively abrupt change in thickness and lateral facies distribution point to a regional paleotectonic high situation of Q 17 compared to the surrounding (Q 16, 18). The enormous shoal accumulation in Q 17 in comparison to the higher portion of low energetic carbonates in Q 16 within a short distance support this assumption.
- **Observed lateral facies succession and reservoir prediction**
  The shoal geobodies in fundamental cycles 4 to 8 and 10 & 11 are largely composed of cross-bedded, well sorted shell-hash grainstones (LFT 10). These shoals have excellent poro-perm properties. They only pass sometimes to mixed shell hash and well sorted oolitic grainstones (LFT 9a) in the shoal tops, what decreases their permeabilities.

Panel 5: Northern NW-SE Correlation Cross Section

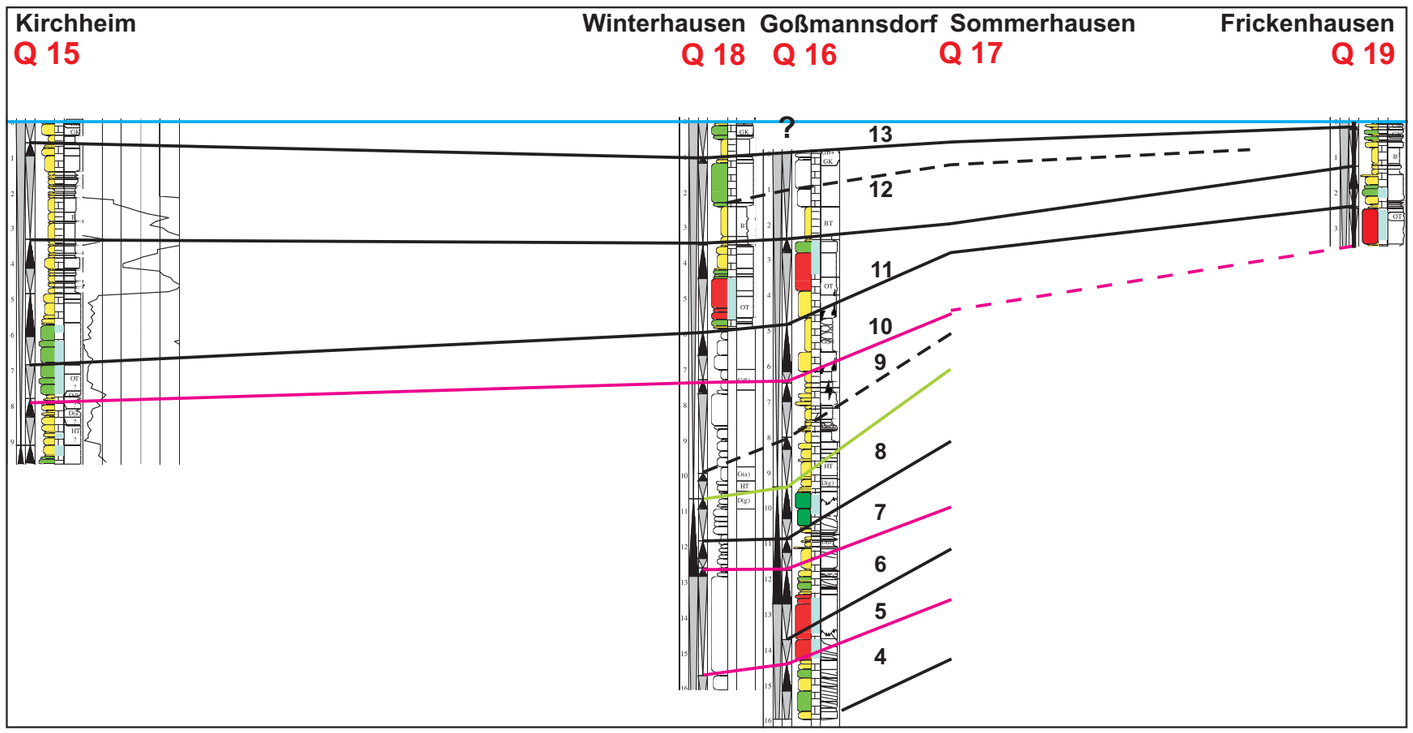

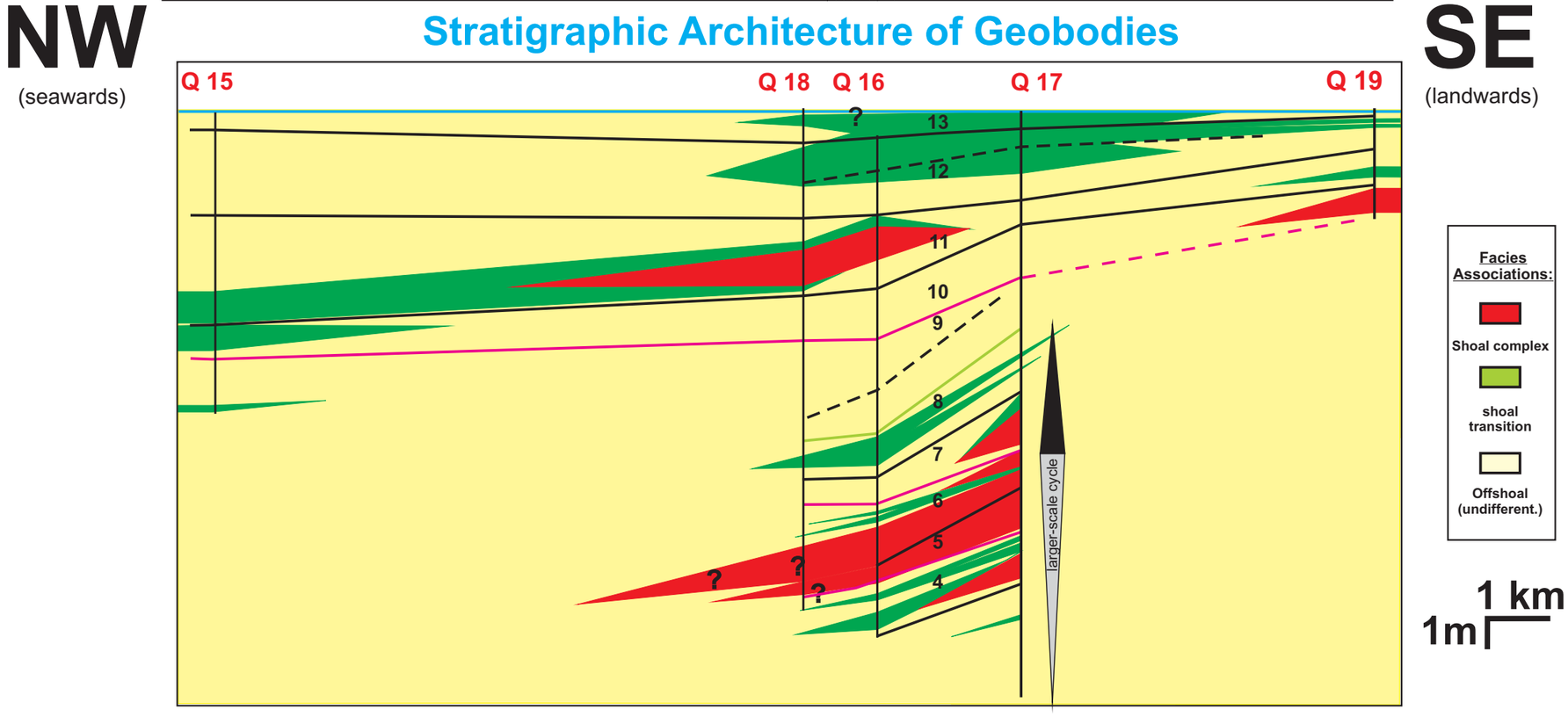

Fig. 26: Correlation cross section 5 & stratigraphic architecture of geobodies. Note seaward stepping of shoal reservoir bodies and increase in shoal facies towards the peak regression of the larger-scale cycle and landward stepping plus decrease in shoal facies during larger-scale transgression.

6. Mapping of Facies and Reservoir Properties

6.1 Mapping strategy

The following strategy was applied for generating all maps:

1.) For drawing isopach maps, areas between two data points were linearly interpolated by the following equation:

$$\text{Missing data} = \frac{\text{Distance between 2 datapoints}}{\text{Difference of data between 2 datapoints (\%,mD,m etc.)}} \text{ X Difference to next isoline (\%, mD, m etc.)}$$

2.) If a present data point is 0 or unknown, the distance between the data points is halved and treated as equivalent to 0. (Example: The distance between 2 data points is 6 km and one of them is 0 or unknown, then a new data point in 3 km distance is interpolated as 0 data point). **Notice**: In order to highlight the shoal geobodies, the data points with shoal facies thicknesses below 0,5 m and < 2,5 % porosity as well as < 5 mD permeability were not considered in the maps.

3.) Data points with a distance of more than 10 km without data control in between were not tied together.

4.) All isopach maps were drawn by hand to ensure that no isopach errors arise in areas with low data density or lack of data and to consider the exceptional cases described in points 2. and 3.

6.2 Facies maps

To illustrate the distribution and evolution of shoal geobodies through time, 4 fundamental cycles were chosen for mapping of facies and shoal thickness. Fundamental cycles 5 and 6 represent the uppermost regressive part of the large-scale hemi-cycle, while fundamental cycles 7 and 8 form the transgressive part. Furthermore, the selected time slices show the most pronounced variations concerning thickness and position of the shoal bodies.

6.2.1 Shoal lithofacies distribution per fundamental cycle (picked at peak regression of the fundamental cycles) (Fig. 27)

Fundamental differences can be observed in shoal facies distribution during larger-scale regression and transgression.
Firstly, the size of shoal bodies (red to orange colored) increases towards the large-scale peak regression (cycle 6) while the bodies are generally smaller during large-scale transgression.
Secondly, the central oolite-shoal facies (LFT 9a, red colored) is virtually absent during transgressive cycles 7 and 8. This implies that the reservoir volumes decrease during the overall transgressive cycle, but reservoir quality may increase caused by the lower proportion of low permeable oolite-central shoal facies towards overall transgression.
In addition, the lithofacies composition of shoal geobodies during large-scale regression (cycles 5 & 6) is more uniform than during transgression. The concentrically arranged shoal lithofacies types are oolitic grainstones, forming the shoal center (LFT 9a), fringed by shell-dominated shoal facies, i.e. shell hash- (LFT 10) and ooidal-skeletal grainstones (LFT 13b). In contrast, during the overall transgressive phase, shoal bodies are composed exclusively of shell-dominated shoal facies, while pure oolite grainstones rarely appear.

6.2.2 Cumulative thickness distribution of shoal facies per fundamental cycle (Fig. 28)

The following abbreviations are used in this text to quantify shoal dimensions:
l_{body} = length of shoal body [km], t_{max} = maximum shoal thickness [m], $t_{average}$ = average thickness of all shoal bodies [m] within a fundamental cycle.

The major shoal body in fundamental cycle 5 is located in the middle of the study area with a length of 10 km and a width of 6,8 km. Besides, the southern flank has relatively steep slopes, while the northern side descends much smoother. The maximum shoal thickness is reached in Q 11 with 2,25 m and Q 13 with 2 m.
A small patch-like shoal exist in the north, with approximately similar orientation (t_{max} = 1,05 m in Q 17, l_{body} = 5 km) and in southern direction, with SW-NE orientation (t_{max} = 0,8 m in Q 3, l_{body} = 2 km).

During fundamental cycle 6 the major shoal body increases enormously in dimension. The total lengths now amounts 17 to 18,5 km (E-W), the total width in N-S direction is 8 km. The shape changed to a boomerang-type, with tails pointing to the NE and NW. Again, the southern side of

Distribution map of shoal facies per cycle (at peak regression)

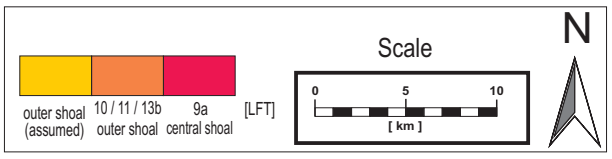

regressive phase

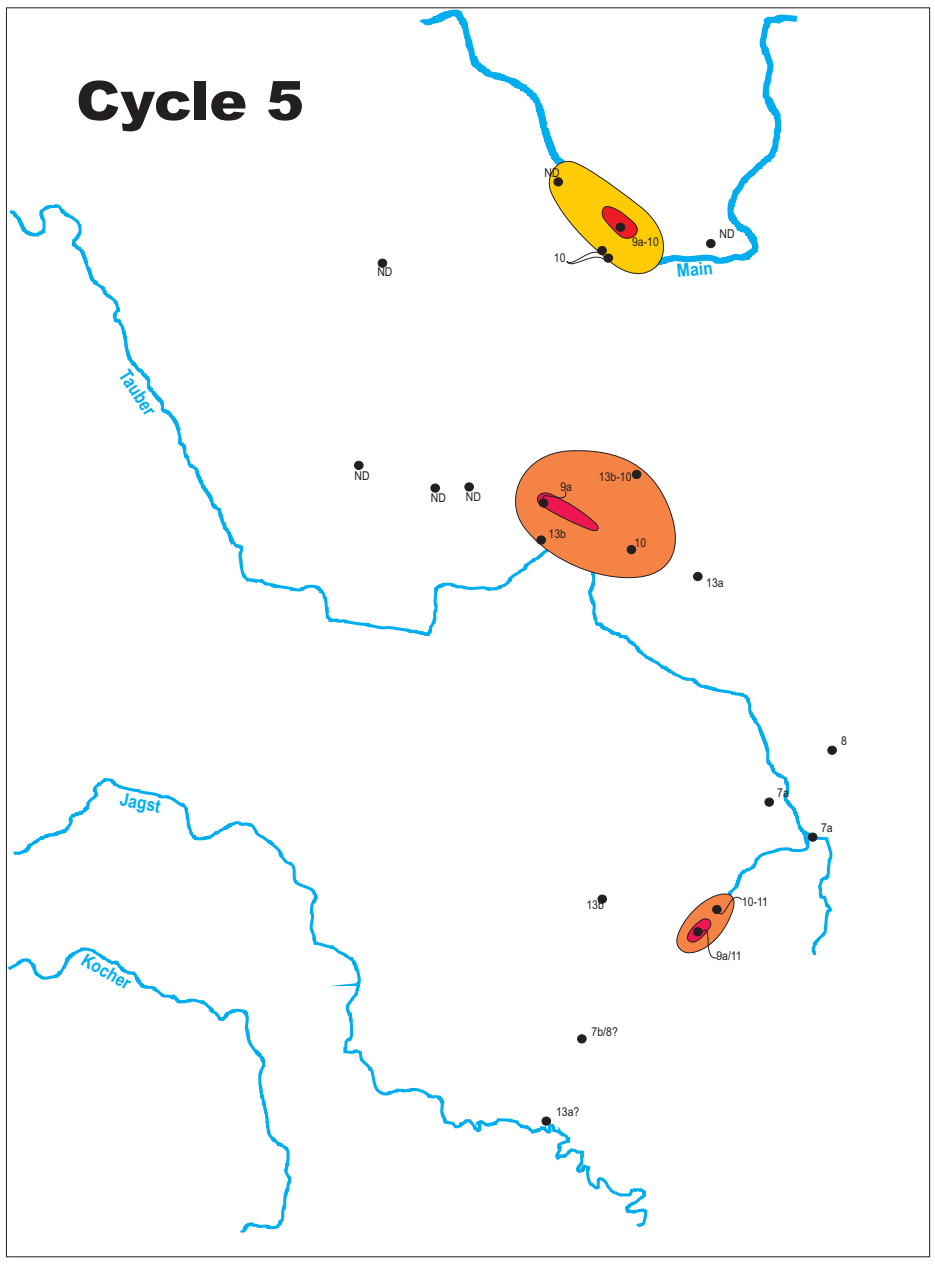

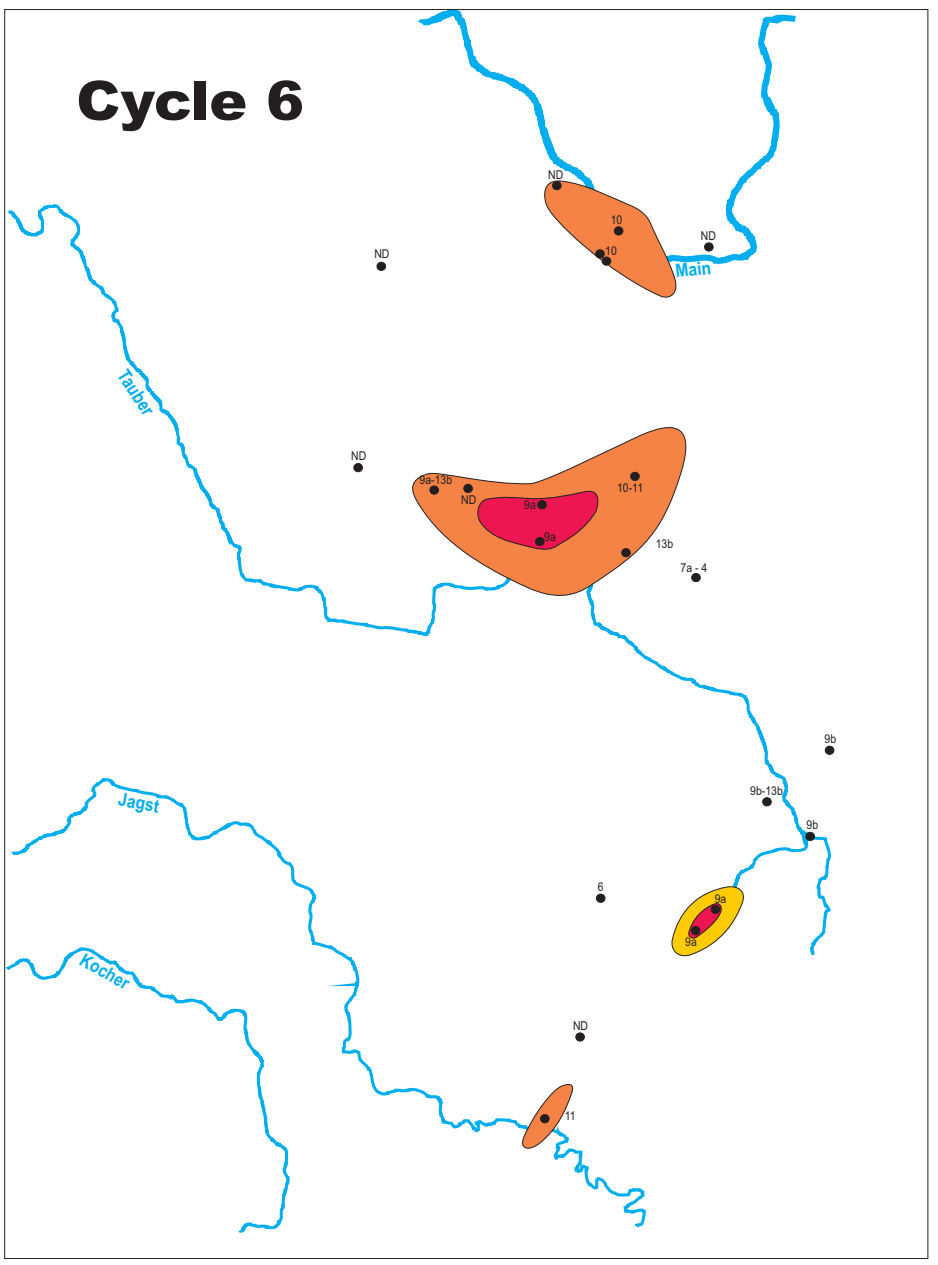

transgressive phase

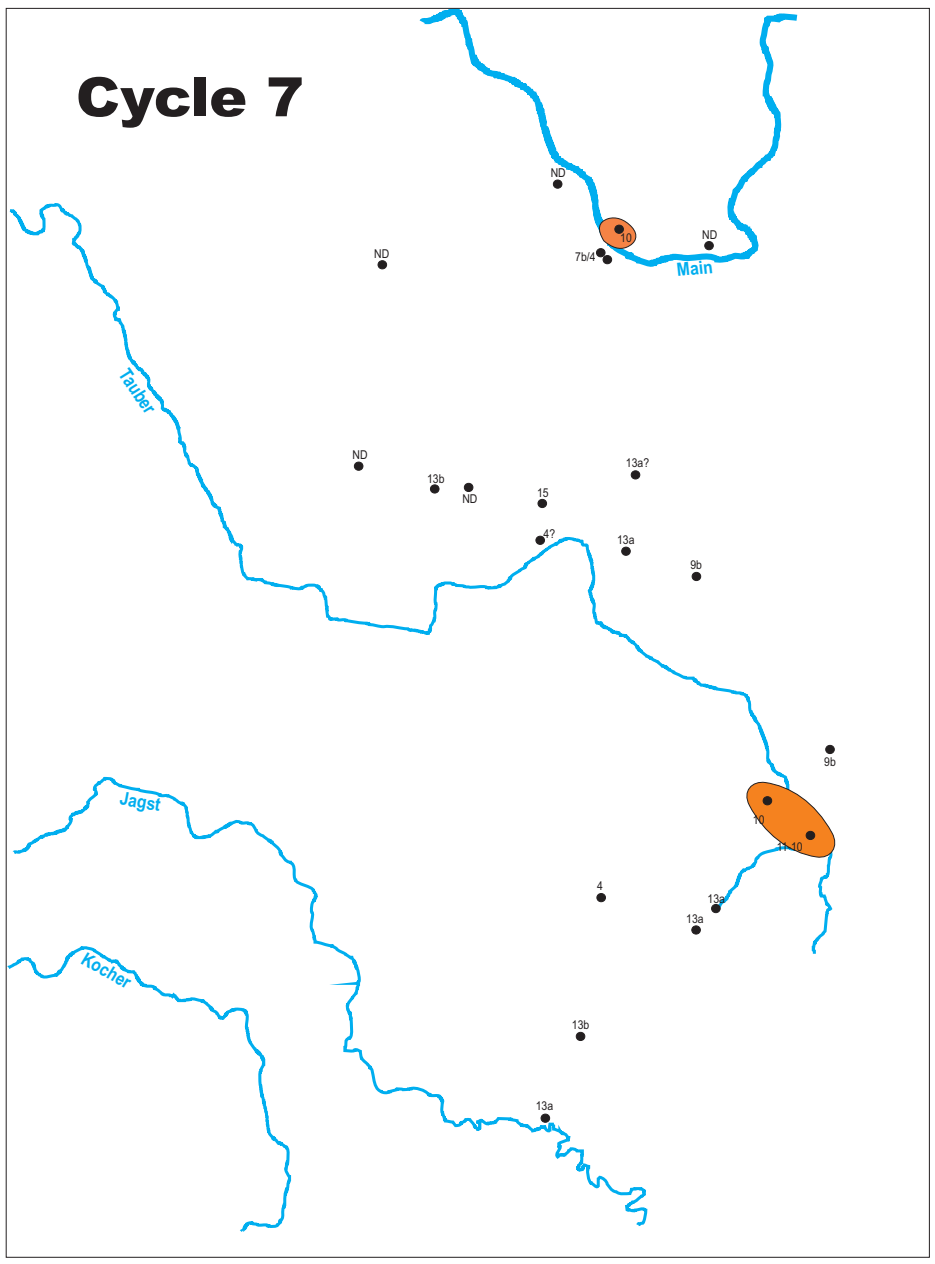

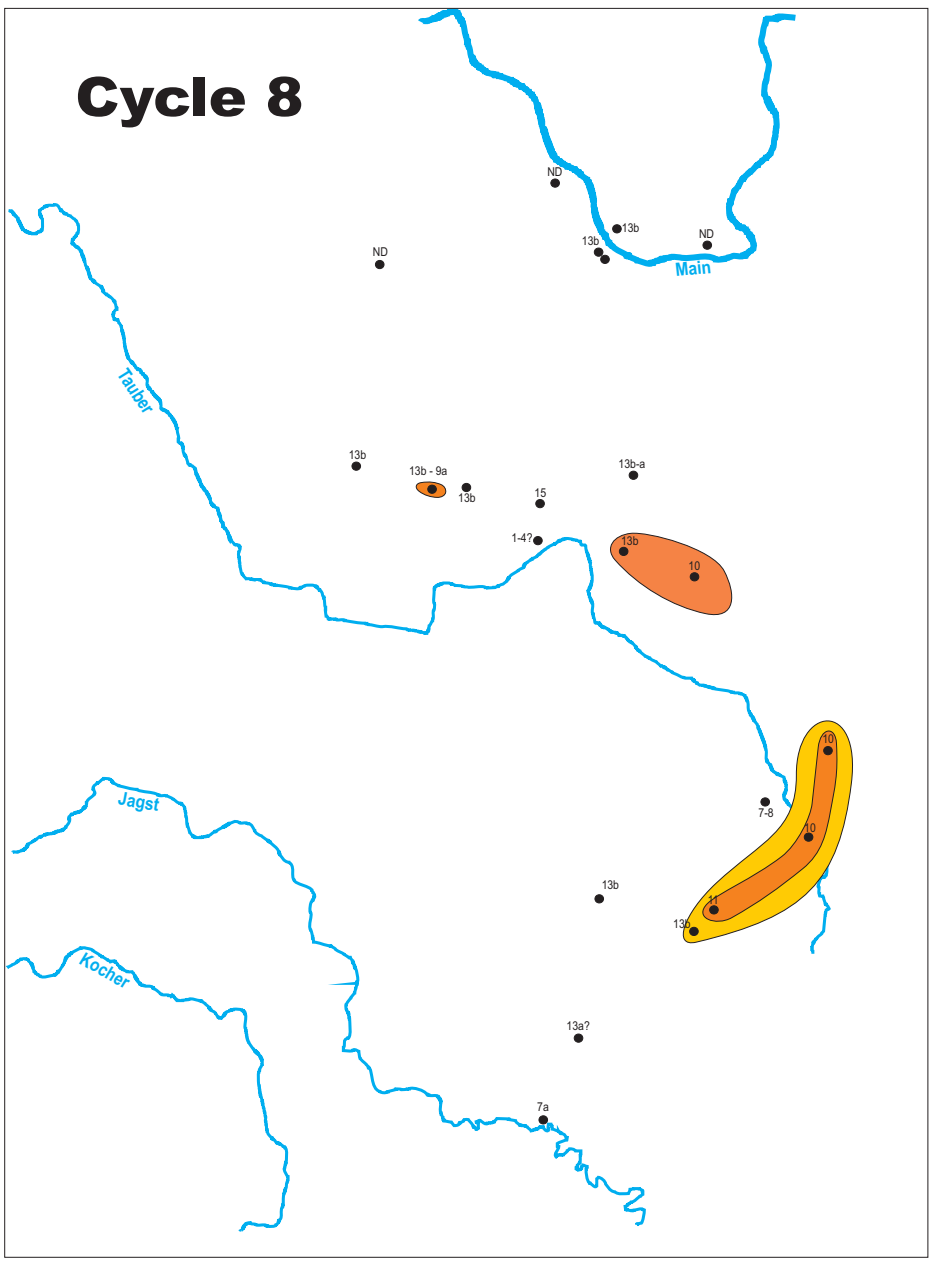

Fig. 27: Shoal lithofacies type distribution at peak regression of fundamental cycles. Note the increase of central- and outer shoal facies towards cycle 6 and the general decrease in shoal facies including the lack of central shoal facies in cycles 7 & 8.

the body decreases rapidly in thickness, while the south-eastern part decreases much smoother. The thickness, opposite to cycle 5, is half as high and amounts 1 m in average (t_{max} = 1,3 m in Q 14 and C 2).
The patch-like shoals in northern and southern direction are located in the same position as before. They increase in thickness (t_{max} = 1,2 m in Q 16 and t_{max} = 1,05 in Q 3) and dimension (Northern shoal: l_{body} = 10 km, Southern shoals: l_{body} = 6 km).

Most shoal bodies disappear in fundamental cycle 7. A tiny body exists in the north (t_{max} = 1 m in Q 17, l_{body} = 2,5 km), while a new body appears in a more landward (SE-) position. This geobody strikes in NW-SE direction, with a lengths of 6,5 km and a widths of 3 km. Its thickness varies between 1,25 m in Q 7 and 0,9 m in Q 6.

In fundamental cycle 8 the south-eastern shoal body still exists but is completely changed its shape, dimension and orientation. The string-like geobody is elongated in SSW-NNE direction, approximately 10 km in length and a width of max. 1 km. The thickness is minimal with 0,6 m in average.
Another body occurs in a position landwards of the main shoal body described in cycle 5 and 6. This body shows the same ENE-WSW orientation t_{max} is 0,9 m in Q 12 and l_{body} is 6 km long.

Interpretation and discussion:
A maximum large-scale regression during fundamental cycle 6 is supported by the following observations:

- A decrease in accommodation space from cycle 5 to 6, recognizable by a decreasing maximum and average shoal thickness (t_{max} = 2.25 m in cycle 5 to 1,3 m in cycle 6, besides $t_{average}$ = 1 m in cycle 5 and 0,95 m in cycle 6).
- An increase in the dimension of shoals together with an increase in grain-dominated facies in general.
- The basinward extension of the shoal geobodies. This probably reflects a shallowing and smoothing of the paleotopographic environment.

The shape of the main shoal geobody (in the middle of the study area) and its steep southern margin compared to its smooth northern slope can be explained by the prevailing paleowind- and wave direction from southwest in northeastern direction. This caused a leeward accretion of sediment towards the sheltered backside of the geobody. Such forms are commonly described in

Isopach map of cumulative thickness of shoal facies association per cycle

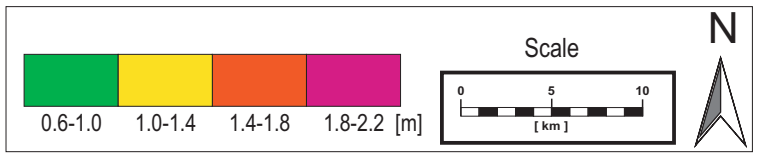

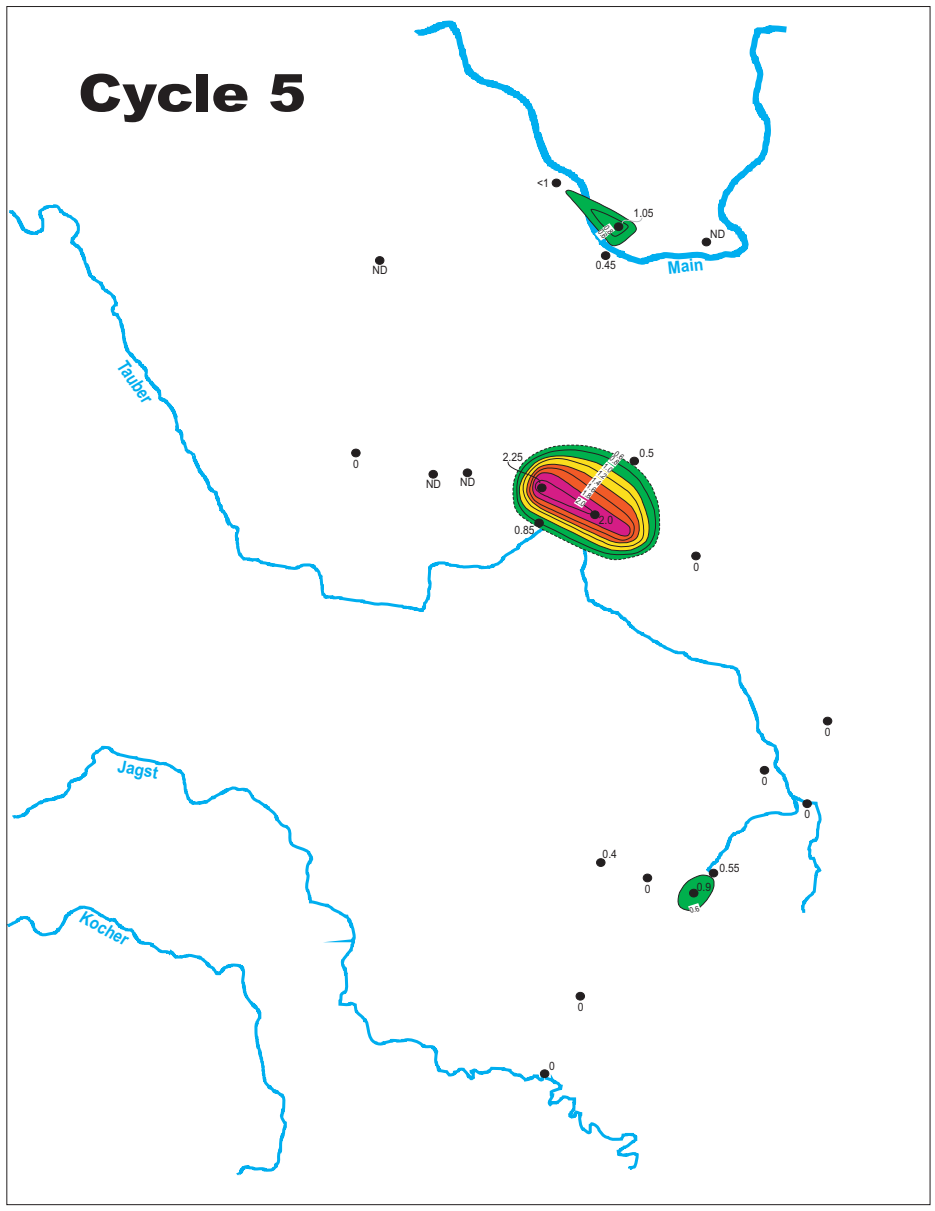

regressive phase

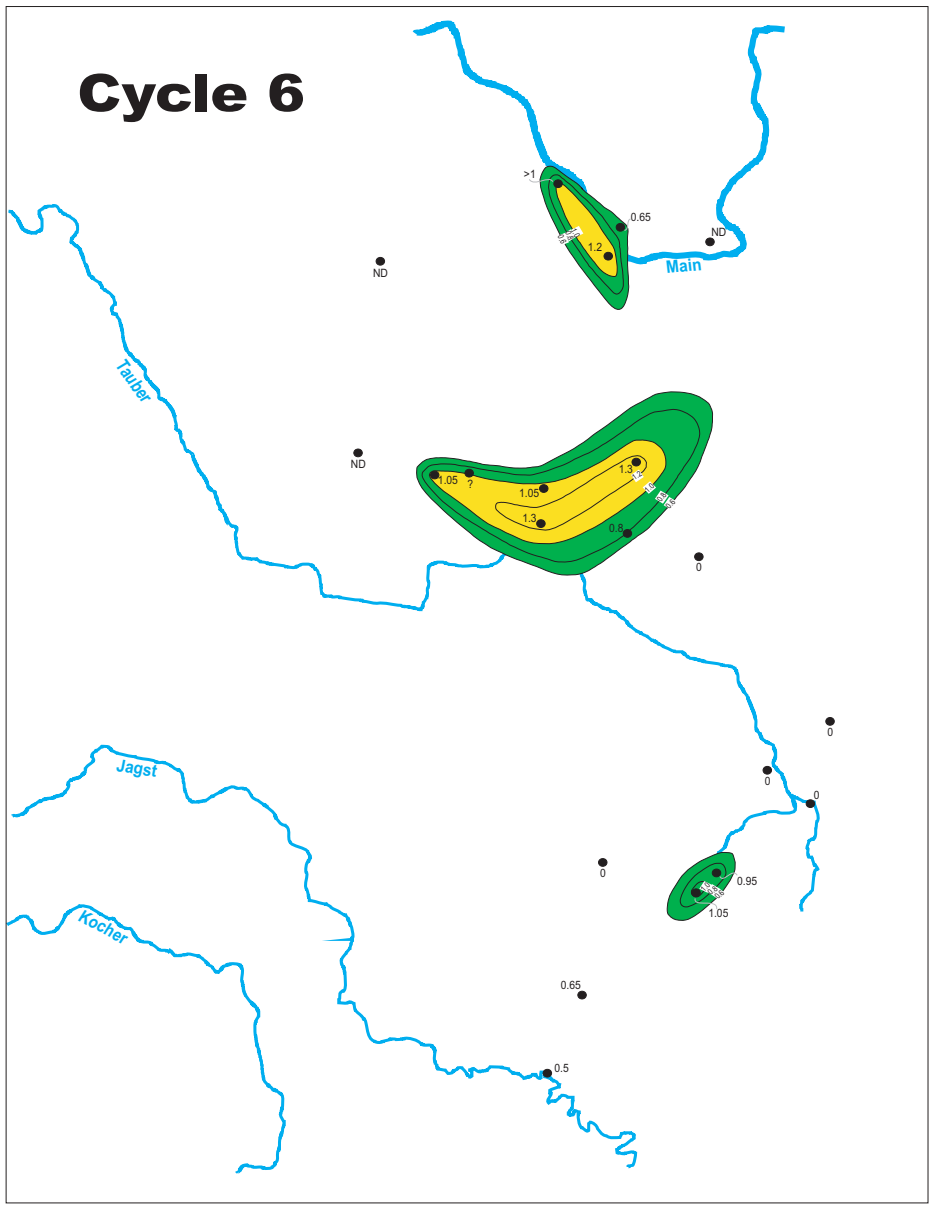

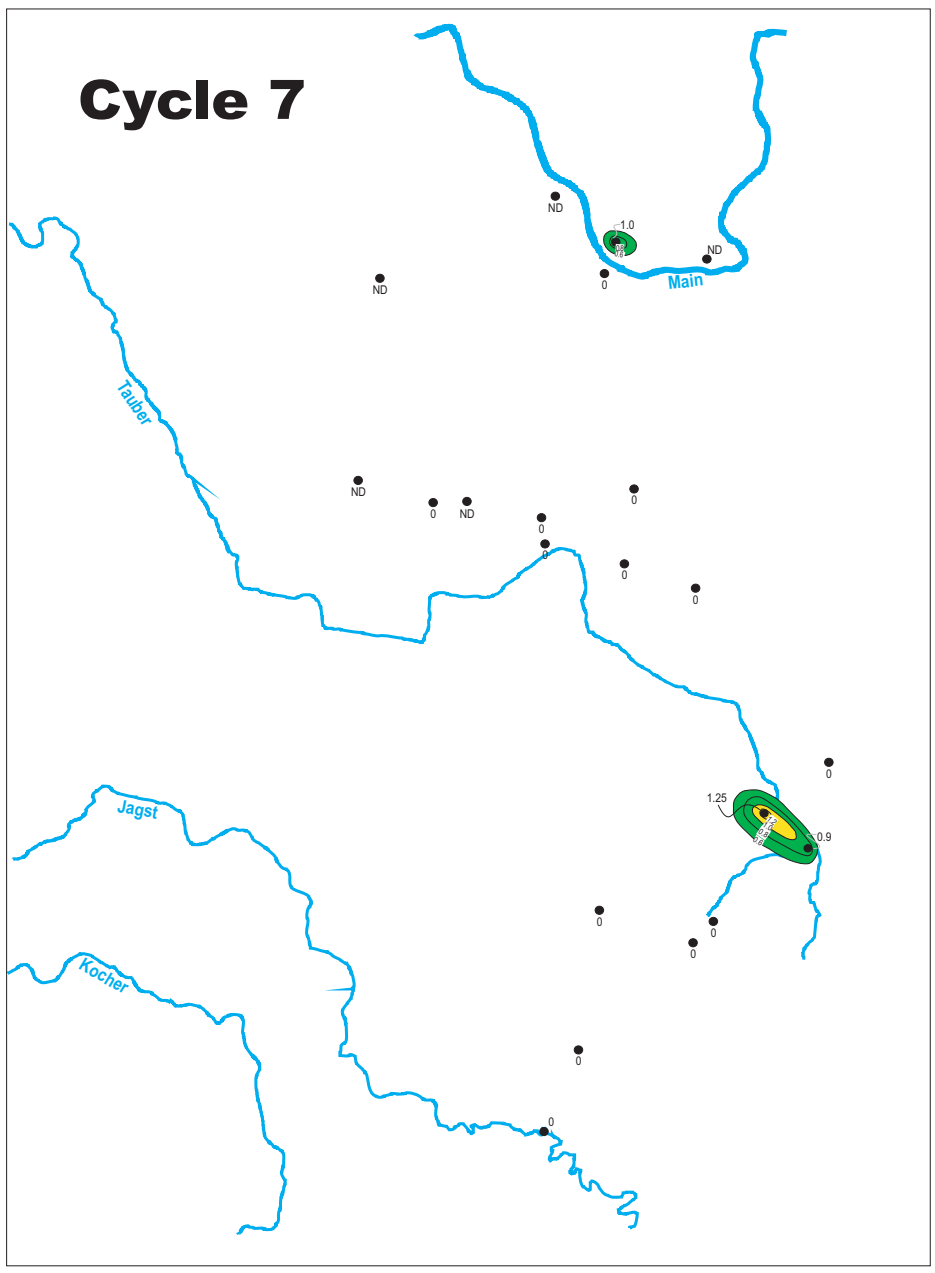

transgressive phase

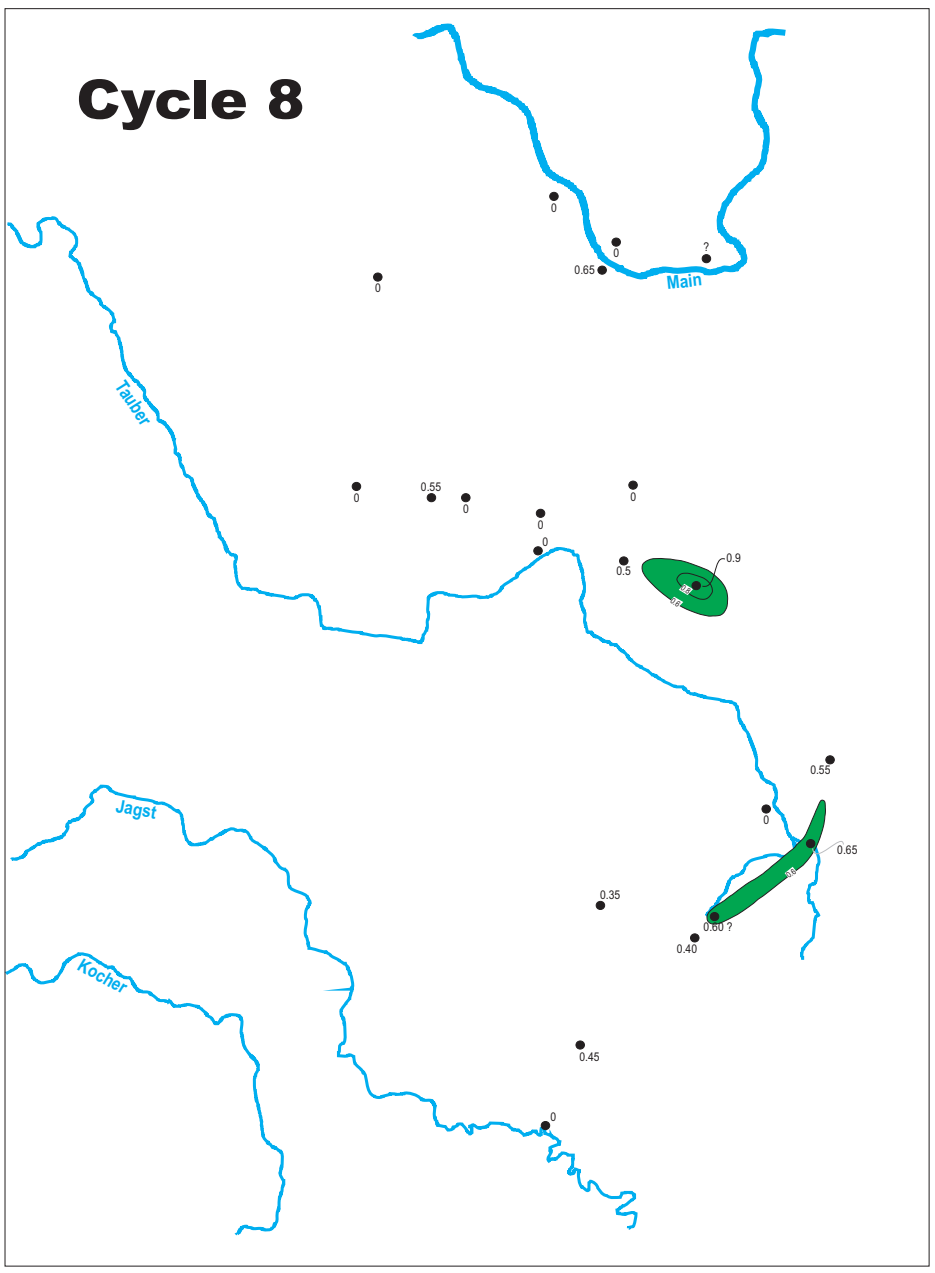

Fig. 28: Cumulative thickness distribution of shoal facies for fundamental cycles 5 - 8. Note the increasing dimension and thickness of shoal facies together with its maximum basinward shift (NW /N) towards fundamental cycle 6, reflecting peak regression on the larger cycle scale.

the literature, for instance the modern tombolo-shaped bodies of the Persian Gulf (i.e. KIRKHAM, 1997).

A maximum large-scale transgression during fundamental cycle 7 and 8 is supported by the following observations:

- A decrease in shoal body dimensions and a decrease in grain-dominated facies. At the same time increasing mud-dominated facies, bioturbation and bed-thicknesses.
- The apparent landward shift and much smaller extensions of the geobodies. This reflects a deepening of the depositional environment.

Summary:

The enormous increase in the dimensions of shoal geobodies (up to 18,5 km) from cycle 5 to 6 , together with its maximum basinward shift reflects the growth and seaward stepping of these bodies, triggered by an overall regression.
During this period the evolution of geobodies with steep slopes in southern- and smooth slopes in northern direction can be observed. These shapes are formed by leeward carbonate sand transport by prevailing paleocurrents and winds.
The disappearance and extreme decrease in shoal body dimensions (up to 2 km) in cycles 7 and 8, together with a landward stepping trend, documenting retrogradation of the carbonate shoals caused by an overall transgression.

6.3 Poro-perm maps (Figs. 29 - 31)

This study concentrates on mapping of shoal reservoir bodies. In order to compare details of the different geobodies, the most important properties were summarized in Table 4.
For generating permeability maps, the permeability values are picked at the level of peak regression in each fundamental cycle and are illustrated in Fig. 29 as overlay over the maps depicting the shoal facies distribution at the level of peak regression.

	Reservoir body in study area :	Dimension of reservoir bodies		Reservoir Quality *= (number of datapoints / total poro-perm samples)					
C #	a) Location b) Orientation	Max. lenghts	Max. widths	$\Phi_{max.}$ [%]	Φ_{mean} [%]	Kh_{max} [mD]	Kh_{mean} [mD]	Evaluation	Remarks, Trends
5	a) Central b) ENE-WSW	10 km	7 km	20,9 in Q13	8 (4/34)*	187 in Q11	24,3 (3/32)*	Very good	Slow, smooth decrease of reservoir dimension and quality to NE, in contrast to rapid decrease to all other directions.
5	a) SE b) SW-NE	9 km	5 km	16,5 in Q5	11,7 (2/8)*	51 in Q5	26,5 (2/7)*	Good	Relatively proportionate lateral decrease of the reservoir body and its quality. Reservoir center is located in Q5.
5	a) North b) NW-SE to N-S	8-9 km	3-4 km	14,5 in Q16	8,1 (2/10)*	14 in Q16	3,2 (2/10)*	Medium	Triangular reservoir body decreases proportional in quality towards all sides.
6	a) Central b) ENE-WSW to SW-NE	15-18 km	8 km	15,6 in C 2	8,6 (5/21)*	207 in C 2	13,9 (4/19)*	Very Good	Boomerang-type shape of reservoir body with slow, smooth decrease in reservoir dimension and quality to NE, and rapid decrease to SW.
6	a) SE b) SW-NE	10 km	5 km	23,9 in Q3	11,9 (2/5)*	48 in Q3	17,8 (2/4)*	Good	Smooth decrease in reservoir dimension and quality to NE and rapid decrease to all other directions.
6	a) South b) SW-NE	Min. 10 km	Min. 5 km	12,9 in Q1	8,5 (1/2)*	188 in Q1	98,8 (1/2)*	Very good	Smooth decrease in reservoir dimension and quality to NE. Total reservoir dimension and quality to SW is unknown.
6	a) North b) NW-SE to N-S	12-13 km	6-7 km	19,7 in Q17	14,1 (2/15)*	42 in Q17	12 (2/15)*	Good	Triangular reservoir body decreases proportional in quality towards all sides.
7	a) SE b) SE-NW	10 km	5-6 km	23,7 in Q7	15,9 (2/20)*	242 in Q7	112,4 (2/19)*	Very good	Relatively proportionate lateral decrease of the reservoir body and its quality.
7	a) North b) SE-NW to E-W	2-3 km	1,5-2,5 km	14,6 in Q17	6,6 (1/6)*	7 in Q17	2,8 (1/5)*	Medium	Relatively proportionate lateral decrease of the reservoir body and its quality.
8	a) SE b) N-S to SW-NE-NW	16,5-17,5	5-6 km	22,8 in Q8	17,6 (3/13)*	139 in Q6	56,7 (3/13)*	Very good	String- to boomerang like form of reservoir body with constant lateral decrease of dimension and quality.
8	a) Central-E b) SE-NW	9-10 km	4-5 km	12,5 in Q12	10 (1/7)*	17 in Q12	4 (1/7)*	Medium	Relatively proportionate lateral decrease of the reservoir body and its quality.
8	a) Central-W b) W-E to NW-SE-	3,5 km	1,5-2 km	4,6 in Q9	4,6 (1/1)*	2,9 in Q9	2,9 (1/1)*	Poor	Relatively proportionate lateral decrease of the reservoir body and its quality.

Table 4: Dimension and quality of shoal reservoir bodies during fundamental cycles 5 to 8.

6.3.1. Permeability distribution per fundamental cycle (picked at peak regression of the fundamental cycles) (Figs. 29 A & B))

The highest permeabilities are apparently concentrated either in the shell hash facies (LFT 10) or even more in the ruditic bioclastic grainstones (LFT 11), if present, but never in the oolitic grainstones (LFT 9a), as seen in the shoal bodies of fundamental cycles 5 & 6.
These results in the following reservoir quality distribution: Maximum permeabilities are located mostly in more landward (sheltered) position of the shoal bodies due to the occurrence of LFT 11 on the backshoal part. In cases where LFT 11 is not developed (e.g., major shoal in cycle 5 or northern shoal in cycle 6), best permeabilities were observed in LFT 10, also preferred on the landward side. Oolite-dominated central shoal parts (LFT 9a) as well as seaward parts however show lower permeabilities.
Altogether an increase in permeability in fundamental cycles 7 & 8 compared to the previous cycles 5 & 6 is reflected by the predominant red (20-60 mD), magenta (60-100 mD) and blue (>100 mD) stained shoal reservoir bodies.
This means that the large-scale transgressive trend seams to have a large influence on the permeability distribution due to the accumulation of predominantly shell-dominated shoal facies types (LFT 10 & 11) in contrast to minor oolite shoal facies (LFT 9a).

6.3.2 Maximum permeability- and maximum porosity distribution per fundamental cycle (Fig. 30 & 31)

In contrast to the above discussed maps showing the permeability at the levels of peak regression per fundamental cycles, the maps of Figs. 30 & 31 represent the maximum values within a complete fundamental cycle.

Maximum porosity and permeability maps show essentially the same pattern and are therefore described together:
The prominent increase in reservoir body dimensions from cycle 5 to cycle 6 and their decrease in size together with a landward (E/SE) shift during cycles 7 and 8, reflect the large-scale regressive / transgressive trends.

Poro-perm values are higher during large-scale transgression, highlighted by a much higher portion of red, magenta and blue color-coded areas, which reflect high to very high porosities (12,5 – 25 %) and permeabilities (20 - >100 mD).

Click for Permeability Distribution

Distribution map of shoal facies per cycle (at peak regression)

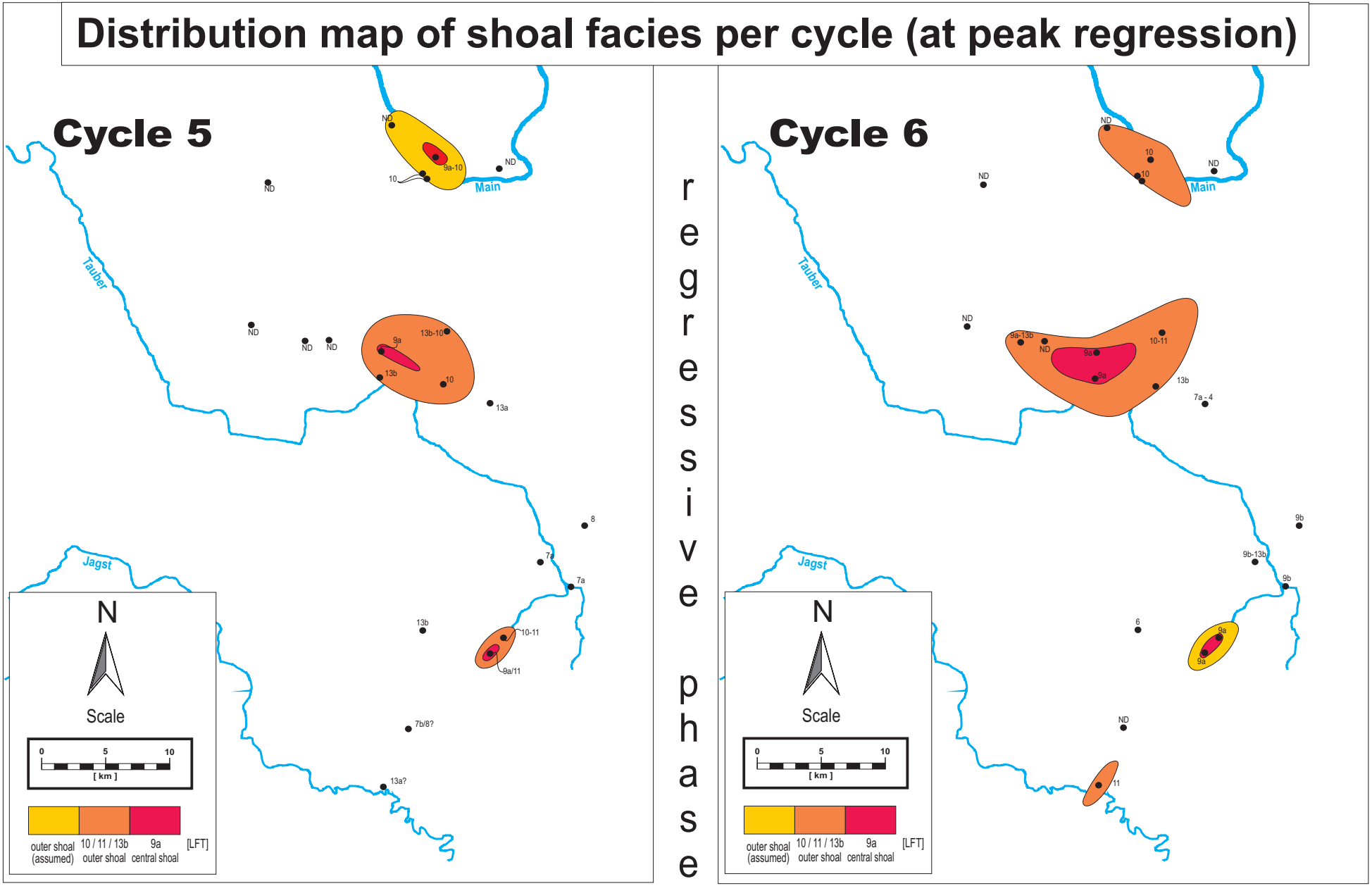

Click for Permeability Distribution

Distribution map of shoal facies per cycle (at peak regression)

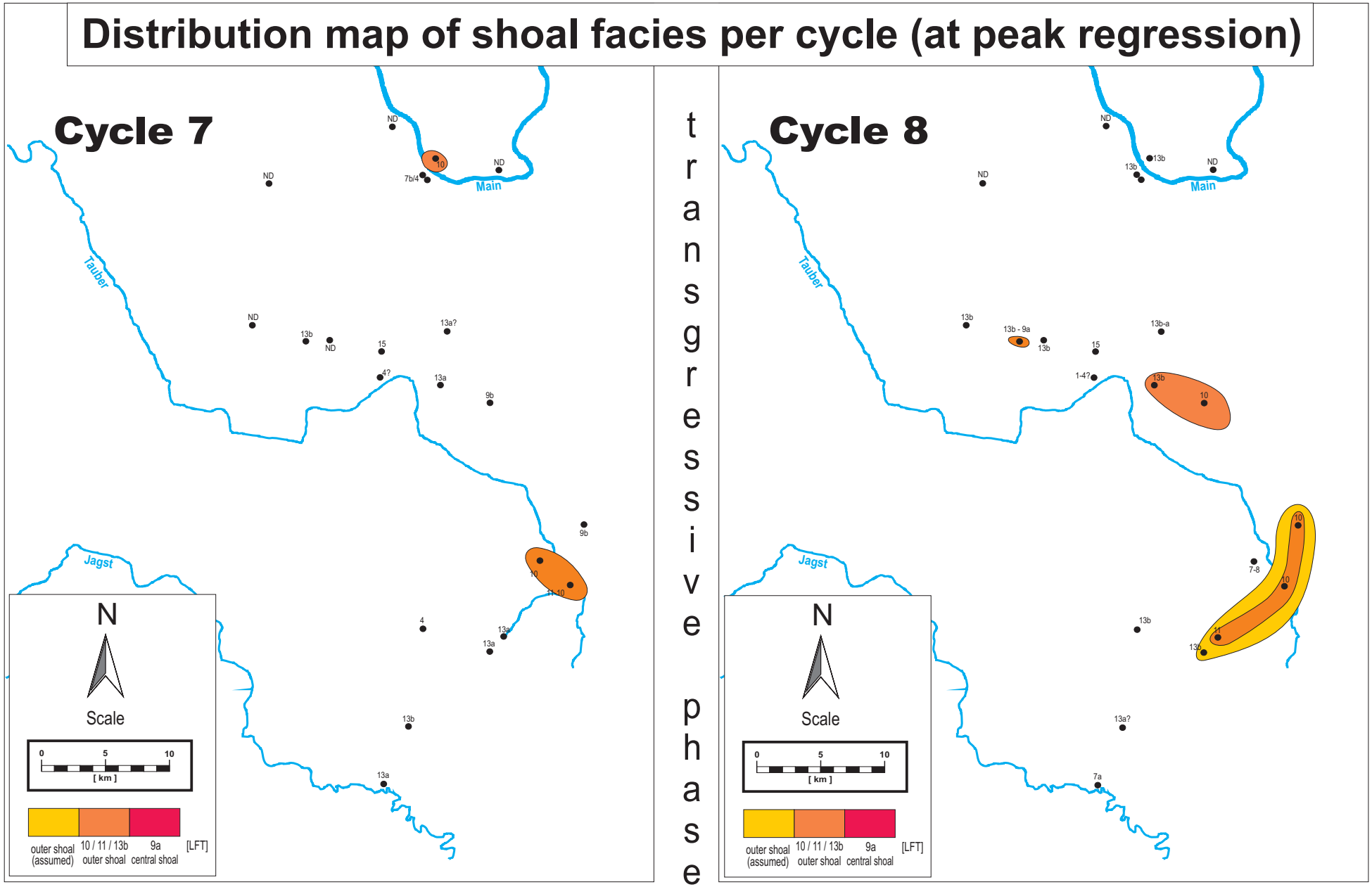

Maximum porosity distribution per cycle (shoal facies only)

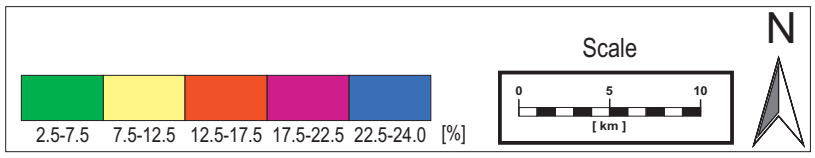

regressive phase

transgressive phase

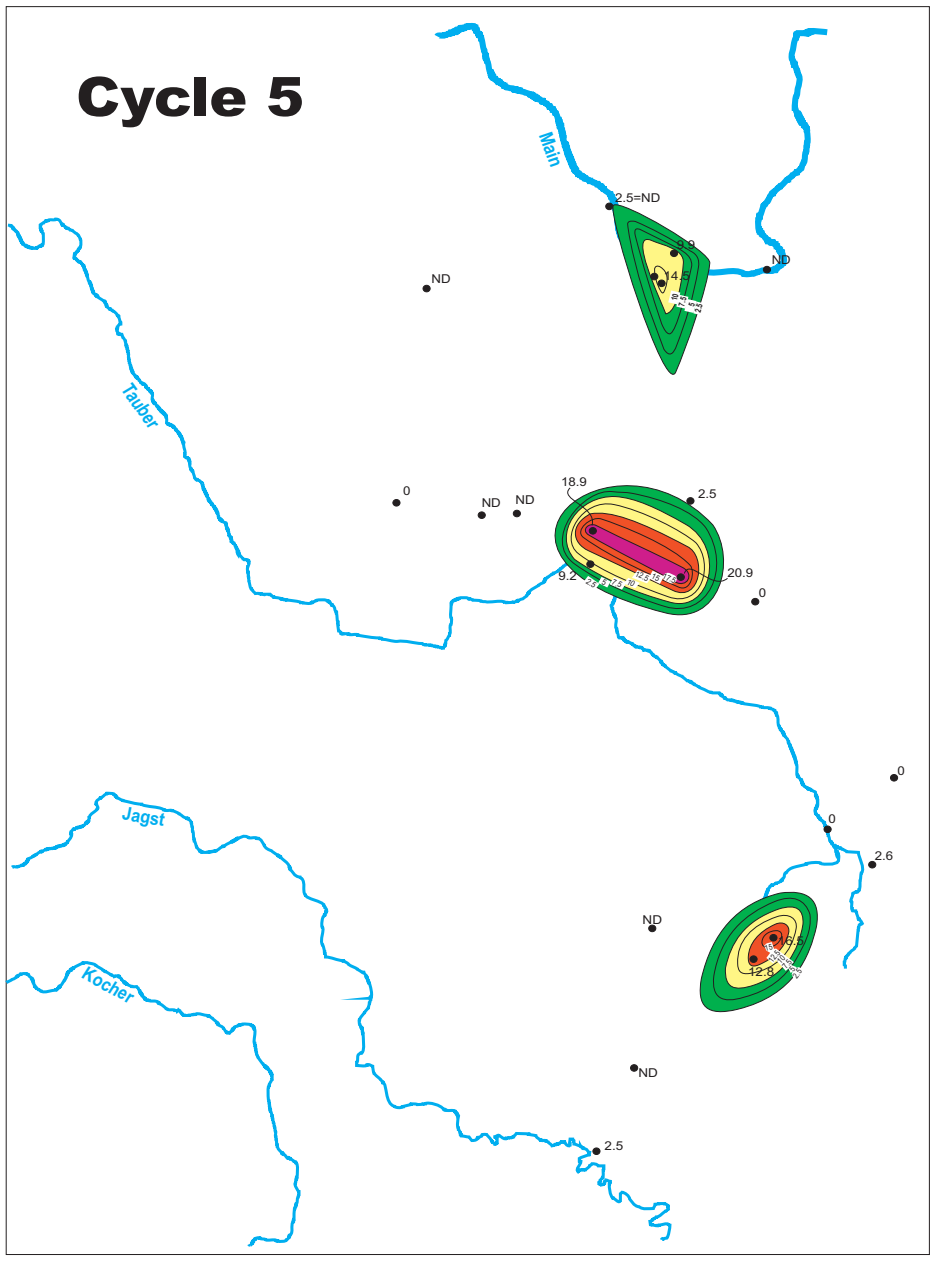

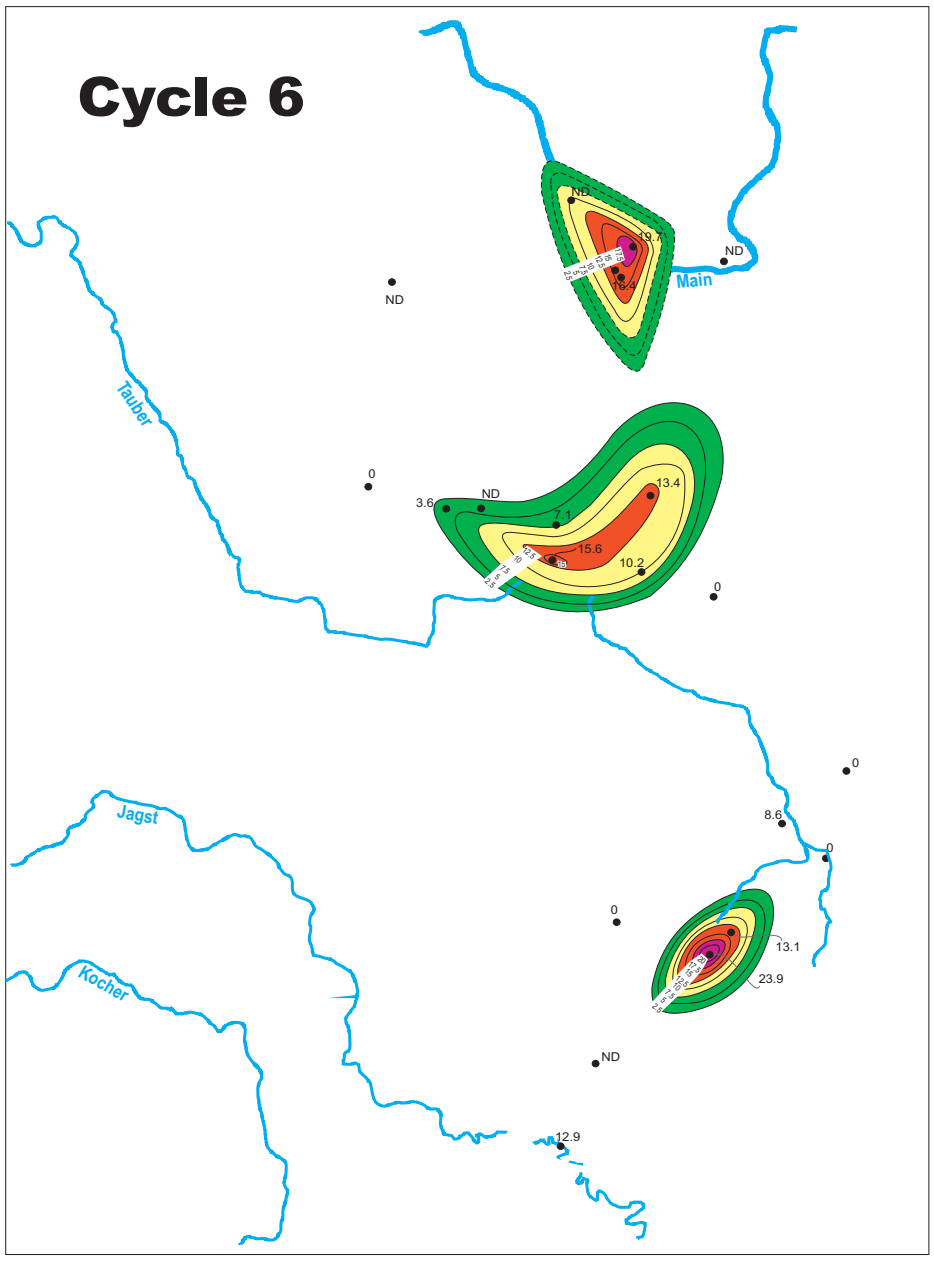

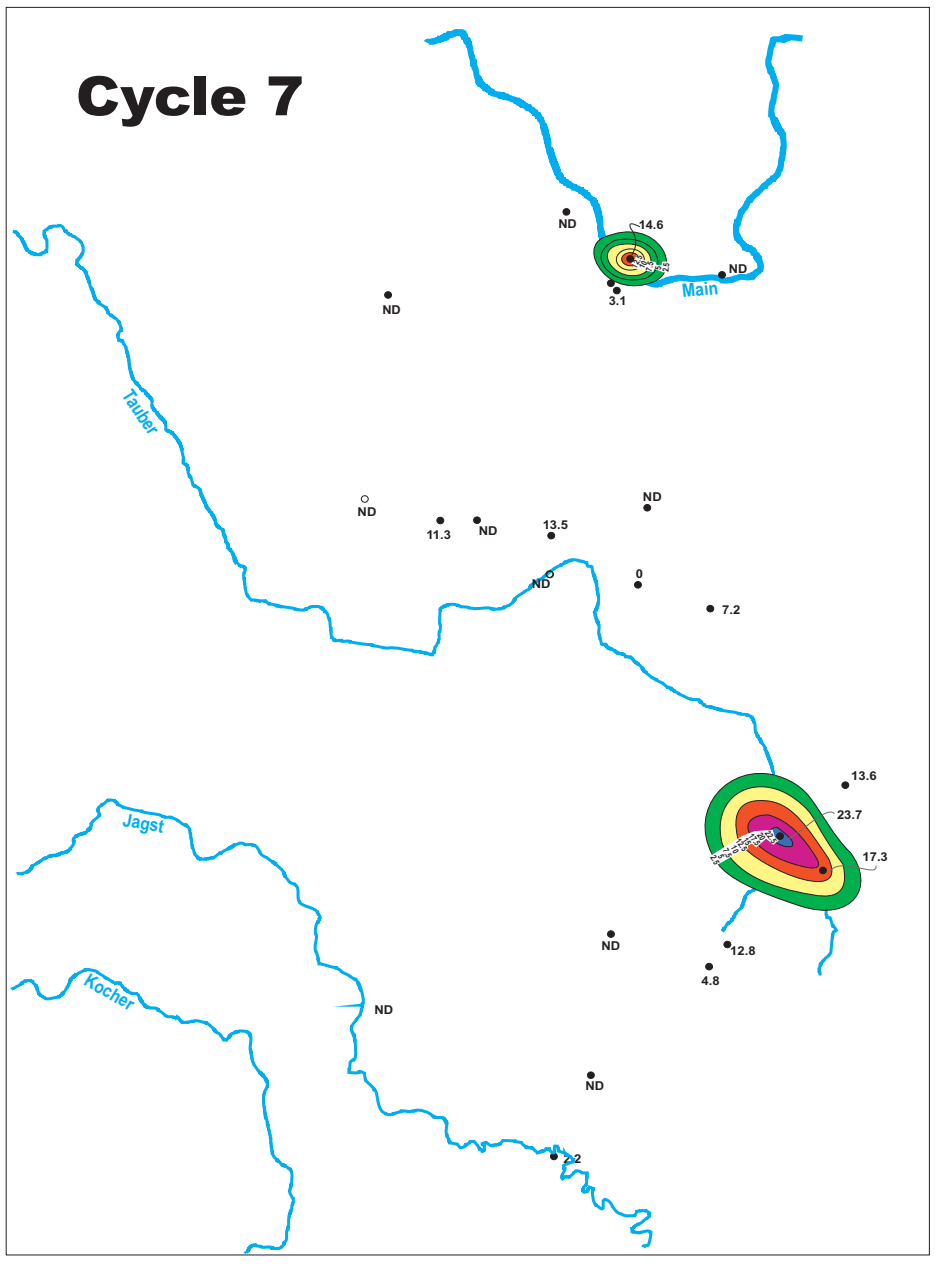

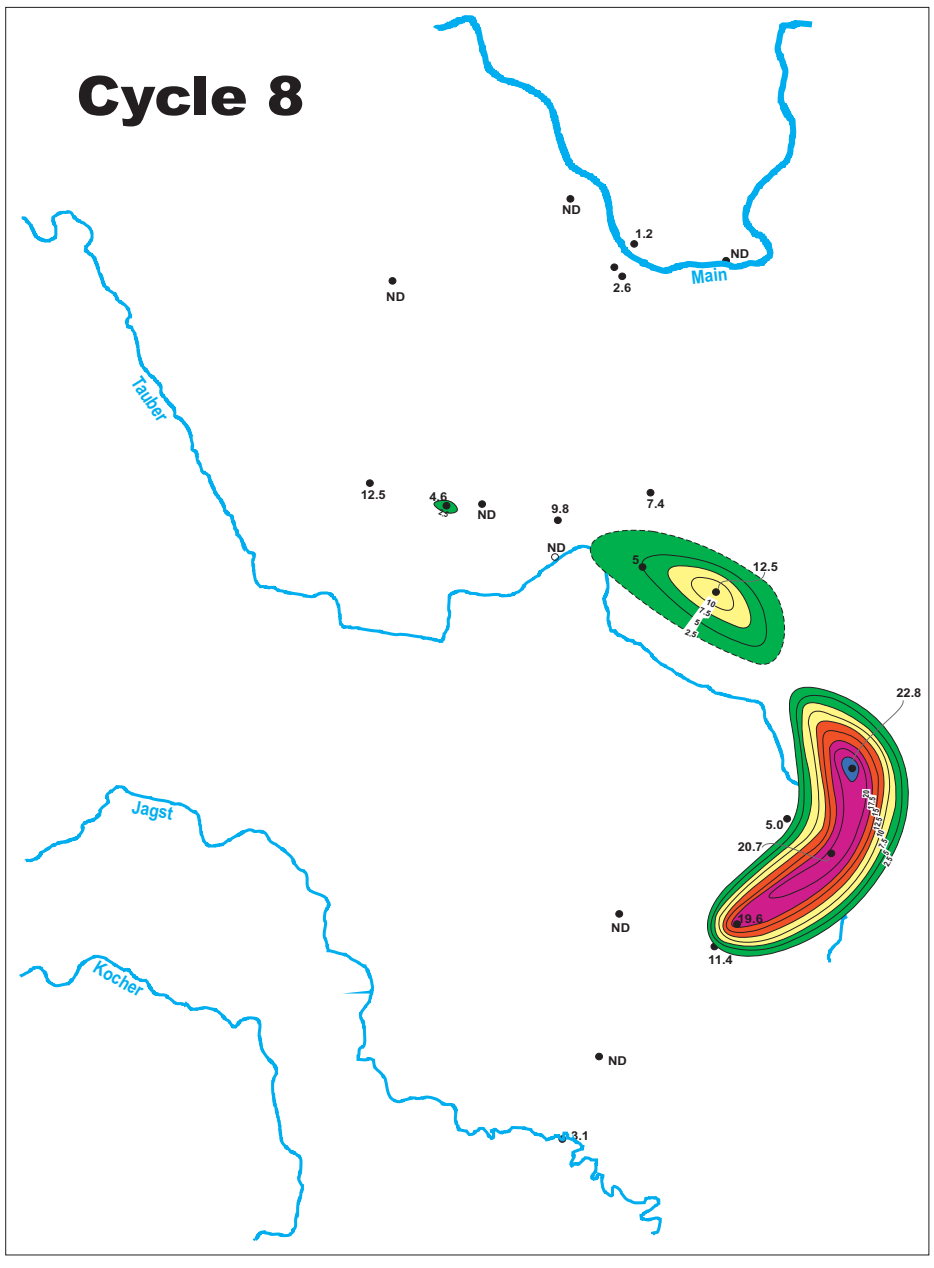

Fig. 30: Isopach map of maximum porosity in fundamental cycles 5 to 8. Note the slightly higher porosity values during maximum larger-scale transgression (cycle 8), indicated by a higher portion of red, magenta and blue stained reservoir areas, reflecting high to very high porosities (12,5 - 25 %).

Maximum permeability distribution per cycle (shoal facies only)

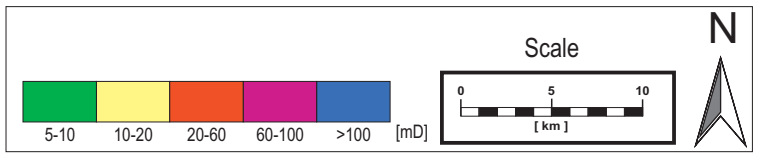

regressive phase

transgressive phase

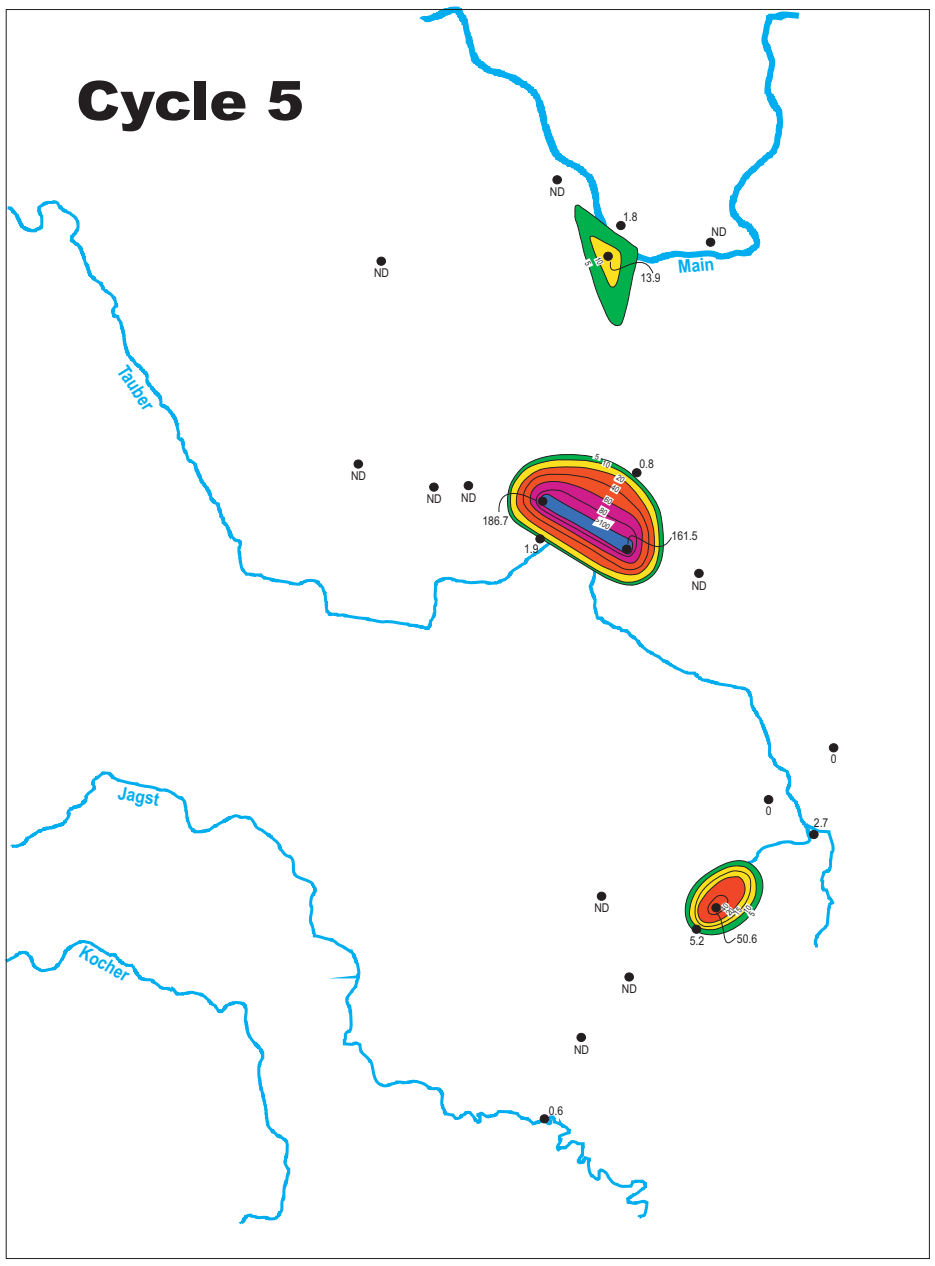

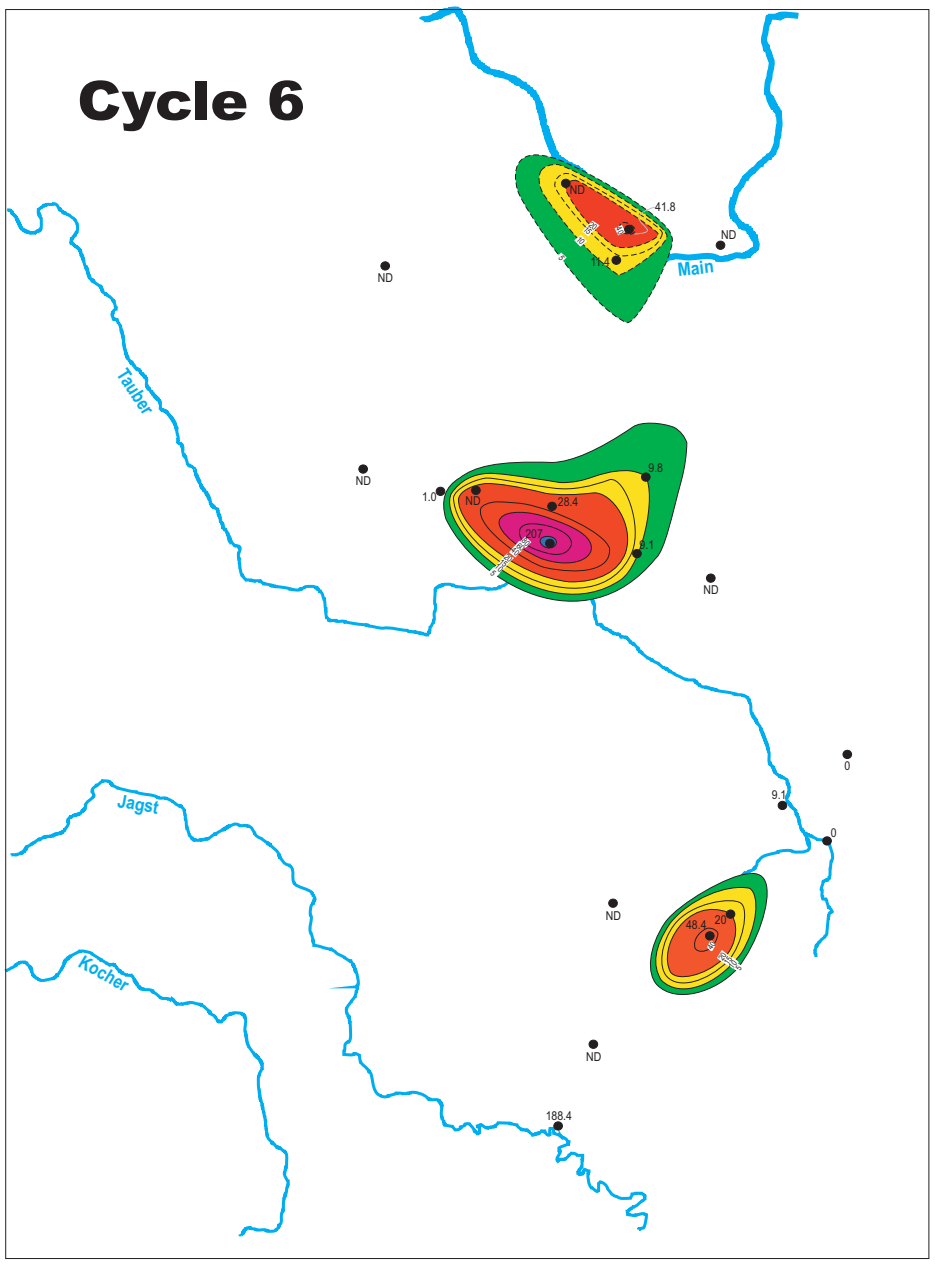

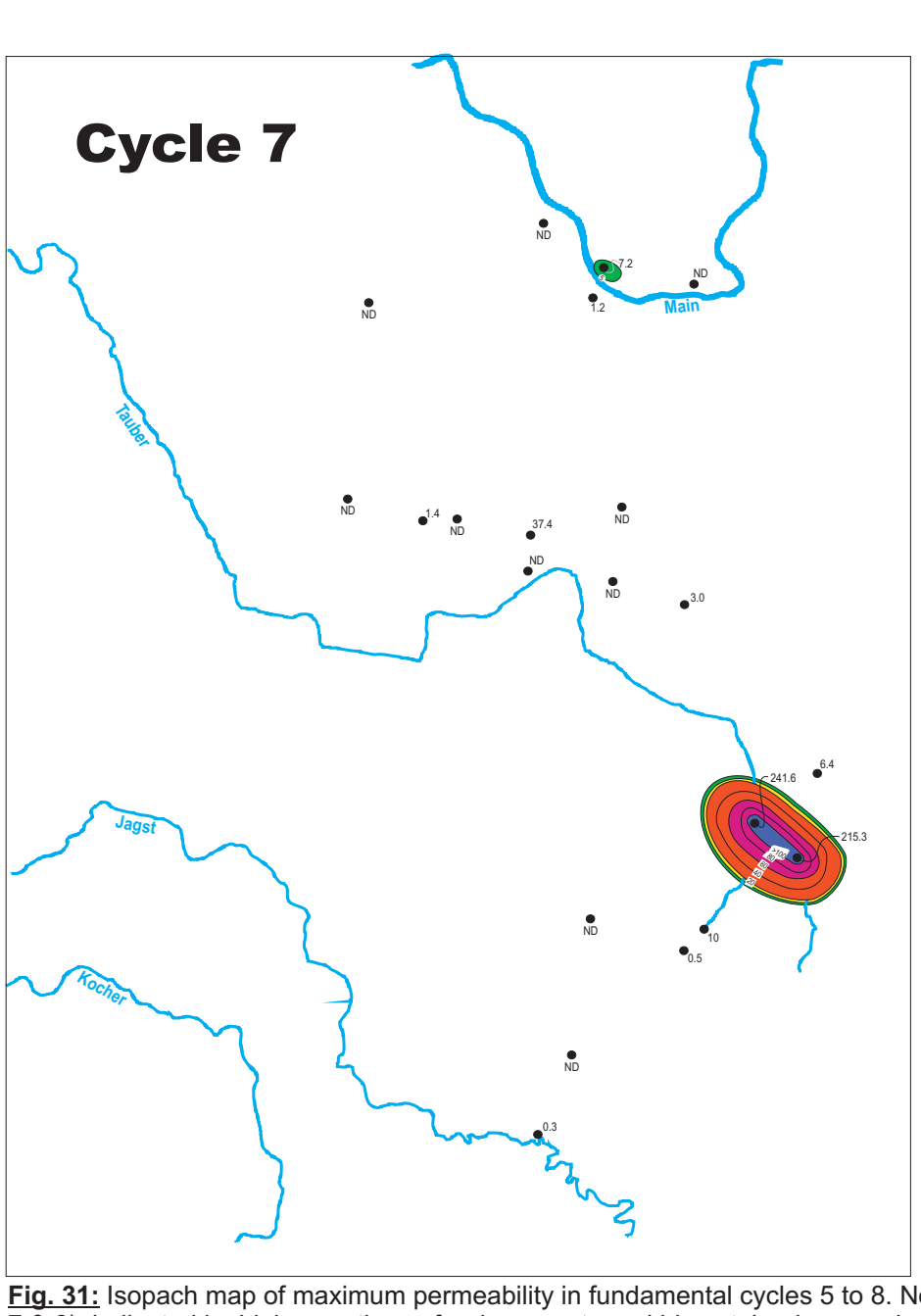

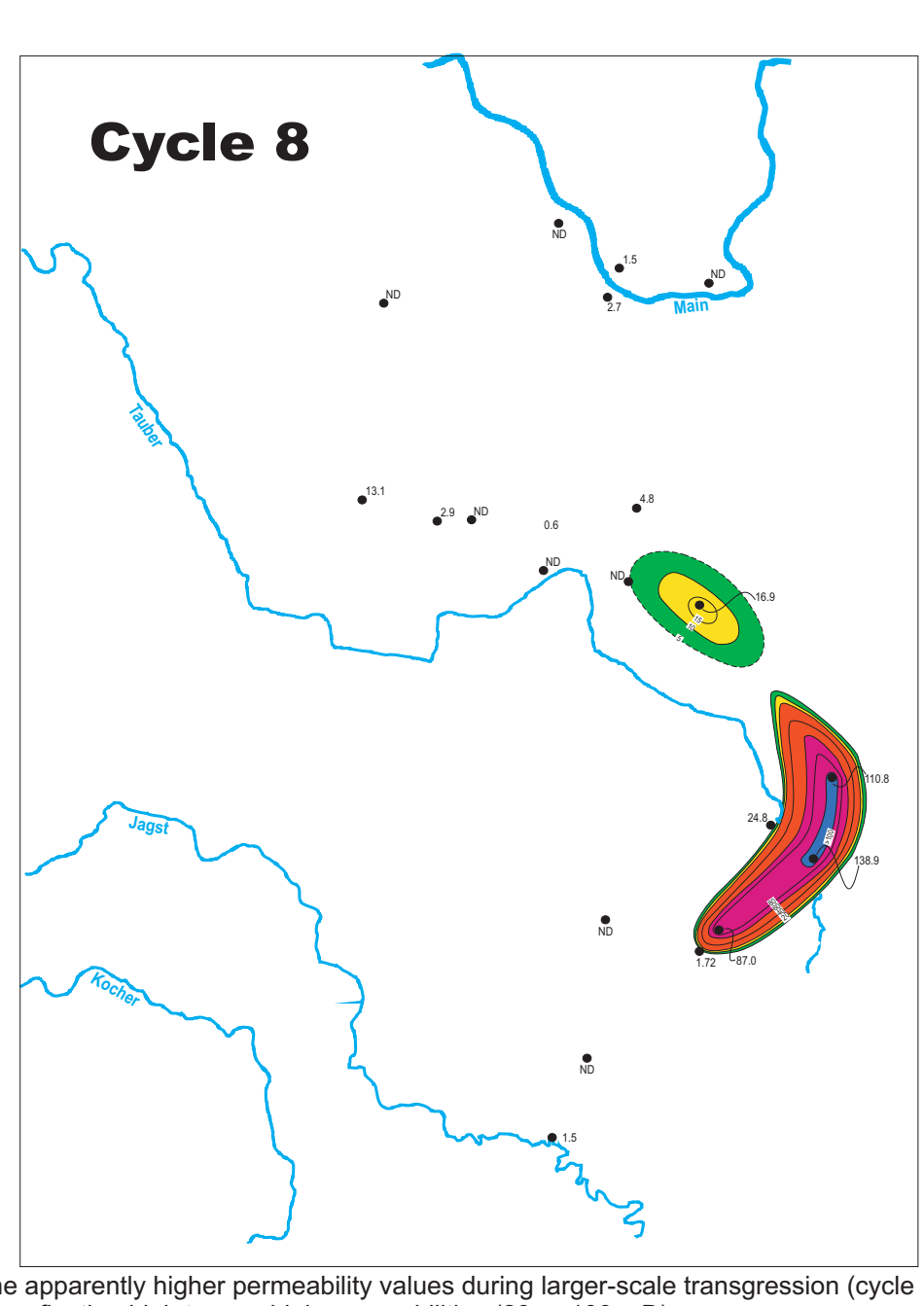

Fig. 31: Isopach map of maximum permeability in fundamental cycles 5 to 8. Note the apparently higher permeability values during larger-scale transgression (cycle 7 & 8), indicated by higher portions of red, magenta and blue stained reservoir areas, reflecting high to very high permeabilities (20 - >100 mD).

7. Implications for Reservoir Characterisation: Geometry of Sedimentary Bodies, Facies Prediction and Poro-Perm Distribution

7.1 Geometry of sedimentary bodies

The overall geometry of the carbonate sandbodies is recognizable best on the facies maps (Figs. 27 & 28). Most sedimentary bodies show an elongated oval geometry. A boomerang-typed shape occurs in fundamental cycle 6. The topography of the individual sandbodies can be described as slightly asymmetrical „mounds“, with shallow inclined landward- and steeper dipping seaward side. During overall peak regression (fundamental cycle 6) carbonate sands are most widespread. Shoals are arranged rather as solitary bodies aligned either roughly parallel or perpendicular to the shoreline. These carbonate bodies move seawards during large-scale regression and landwards during transgression (see Fig. 28, fundamental cycles 5 to 7).

Length / thickness ratios of shoal bodies

Table 5: Approximate size / thickness ratios of investigated sedimentary bodies of shoal facies only, deduced from facies maps and 2-D stratigraphic cross sections.

Cycle	Length / Thickness Ratios of „shoal“* bodies *(shoal facies association) (ratio = x 10^3 m)			
8		10 km / 0.6 m (Q 3+8) ratio: 16,7	6 km / 0.9 m (Q 12-13) ratio: 6,7	
7		6.5 km / 1.3 m (Q 6, 7) ratio: 5		2.5 km / 1 m (Q 17) ratio: 2,5
6		6 km / 1.1 m (Q 3, 5) ratio: 5,5	18.5 km / 1.3 m (Q 9-14) ratio: 14,2	12.5 km / 1.2 m (Q 16-18) ratio: 8,3
5		2 km / 0.8 m (Q 3) ratio: 2,5	10 km / 2.3 m (Q 11, 13) ratio: 4,3	5 km / 1.1 m (Q 17) ratio: 4,5
4			4.5 km / 1 m (C 2) ratio: 4,5 4 km / 0.5 m (Q 12) ratio: 8	2.5 km / 0.8 m (Q 17) ratio: 3,1
3		5 km / 1.2 m (Q 3+5) ratio: 4,2		
2	5.5 km / 0.85 m (Q 2) ratio: 6,5	>10 km / 1.4 m (Q 3,4,5) ratio: >7,1		
1	~ 5 km / 0.75 m (Q 1) ratio: 6,6			

The approximate length / thickness ratios through time, as listed in Table 5, are taken from the facies- and poro-perm maps (Figs. 28 to 31) and cross section panels (Figs. 22-26).
The length / thickness ratios are also shown in Fig. 32 A, where most shoal bodies cluster between 0,8 and 1,4 m in thickness, corresponding to a length of 4 - 6 km. This ratio is independent of the position within the large-scale cycle.
Isolated large deviations concerning thickness and length were observed mainly at fundamental cycle 5 (thickness: 2,3 m), 6 (length: 18,5 km) and 8 (10 km in length, but just 0,6 m thick). The strongest deviations from the average ratio appear to occur towards the maximum regression / transgression of the larger cycle scale, but are not predictable.
A similar length / thickness ratio is also apparent for the porous (reservoir) portion of shoal bodies, shown in Fig. 32 B.

7.2 Facies distribution & reservoir quality

In order to illustrate the proportion of porous shoal facies out of the total shoal facies, the distribution of „shoal reservoir facies“ was marked by light blue bars in the stratigraphic cross-sections Figs. 22 to 26. The evolution and dimensions of shoal reservoir facies (blue stained) through time is exemplified in Fig. 33, where changes in thickness and extension of porous carbonates can easily be traced. Within the shoal bodies, good to excellent reservoir quality occurs preferentially under the following conditions:

1. **In shell hash facies (LFT 10) and ruditic bioclastic grainstones (LFT 11) (see Figs. 29 A & B).**
   Both shell-dominated lithofacies types have a high portion of interparticle pore space additionally to their moldic porosity and therefore exhibit excellent poro-perm properties.
2. **On the landward, wind-sheltered leeward side of shoal bodies (see Figs. 29 A & B).**
   Episodic accumulation events (e.g. by storm spillovers), result in coarse grained lithofacies types 10 & 11, with a low degree of post-event reworking at sheltered „backshoal“ positions. Therefore large volumes of interparticle pore space may be preserved.
3. **During large-scale transgression.**
   During large-scale transgression, shell-dominated shoal facies types with good permeabilities predominate; while low-permeable oolite shoal facies is less abundant (see Figs. 29 B & 31).

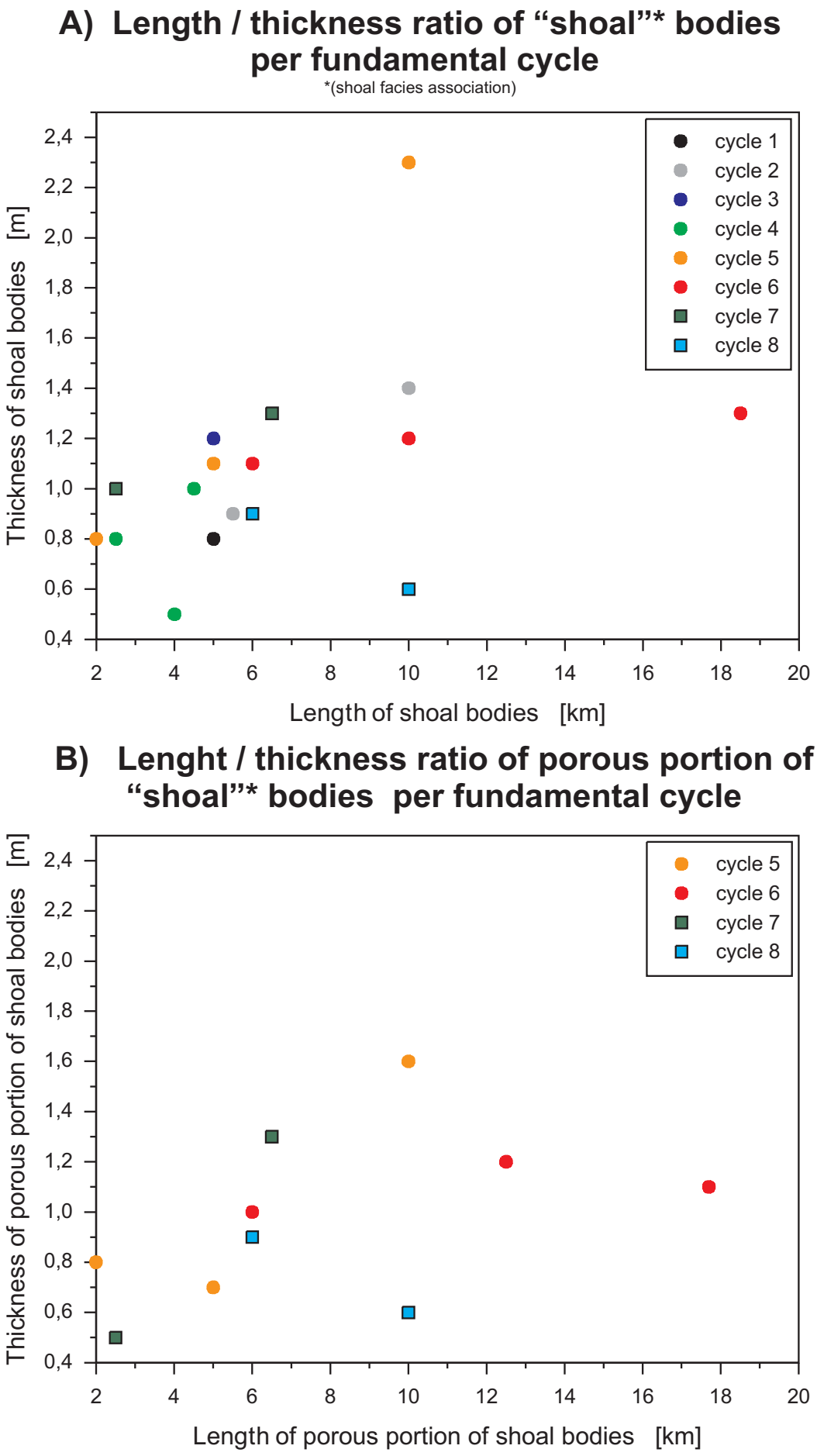

Fig. 32: A) The average thickness of shoal bodies is approximately 1 m, which corresponds to shoal body length of 4 to 6 km. Considerable deviations concerning thickness and length were observed mainly during cycles 5 and 6 (max. regression of large-scale cycle).
B) This relationship is roughly valid also for the porous reservoir portion of shoal bodies.

Stratigraphic Architecture of Shoal Reservoir Bodies (NW-SE)

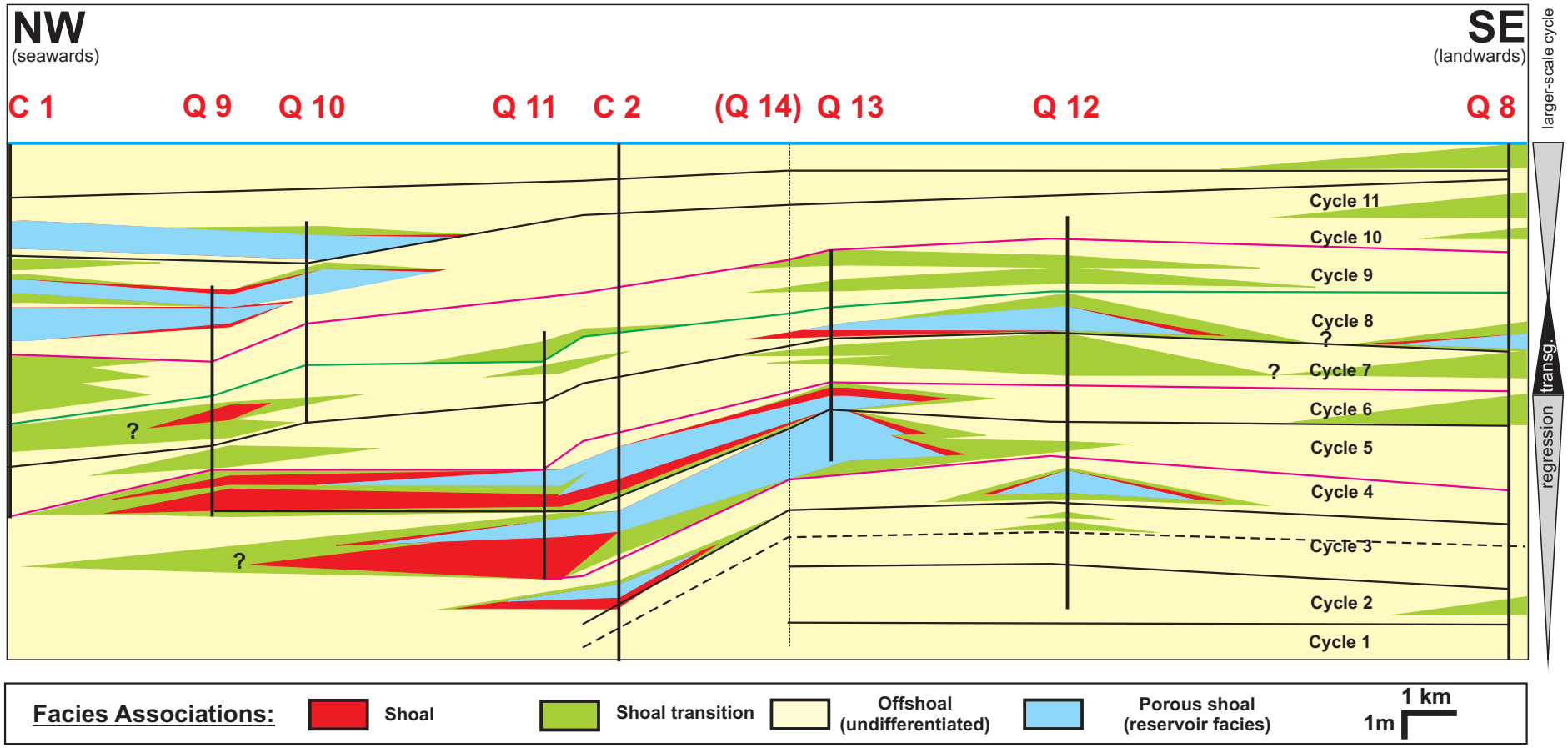

Fig. 33: Evolution and dimensions of shoal reservoir facies (blue stained) through time. Note the increase in shoal- (red) and porous shoal facies (blue) and its maximum seaward extension during larger-scale regression. Highest reservoir potential within the shoal bodies is located on the more landward, wind-sheltered leeward side (most evident on shoal bodies of cycles 5 & 6)

7.3 Controlling factors

7.3.1 Cyclicity

Hierarchical eustatic sealevel oscillations are one of the most important driving factors. The relationship between hierarchical cycle stacking pattern and vertical and lateral facies distribution was already discussed in chapters 4 to 6. The most voluminous reservoir facies are always developed during overall peak regression while the best reservoir quality was observed during large-scale transgression.

7.3.2 Paleotectonic

Underlying Variscan structural zones fundamentally control Triassic facies as pointed out in previous publications (e.g. AIGNER, 1985 or KRIMMEL, 1980). Isopach maps for different stratigraphic units within the Upper Muschelkalk, published by RAUSCH & SIMON (1988) illustrate rapid, subregional variations in thicknesses of subsequent time slices. This phenomenon can only be explained by differential subsidence with paleotectonic uplift or lower subsidence phases. A prominent paleohigh is the so-called „Gammesfeld high".
This paleotectonic pattern is also illustrated by the Lower Keuper isopachs, roughly tracing the underlying Muschelkalk, following the „Gammesfeld high", as shown in Fig. 34. The overall distribution of „Quaderkalk" shoal facies occurs on top of this regional paleohigh (Fig. 34). Within this regional paleotectonic high, it is quite difficult to predict the exact position of individual shoal reservoir bodies.

However, a comparison of the shoal facies maps (Figs. 27 & 28), the stratigraphic architecture of geobodies (Figs. 22 – 26) and maps of structural elements showed:

A) Shoal bodies repeatedly formed at almost the same locations during different timeslices.
B) „Centers" of preferred shoal accumulation are always situated on presently well-known subregional anticlines, separated by well-established synclines (see Fig. 35).

The most important shoal body „centers" are:

1) Gammesfeld / Bettenfeld (Q 3/5) in the south, situated on the „Schrozberger anticline".
2) Lenzenbrunn (Q 11) to Aub (Q 14) in the center, situated on the „Niederrimbacher anticline".
3) Sommerhausen (Q 17) in the north of the study area, situated on the „Goßmannsdorfer anticline".

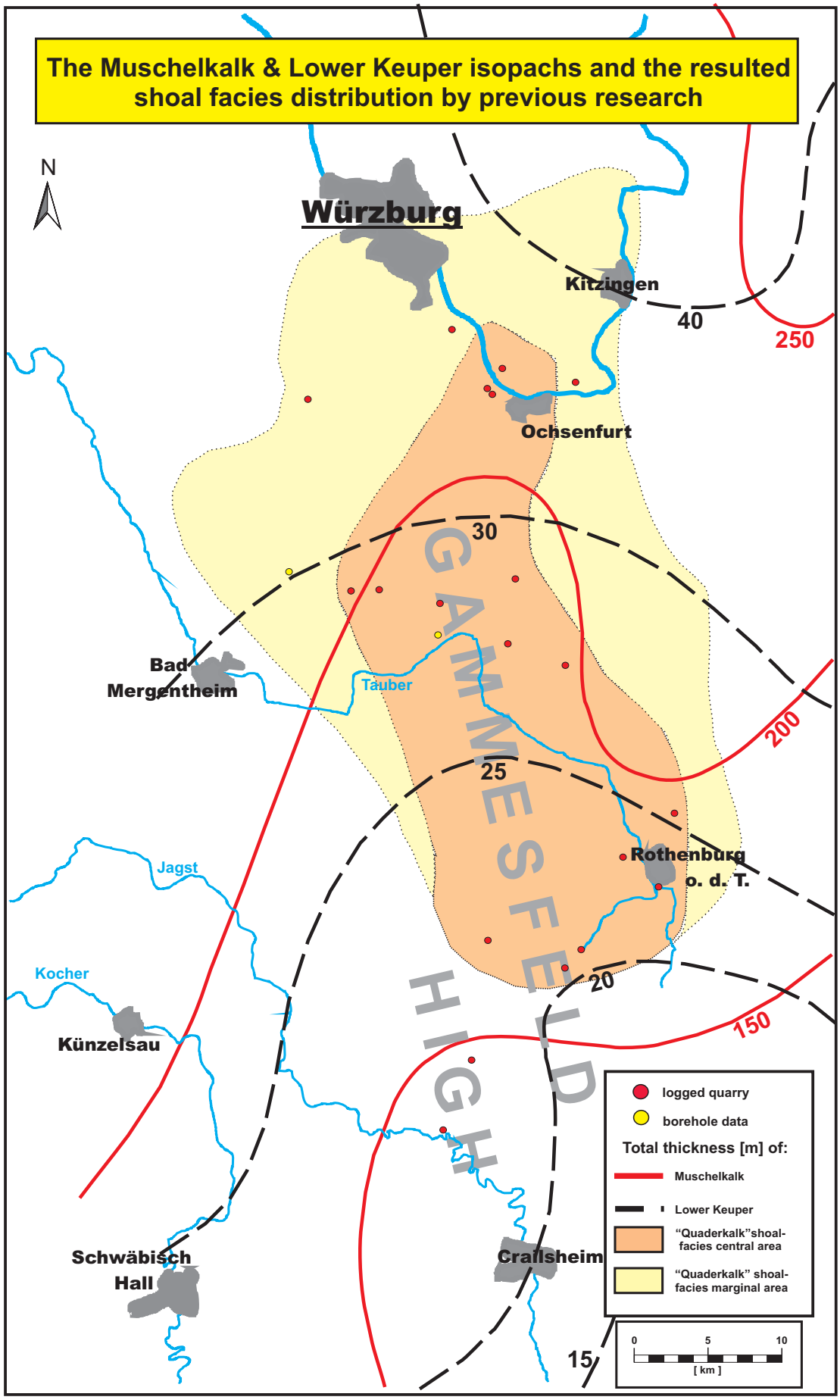

Fig. 34: This map shows that the Lower Keuper isopachs roughly follow the pattern of the underlying Muschelkalk, tracing the prominent paleotectonic "Gammesfeld High". Numerous previous investigations ,e.g. of WAGNER (1913), SCHUSTER (1928), RUTTE (1957), DREXLER (1964) and AUST (1969) resulted in the "Quaderkalk" shoal facies distribution map, oriented along the Gammesfeld- anticline. A prediction of the exact position of shoal reservoir bodies on this paleohigh with the available dataset is quite difficult.

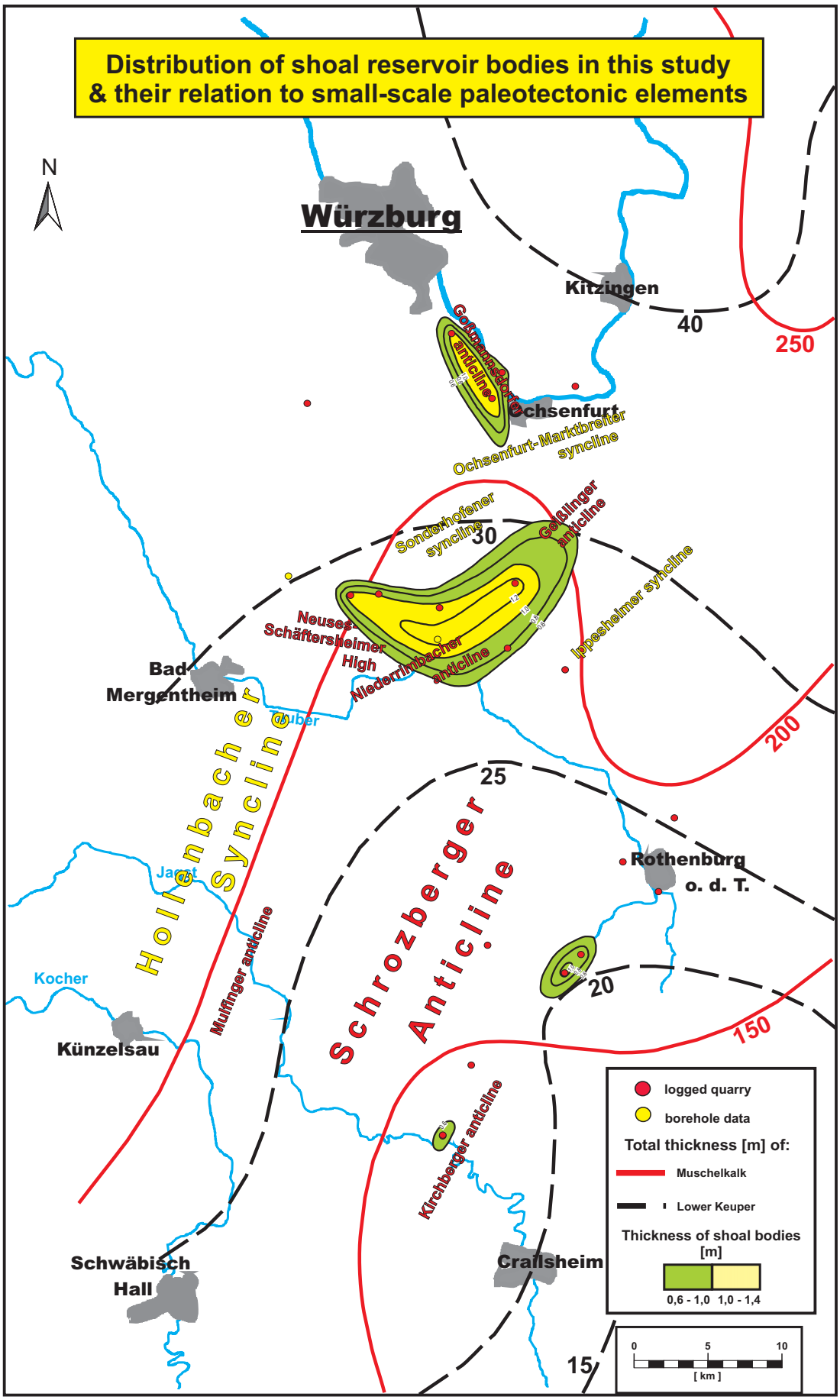

Fig. 35: This map emphasizes the importance of knowledge of the smaller-scale paleotectonic situation. Preferred shoal accumulation was observed at presently well-known anticlines (red marked). These shoal bodies are separated by well-established synclines again (yellow marked). Additionally the particular shoal bodies roughly follow the Muschelkalk / Unterkeuper isopachs and clearly cluster around their peaks. This map also demonstrates the improved prediction of exact shoal reservoir body positions by integration of smaller-scale, subregional paleotectonic datasets plus regional isopach maps.

This pattern suggests, that the evolution of carbonate shoal bodies with reservoir potential is controlled by smaller-scale paleotectonic elements within a regional paleotectonic high (compare Figs. 34 & 35).
Thus exact positions of shoal reservoir bodies may be predicted only by integrating subregional-scale structural information in addition to regional data (e.g. isopach maps).

7.3.2 Paleocurrents

Abundant storm-generated sedimentary structures like hummocky cross-stratification and tempestites, a high degree of amalgamated, cross-bedded event sheets, the relationship between foreset direction and wave ripple orientation are indicative for a high-energetic wind/storm-dominated hydrodynamic regime.
Paleocurrent data were measured in trough cross-bedded carbonate sanddunes. They were taken from the skeletal and oolitic grainstone units between the „Tonhorizont ζ“ and the „Dolomitischer Mergel α“ (fundamental cycles 5 & 6), supplemented by measurements from KOSTIC (2001) and AIGNER (1985). The results are summarized in Fig. 36 and show a predominant alongshore transport towards the NE / NNE. In addition onshore (E, SE) and offshore (NW, W) directed sediment transport was measured.
AIGNER (1985) reconstructed the dynamic processes on the Upper Muschelkalk carbonate ramps. Northeastern winds and storms induced combined geostrophic bottom flows, while surface water flows were forced by the Coriolis effect (Ekman-transport) onshore (eastwards). The landward transport of surface water caused a water build-up (formation of spillovers) which was compensated by offshore directed bottom return flows (erosion of surge channels and deposition of proximal tempestites). Fig. 10 provides a 3-D model of depositional environment including the paleocurrents.
Some tidal paleocurrent influence is likely as evidenced by opposite dips in some trough cross-bedded carbonate sandwave (see also KOSTIC, 2001). Tidal processes however play a minor role in shoal evolution compared to the storm-dominated hydrodynamic regime.
The frequently observed orientation of carbonate sand bodies either in SW-NE- (alongshore) direction or perpendicular in SE-NW- (onshore / offshore) direction can be explained by the prevailing sediment transport mainly alongshore (storm-induced geostrophic currents) as well as onshore (diversion of surface currents by Coriolis effect) and additionally offshore (by bottom return flows). The slightly asymmetrical geometry of most shoal complexes with steeper southern margins compared to smoother northern slopes may be explained by windward / leeward effects.

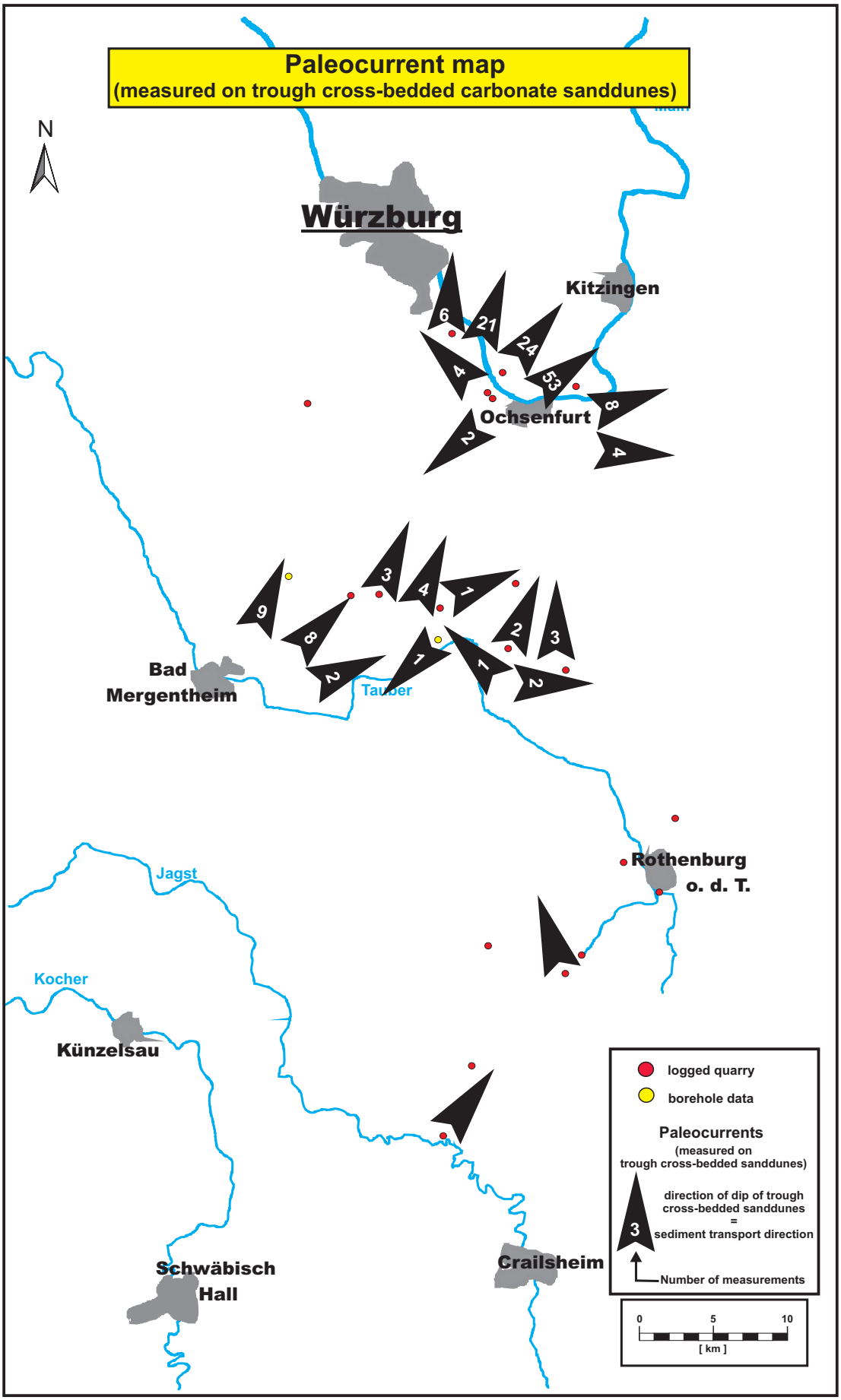

Fig. 36: Paleocurrent measurements show a predominant alongshore (NE / NNE) sediment transport by storm induced geostrophic currents. Subordinate onshore (E / SE) oriented carbonate sand bodies as well as offshore (NW / W) transport occur. Northern paleocurrent data (Q 17) are taken from KOSTIC (2001) and southern data (Q 1 & 3) are taken from AIGNER (1985).

8. Summary of Results (see Fig. 37) Note: (*= Average values)

The purpose of this outcrop analog study was a detailed analysis of the architecture, high-resolution sequence stratigraphy and poro-perm distribution of shelly-oolitic reservoir bodies on a shallow carbonate ramp. The Muschelkalk represents excellent outcrop analogs for epeiric carbonate systems in the Middle East (e.g. Khuff, Hanifa, Arab reservoirs). The following general patterns were recognized:

1. Lithofacies types with reservoir quality are coarse arenitic to ruditic, shelly grainstones, characterized by primary interparticle pore space enhanced by separate-vug (moldic) porosity.
2. The lithofacies types are arranged in 3 facies associations (shoal, transitional shoal and offshoal facies association). The best reservoirs are the shoal facies association.
3. The internal structure of shoal geobodies is more complex than known so far, with several facies types that are concentrically arranged. Generally shell hash grainstones are fringing the oolitic shoal center.
4. The best reservoir facies types are (1) shell hash grainstones ($\Phi^* = 15$ %, $k^* = 45$ mD) and (2) poorly sorted, bioclastic grainstones ($\Phi^* = 13$ %, $k^* = 82$ mD), both on the wind-sheltered leeward sides of the shoals.
5. In order to relate lithofacies types to their petrophysical properties, their rock-fabric (modified DUNHAM textures) was linked to the pore-types, resulted in petrophysical rock-fabric types (LUCIA, 1999) with distinct poro-perm properties, reflecting their specific reservoir potential.
6. Diagenesis was mostly porosity-destructive with four marine cementation phases. Porosity creation took place by (meteoric) leaching after initial early diagenesis.
7. Meter-scale shallowing (-deepening) cycles form the smallest stratigraphically correlatable units (fundamental cycles). Shoal facies occur in the top parts of these cycles.
8. The stacking pattern of these fundamental cycles builds larger-scale regressive and transgressive trends.
9. Within a larger-scale regression a systematic increase in the abundance, size and thickness of shoal bodies was observed. Central oolite shoal facies are prominently developed.
10. During large-scale transgression, shoal bodies decrease in number and size, but porosity and mainly permeability is increased due to the predominance of shelly shoal facies in contrast to low-permeable oolite shoal facies.

11. The geometries and dimensions of the shoal reservoir bodies display the following general patterns:
    a) Shoals are oval elongated geobodies, oriented parallel or perpendicular to the shoreline (Fig. 37). Their slightly asymmetrical topography is caused by a shallow inclined landward- (leeward) and steeper dipping seaward (windward) side.
    b) Individual shoal reservoir bodies are up to 18 km x 8 km in extend and up to 2 m thick.
    c) Length / thickness proportions of shoal bodies indicate that the average thickness is approximately 1 m what seams to correspond in length to 4 – 6 km. This relationship is also valid for the porous reservoir portion of shoal geobodies.
12. High resolution sequence stratigraphic correlations (of 21 logs) document the vertical and lateral distribution and general seaward stepping of the shoal bodies during large-scale regression, building multiple reservoir storeys (Fig. 37).
13. Three factors are considered to control the distribution and evolution of carbonate shoal complexes with reservoir potential:
    a) Cyclicity, controlled by hierarchical eustatic sealevel oscillations: Preferred accumulation of grainstones with primary interparticle porosity enhanced by meteoric leaching is restricted to shallow water sites during maximum regression.
    b) Regional differential subsidence of basement blocks: (1) Generally preferred shoal facies accumulation takes place on regional, paleotectonic highs caused by subtle paleotectonic uplift or lower subsidence rates. The exact position of shoals reservoir bodies on the regional highs are difficult to predict. (2) Individual shoal bodies appear to be located on local, small-scale paleotectonic highs which correspond to subtle, present-day anticlines, separated by synclines within the regional-scale high. Thus prediction of shoal reservoir bodies may be possible by integration of subregional structural data.
    c) Paleocurrent, storm and wind direction: Shapes, alignment and extension of shoal bodies are influenced by their effects on sediment dynamics.

The present outcrop analog study demonstrates that the reservoir potential of investigated shoal geobodies appears to follow systematic rules. These are likely to be useful for predicting the reservoir architecture in productive hydrocarbon provinces of the storm-dominated carbonate ramp type. Furthermore the quantitative data provided by these outcrop analogs may be used as input data for building static reservoir models.

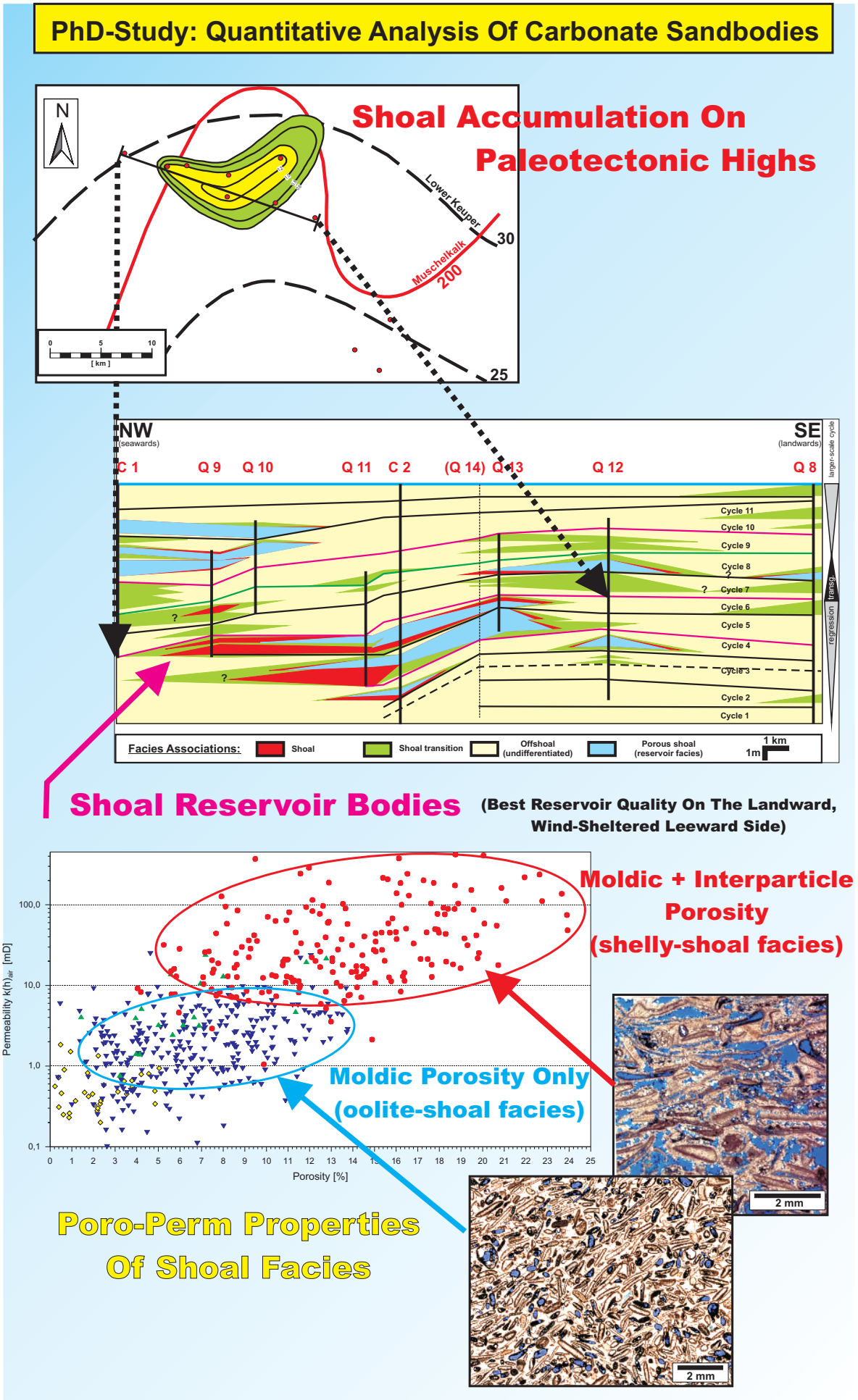

Fig. 37: The present outcrop analog study demonstrates that the reservoir potential of investigated shoal geobodies follows systematic stratigraphic and paleotectonic trends.

9. Acknowledgements

First of all, I would like to express my love and highest gratitude to my girlfriend Silke for her infinite patience, tolerance, encouragement and intense support during the whole project. Thank you for ALL.

Special thanks are due to Prof. Dr. T. Aigner who supervised this work in his unrivaled enthusiastic manner. The creative discussions with him as well as his ideas, experience, supervision and improvement influenced not only the quality of this work but also my education as sedimentologist in a very special way.

Furthermore I would like to thank Prof. Dr. H-P. Luterbacher for his examination of this PhD thesis.

In particular I want to thank my companion, the Muschelkalk-champion Ravi Borkhataria who created a comfortable, personal, very productive scientific atmosphere in our office. Continuous exchange, fruitful discussions and his stimulating ideas make our common Muschelkalk-time unique, not to forget our countless opulent dinners at the institute and so much more.

I am also very grateful to Dr. H. Hagdorn and at the Geological Survey of Bavaria Dr. H. Weinig and Dr. W. Freudenberger for their collaboration (cores, literature etc.), initial introduction and navigation to the outcrops of the Lower Franconian Upper Muschelkalk.

Especially I would like to thank Dr. M. Pöppelreiter (NAM / Shell) for his effort to give this research project publicity at Shell and his extreme engagement for the Muschelkalk field workshops, especially as editor of the excellent guide book. His report examinations, challenging questions, discussions and ideas strongly enriched this study.

Thanks go to the present and former colleagues of the research group „sedimentary geology“ at Tuebingen University for the comfortable atmosphere and their openness for discussions and cooperativeness, especially M. Ruf, R. Borkhataria, B. Kostic (the Muschelkalk experts), M. Schuh (the computer guru), Dr. U. Asprion, Dr. J. Hornung, Dr. W-D. Junghans (the wise men), E. Link (my Lord of the Ring companion) and F. Prousa (the traveler).

A special thank to the (former-) „Darmstadt University companions“ R. Meinke, Dr. A. Götz (Halle), Dr. S. Feist-Burkhardt (London) and N. Rameil (Fribourg). Your familiar ambience and warm, hearty welcome at conferences and field trips is highly appreciated.

I am also grateful to the NAM delegation, K. Pipping, G. Hoetz and G. Louwaars for their collaboration, interest and discussion contributions concerning this outcrop analog study.

The following persons, quarry operators and owners are gratefully acknowledged for their help, information and access to their outcrop(s):
Fa. Renninger Steinbruch-Erdbau (Giebelstadt) in particular Mr. Renninger & Mr. Gast, Fa. Vetter Stein-Industrie (Eltmann), Fa. Kraemer Bau- & Steinindustrie (Ochsenfurt), A. Wirths Steinwerke (Geroldshausen), Fa. Manger Schotterwerke (Aub), A. Baumann Steinbruch (Buch), K. & K. Bopp, A. & A. Krieger (Lenzenbrunn), B. Schenk (Riedenheim), G. Völkert (Nassau), S. Scheubert (Bernsfelden), A. Göller (Bernsfelden), Mr. Schor (Westfränkische Schotterwerke, Marktbegel), K. Breitenbücher Schotterwerk-Baugeschäft (Steinsfeld), Fa. Soldner Schotterwerke, especially A. Baumann (Dürrenhof), T. Hepp Bauunternehmung-Baustoffe (Rothenburg), Fa. Schneider Schotterwerke (Gammesfeld), in particular Mr. Schneider himself, Fa. SHS Steinbruchbetriebe, in particular Mr. Klenk, Mr. Hayh, Mr. Kreidel & Mr. Eckart (Schrozberg), K. Wüstler Steinwerke (Kirchberg).

Fam. Berghold (Röttingen), Fam. Weininger (Steinsfeld), Fam. Brand (Reichenberg), M. Kupfer & J. Faul (Würzburg) are gratefully acknowledged for their pleasant accommodation during the field work phase.

Last but not least I thank the sponsor Shell International Exploration and Production B.V. (Rijswijk) for the financial support of EMR-project (CP – 00621), especially Dr. G. Warrlich and Dr. J. Borgomano (SEPTAR) for examination and suggestions.

10. References

Aigner, T., (1985) : Storm depositional systems. Dynamic stratigraphy in modern and ancient shallow marine sequences. – Lecture Notes in Earth Sciences No. 3, Springer, Berlin.

Aust, H., (1969) : Lithologie, Geochemie und Paläontologie des Grenzbereiches Muschelkalk-Keuper in Franken. – Abh. Naturwiss. Ver. Würzburg, **10** : 3-155.

Bachmann, G.H. & Gwinner, M.P., (1971) : Nordwürttemberg. – Sammlung Geolog. Führer, No. 54, Gebr. Borntraeger.

Bachmann, G.H., (1973) : Die karbonatischen Bestandteile des Oberen Muschelkalks (Mittlere Trias) in Südwest-Deutschland und ihre Diagenese. – Arb. Inst. Geol. Paläont. Univ. Stuttgart, N.F. 68 : 1 – 99.

Bachmann, G.H., (1979) : Bioherme der Muschel *Placunopsis ostracina* v. Schlotheim und ihre Diagenese. – N. Jb. Geol. Paläont. Abh. **158**, Stuttgart : 381 – 407.

Bathurst, R.G.C., (1975) : Carbonate sediments and their diagenesis. Elsevier, Amsterdam : pp. 658.

Behr, H.J., Engel, W., Franke, W., Giese, P., & Weber, K. (1984) : The Variscan Belt in Central Europe : Main structures, geodynamic implications, open questions. – Tectonophysics, 109: 15 – 40.

Choquette, P.W. & Pray, L.C., (1970) : Geologic nomenclature and classification of porosity in carbonates. – Bull. AAPG, Geol. **54**/2 Littleton, Col. : 107-250.

Dercourt, J., Ricou, L.E., Wrielynck, B. (eds.) (1993) : Atlas Tethys Paleoenvironmental maps. Gauthier-Villars, Paris.

Dott, R.H.Jr. & Bourgeois, J., (1982) : Hummocky stratification: Significance of its variable bedding sequence. – Geol. Soc. Am. Bull., 93 : 663 – 680.

Drexler, P., (1964) : Der Quaderkalk im Hauptmuschelkalk Frankens (Eine geowissenschaftliche Studie). – Diss. Univ. Würzburg: 140pp.

Dunham, R.J., (1962) : Classification of carbonate rocks according to depositional texture. – Mem. AAPG **1**, Tulsa : 108-121.

Flint, St. & Bryant, I.D. (eds.),(1993) : The geological modeling of Hydrocarbon Reservoirs and Outcrop Analogies. - IAS Special Publication No. **15**, Blackwell Scientific Publications, London.

Geyer, O.F. & Gwinner, M.P., (1991) : Geologie von Baden-Würrtemberg. – Schweizerbart, Stuttgart.

Goldhammer, R.K., Oswald, E.J., and Dunn, P.A., (1991) : Hierarchy of stratigraphic forcing: Example from the Middle Pennsylvanian shelf carbonates of the Paradox Basin; in E.K. Franseen, W.L. Watney, C.G. Kendall, and W. Ross, (eds.), Sedimentary Modeling: Computer Simulations and Methods for improved Parameter Definition. - Kansas Geological Survey Bulletin 233 p. : 361-413.

Hagdorn, H., (1982) : The „Bank der kleinen Terebrateln“ (Upper Muschelkalk, Triassic) near Schwäbisch Hall (SW-Germany) – a tempestite condensation horizon. In: Einsele, G. & Seilacher, A. (eds.), Cyclic and event stratification. – Springer, Berlin : 263-285.

Hagdorn, H. & Simon, T., (1985 + 1988) : Geologie und Landschaft des Hohenloher Landes. – Jan Thorbecke Verlag, Sigmaringen : 88 - 94.

Hagdorn, H. (eds.), (1991) : Muschelkalk – A field guide. – Goldschneck, Stuttgart, Korb : 12.

Hagdorn, H., Horn, M. & Simon, T., (1993) : Vorschläge für eine Lithostratigraphische Gliederung und Nomenklatur des Muschelkalks in Deutschland. – In: Hagdorn, H. & Seilacher, A., [Hrsg.]: Muschelkalk. Schöntaler Symposium 1991. – Sonderbde. Ges. Naturkde. Württ., Band 2. – Goldschneck, Stuttgart, Korb : 39 – 46.

Hatzold, W., (1981) : Zum Quaderkalk (Trias,mo) Frankens. – J. ber. Mitt. Oberrhein. Geol. Ver., N.F., 63: 211-217, Stuttgart.

Hüssner, H., (1991) : Rifftypen im Muschelkalk Süddeutschlands. - In: Hagdorn, H. & Seilacher, A., [Hrsg.]: Muschelkalk. Schöntaler Symposium 1991. – Sonderbde. Ges. Naturkde. Württ., Band 2. – Goldschneck, Stuttgart, Korb : 261 – 269.

Kerans,C. & Tinker, S., (1997) : Sequence Stratigraphy and Characterization of Carbonate Reservoirs. – SEPM Short Course No. 40, Tulsa : 130 pp.

Kirkham, A., (1997) : Shoreline evolution, aeolian deflation and anhydrite distribution of the Holocene, Abu Dhabi. – Geo Arabia, Vol. 2, No. 4 : 403 – 416.

Kostic, B., (2001) : Sedimentäre Strukturen, Fazies und Poroperm-Eigenschaften in ausgewählten „Karbonatsanden“: Quaderkalk, Oberer Muschelkalk. – Diploma Thesis, University of Tübingen, unpublished.

Kozur, H., (1974) : Biostratigraphie der germanischen Mitteltrias. – Freib. Forschungsh., C 280: 7-56.

Krimmel, V., (1980) : Epirogene Paläotektonik zur Zeit des Keupers (Trias) in Südwest-Deutschland. – Arb. Inst. Geol. Paläont. Univ. Stuttgart, N.F. 76 : 1-74.

Lucia, F.J., (1983) : Petrophysical parameters estimated from visual description of carbonate rocks: a field classification of carbonate pore space. – J. Pet. Technol. March : 626-637.

Lucia, F.J., (1995) : Rock fabric / petrophysical classification of carbonate pore space for reservoir characterization. – Bull. AAPG 79/9 : 1275-1300.

Lucia, F.J., (1999) : Carbonate reservoir characterization. – Springer, Berlin : 226 pp.

Marsaglia, K.M. & Klein, G. de V., (1983) : The paleogeography of Paleozoic and Mesozoic storm depositional systems. – J. Geology, 91 : 117-142.

Matthews, R.K., (1984) : Dynamic Stratigraphy. – Prentice-Hall, New Jersey, 2nd ed., 489 pp.

Pöppelreiter, M., (1999) : Controls on epeiric successions exemplified with the mixed siliciclastic-carbonate Lower Keuper (Ladinian, German Basin). – Tübinger Geowissenschaftliche Arbeiten, Reihe A, Band 51.

Rausch, R. & Simon, T. (1988) : Lithostratigraphische Untersuchungen im Oberen Muschelkalk der östlichen Hohenloher Ebene. – In H. Hagdorn [Hrsg.] : Neue Forschungen zur Erdgechichte von Crailsheim. – Sonderbde. Ges. Naturkde. Württ., Band 1. - Goldschneck, Stuttgart, Korb : 22-42.

Reinhold, C., (1997) : Dog-tooth cements: indicators of different diagenetic environments. – Zbl. Geol. Paläont. Teil 1, H. 10-12, Stuttgart : 1221 – 1235.

Ruf, M., (2001) : Facies distribution, petrophysics and mapping of selected carbonate sand bodies in the Upper Muschelkalk, South German Basin: A reservoir analogue investigation. – Diploma Thesis, University of Tübingen, unpublished.

Rutte, E., (1957) : Einführung in die Geologie von Unterfranken. – Laborarztverlag, Würzburg : 168 pp.

Schauer, M. & Aigner, T., (1997) : Cycle stacking patterns, diagenesis and reservoir geology of peritidal dolostones, Trigonodus-Dolomit, Upper Muschelkalk (Middle Triassic, SW-Germany), Facies 37: 99-114.

Schuster, M., (1928) : Abriß der Geologie von Bayernr r.d. Rh. – VI. Abt. – Oldenbourg u. Pilot & Loehle, München : 119 S.

Smith, A., Hurley, A.M., & Briden, J., (1981) : Phanerozoic paleocontinental world maps. – Cambridge Univ. Press, Cambridge : pp. 102.

Strasser, A. & Davaud, E., (1983) : Black pebbles of the purbeckian (Swiss an French Jurassic): lithology, geochemistry and origin. – Eclogae Geol. Helv. 76 : 551 – 580.

Tucker, M.E., & Wright, V.P., (1990) : Carbonate sedimentology. – Blackwell Sience Ltd : 314 – 364.

Vail, P.R., (1987) : Seismic stratigraphy interpretation using sequence stratigraphy: In Bally, A.W., Atlas of seismic stratigraphy. - Am. Association of Petroleum Geologists, Studies in Geology Nr.**27**, v. 1 : 1-10.

Vollrath, A., (1955) : Zur Stratigraphie des Hauptmuschelkalks in Württemberg. – Jh. geol. L.-A. Baden-Württ., **2**: 79-168.

Wagner, G., (1913) : Beiträge zur Stratigraphie und Bildungsgeschichte des oberen Hauptmuschelkalks und der unteren Lettenkohle in Franken. – Geol. Paläont. Abh., N.F., **12**:1-180.

Ziegler, P.A., (1982) + (1990): Geological Atlas of Western and Central Europe. – Elsevier & Shell Intern. Petrol. Maatschappij B.V., Amsterdam, New York.

I

P L A T E S

Plates 6 - 23:

Atlas of Lithofacies Types and their Petrophysical Properties

Note used abbreviations:

r = rare

r-p = rare to present

p = present

p-c = present to common

c = common

a = abundant

Lithofacies Type 1a/b “nodular / massive mudstone”

Description

Texture [Dunham]: Mudstones.

Lithology & color: 1a: Limestone, partly argillaceous / marly, dark- to medium grey. 1b: Dolo-limestones, rarely dolostones, yellowish grey, beige.

Physical sedimentary structures: 1a: Mostly vague or absent lamination resulting massive appearance (c) or nodular fabric due to differential compaction and / or bioturbation (p-c). 1b: Nodular to massive appearance caused by intense bioturbation, primary sedimentary structures are completely obliterated.

Biogenic sedimentary structures: 1a: Weak to intense bioturbated. Burrows of: *Teichichnus* (a), *Rhizocorallium* (c), *Planolites / Paleophycus* (p-c) and *Thalassinoides* (p) plus a large number of poorly defined ichnofabrics are observed. 1b: Intense bioturbation of *Teichichnus* (c) and patchy, poorly defineable burrows (a) cause a mainly mottled fabric.

Grainsize & sorting: 1a/b: Well to moderately sorted, calcilutites, rarely calcisiltites.

Components & frequency: 1a/b: Peloids (r-p), mostly fecal pellets (c), fine bioclastic debris (p), quartz (p).

Thickness: Several cm- to stacked dm-scale sets.

Interpretation

Lithofacies type 1 is almost exclusively composed of lime mud, the accumulation by suspension settling and lack of grain production reflects deposition in very low-energy settings.

1a: Dark to medium grey colored, massive / nodular mudstones are interpreted as distal deposits situated around the storm-wave-base (deeper ramp), depending on the presence / lack of physical sedimentary structures. Indicative is additionally the existing ichnofacies. *Thalassinoides*-, abundant *Teichichnus*- and *Planulites / Paleophycus*- burrows display, according to the paleoecological trends of AIGNER (1985), the transitional area between shallow and deeper ramp, while frequent *Rhizocorallium*-burrows reflect deeper ramp settings. Dark colors and low level or lack of bioturbation are interpreted as evidence for restricted / reduced depositional conditions.

1b: The yellow-beige colored massive / nodular dolo-mudstones already indicates dolomitization. Dolo-lime muds are well-known in very shallow lagoonal- up to supratidal environments (TUCKER & WRIGHT, 1990). They are interpreted as shallow, lagoonal deposits on account of its association to LFT 2b, 3 & 5 and its intense bioturbation of unknown sediment feeders and *Teichichnus*.

The nodular / massive mudstones are interpreted either as distal, low energy deep ramp deposits, situated around the storm-wave-base or as sheltered, nearshore, shallow lagoonal deposits depending on color, lithology, facies association and ichnofacies

Porosity & Permeability

Pore types and occurrence:

(Choquette & Pray, 1970): No pores.

(Lucia, 1999) : No pores.

Rock-Fabric types (Lucia, 1999): No rock-fabric type was defined.

Average Porosity & Permeability Values

No samples are measured.

Poro-perm values are expected below measuring limit.

Conclusion:

The nodular / massive mudstones of LFT 1 are considered as tightly cemented concerning their lutitic grainsize which controls Φ & k.

Poro-perm properties may be slightly increased depending on the degree of dolomitization and the dolomite crystal size of nodular, bioturbated dolo-mudstones of subtype 1b.

Lithofacies Type 1a/b “nodular / massive mudstone”

Photodocumentation of LFT 1a

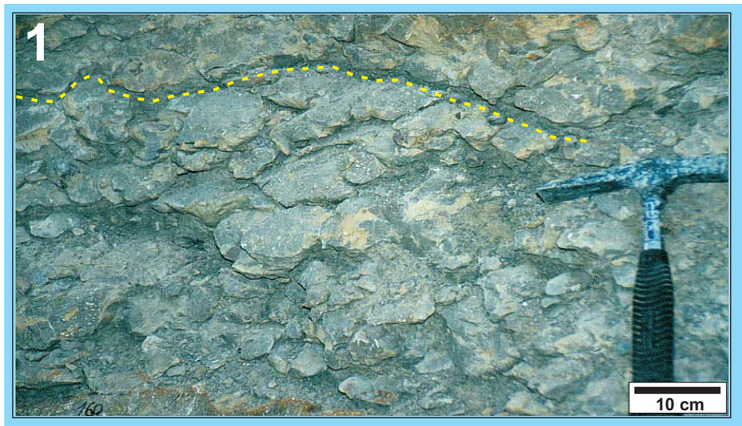

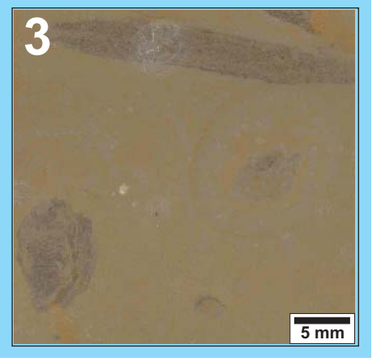

1) The nodular appearance and the dark grey color is indicative for lithofacies type 1a. Each mudstone bed is separated by thin marl drapes (see stippled line).

2 & 3) 1a-type mudstones are either nodular and intensely bioturbated, like example in Fig. 2 or rather massive and weaker bioturbated, as shown in Fig. 3. Level of bioturbation and ichnofacies gives important indications for the respective depositional environment. The dominance of *Teichichnus*- spreiten and the large *Thalassinoides*- burrow (see arrow) ascribes this slab to the transitional area between shallow and deep ramp (according to AIGNER, 1985). The high level of bioturbation reflects aerobic conditions. The *Planolites*- type burrows in Fig. 3 however reflects a deeper ramp setting with rather restricted, poorer (ichnofaunal) living conditions illustrated by its lower bioturbation-index.

Photodocumentation of LFT 1b

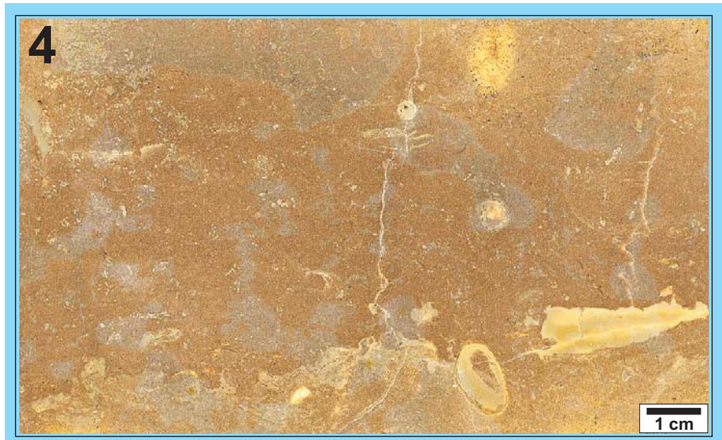

4 & 5) In contrast to the nodular / massive LFT 1a mudstones, the 1b-type dolo-mudstones are bright colored, due to the higher level of dolomitization and bioturbation. Note: Stronger dolomitized patches are linked to distinct borrows. Indicative for LFT 1b is in general the mottled, patchy appearance caused by intense bioturbation, reflecting aerobic conditions. Abundant *Teichichnus*- burrows, like in Fig. 5, are characteristic for these shallow, lagoonal mudstones.

Lithofacies Type 2a/b “laminated & scoured mud- to wackestone”

Description

Texture [Dunham]: Mudstones & mud- to wackestones.

Lithology & color: 2a: Limestone, medium grey. 2b: Limestone / dolo-limestone, beige, light to yellowish grey.

Physical sedimentary structures: 2a: Stacked low angle- to even laminated, mm- to cm-scale calcisiltitic laminae (c), partly interrupted by small-scale scour surfaces, hummocky cross-stratification (p), (micro-) grading (p), washed out trace fossil tiers (c), tool marks (p). 2b: Parallel lamination of calcisiltites (c) and / or fine dolomite crystals (p), lamination often vague or destroyed by bioturbation and therefore massive appearance.

Biogenic sedimentary structures: 2a /b: Weak to moderate bioturbated. *Teichichnus*-, *Rhizocorallium-, Planolites*- and patchy undefineable burrows occur in both subtypes.

Grainsize & sorting: 2a/b: Well to moderately sorted, calcilutite to calcisiltite.

Components & frequency: 2a/b: Peloids (p-c), fine bioclastic debris (c), quartz (p), shell fragments (r-p), small, well-rounded lithoclasts (p).

Thickness: Several cm- to few dm-scale sets.

Interpretation

Laminated lime-mud, caused by suspension settling, reflect quite, low-energetic conditions, while predominant siltitic particles, arranged in mm- to cm- scale (partly micro-graded) laminae, point to episodic storm-induced sediment supply. Scour surfaces indicates storm-reworking.

2a: Low-angle lamination mostly (micro-) hummocks indicate combined flows by storms and paleocurrents (DOTT & BOURGEOIS, 1982). These features, exclusively rounded lithoclasts plus the minor portion of macro-fossils point to a distal subtidal depositional environment as located between middle- and deeper ramp.
2b: The frequent higher degree of dolomitization, initially induced along burrows and the usually high level of bioturbation, plus the association to lithofacies types 3 & 5 indicates a very shallow backshoal, lagoonal setting. The lack of macro-fossils in this case may reflect deviations in marine water quality (salinity, nutrient content etc.).
2a & b: *Rhizocorallium-, Planolites*- as well as *Teichichnus*- burrows are typical traces of sediment feeders, reflecting low energy soft-bottom substrates due to calcilutitic background sedimentation. The first two are more ascribed to deeper ramp areas (LFT 2a), while *Teichichnus* occurs in both, lagoonal and deeper ramp settings (compare e.g. with AIGNER, 1985).

The laminated & scoured mud- to wackestones are interpreted as distal low-energy deposits (deeper ramp), while the laminated & scoured dolo-mudstones are interpreted as low-energy backshoal deposits, located within a very shallow (protected) lagoonal area. Both lithofacies types are influenced by storm-events and bioturbation

Porosity & Permeability

Pore types and occurrence:

(Choquette & Pray, 1970): No pores.

(Lucia, 1999) : No pores.

Rock-Fabric types (Lucia, 1999): No rock-fabric type was defined.

Average Porosity & Permeability Values

No samples are measured.

Poro-perm values are expected below measuring limit.

Conclusion:

Poro-perm properties of mud-dominated limestones like LFT 2 are generally controlled by their mud size (here calcilutite & calcisiltite). Minor pore space was further decreased by compaction and diagenesis. LFT 2 is therefore considered as tightly cemented.

Rare exceptions of slightly increased poro-perm properties are assumed in mud- to wackestones with dolomitic proportions, where dolomite crystal size controls Φ & k values.

Lithofacies Type 2a/b “laminated & scoured mud- to wackestone”

Photodocumentation of LFT 2a

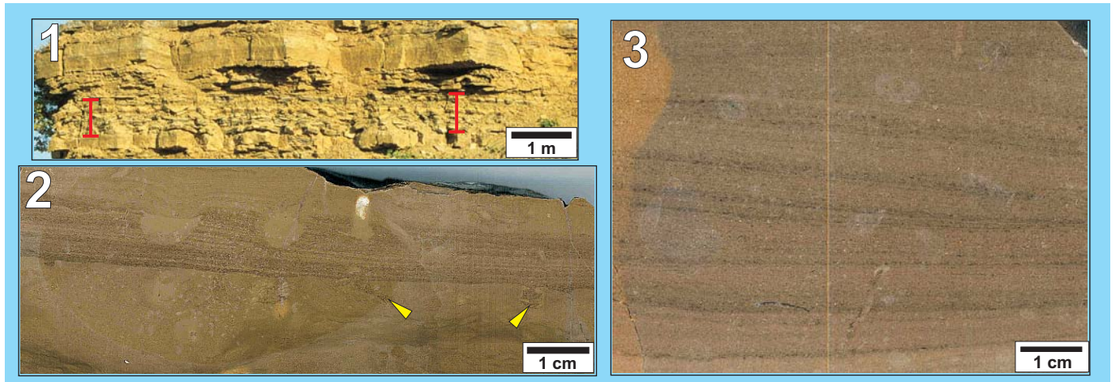

1) The marked succession shows stacked, laminated, scoured mud- to wackestones with dm-scale bed thicknesses. Each set is separated by mm-thin marl drapes.

2) Typical laminated, scoured mud- to wackestone slab with weakly erosive scour surfaces and calcisiltitic laminated lags due to reworking and supply of single storm-events are most indicative for LFT 2a. Washed-out burrows (arrow) and weak to moderate post-event bioturbation from top are further characteristic features.

3) Storm reworking is indicated in this slab by low angle calcisiltitic laminae. Their upward curved stratification point to hummocky cross-stratification reflecting combined flows induced by the interaction of storms and currents (see DOTT & BOURGEOIS, 1982).

Photodocumentation of LFT 2b

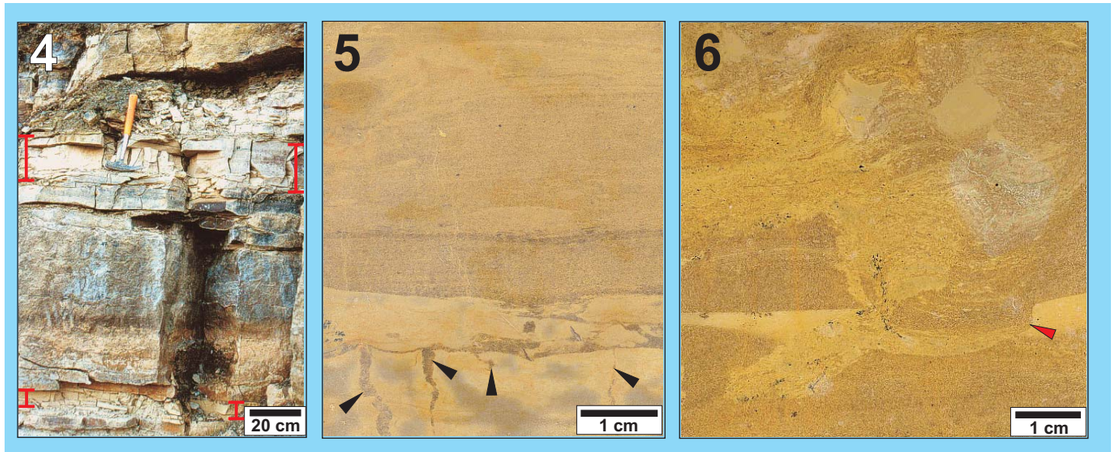

4) Laminated dolo-mudstones are easy recognizable in the field due to their yellow - beige color and massive appearance. The cm- to few dm- thick beds (see brackets) are frequently subject to intense erosion and therefore mostly form hollows in outcrop walls.

5) This slab illustrates all features of a laminated, scoured dolo-mudstone: Stacking of cm- scale calcilutitic or calcisiltitic laminae, frequently scoured by succeeding laminae and the beige color due to the certain level of dolomitization. Dolo-mudstones of the 2b type are commonly bioturbated by burrows of sediment feeding organisms, indicating soft muddy substrates. The black arrows mark likely mud cracks, indicating a subaerially exposed (semi-) consolidated substrate. This supports the interpretation of a very shallow (up to intertidal) lagoonal setting.

6) The usually moderate bioturbation of LFT 2b by feeding structures, here *Teichichnus*- spreiten (see arrow), destructs the characteristic fabric as shown in Fig. 5. Remnants of lamination and scours are visible at the bottom of this bed.

Lithofacies Type 3 “oncolitic wackestone”

Description

Texture [Dunham]: Wackestones.

Lithology & color: Limestone, medium to light grey, greenish grey, beige.

Physical sedimentary structures: Stratification mostly very vague or destroyed, leading to a massive appearance.

Biogenic sedimentary structures: Mostly nodular bedding due to moderate to intense bioturbation of *Teichichnus*- or *Rhizocorallium* burrows and undefined burrows.

Grainsize & sorting: Poorly sorted, coarse calcarenites to medium calcirudites.

Components & frequency: Oncoids (p-c), shells (c), partly bored, with micritic envelopes (p-c), peloids (p-c), black pebbles (r-p), gastropods (r), black debris (r), ophiure ossicles (r), intraclasts (poorly rounded) (r).

Thickness: Cm- to dm-scale sets.

Interpretation

Muddy, poorly sorted, coarse grained oncolitic wackestones and the high degree of bioturbation reflecting a low to moderate hydroenergetic depositional environment.

Oncolites, formed by algae (*Sphaerocodium kokeni*) colonization as well as micritic envelopes and bored shells, caused by microboring organisms indicate quiet, shallow water conditions within the photic zone. Black pebbles however have a variety of origins ranging from staining by organic solutions (in soils), blackening during fires and pyritization, but generally are associated with subaerial exposure surfaces and therefore point to nearshore (lagoonal) settings (see STRASSER & DAVAUD, 1983, STRASSER, 1984, SHINN & LIDZ, 1988).

The oncolitic wackestones are interpreted as backshoal deposits located within a shallow, quiet lagoonal setting

Porosity & Permeability

Pore types and occurrence:

(Choquette & Pray, 1970): Microporosity / dolomitic intercrystalline porosity (r) (assumed).

(Lucia, 1999) : Intergranular / micrporosity (r) (assumed).

Rock-Fabric types (Lucia, 1999): No rock-fabric type was defined.

Average Porosity & Permeability Values

No samples are measured. Low poro-perm values are expected.

Conclusion:

Oncolitic wackestones are considered as tightly cemented due to the lack of dissolved components and a high portion of mud.

Dolomitization, mainly of burrows and bioturbated parts may slightly increase the poro-perm properties of LFT 3.

Photodocumentation

This slab shows all characteristic features of LFT 4:

Oncoids (see red arrows). Their regular shapes in this slab requires frequent over-turning and therefore reflects continuous reworking.

Black pebbles, the largest are marked by black arrows, are ascribed to nearshore settings (peri-/ intertidal, see e.g. STRASSER & DEVAUD, 1983).

Thick **micritic envelopes**, here around very large unbroken shells (white arrows) reflecting relatively quiet shallow marine conditions.

Intense bioturbation, (see mottled fabric) indicates to quiet depositional environments.

Lithofacies Type 4 “bioturbated bioclastic wacke- to packstone”

Description

Texture [Dunham]: Wackestones & wacke- to packstones.

Lithology & color: Limestone: Medium to light grey, greenish, beige.

Physical sedimentary structures: Frequently poorly or vague stratified (c) and therefore massive appearance.

Biogenic sedimentary structures: Nodular bedding (c) by moderate to intense bioturbation, *Teichichnus-*, *Rhizocorallium-* & undefined borrows (c).

Grainsize & sorting: Moderately to poorly sorted, coarse calcarenites to medium calcirudites.

Components & frequency: Shells (c), brachiopods (p-c), fragmented as well as wholly preserved, ooids (p-c), coated grains (p-c), bio- & intraclasts (p-c), peloids (p), black pebbles (r-p).

Thickness: Cm- to dm-scale sets.

Interpretation

Wackestone texture, moderate to poor sorting and coarse particle sizes as well as partly intense bioturbation attests moderate hydroenergetic conditions and rather quiet depositional environments.

Ooids (mostly dolomitized), coated grains and the exclusive occurrence of bivalve shells indicate shallow water origin, while mainly brachiopod- composed wackestones points to open marine, more distal settings.

The bioturbated bioclastic wackestones are interpreted, depending to their composition, as distal mid ramp to deep ramp deposits or shoal (spillover-) derived backshoal / lagoonal deposits

Porosity & Permeability

Pore types and occurrence:

(Choquette & Pray, 1970): Moldic (r-p), vug (r-p).

(Lucia, 1999) : Separate-vug (r-p).

Rock-Fabric types (Lucia, 1999): Bioturbated bioclastic wackestones & wacke- to packstones with separate-vug porosity *(4-sv)*

Average Porosity & Permeability Values

4-sv (n=15 plug samples)

Φ = 2,96 %, $k(h)_{air}$ = 0,80 mD, $k(v)_{air}$ = 0,81 mD

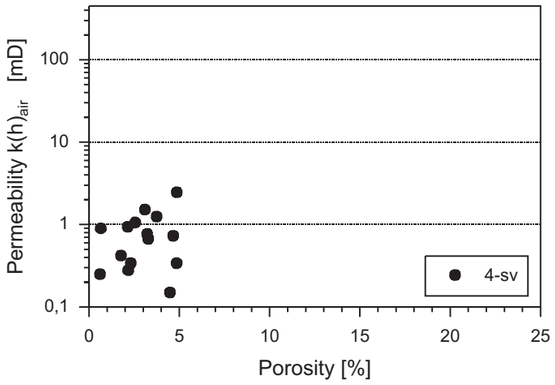

Conclusion:

The particle composition essentially determines the porosity of the respective bioclastic wackestone. Constituents like ooids and bivalves are more frequently dissolved and therefore slightly increase the porosity of LFT 4 in contrast to rarely dissolved brachiopods.

Permeability and reservoir potential is low.

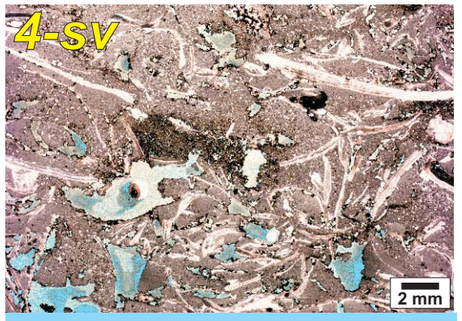

In rare cases non-fabric selective vuggy pores (blue stained) increase porosity above 5% and permeability above 1 mD.

Lithofacies Type 4 “bioturbated bioclastic wacke- to packstone”

Photodocumentation

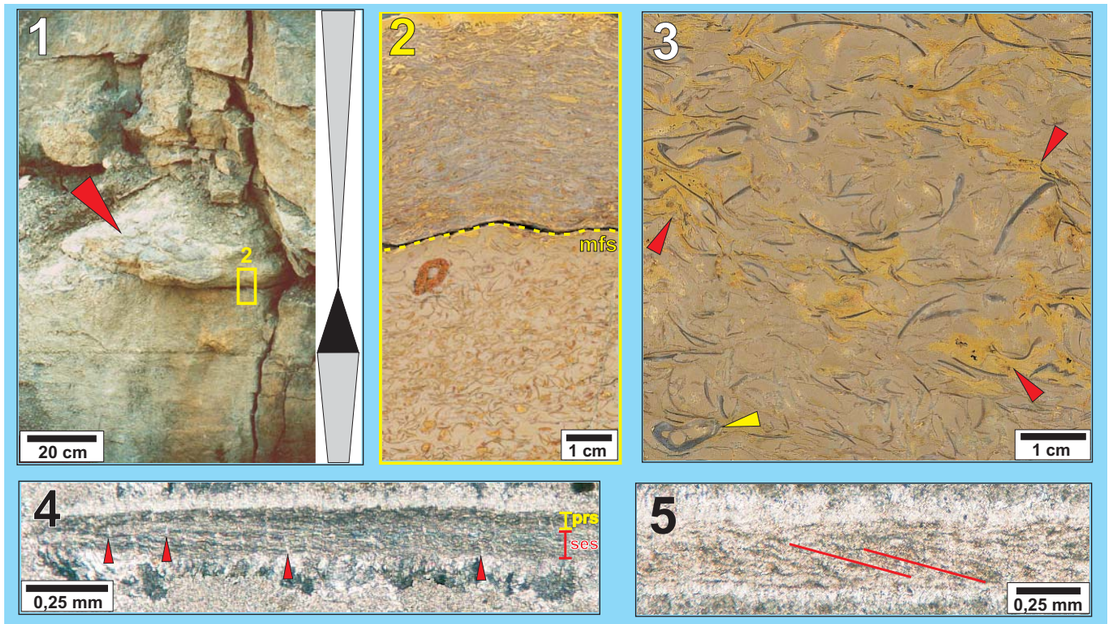

1) Bioturbated bioclastic wackestones & wacke- to packstones within a fundamental cycle are mostly observed in the transgressive hemi-cycle and / or the initial regressive hemi-cycle part (here below and above the marked *Placunopsis*-bioherm).
2) Detailed view of Fig. 1 (see frame) showing a bioclastic wacke- to packstone slab, reflecting moderate to low hydrodynamic conditions, succeeded by a *Placunopsis* boundstone (LFT 14), indicating very low sedimentation rates within a quiet setting (mfs = max. flooding surface).
3) Predominantly large brachiopod shells, even completely preserved (yellow arrow), the lack of shallow marine indicators (ooids etc.) and intense bioturbation (dolomitic patches, red arrows) point to open marine conditions and a rather quiet deeper ramp setting.
4 & 5) The illustrated microstructures of brachiopod shells emphasize the excellent preservation potential of these open marine bioclastic wackestones of LFT 4. In Fig. 4 the upper calcareous primary layer (prs, dark grey) may be distinguished from the lower secondary layer (ses) consisting of inclined calcitic rods (fibres, medium grey, indicated in Fig. 5 by red lines). The perforations (red arrows), regularly penetrating the shell from the inside, point to an endopunctate brachiopod shell, typical for e.g. terebratulides.

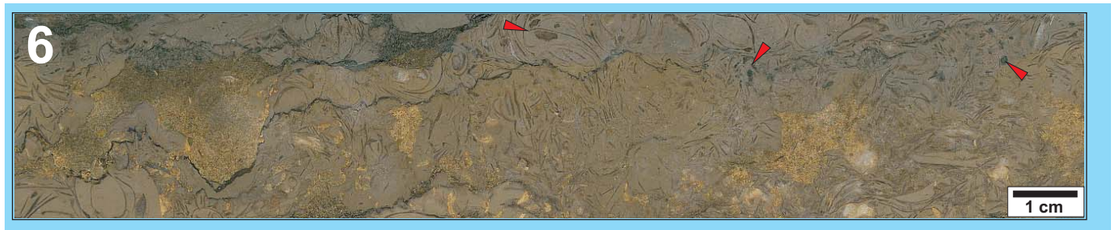

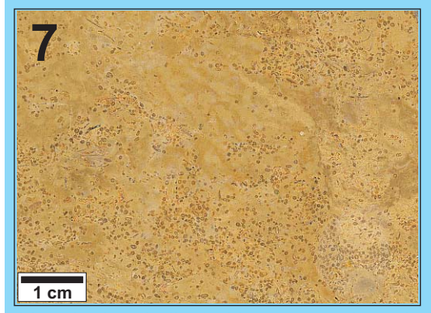

6) The admixture of particles, predominantly bivalve shells plus black pebbles (arrows), representing backshoal environment. According to STRASSER & DAVAUD, (1983) black pebbles are ascribed to near-shore lagoonal settings. Wave-dominated hydrodynamic conditions may attested by edge-wise fabrics of shells indicating oscillatory flows while dolomitic patches due to intense bioturbation appear during lower energetic background sedimentation.
7) This slab is another example of a bioturbated bioclastic wackestone. Indicators for its backshoal / lagoonal origin are: Large, mostly dolomitized ooids and coated grains (remnants of shoal spillover events), exclusively bivalve shells and intense bioturbation (indicated by a general mottled fabric and burrows, e.g. *Teichichnus*, on the right-hand side).

Lithofacies Type 5a/5b “oncolitic packstone / black pebble packstone”

Description

Texture [Dunham]: Packstones.

Lithology & color: Limestone, 5a: Beige, yellow to light grey. 5b: Medium to light grey.

Physical sedimentary structures: 5a: Even- lamination (p), more often vague and therefore massive appearance. 5b: Parallel lamination by aligned components (c), rarely low angle cross-bedding.

Biogenic sedimentary structures: 5a/b: Moderate bioturbation, patchy by poorly defineable burrows.

Grainsize & sorting: 5a/b: Poorly sorted, coarse calcarenites to medium calcirudites.

Components & frequency: 5a: Oncoids (c), bored shells (c) fragmented as well as whole body preserved + micritic envelopes (p-c), coated grains (p), ooids (r). 5b: Black pebbles (c), shells (c) + micritic envelopes (p-c), peloids (p).

Thickness: Cm- to dm-scale sets.

Interpretation

Texture, poor sorting and ruditic particle sizes reflecting a moderate, not constant paleo-hydroenergy.

5a: The oncolite packstone is mostly associated with the oncolite grainstone (LFT 12) and therefore is interpreted as marginal channel or oncolite channel deposit.
5b: The laminated to low angle cross-bedded black pebble packstone is interpreted as storm-induced event sheet into a quiet, lagoonal setting.

5a: Oncolites, micritic envelopes and bored shells points to quite shallow water conditions within the photic zone, displayed by microbial borers and algal growth on particles.
5b: Black pebbles indicate nearshore setting (STRASSER & DAVAUD, 1983)

The oncolitic packstones are interpreted as oncolite channel deposits, the black pebble packstones are interpreted as event sheets. Both facies types are located within the shallow subtidal backshoal area (lagoon)

Porosity & Permeability

Pore types and occurrence:

(Choquette & Pray, 1970): Moldic (p), intergranular (r).

(Lucia, 1999) : Separate-vug (p), interparticle (r).

Rock-Fabric types (Lucia, 1999): Oncolitic / black pebble packstones with

separate-vug porosity *(5a/b-sv)*

separate-vug & interparticle porosity *(5a-sv+ip)*

Average Porosity & Permeability Values

5a/b-sv (n=4 plug samples)

Φ = 5,49 %, $k(h)_{air}$ = 1,46 mD, $k(v)_{air}$ = 1,08 mD

5a-sv+*ip* (n=2 plug samples)

Φ = 9,93 %, $k(h)_{air}$ = 11,94 mD, $k(v)_{air}$ = 2,69 mD

Conclusion:

Poro-perm properties in oncolitic / black pebble packstones are controlled by the frequency and size of dissolved particles. The reservoir properties of *5a/b-sv* are rather low.

A rare exception are dolomitized oncolitic packstones, where dolomite crystal size controls additional interparticle pore size *(5a-sv+ip)*. In this case Φ & k values are moderate.

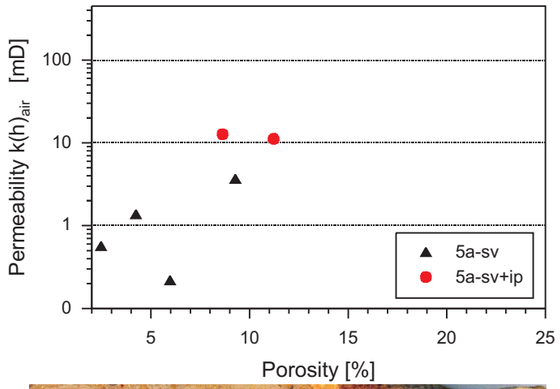

The vast majority of oncolitic or black pebble packstones show some separate-vug porosity (see red arrows). In this slab sample additionally dolomitized particles (yellow / orange colored) occur.

Lithofacies Type 5a/5b “oncolitic packstone / black pebble packstone”

Photodocumentation

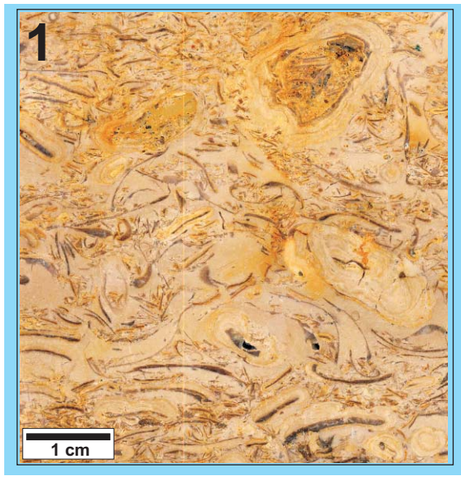

1) Bioclast nuclei are coated by the calcareous algae *Sphaero-codium kokeni* forming cm-size oncoids. Irregular lensoid growth reflects repeated reworking. The colonization by algae indicates shallow water conditions within the photic zone. A formation under fluctuating hydrodynamic activity in channels within a lagoon is assumed.

2) Larger oncoids show multi-phase algal coatings, often interrupted by boring organisms (see arrows) indicating inter-mittence of growth and episodes of reworking (e.g. by storms).

3 & 4) The difference of lithofacies subtype 5b is the abundance of black pebbles instead of oncolites. Black pebbles are ascribed to near-shore (STRASSER & DAVAUD, 1983), lagoon-al settings. Storm influence is indicated by aligned components and sheet-like geo-metries with concen-tration of black pebbles.

Lithofacies Type 6 “laminated skeletal-ooidal packstone”

Description

Texture [Dunham]: Packstones.

Lithology & color: Limestone, light grey to beige.

Physical sedimentary structures: Frequently parallel lamination (a) by aligned skeletal grains, low angle lamination (p), geopetal fabric (p).

Biogenic sedimentary structures: Weak (-moderate) patchy bioturbation, undefined burrows.

Grainsize & sorting: Moderately to poorly sorted, very coarse calcarenite to fine calcirudite.

Components & frequency: Aligned fragmented shells (c) with micritic envelopes (p-c), ooids (c) in various sizes, partly dolomitized, peloids (p), coated grains (r-p), brachiopods (r), intraclasts (r).

Thickness: Cm- to dm scale beds.

Interpretation

Mud-dominated texture and poor sorting attests relatively low energetic background sedimentation. Event sheets of even-laminated aligned components point to phases of episodic higher water-energy, probably induced by storms.

The assemblage of mainly ooids and shells with micritic envelopes indicates supply from the proximal shoal flanks. Lithofacies type 6 is associated with the more proximal facies type 13a.

The laminated skeletal-ooidal packstones are interpreted as storm-generated proximal event sheets, fringing the central shoal area (transition zone to deeper ramp)

Porosity & Permeability

Pore types and occurrence:

(Choquette & Pray, 1970): Moldic (r-p).

(Lucia, 1999) : Separate-vug (r-p).

Rock-Fabric types (Lucia, 1999): Laminated skeletal-ooidal packstones with

separate-vug porosity *(6-sv)*

Average Porosity & Permeability Values

6-sv (n=5 plug samples)

Φ = 4,49 %, $k(h)_{air}$ = 1,12 mD, $k(v)_{air}$ = 0,68 mD

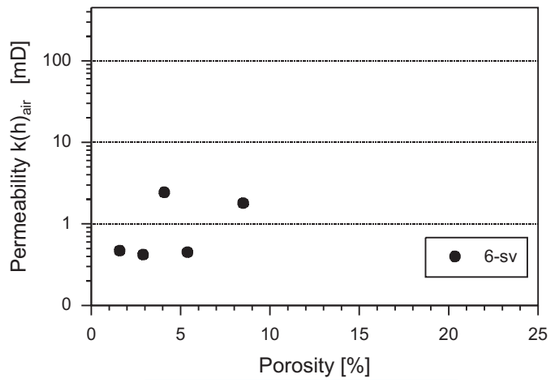

Conclusion:

Poro-perm properties of laminated skeletal-ooidal packstones depend on the number and size of dissolved components. In spite of some oomoldic porosity, reservoir potential of LFT 6 is poor to very poor.

The thin section scan of a laminated skeletal-ooidal packstone demonstrates the very poor reservoir properties of rock-fabric type *6-sv*. Poro-perm properties of this example:
Φ = 1,59 % and k(h) = 0,47 mD, k(h) = 0,30 mD.

Lithofacies Type 6 “laminated skeletal-ooidal packstone”

Sedimentologic log & GR-signature

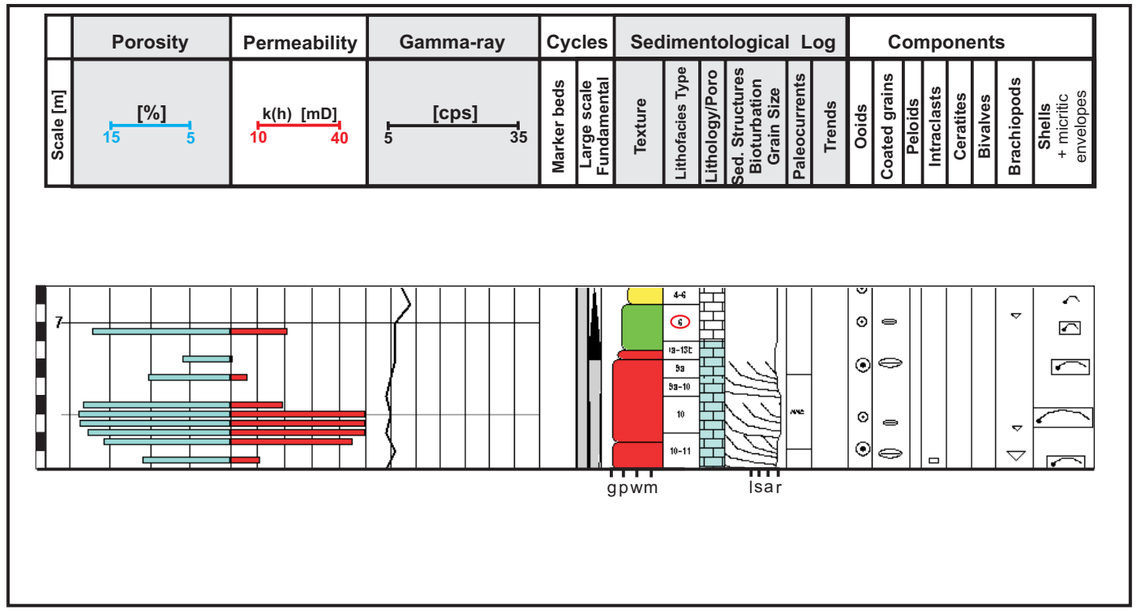

Photodocumentation

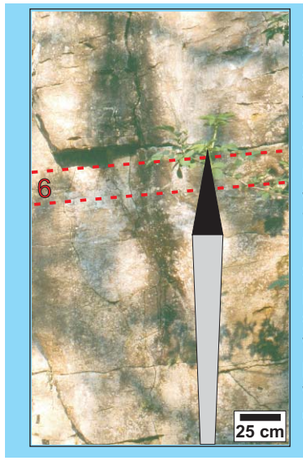

Decreasing hydrodynamic conditions are displayed by this 20 cm thick bed of a laminated skeletal-ooidal packstone (LFT 6) on top of a m-scale oolite sandwave (LFT 9a).
The stacking of cross-bedded oolitic grainstone sets are interpreted as regressive part of a fundamental cycle, while the skeletal-ooidal packstone is located within the transgressive cycle part.

Skeletal-ooidal packstones occur as fringes around the shoal complexes. In some cases foreshoal and backshoal types can be distinguished. Relatively large, dolomitized (yellow) ooids, very large shell fragments, blackened components and increased bioturbation, like in this slab point to a quiet backshoal setting.

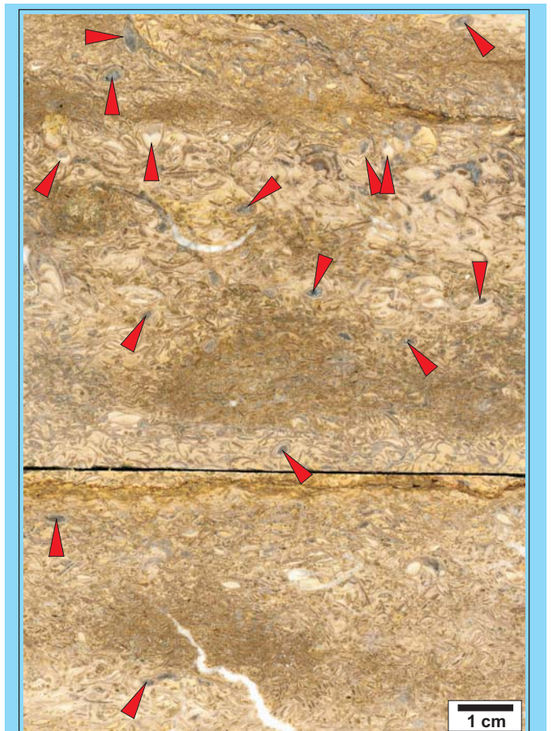

This core-slab shows all features of LFT 6: Even-lamination by aligned shells, presence of fragmented as well as whole body shells (note geopetal fabrics, indicated by red arrows), patch-like accumulation of ooids in certain layers and moderate to poor sorting.

Lithofacies Type 7a “poorly sorted bioclastic packstone”

Description

Texture [Dunham]: Wacke- to pack- & packstones.

Lithology & color: Limestone & dolo-limestone, medium-light grey, beige.

Physical sedimentary structures: Poorly stratified, vague lamination (c), parallel- to low angle lamination (p), umbrella structures (p-c), sharp erosive basis (p), faintly graded (r-p).

Biogenic sedimentary structures: Weak to moderate bioturbation, patchy (dolomitized) burrows (p), *Rhizocorallium*- type burrows (p).

Grainsize & sorting: Poor sorted, fine to medium calcirudites.

Components & frequency: Fragmented as well as whole body preserved brachiopods (a), original preservation of shell structure (c), shells (p) with micritic envelopes (r), bio- and intraclastic debris (p), peloids (r).

Thickness: Cm- to dm-scale sheets.

Interpretation

Poorly sorted, coarse bioclastic wacke- to packstones, common umbrella structures and whole body preserved brachiopods attests episodic higher energetic event sedimentation, probably induced by storms, interrupting lower background sedimentation.

The common occurrence of brachiopods compared to bivalve shells and minor amounts or lack of micritic envelopes, ooids and coated grains point to a more distal, open marine setting of lithofacies type 7a.

The poorly sorted bioclastic wacke- to packstones are interpreted as storm-generated distal offshoal event sheets (deeper ramp)

Porosity & Permeability

Pore types and occurrence:

(Choquette & Pray, 1970): Moldic (p).

(Lucia, 1999) : Separate-vug (p).

Rock-Fabric types (Lucia, 1999): Poorly sorted bioclastic wacke- to packstones with separate-vug porosity *(7a-sv)*

Average Porosity & Permeability Values

7a-sv (n=22 samples)

Φ = 3,99 %, $k(h)_{air}$ = 2,02 mD $k(v)_{air}$ = 1,29 mD

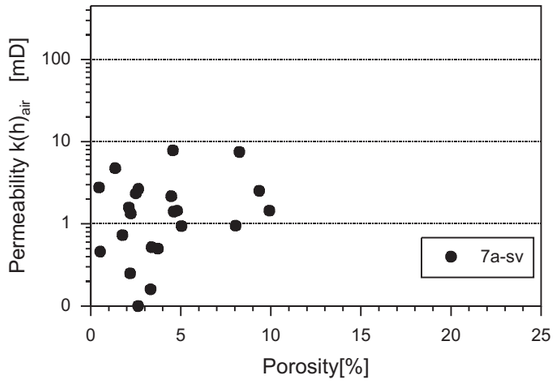

Conclusion:

Amount and size of dissolved particles determine poro-perm properties of poorly sorted bioclastic wacke- to packstones. Brachiopods as main constituent are rarely dissolved, therefore the reservoir potential of LFT 7a is poor.

Minor dolo-mud-dominated fabric occur. In this case additional dolomite crystal size controls connecting pore size, leading to slightly increased poro-perm values.

In brachiopod-shell-dominated bioclastic sheets like LFT 7a, dissolved components are rather rare. The selective dolomitisation around shells (probably due to bioturbation) may increase porosity of this facies.

Lithofacies Type 7a “poorly sorted bioclastic packstone”

Photodocumentation

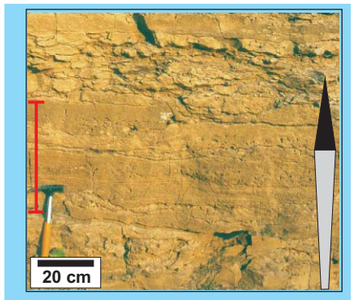

This even-laminated package composed of LFT 7a (marked red) within wackestones (below) and mudstones (above) is interpreted as most regressive part within this fundamental cycle.

Some features of LFT 7a (sheet marked red) are well visible in this core slab. Sharp erosive base, poor sorting and stratification of a coarse-sized bioclastic wacke- to packstone with abundant brachiopods indicate a storm-generated distal event sheet. Note post-event, quiet, muddy background sedimentation.

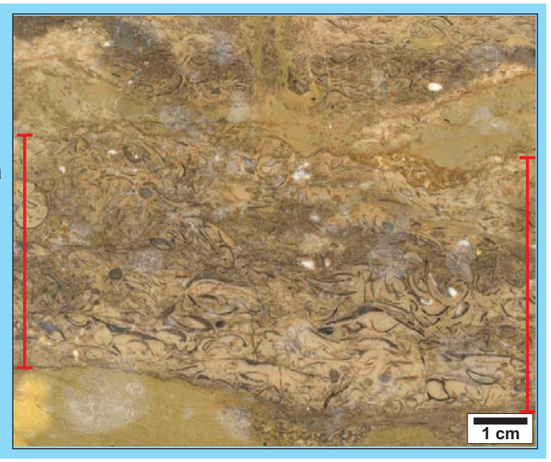

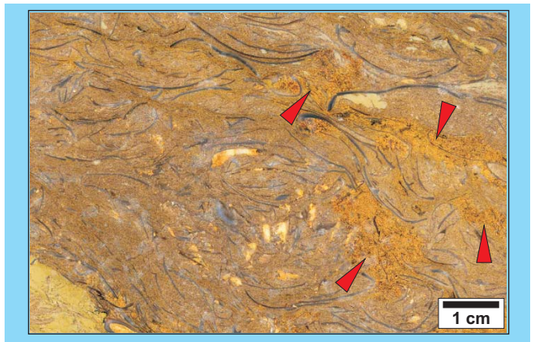

Dolomitic patches, probably due to bioturbation, slightly increase poro-perm properties of LFT 7a.

Main constituent of LFT 7a are large brachiopods indicateing open marine conditions and a deeper ramp setting.

Lithofacies Type 7b “laminated bioclastic wacke- to packstone”

Description

Texture [Dunham]: Wacke- to pack- & packstones.

Lithology & color: Limestone & dolo-limestone, medium-light grey, beige.

Physical sedimentary structures: Frequently parallel- to low angle lamination (c) by aligned shells, sharp erosive basis (p).

Biogenic sedimentary structures: Weak to moderate bioturbation, patchy burrows (p).

Grainsize & sorting: Well to moderately sorted, fine to medium calcirudites.

Components & frequency: Fragmented (bivalve-) shells (a), bored shells may occur as well as micritic envelopes (p), gastropods (r-p), bio- and intraclastic debris (p), brachiopods (r).

Thickness: Cm- to dm-scale sheets.

Interpretation

Frequent parallel- to low angle lamination of erosive scoured layers, mainly composed of fragmented bivalve shells indicate fluctuating hydrodynamic conditions probably caused by storm activity, generating shoal derived event sheets and / or spillover deposits.

The well to moderate sorting of shell fragments and other bioclasts reflect more frequent reworking and transportation. The minor appearance or lack of brachiopods points to a proximal shoal origin of the skeletal components.

The laminated bioclastic wacke- to packstones are interpreted as storm-generated, shoal derived, proximal to medial flanking event sheets and / or spillover lobes (transition shallow to deeper ramp and backshoal)

Porosity & Permeability

Pore types and occurrence:

(Choquette & Pray, 1970): Moldic (p), solution enlarged molds (r), vug (r).

(Lucia, 1999) : Separate-vug (p), touching-vug (r).

Rock-Fabric types (Lucia, 1999): Laminated bioclastic wacke- to packstones with

separate-vug porosity *(7b-sv)*

separate-vug & touching-vug porosity *(7b-sv+tv)*

Average Porosity & Permeability Values

7b-sv (n=18 plug samples)

Φ = 4,92 %, $k(h)_{air}$ = 1,85 mD $k(v)_{air}$ = 0,85 mD

7b-sv+tv (n=2 plug samples)

Φ = 12,42 %, $k(h)_{air}$ = 22,73 mD $k(v)_{air}$ = 3,70 mD

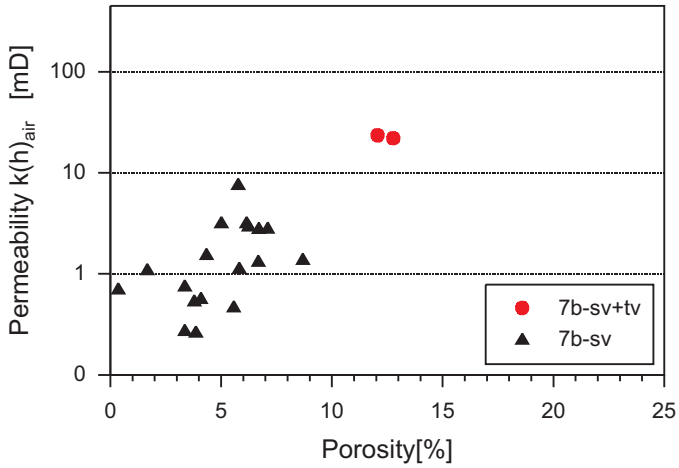

Conclusion:

Reservoir potential of LFT 7b is determined by number and size of dissolved bivalve shells. The porosity is quiet fair but the permeability is poor due to the lack of pore connection.

In rare cases vug to vug connection by solution enlarged moldic pores (partly stylolithes) is present causing touching-vug porosity and therefore increasing the poro-perm properties.

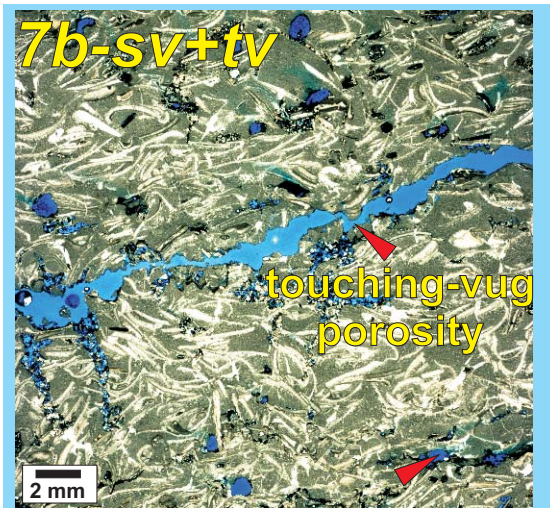

Lithofacies Type 8 “graded bioclastic packstone sheets”

Description

Texture [Dunham]: Wacke- to pack- & packstones.

Lithology & color: Limestone, medium grey.

Physical sedimentary structures: Grading (a) and parallel lamination by aligned components (a), sharp erosive basis (c), umbrella structures (p-c), wave rippled or hummocky cross-stratified tops (r-p), amalgamation (p-c).

Biogenic sedimentary structures: Weak to moderate bioturbation from top, patchy, muddy burrows (p), *Rhizocorallium-, Teichichnus- & Planolites / Palaeophycus- burrows* (p).

Grainsize & sorting: Upward increasing level of sorting, mostly moderate to poorly sorted, upward decreasing grainsizes, medium calcirudites to calcisiltites.

Components & frequency: Shells (c) with micritic envelopes (p), brachiopods (p), bio- & intraclasts (p-c), peloids (p).

Thickness: Cm- scale sheets commonly amalgamated to few dm-scale composite sheets.

Interpretation

Scoured erosive bases of graded, moderate to poorly sorted, bioclastic packstone sets are typical features of single high-energy events, such as storms. Short term and rapid sedimentation is indicated e.g. by umbrella structures. Grading and parallel orientation of components as well as increasing mud content and wave ripples on tops reflect slow post-event accumulation and a rapid decrease in hydroenergy.

The various variable components indicate variable origin of sediment, e.g. shells with micritic envelopes hints to rather proximal- while brachiopods points to open marine sediment sources.

The graded bioclastic packstones sheets are interpreted as storm-generated offshoal tempestites (transition shallow to deep ramp)

Porosity & Permeability

Pore types and occurrence:

(Choquette & Pray, 1970): Moldic (p).

(Lucia, 1999) : Separate-vug (p).

Rock-Fabric types (Lucia, 1999): Graded bioclastic wacke- to packstones sheets with separate-vug porosity *(8-sv)*

Average Porosity & Permeability Values

8-sv (n=7 samples)

Φ = 3,14 %, $k(h)_{air}$ = 2,24 mD $k(v)_{air}$ = 0,86 mD

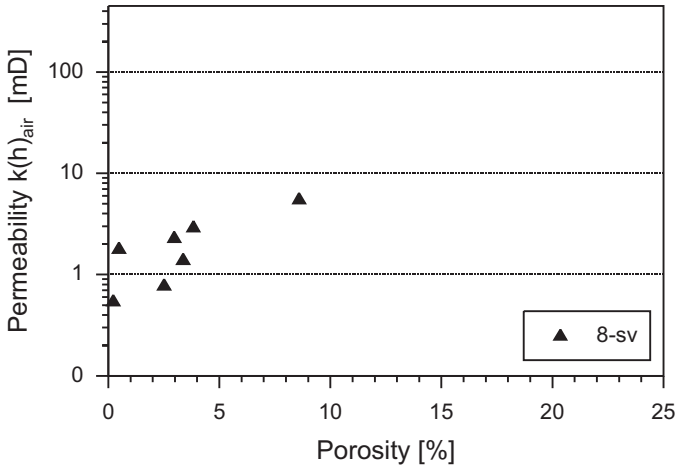

Conclusion:

The highest amount of bivalve shells is accumulated at the basis of these sheets, forming poorly sorted, coarse grained skeletal lags. The mud-dominated matrix however hinders an interconnection of moldic pores. The upward decreasing grainsize and the increase in mud further reduces the poro-perm-properties of LFT 8.

Generally the reservoir potential is moderate to poor.

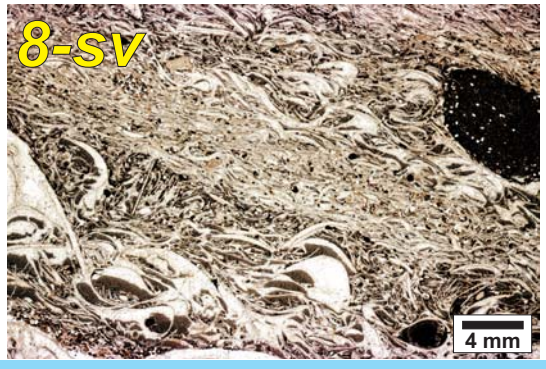

The amount of dissolved components in LFT 8 is rather low. The mud-dominated matrix additionally hinders the connectivity of moldic pore space.

Lithofacies Type 9a “cross-bedded oolitic grainstone”

Description

Texture [Dunham]: Grainstones.

Lithology & color: Limestone, light grey to white, beige.

Physical sedimentary structures: Most frequently high angle cross-bedding as trough cross-bedding (a), planar-tabular cross-bedding (p), partly massive.

Biogenic sedimentary structures: Few shallow penetrating burrows from top.

Grainsize & sorting: Well to moderately sorted, medium to very coarse calcarenite.

Components & frequency: Ooids (a) partly dolomitized, coated grains (c), aligned fragmented shells with micritic envelopes (p) concentrated on bedding planes, fine bioclastic debris (p).

Thickness: Dm-m-scale sandwaves- and dunes as well as dm-scale ripple sets, stacking to meter-scale sets.

Interpretation

Grainstone texture, good sorting and cross-bedding of carbonate sandbodies attests frequent high hydrodynamic conditions as caused by e.g. frequent storm events.
This also explains minor bioturbation.

Necessary $CaCO_3$ supersaturated seawater as well as endolithic and epilithic algae for production of oolites and coated grains indicate shallow water conditions within the photic zone.

The cross-bedded oolitic grainstones are interpreted as the central oolite-dominated shoal, accumulated as sanddunes and mega ripples on the shallow ramp

Porosity & Permeability

Pore types and occurrence:

(Choquette & Pray, 1970): Oomoldic (a), intercrystal. (c).

(Lucia, 1999) : Separate-vug (a), intercrystalline (c).

Rock-Fabric types (Lucia, 1999): Cross-bedded oolitic grainstones with

separate-vug porosity *(9a-sv)*

intercrystalline porosity *(9a-ic)* due to dolomitization of ooids

Average Porosity & Permeability Values

9a-sv (n=4 samples)

Φ = 6,79 %, $k(h)_{air}$ = 4,63 mD, $k(v)_{air}$ = 1,43 mD

9a-ic (n=11 samples)

Φ = 6,79 %, $k(h)_{air}$ = 0,82 mD $k(v)_{air}$ = 0,86 mD

Conclusion:

Poro-perm properties of oolitic grainstones are fair to poor depending on preservation of oomoldic pore space & late diagenetic cementation of pores (B-cement & dolomite).

Interparticle pore space is always cemented.

Best reservoirs of separate-vug oolite bar deposits are located in the center of shoal geobodies, where under shallow water conditions ooids are influenced by fresh water dissolution and / or subaerial exposure.

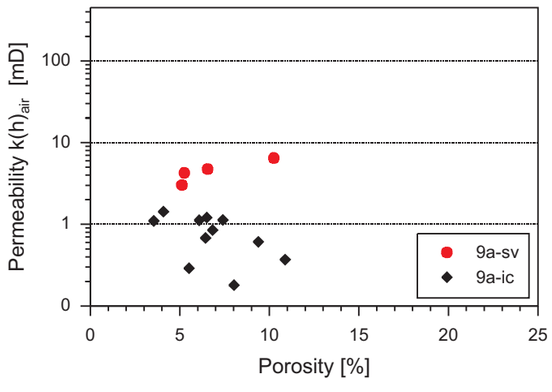

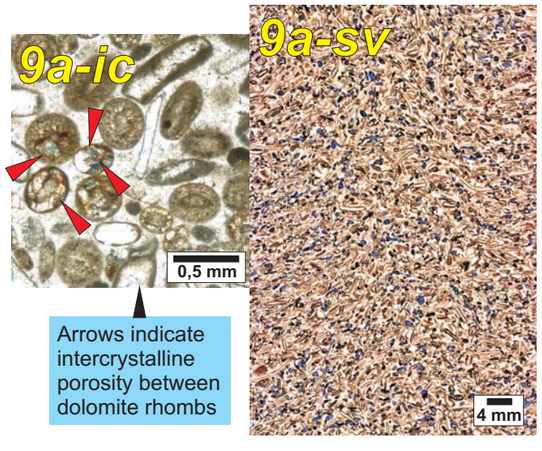

Arrows indicate intercrystalline porosity between dolomite rhombs

Lithofacies Type 9a “cross-bedded oolitic grainstone”

Sedimentologic log & GR-signature

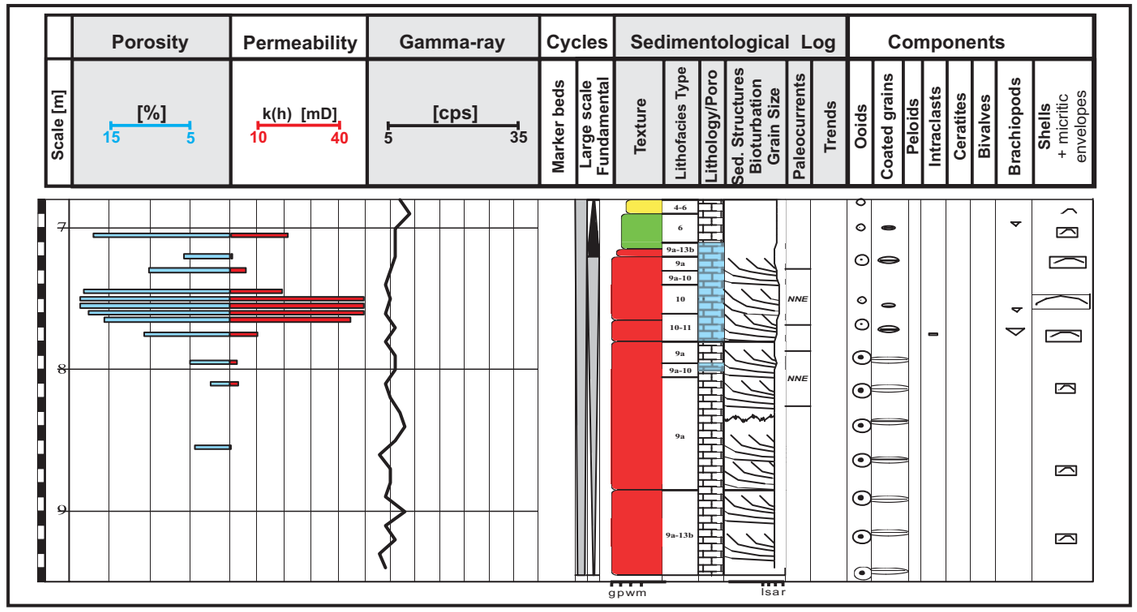

Photodocumentation

Trough cross-bedded oolite sandwave dipping in north-eastern direction, which corresponds to major paleocurrent and wind direction.

Slab scan of a typical oolitic grainstone, faintly cross-bedded. Shell fragments with micritic envelopes are concentrated on bedding planes.

Oomoldic pores (blue stained) by dissolution of the aragonitic cortex. Note: Fringe of early diagenetic radial fibrous marine cement around components.

The assemblage of components is characteristic for shallow water carbonates, e.g. ooids of various diameters and laminae, coated grains and shell fragments with micritic envelopes.

Lithofacies Type 9b “laminated fine debris pack- to grainstone”

Description

Texture [Dunham]: Pack- to grain- & grainstones.

Lithology & color: Limestone, beige.

Physical sedimentary structures: Frequently parallel lamination (a), low angle cross-bedding (p), partly vague lamination (massive appearance).

Biogenic sedimentary structures: Poorly defined burrows may be present.

Grainsize & sorting: Well sorted, fine to coarse calcarenite.

Components & frequency: Bioclastic debris (a), micro-lithoclasts (p), siliciclastic debris/ quartz (p), shell fragments (r).

Thickness: Dm-scale sets and bar deposits stacking to m-scale sets.

Interpretation

Abundant cm-dm-scale lamination up to low angle cross-bedding combined with good sorting and grainstone texture of pure calcarenites points to frequent very high-energy hydrodynamic conditions as caused by permanent current action. Minor bioturbation supports this assumption.

Heavy fragmentation mainly of allochems and the presence of subordinate micro-lithoclasts as well as siliciclastic grains (concentrated in discrete laminae) indicates a near-coast depositional environment with input of coastal clastics.

The laminated fine debris pack- to grainstones are interpreted as wave-induced beach deposits and backshoal beach bars

Porosity & Permeability

Pore types and occurrence:

(Choquette & Pray, 1970): Intergranular (c), moldic (p).

(Lucia, 1999) : Interparticle (c), separate-vug (p).

Rock-Fabric types (Lucia, 1999): Laminated fine debris pack- to grainstones with

separate-vug + interparticle porosity *(9b-sv+ip)*

Average Porosity & Permeability Values

9b-sv+ip (n=18 samples)

Φ = 6,91 %, $k(h)_{air}$ = 4,75 mD, $k(v)_{air}$ = 5,52 mD

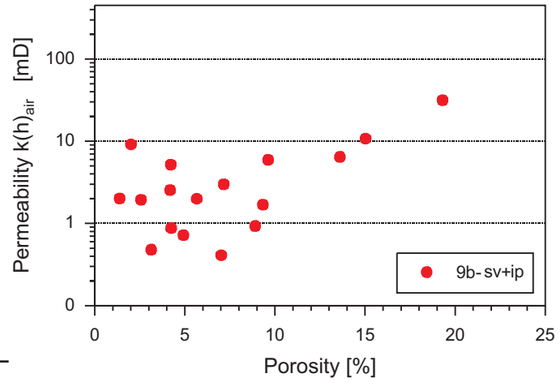

Conclusion:

Poro-perm properties of fine debris pack- to grainstones are fair to poor depending on grainsize and sorting which controls preservation and volume of interparticle pore space. The proportion of biomoldic porosity is low (remnants of bivalves).

These marginal reservoirs are located in a short distance landwards of the shoal deposits as separate bars and banks.

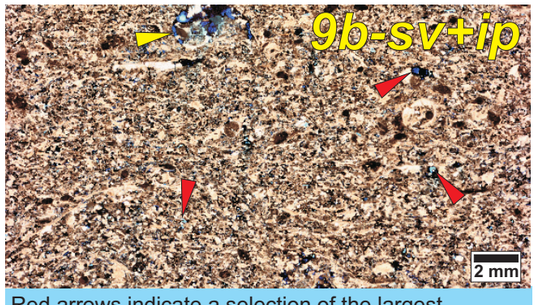

Red arrows indicate a selection of the largest interparticle pores (blue stained) between calcarenitic grains.
The yellow arrow points to rare separate-vug porosity.

Lithofacies Type 9b “laminated fine debris pack- to grainstone”

Sedimentologic log & GR-signature

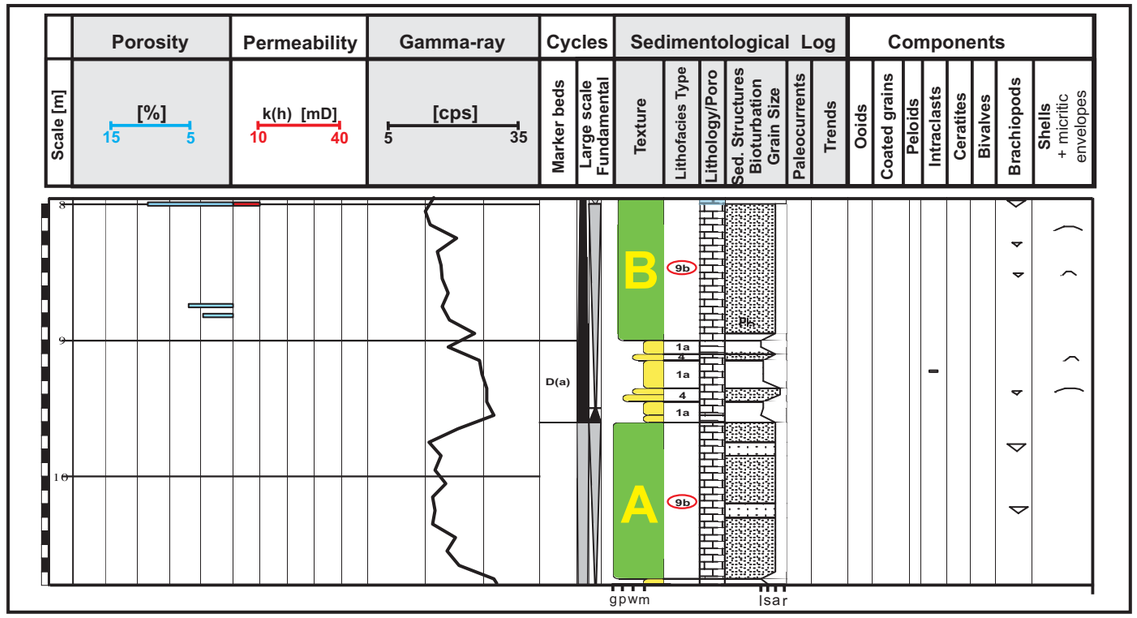

Photodocumentation

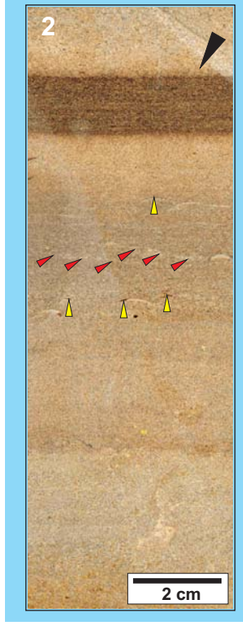

1) Horizonts A + B (also displayed on sedimentologic log) consists of pure calc-arenites of the 9b lithofacies type. This m-scale units are interpreted as backshoal beach bars formed by permanent wave action. The shown geobodies extend several km´s and wedge out towards NW (seawards).

2) The slab is taken from the top of horizont B in Fig.1. Parallel lamination and faintly low angle cross-bedding (red arrows) are characteristic features of LFT 9b as well as siliciclastic grain-dominated laminae (brown laminae, black arrow).
Solitary shell fragments cause subordinate biomoldic porosity (yellow arrows).

That grainsize and level of sorting controls preservation and volume of interparticle pore space is excellently documented in this thin-section scan. Blue stained interparticle pores are concentrated on laminae consisting of elongated grains (remnants of fragmented shells).

Lithofacies Type 10 “shell hash pack- to grainstone”

Description

Texture [Dunham]: Pack- to grainstones and grainstones.

Lithology & color: Limestone, light grey, beige, white.

Physical sedimentary structures: High angle cross-bedding, frequently as trough cross-bedding (a), planar cross-bedding (p), rarely massive or vague lamination.

Biogenic sedimentary structures: Few shallow penetrating burrows from top.

Grainsize & sorting: Well to moderately sorted, very coarse calcarenite to fine calcirudite.

Components & frequency: Disarticulated & fragmented shells with micritic envelopes (a), coated grains (c), bioclastic detritus (p). Rare components are: brachiopod fragments, ooids, intraclasts.

Thickness: Dm-scale event sheets and sandwaves to meter-scale composed sets.

Interpretation

Grainstone texture, crushed shells, good sorting and cross-bedded bars and banks indicate sediment accumulation and transportation by permanent current action and frequent storm events.

The dominance of micritic envelopes and coated grains, caused by boring algae reflects shallow water conditions within the photic zone.

The shell hash pack- to grainstones are interpreted as the shell-dominated part of the shoal (shallow ramp position)

Porosity & Permeability

Pore types and occurrence:

(Choquette & Pray, 1970): Moldic (a), interparticle (c).

(Lucia, 1999) : Separate-vug (a), interparticle (c).

Rock-Fabric types (Lucia, 1999): Shell hash grain-dominated packstones and grainstones with

separate-vug **and** interparticle porosity *(10-sv+ip)*

separate-vug porosity only *(10-sv)*

Average Porosity & Permeability Values

10-sv+ip (n=86 samples)

Φ = 15,05 %, $k(h)_{air}$ = 45,41 mD, $k(v)_{air}$ = 43,63 mD

10-sv (n=64 samples)

Φ = 8,17 %, $k(h)_{air}$ = 2,99 mD, $k(v)_{air}$ = 3,17 mD

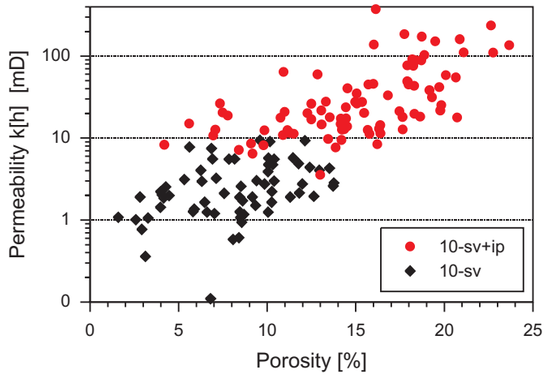

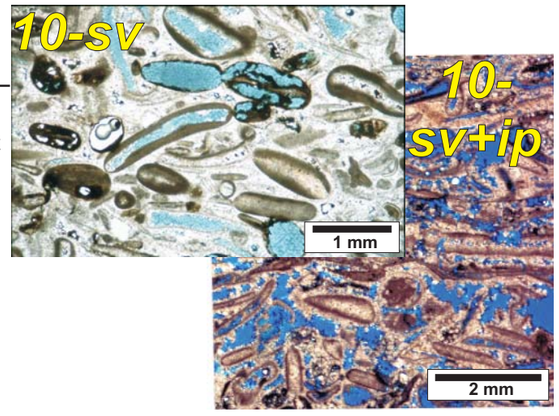

Conclusion:

Grainsize and level of sorting is influenced by permanent current action and frequent storm events.
Both properties control the preservation and volume of interparticle pore space.

Best reservoirs of LFT 10 are located on the wind-sheltered leeward sides of shoal bodies due to the larger grainsizes of shells (by lower hydroenergy) and better preservation of primary interparticle porosity.

Lithofacies Type 10 “shell hash pack- to grainstone”

Sedimentologic log & GR-signature

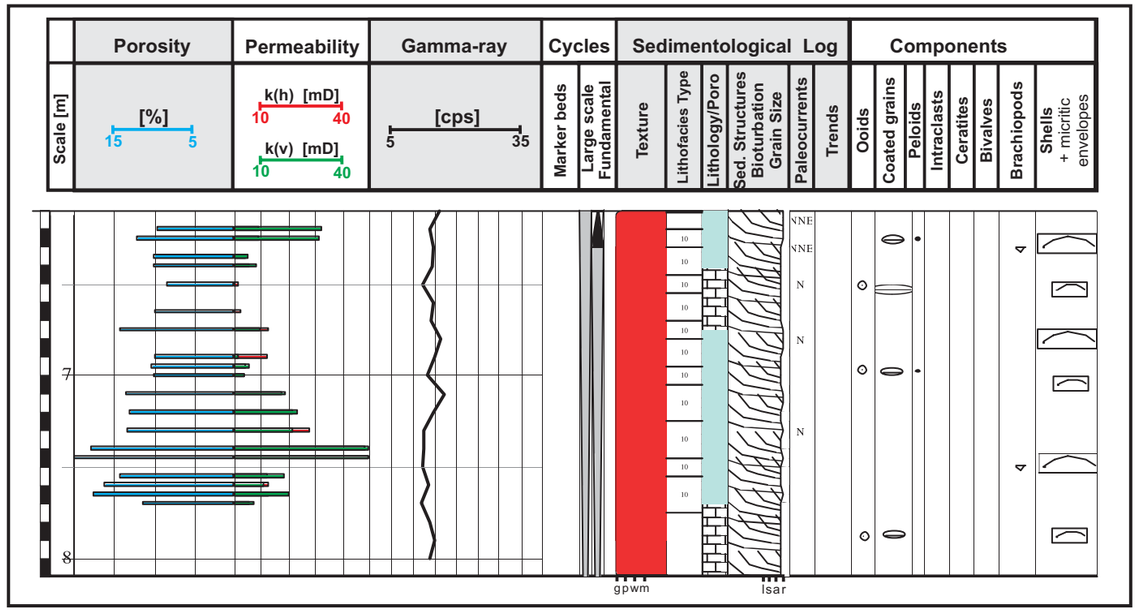

Photodocumentation

Approximately 50 cm set of a cross-bedded subtidal carbonate sanddune (A) of pure shell hash, succeeded by dm-scale ripple sets (B).

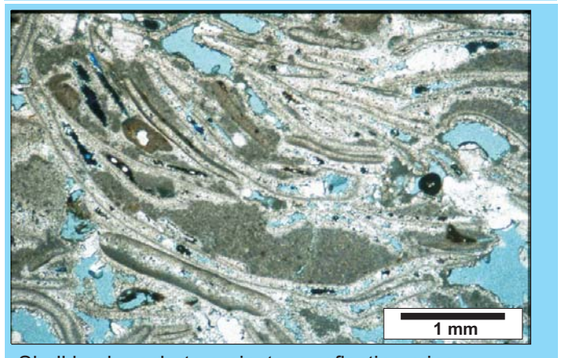

Shell hash pack- to grainstone reflecting minor fluctuations in hydrodynamic conditions. Note high interparticle porosity in spite of lime mud content.

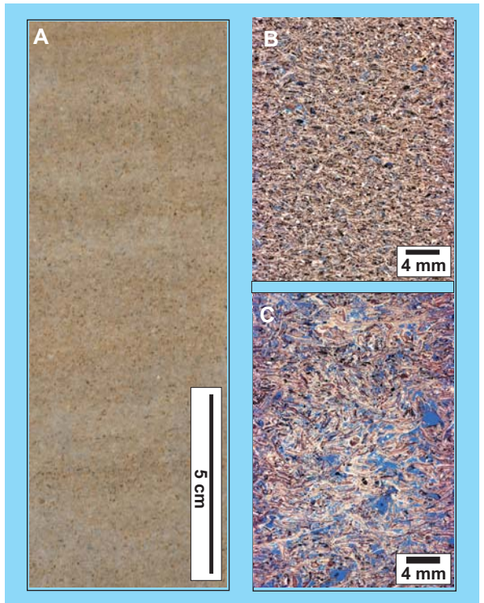

A) Slab of a typical shell hash grainstone, faintly cross-bedded, well sorted, very coarse calcarenite.
Grainsize and level of sorting control preservation and volume of primary interparticle pore space.
Compare thin section scans B) and C) for visualisation.
B) Smaller particle size and better sorting cause smaller interparticle pore space.

Lithofacies Type 11 “poorly sorted bioclastic pack- to grainstone”

Description

Texture [Dunham]: Pack- to grain- & grainstones.

Lithology & color: Limestone, light grey, beige.

Physical sedimentary structures: Frequently parallel lamination (c) or faintly high angle cross-bedding (c), partly massive appearance, umbrella structures (c).

Biogenic sedimentary structures: Poorly defined burrows may be present.

Grainsize & sorting: Poorly sorted, fine to medium calcirudites.

Components & frequency: Commonly aligned shells and brachiopods (a), fragmented as well as whole body with micritic envelopes (a), coated grains (p), ooids (p), lithoclasts (r).

Thickness: Dm-scale sets that rarely stack to m-scale beds.

Interpretation

Calciruditic, poorly sorted, mostly laminated sets of fragmented and well preserved skeletal components points to episodic high-energy conditions as caused by single storm events. Characteristic features are umbrella structures as well as remnants of interparticle micrite demonstrating no post-event reworking by wave action.

The skeletal composition indicate an origin of proximal foreshoal- (brachiopods) to shoal setting (shells with common micritic envelopes, coated grains, ooids). The mixture of fragmented and whole body components attests rapid hydrodynamic fluctuations.

The poorly sorted bioclastic pack- to grainstones are interpreted as storm induced event-sheets without subsequent reworking, located at the landward wind-sheltered leeward flank of the shoal body

Porosity & Permeability

Pore types and occurrence:

(Choquette & Pray, 1970): Moldic (a), interparticle (c), shelter (p).

(Lucia, 1999) : Separate-vug (a), interparticle (c).

Rock-Fabric types (Lucia, 1999): Poorly sorted bioclastic pack- to grainstones with

separate-vug & interparticle porosity *(11-sv+ip)*

Average Porosity & Permeability Values

11-*sv+ip* (n=56 samples)

Φ = 12,92 %, $k(h)_{air}$ = 82,12 mD, $k(h)_{air}$ = 84,51 mD

Conclusion:

Poro-perm properties of poorly sorted bioclastic pack- to grainstones are good to very good due to fast and short accumulation periods, resulting in coarse and poorly sorted sheets with large pore volumes and excellent preserved interparticle pore space.

Strong moldic porosity can be explained by subaerial exposure and influence of fresh water dissolution.

Best reservoirs are located on the wind-sheltered leeward flank of the shoal body.

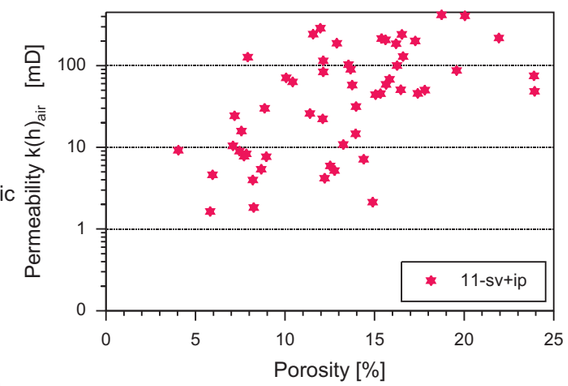

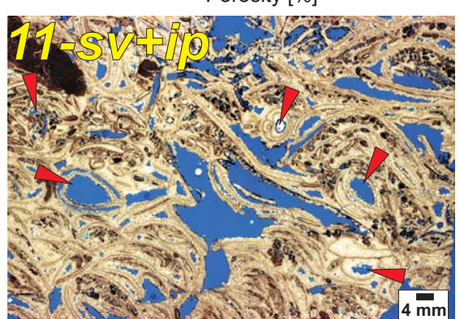

Apparent major primary interparticle porosity is commonly increased by separate-vug (moldic, intraparticle & shelter) porosity. A selection is indicated by red arrows.

Lithofacies Type 11 “poorly sorted bioclastic pack- to grainstone”

Sedimentologic log & GR-signature

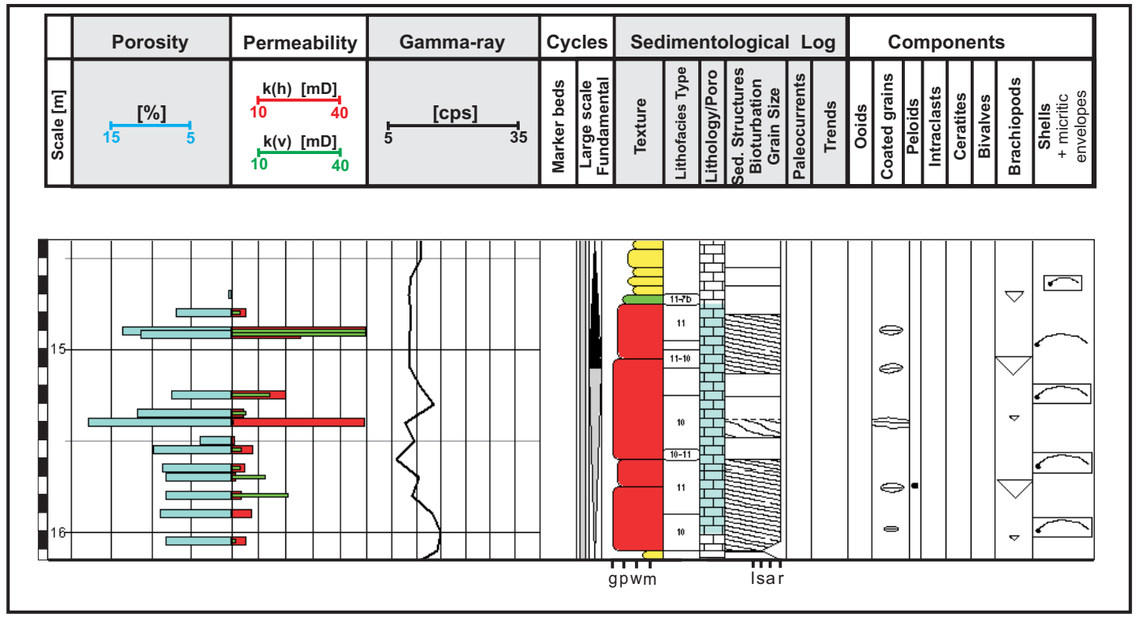

Photodocumentation

Set A is composed of some cm-thick poorly sorted calcirudite sheets of LFT 11, faintly cross-bedded (stippled lines), succeeded by shell hash (set B).

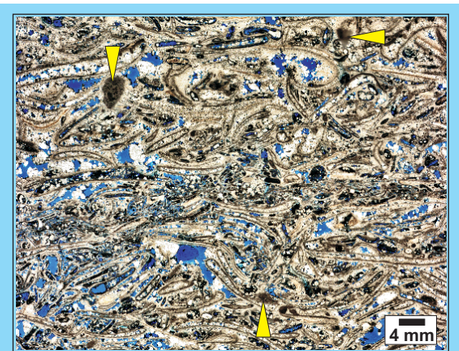

Typical features of poorly sorted coarse calcirudites are remnants of micrite (yellow arrows) & cruedly aligned shells. Pore space (blue) is easy to recognize.

1)The slab shows cm-scale sets and parallel lamination or faintly cross-bedding of LFT 11. Note bright micritic mud trapped below shells (umbrella structures, red arrow). These structures are indicators of rapidly decreasing hydro-dynamic energy after storm events and little sediment reworking.

2) Detail of the thin section scan on the left side: Interparticle and separate-vug porosity is reduced by early dia-genetic radial fibrous cement fringes (a), succeded by dolomite (d), dog-tooth cement (b) and equant blocky spar cement (c).

Lithofacies Type 12 “oncolitic pack- to grainstone”

Description

Texture [Dunham]: Pack- to grain- & grainstones.

Lithology & color: Limestone, beige.

Physical sedimentary structures: Trough cross-bedding (c), lamination by aligned skeletal grains, channel geometries are observed.

Biogenic sedimentary structures: No or weak bioturbation of undefined burrows.

Grainsize & sorting: Poorly sorted, fine to medium calcirudites.

Components & frequency: Oncoids (p-c), fragmented shells (p-c) with micritic envelopes (c), bored shells (p), coated grains (p), (dolomitized) ooids (p-c), fine bioclastic debris (p).

Thickness: Dm-scale sets.

Interpretation

Trough cross-bedding and texture of oncolitc pack- to grainstones attests high energetic paleocurrent conditions. Poor sorting and coarse particle sizes point to non-constant or fluctuating sediment transport. LFT 12 commonly occur in basal lag position of channel-like geometries and therefore was interpreted as channel-fill of storm and tidal channels.

Endolithic and epilithic algae for production of oncolites and micritic envelopes indicate shallow water conditions within the photic zone of the source area of these cannel-fills.

The oncolitic- pack- to grainstones are interpreted as channel-fills of / from an shallow lagoonal environment (shallow ramp)

Porosity & Permeability

Pore types and occurrence:

(Choquette & Pray, 1970): Interparticle (c), moldic (c).

(Lucia, 1999) : Interparticle (c), separate-vug (c).

Rock-Fabric types (Lucia, 1999): Oncolitic pack- to grainstones with

separate-vug & interparticle porosity *(12-sv+ip)*

Average Porosity & Permeability Values

12-sv+ip (n=4 samples)

Φ = 11,52 %, $k(h)_{air}$ = 21,98 mD, $k(v)_{air}$ = 21,23 mD

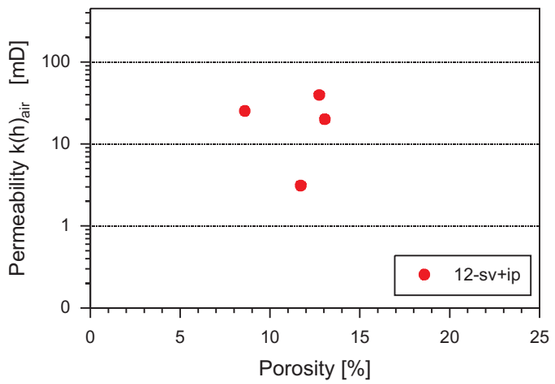

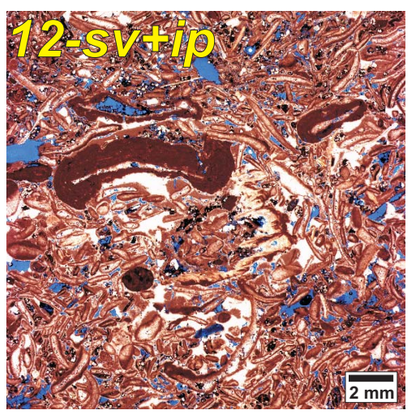

Conclusion:

Poro-perm properties of poorly sorted oncolitic pack- to grainstones are good due to fast but episodic sedimentation periods and presumably short distance transportation, resulting in coarse and poorly sorted channel-fills where large volume of interparticle pore space was preserved.

Moldic porosity can be explained by subaerial exposure and influence of fresh water dissolution.

Occurrence of oncolite channels is limited to most landward positions.

Lithofacies Type 12 “oncolitic pack- to grainstone”

Sedimentologic log & GR-signature

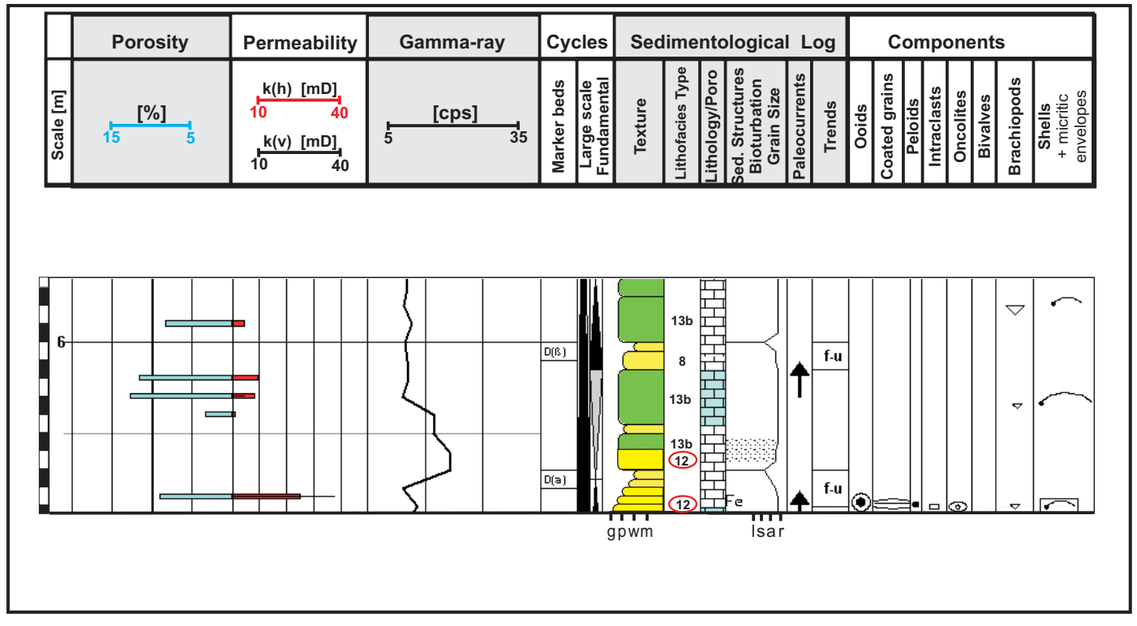

Photodocumentation

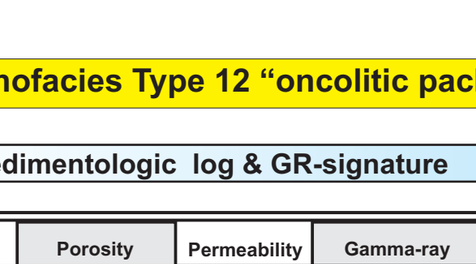

The stippled line indicates high angle cross-bedding of red marked dm-scale set composed of oncolitic pack- to grainstone. The coarse NW dipping laminae indicate sediment transport perpendicular to the coastline.

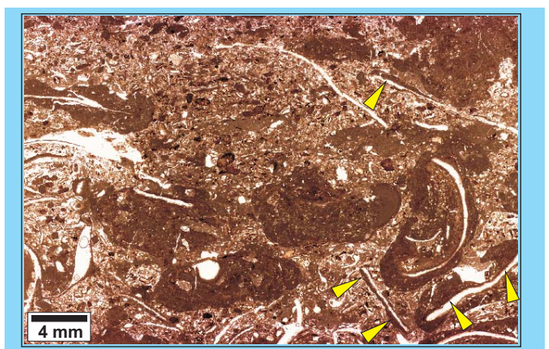

Frequent one-sided growth of algal laminae on shells (yellow arrows) indicates a quiet lagoonal setting as origin. Abundant fecal pellets support this assumption.

1)This slab is a characteristic example of an oncolitic grainstone reflecting high hydro-dynamic conditions while coarse grainsize and poor sorting point to non-constant, rather episodic periods of sediment transportation. Common oncolites and abundant ooids are typical components of shallow water carbonates. Obvious moldic (black arrows) and large vug porosity (red arrows) occurs more often in very shallow environments by subaerial exposure or fresh water dissolution.

2) Detail view of the slab top above.

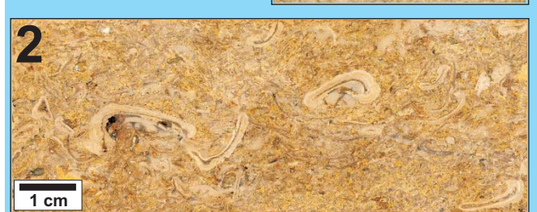

Lithofacies Type 13a “ooidal-skeletal pack- to grainstone”

Description

Texture [Dunham]: Pack- to grain- & grainstones.

Lithology & color: Limestone, light grey, beige.

Physical sedimentary structures: Mostly vague or faintly parallel lamination (c), cm-scale successions of oolites or skeletal grains (a), umbrella structures (p-c).

Biogenic sedimentary structures: Weak bioturbation of undefined burrows.

Grainsize & sorting: Moderately to poorly sorted, very coarse calcarenites to fine calcirudites.

Components & frequency: Cruedly aligned shells (c) at different levels of fragmentation, with micritic envelopes (p-c), coated grains (c), ooids (c), intraclasts & debris (p), brachiopods (r).

Thickness: Cm-scale sets stack to dm-scale, rarely to m-scale beds.

Interpretation

Coarse calcarenitic to calciruditic, poorly sorted and laminated ooidal-skeletal pack- to grainstone sets indicate episodic high-energy events as caused by storm events. Frequent umbrella structures point to rapid accumulation without further transportation.

The changing composition of oolite- or skeletal-dominated laminae or mixtures of both attests supply of changing production areas. Shells with common micritic envelopes are predominantly supplied from proximal shoal flanks, while calcitic oolites are oolite-shoal derived. Dolomitized oolites probably come from backshoal areas.

The ooidal-skeletal pack- to grainstones are interpreted as storm induced event-sheets and / or spillover lobes besides the shoal

Porosity & Permeability

Pore types and occurrence:

(Choquette & Pray, 1970): Moldic (a), interparticle (p).

(Lucia, 1999) : Separate-vug (a), interparticle (p).

Rock-Fabric types (Lucia, 1999): Ooidal-skeletal pack- to grainstones with

separate-vug porosity *(13a-sv)*

separate-vug & interparticle porosity *(13a-sv+ip)*

Average Porosity & Permeability Values

13*a-sv* (n=57 samples)

Φ = 5,76 %, $k(h)_{air}$ = 2,80 mD $k(v)_{air}$ = 2,40 mD

13*a-sv+ip* (n=18 samples)

Φ = 9,26 %, $k(h)_{air}$ = 28,30 mD $k(v)_{air}$ = 24,82 mD

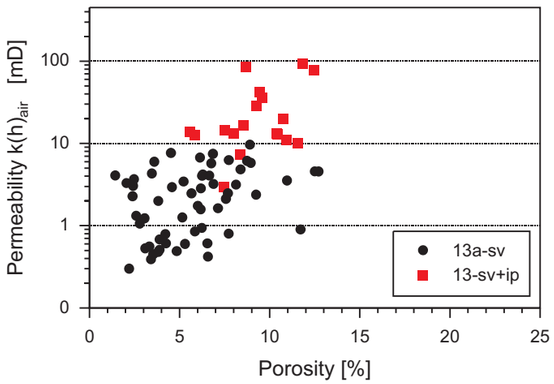

The vast majority of porosity in ooidal-skeletal pack- to grainstones is caused by dissolution of ooids (blue stained) and minor bivalve shells (red arrows). Primary interparticle porosity is rather exceptional.

Conclusion:

Poor sorting of ooidal-skeletal pack- to grainstones due to rapid sedimentation may preserve some primary interparticle pore space, resulting high-k streaks. However the vast majority of interparticle space is cemented.

Discrete dissolution of ooids and subordinate shells result abundant separate-vug porosity.

Lithofacies Type 13a “ooidal-skeletal pack- to grainstone”

Sedimentologic log & GR-signature

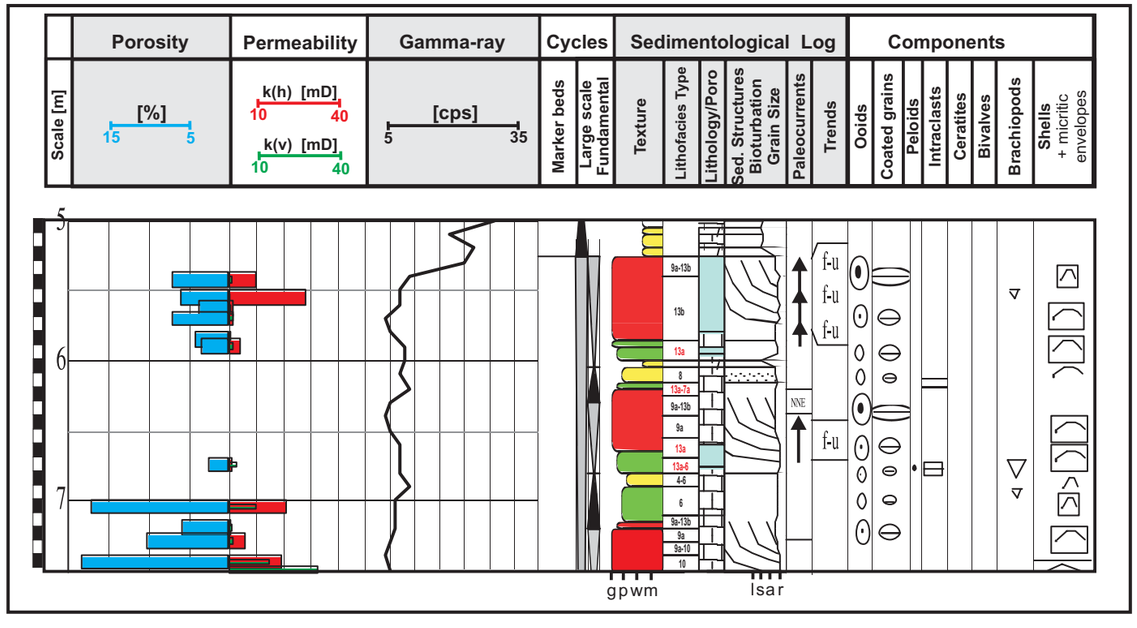

Photodocumentation

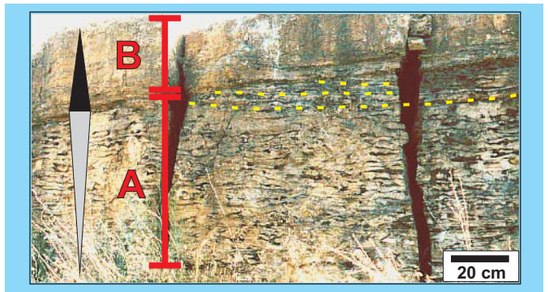

Set A reflects high hydroenergetic conditions interpreted as regressive fundamental hemi-cycle. Note high angle cross-bedding truncated at the set top (stippled lines). Decreasing energy is reflected by set B composed of LFT 13a representing the transgressive hemi-cycle part.

Non-constant high hydroenergy is reflected by frequent remnants of micrite and poor sorting of LFT 13a.

1) The lower slab part shows characteristic cm-scale successions of oolite-dominated (a) and shell-dominated (b) laminae of an ooidal-skeletal pack-to grainstone. An indication of fluctuating hydroenergy as caused by storm induced event-sheets or spillover lobes. The upper part is high angle cross-bedded and oolites and shells are mixed. This attests increasing hydroenergy.

2) Relatively poor sorting of dolomitized ooids and large shell fragments as well as inter-skeletal mud characterize the appearance of LFT 13a.

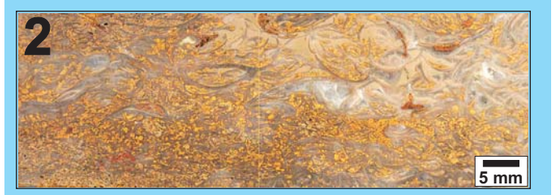

Lithofacies Type 13b “cross-bedded ooidal-skeletal pack- to grainstone”

Description

Texture [Dunham]: Pack- to grain- & grainstones.

Lithology & color: Limestone, light grey, beige.

Physical sedimentary structures: (Trough-) cross-bedding (c), parallel lamination (c) by aligned skeletal grains, cm-scale laminae of oolites or skeletal grains (a).

Biogenic sedimentary structures: Weak bioturbation of undefined burrows.

Grainsize & sorting: Moderately to well sorted, very coarse calcarenites to fine calcirudites.

Components & frequency: Aligned fragmented shells (c) with micritic envelopes (c), coated grains (c), ooids (c), intraclasts & debris (p), brachiopods (r).

Thickness: Cm-dm scale laminae stack to several dm- up to meter-scale beds.

Interpretation

Frequent cross-bedding and moderate to well sorting of ooidal-skeletal pack- to grainstones attests constant higher hydrodynamic conditions as displayed in LFT 13a for comparison. The formation of LFT 13b reflects higher storm frequencies, additionally wave and tidal action.

The composition of oolites and fragmented shells with micritic envelopes points to a changing supply from the central oolite-dominated shoal and the proximal flanking shell hash zone.

The cross-bedded ooidal-skeletal pack- to grainstones are interpreted as transition of oolite to shell hash-dominated shoal (shallow ramp position)

Porosity & Permeability

Pore types and occurrence:

(Choquette & Pray, 1970): Moldic (a), interparticle (p-c).

(Lucia, 1999) : Separate-vug (a), interparticle (p-c).

Rock-Fabric types (Lucia, 1999): Cross-bedded ooidal-skeletal pack- to grainstones with

separate-vug porosity *(13b-sv)*

separate-vug & interparticle porosity *(13b-sv+ip)*

Average Porosity & Permeability Values

13b-sv (n=68 samples)

Φ = 6,65 %, $k(h)_{air}$ = 2,28 mD, $k(v)_{air}$ = 1,81 mD

13b-*sv+ip* (n=14 samples)

Φ = 9,08 %, $k(h)_{air}$ = 60,35 mD, $k(v)_{air}$ = 12,54 mD

Conclusion:

Primary interparticle pore space may be preserved during periods of intense sediment accumulation, typically storm events and wave action. The amount of interparticle porosity is commonly reduced by diagenetic cementation.

Discrete dissolution of ooids and subordinate shells result abundant separate-vug porosity.

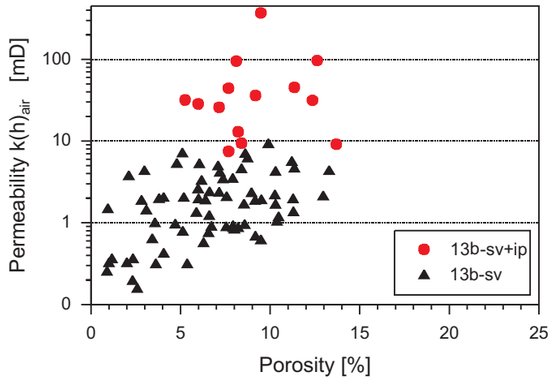

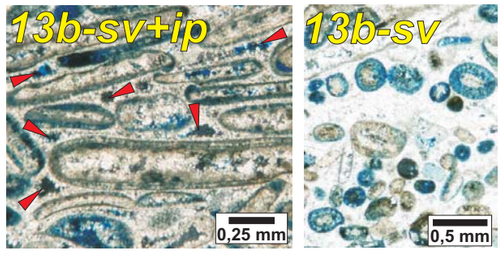

Abundant oomoldic and subdominant biomoldic porosity are the most common porosity types in laminated, moderate sorted ooidal-skeletal pack- to grainstones. Primary interparticle porosity (indicated by red arrows) is less common depending on cementation.

Lithofacies Type 13b “cross-bedded ooidal-skeletal pack- to grainstone”

Sedimentologic log & GR-signature

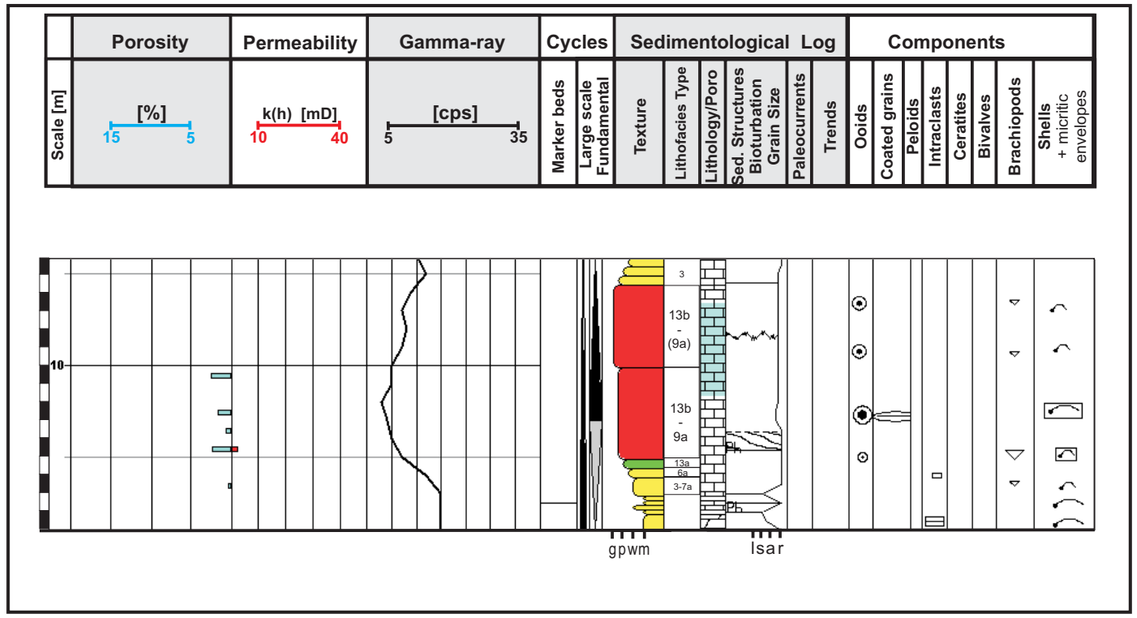

Photodocumentation

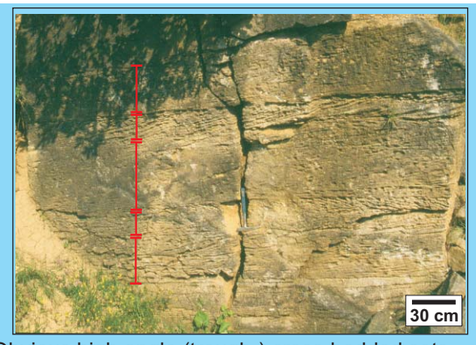

Obvious high angle (trough-) cross-bedded sets stack to a m-scale shoal. The individual coarse NE and SW dipping sets indicate sediment transport approximately parallel to the coast.

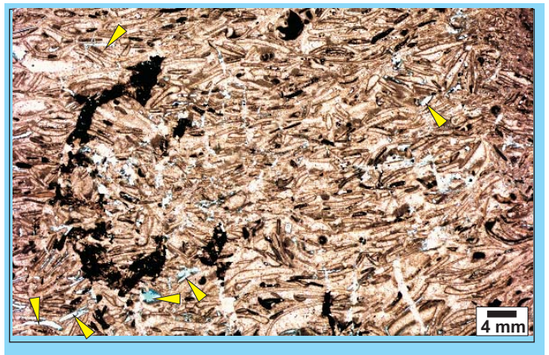

This unit dominated by fragmented bivalves shows discrete dissolution of shells (indicated by arrows).

1)The lower slab part is a good example of a typical high angle cross-bedded ooidal-skeletal pack- to grainstone of the 13b type. This part indicates a high hydrodynamic energy, that decreases to the upper slab part, visible by a continuously lower level of sorting, increasing grainsizes and lime mud content (red arrows). The upper part rather belongs to lithofacies type 13a.

2) Abundant dissolved ooids may be filled by later dolomite precipitation. Dolomite rhombs are indicated by red arrows.

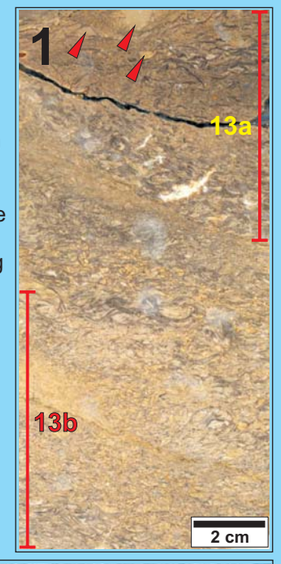

Lithofacies Type 14 "*Placunopsis* boundstone"

Description

Texture [Dunham]: Boundstone.

Lithology & color: Limestone, medium to light grey.

Physical sedimentary structures: Not present.

Biogenic sedimentary structures: Nodular, cauliflower-like individual biostromes, colonizing solid substrate like oolite- or skeletal bars. The vast majority are in-situ grown structures, "roll reefs" which indicate reworking are rare. Bioherms are frequently bored by *Trypanites*-type borings from top and filled by lime mud.

Grainsize & sorting: Well to moderately sorted, medium calcirudites.

Components & frequency: Bivalve *Placunopsis ostracina* (a), peloids (p), other bivalves and brachiopods (r).

Thickness: Cm-scale, mostly dm-scale biostromes, m-scale reefs are exceptions.

Interpretation

Bioherm growth is induced exclusively by the right valve of *Placunopsis ostracina* grown on solid ground, while the left valve is disarticulated and washed away after death of bivalve. As described by HÜSSNER (1991), *Placunopsis*, like other filtrators only accepts minor sediment supply. The concentric accumulation of right shells reflects a very slow bioherm growth. *Placunopsis* bioherms therefore indicate, according to their size, varying periods of time with slow sedimentation rates.

The occurrence of *Placunopsis* bioherms on the seaward flank of the shallow ramp, as described e.g. by AIGNER (1985) and RUF (2001) corresponds to own observations. Bioherms appear preferentially in certain local paleolow positions.

The vast majority of *Placunopsis* bioherms occur at the "Hauptterebratelbank" marker bed, which is interpreted as maximum flooding surface of the large-scale transgression. The described slow sedimentation rates during *Placunopsis* reef growth support the assumption of an overall transgressive phase.

The *Placunopsis* boundstones are interpreted as "patch-bioherms" on the seaward flanks of the shallow ramp

Porosity & Permeability

Pore types and occurrence:

(Choquette & Pray, 1970): No pores.

(Lucia 1999) : No pores.

Rock-Fabric types (Lucia, 1999): No rock-fabric type was defined.

Average Porosity & Permeability Values

No samples are measured.

Expected poro-perm values are below measuring limit.

Conclusion:

As analyzed by BACHMANN (1979) oyster *Placunopsis ostracina* nestles very tightly to the underlaying surface and adjust unevenness by varying thickness growth of calcitic ostracum and primary aragonitc hypostracum.

Rare interparticle space as well as vertical borings are already synsedimentary filled by pelmicrite.

Placunopsis boundstones are therefore considered as tightly cemented.

Lithofacies Type 14 "*Placunopsis* boundstone"

Sedimentologic log & GR-signature

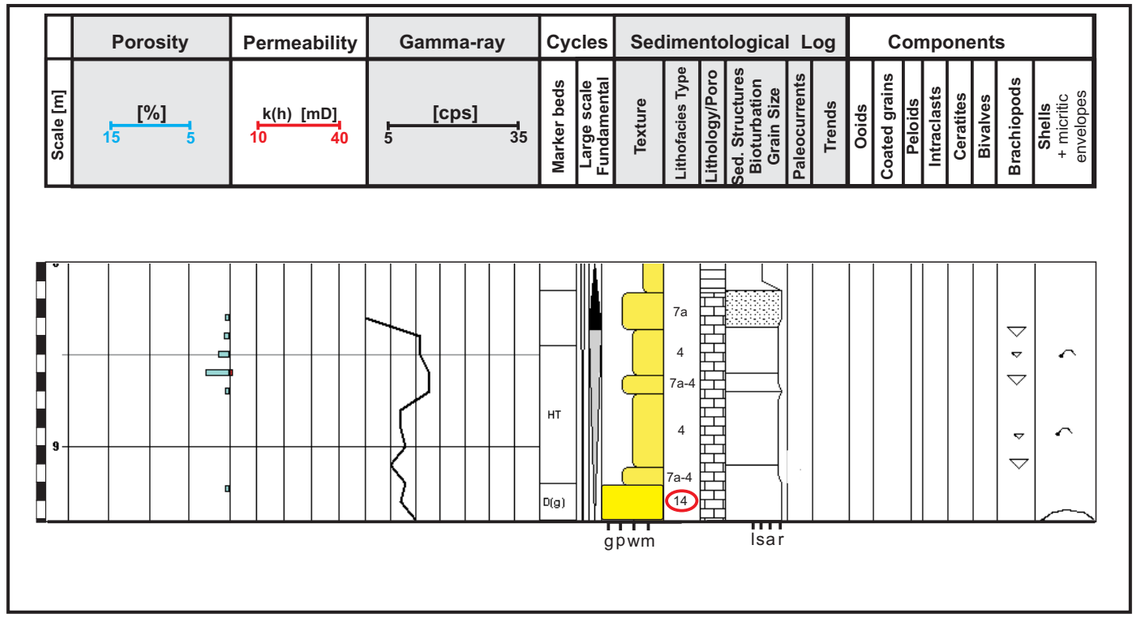

Photodocumentation

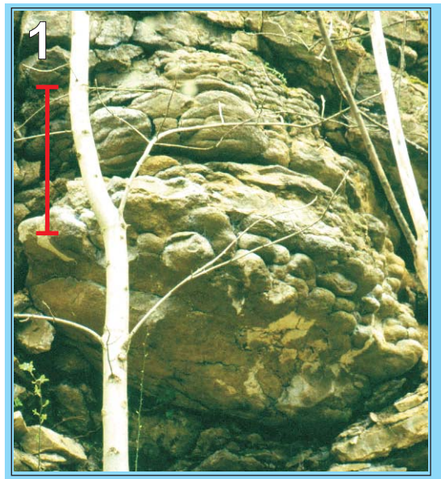

1) Characteristic nodular, cauliflower-like *Placunopsis* "reef". The height of 1,80 m is exceptional.

2) This slice through a bioherm shows typical concentric colonization of *Placunopsis ostracina*. Only the right valves of the oyster-typed shells are nestled together. Therefore these bioherms reflect slow growth and slow sedimentation rates.
Interparticle space and borings are always filled by beige (pel-) micrite (see red arrows).

3) These bioherms exclusively settle on consolidated substrate.

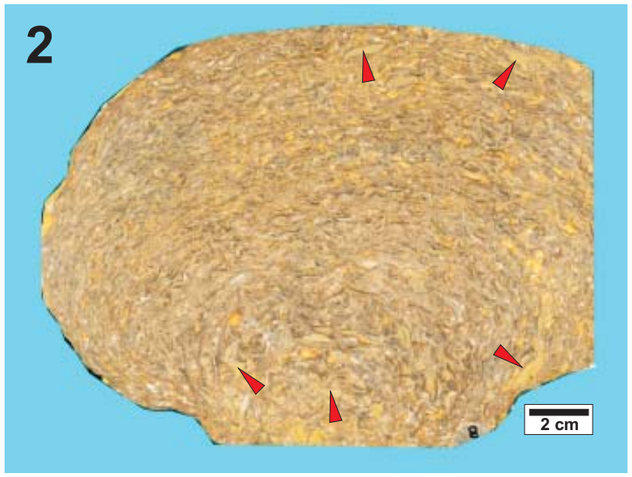

Lithofacies Type 15 “fine laminated dolo-boundstone”

Description

Texture [Dunham]: Dolo-boundstone.

Lithology & color: Dolomitic limestones to dolomites, yellowish grey, beige, yellow.

Physical sedimentary structures: Internal structure is composed of thin (mm-scale), discontinuous, crinkly laminae. Laminae sets are cruedly even, mostly low angle laminated. Siliciclastic and fine sparitic, mm-thin laminae occur.

Biogenic sedimentary structures: Weak to moderate bioturbation by simple burrows (*Planolites*-type).

Grainsize & sorting: Moderately to well sorted, dolo-siltite to medium dolo-arenites.

Components & frequency: Algal laminites / microbial mats, undefined micro-bio- and lithoclasts (r), quartz (p).

Thickness: Cm-scale laminae stack rarely to dm-scale sets.

Interpretation

Millimeter thin, discontinuous, slightly crenulated laminites are interpreted as laminae of microbial mats. Other indicators are sparse speckled as well as concentrated siltitic particles in laminaes due to the ability of microbial mats to trap and bind sediment.

Fine pack- to grainstone layers of silt-sized particles (micro-clasts of different origin) represent storm reworking.

The fine laminated dolo-boundstones are interpreted as algal laminites in a quiet, shallow subtidal to intertidal setting (shallow ramp position)

Porosity & Permeability

Pore types and occurrence:

(Choquette & Pray, 1970): Intercrystal. (p-c), fenestral (p).

(Lucia 1999) : Interparticle (p-c), vug-touching (p).

Rock-Fabric types (Lucia, 1999): Fine laminated boundstones with

interparticle porosity only *(15-ip)*

interparticle porosity & touching-vug *(15-tv+ip)* **??**

Average Porosity & Permeability Values

15-ip (n=3 plug samples)

Φ = 6,27 %, $k(h)_{air}$ = 2,67 mD, $k(v)_{air}$ = 1,54 mD

15-*tv+ip* (n=1 plug sample) **??**

Φ = 13,48 %, $k(h)_{air}$ = 37,39 mD, $k(h)_{air}$ = 24,49 mD

Conclusion:

Poro-perm properties of fine laminated boundstones with interparticle pore space range from poor to fair depending on crystal sizes of dolomite rhombs.

Additional touching-vug porosity in form of fenestral porosity cause an enormous increase in porosity and permeability. Fenestral porosity is probably caused by gas generation from the decomposition of organic matter.

• Uncertain is, if recent weathering has distorted (increased) the original poro-perm values.

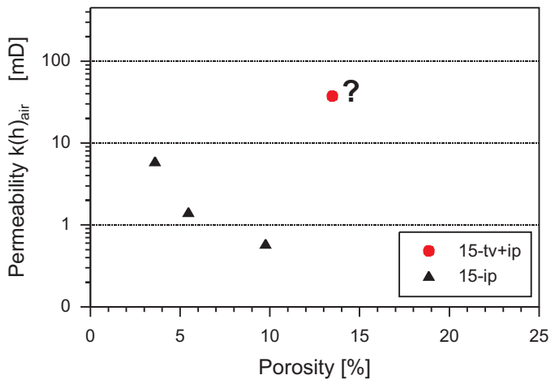

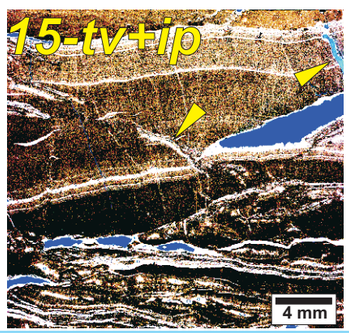

Blue stained fenestral pore space enormously enhance the poro-perm properties of these algal laminites. Some fracture porosity (indicated by yellow arrows) additionally increases touching-vug porosity.

Lithofacies Type 15 “fine laminated dolo-boundstone”

Sedimentologic log & GR-signature

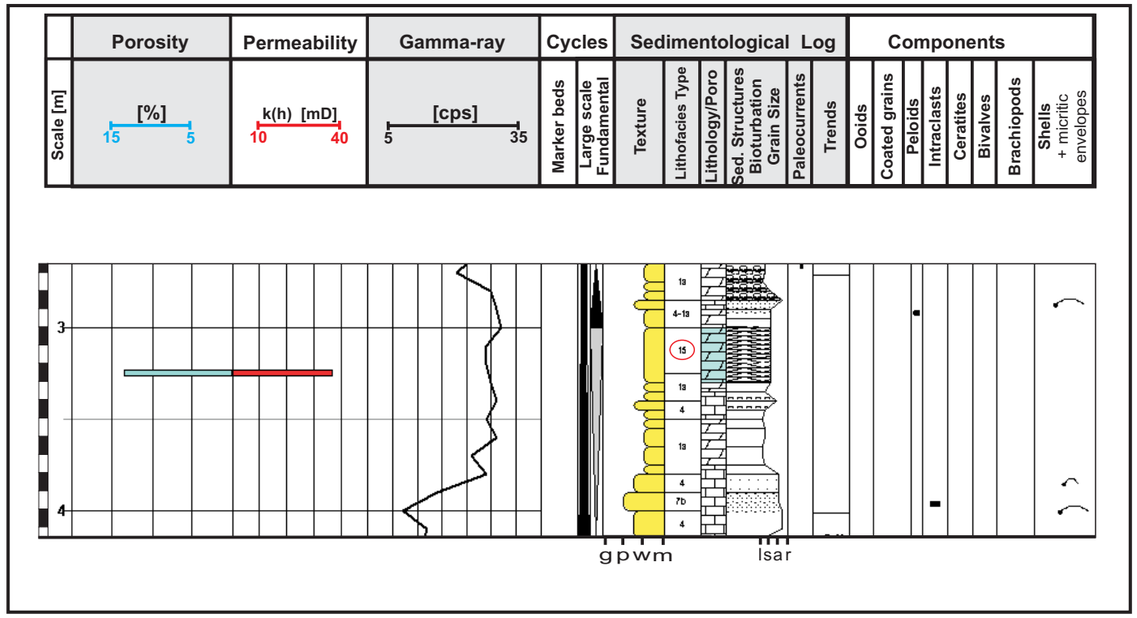

Photodocumentation

Even to faintly low angle laminated dolo-boundstone bed. Internal fine lamination as well as fenestral porosity just can be seen if slabed and polished. See slab example on the right.

Fenestral fabric by elongated touching-vug pores is very well visible. Mm-thin grainstone layers (see arrows) containing micro-bioclasts or intraclasts. Such lag deposits represent storm reworking.

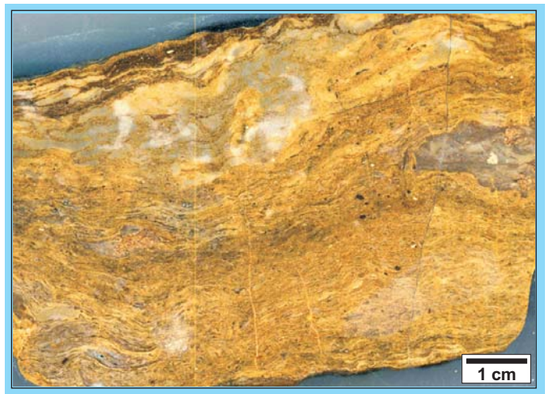

Thin, discontinuous, crenulated laminae mainly contrasts LFT 15 from other physically laminated facies

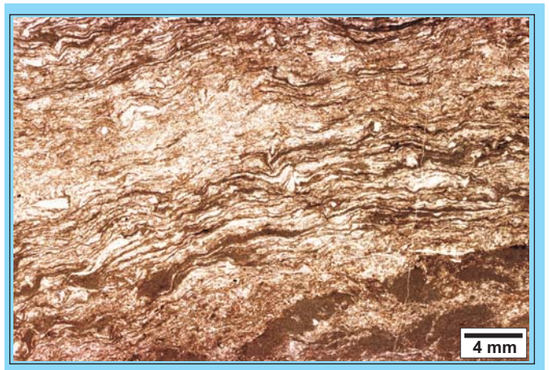

Note typical alternation of microbial- (dark) and sedi-ment layers (bright). Silt-size particles display sediment trapping and binding ability of microbial mats.

II

E N C L O S U R E S

List of Abbreviations

Abbreviations in log sheet header:

- bi = bivalves
- br = brachiopods
- bed contact = strata boundary
- cg = coated grains
- c-u = coursening-up
- fc = fundamental cycle
- f-u = fining-up
- GR = total gamma-ray log [cps]
- in = intraclasts
- k(h) = horizontal permeability [mD]
- k(v) = vertical permeability [mD]
- lc = larger-cycle
- Litho. = lithology
- lithofacies = lithofacies associations
- LFT = lithofacies types
- mb = marker beds
- oo = ooids
- part. size = particle size
- pe = peloids
- poro = porosity [%]
- rf = rare fossils
- sedi. struct. = sedimentary structures
- sh = shells (undifferentiated)
- strata bound. = strata boundary

Abbreviations of marker beds:

- D (a) = Dolomitische Mergel α
- D (ß) = Dolomitische Mergel β
- D (g) = Dolomitische Mergel γ
- G (ß) = Gelbe Mergel α
- G (ß) = Gelbe Mergel β
- G (ß) = Gelbe Mergel γ
- GB = Grenzbonebed
- GK = Grenzglaukonitkalk
- HT = Hauptterebratelbank
- OT = Obere Terebratelbank
- TH (e) = Tonhorizont ε
- TH (z) = Tonhorizont ζ

LEGEND

Sedimentary Structures

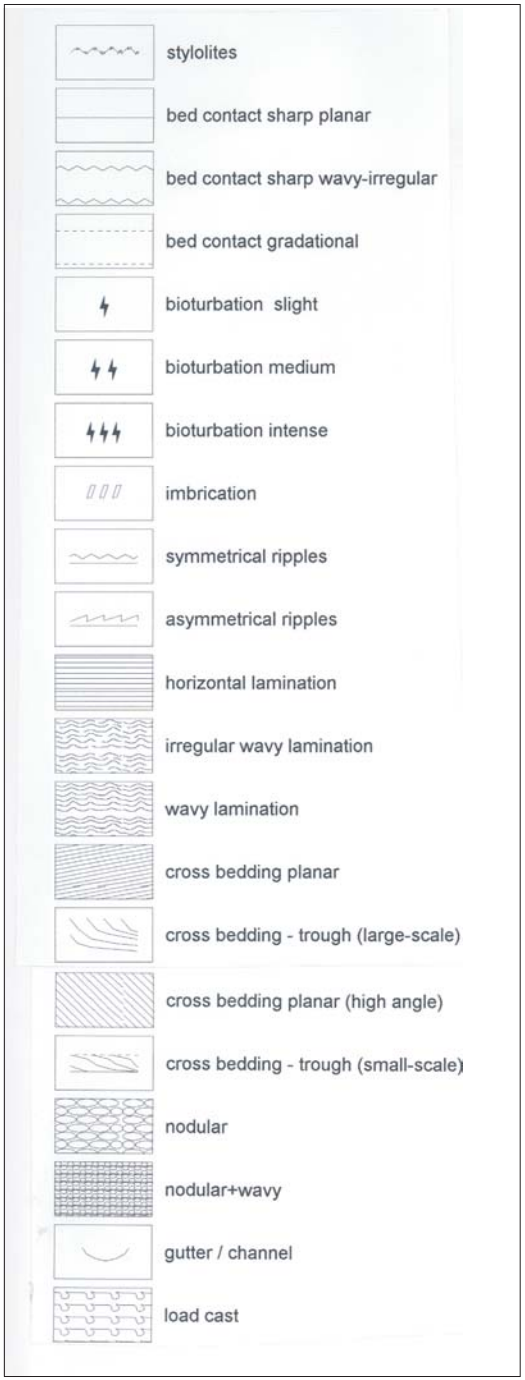

Facies Associations:

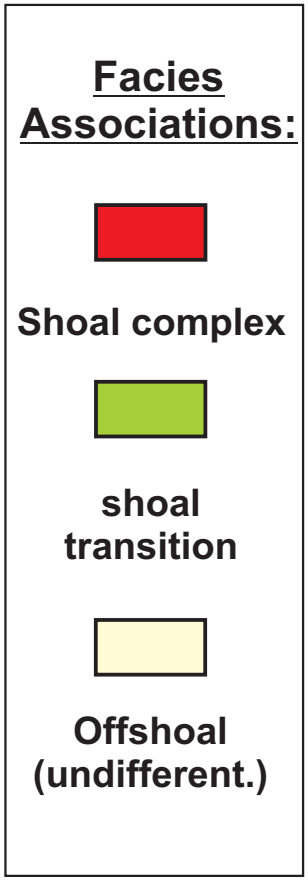

Minerals

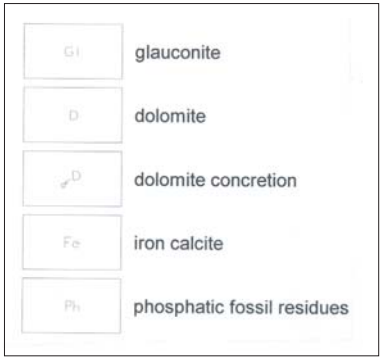

Lithology

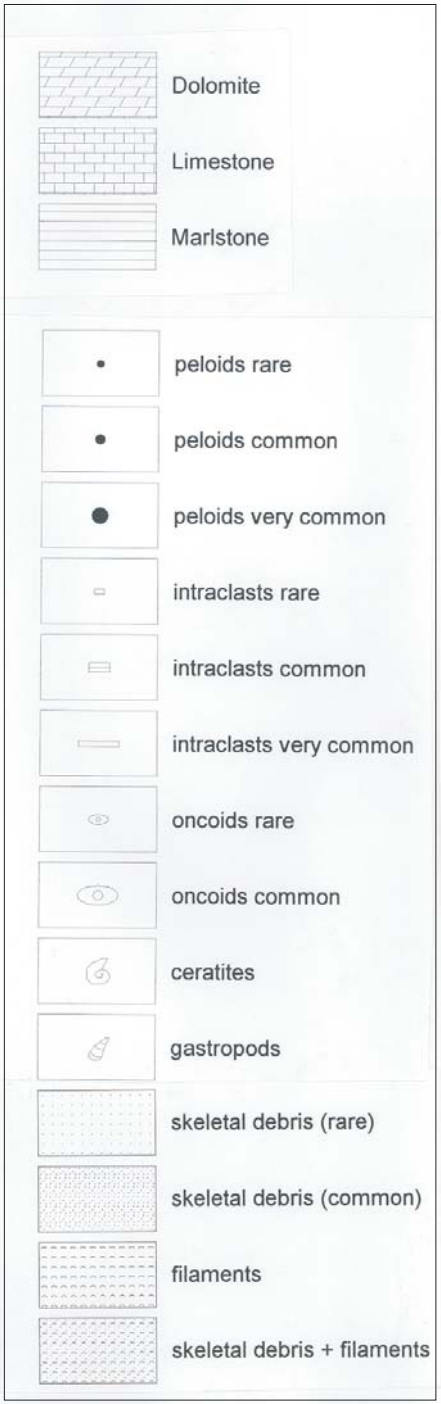

Fossils

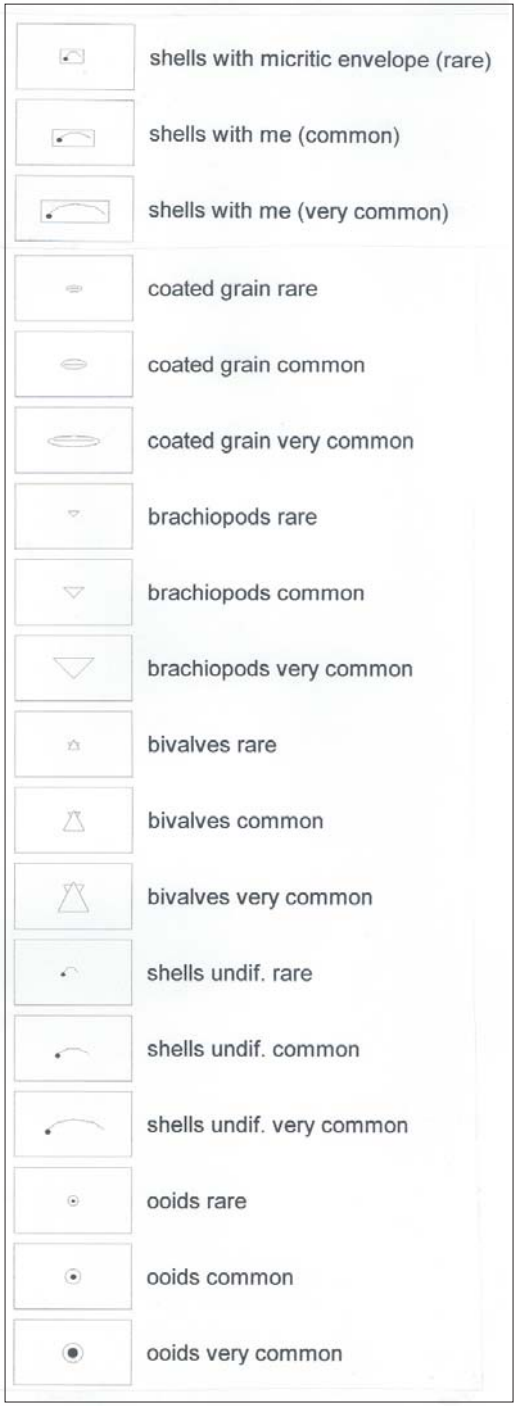

Depth
1:60

poro. [%] 20 0
k(h) [mD] 0 50
k(v) [mD] 0 50
GR [cps] 10 45

mb ld dthofaci LFT th conta a tr oo cg p in rf bi br sh remarks

p#1 struct

pecial

ineral

ticle s
0 11

Weckelweiler (Q 1)

0 1 2 3 4 5 6 7 8 9 10 11 12 13 14 15 16 17 18 19

GB
GK
OT
HT
D(g)
D(ß)
D(a)
TH (z)
TH (e)

f-u
f-u
c-u
f-u
f-u

Ph
Gl
Ph
Gl
Gl
Ph
Gl

double valved brachiopods

black grains, ophiure ossicles common, basis: large shells

large, double valved coenothyris v.

upper part: fine-grained debris + shells
debris partly black
middle: interbedded coarse, bioclastic bed
lower part: fine-grained, large brachiopods
double valved brachiopods available

double valved brachiopods common
dark debris common

dark components + dolomitized particles common

upper part: largely dolomitized, also most ooids, small double valved brachiopods
lower part: partly large intraclasts + ooids

ooids commonly dolomitized, basis: well sorted, glauconite common

ooids mostly dolomitized

basis: large intraclasts, altogether medium sorted

shells commonly dissolved, basis: well sorted

top: large, dark shells, basis: very large components

large oncoids common + large, double valved brachiopods
basis: well sorted

coarse-grained debris + double valved brachiopods

tempestite, basis: large shells

large shells

large double valved brachiopods

unit composed of pure shell hash

large bivalves + brachiop.
large channel

black debris

pure ooid-grainstone, very well sorted, sporadic large bivalves + large brachiopods

medium sorted

dark debris with ophiure ossicles

top: black ooids + coated grains

large bivalves + brachiopods, medium sorted

Brettenfeld (Q 2)

Depth 1:60

No GR mb lfd thofaci LFT.th contadip tr oo cg ein rf bi br sh remarks

10 45

particle s

0 11

GK + BT

OT

D (g)

D (ß)

D (a)

TH (z)

0 1 2 3 4 5 6 7 8 9 10 11 12 13 14 15 16 17

Depth
1:60

poro. [%] 20 0
k(h) [mD] 0 50
k(v) [mD] 0 50
GR [cps] 10 45

mb lf dthofaci LFT.th pecial A Tr Oo cg e In rf bi br sh

p Struc
conta
ticle S
0 11
ineral

Remarks

Gammesfeld (Q 3)

0 1 2 3 4 5 6 7 8 9 10 11 12 13 14 15 16 17 18 19

GK
OT
HTB
D(g)
D(ß)
D(a)
TH
(z)
TH
(e)

Gl Ph D D Fe Gl Gl Gl Gl Gl Gl Ph

f-u
c-u
c-u
f-u
c-u
f-u
f-u
f-u
f-u
f-u
f-u
f-u
c-u

large shells, black peloids
Ooids decreasing up, large shells w/ micrit-residue -> tempestite
small ooids, filaments
fine debris
much skeletal debris
large brachiopods (Coenothyris vulgaris)
ooids dolomitized
large brachiopods + more coated grains in intercaleted layers, well sorted ooid-sand
ooids dolomitized, shells w/ micrit- residue
ooids -> FeC, shells w/ micritic-residue
on top large brachiopods
fine skeletal debris GS
on top + bottom of strata black brachiop.
black peloids common
black peloids, large brachiopods
large brachiopods, well sorted oo-bio GS
black peloids
ooids decreasing up, small Coenothyris
pure ooid GS
Top large brachiopods, Bottom small br.
larger ooids, small brachiopods
Top large brachiopods, ooid - GS, well sorted
poorly sorted
large brachiopods, set height 40 - 50 cm
large shells
filaments common
micritic envelopes decreasing up
pure ooid - cg GS, very well sorted
well sorted, still single brachiopods
ooids decreasing up
ooids increasing up, large brachiopods
micritic envelopes increasing up
well sorted
ooids increasing up
ooids increasing up
very well sorted ooid GS
ooids + cg increasing up
bioturbation increasing up
large ooids, large brachiopods
basis well sorted to very well sorted
pure ooid GS
large brachiopods
ooids decreasing up, brachiopods increasing up
LFT 1, ooids always disolved and replaced by FeC
brachiopods + shells increasing up
shells + brachiop. w/ micrit residue
large micrit intraclasts poorly rounded, poorly sorted
MS - marl alterations
large shells
large brachiopods partly w/ micritic envelopes
basis small shells common
light grey MS - WS
medium grey MS
medium grey MS
dark grey marl
medium grey MS

Schmalfelden (Q 4)

Depth 1:60

Poro [%] 20 0

k(h) [mD] 0 50

k(v) [mD] 0 50

GR[cps] 0 10 45

mb lfd thofaci LFT ithed cont dip tr oo cg ein rf bi br sh

p ructur ar

lineral

ec.lit

art.siz 0 11

remarks

GB + OT

G(ß)

G(a)

HT

D(g)

D(ß)

D(a)

TH (z)

TH (e)

11-7b 11

11-10

10

10-11

11

10

cu

fu

Bonebed

Disarticulated & fragmented brachiopods (c)

Base: Bonebed-layer 1cm

Top: algal-laminites ?, oncoids
poorly sorted, dolomitized ooids
Base: event-sheets, umbrella str.

dolomitized ooids

strongly dolomitized
original content hardly to recognize

strongly dolomitized
dolomitized ooids (p)

yellow-brownish claystone

poorly sorted, large shells

partly dolomitized, large shells

large shells w/ micritic envelopes
Base: well sorted shell hash

yellow massive dolo-mudstone

partly dolomitized

strongly dolomitized

yellow dolomite, w/ mudstone-nodules

poorly sorted, partly dolomitized

Top: poorly sorted, partly dolomitized
Base: moderately sorted

well sorted shell hash
Base: moderately sorted

fine black debris

Top: large, articulated shells
dark fine grained debris common
well - moderately sorted

blackened components

large articulated shells
all components blackened
moderately sorted
Basis: well sorted

moderately - poorly sorted

moderately sorted black pebbles ws

dark components, poorly sorted

fine bioclastic debris

moderately - poorly sorted, ooids
decreasing upwards, shells increasing

upward incresing pure ooid - coated grain grainstone, well sorted

Top: coarser debris, moderately sorted
Base: dark fine debris, poorly sorted

dark debris & components, poor - moderately sorted

poor - moderately sorted

Base: dm-scale, angular intraclasts

Base: large shells, poorly sorted

well sorted

upward decreasing level of sorting

moderately sorted

black debris, ossicles (c)

Base - mid: large intraclasts, poorly s.

poorly sorted

poorly sorted

poorly sorted

black debris, poorly sorted

poorly sorted

altogether moderately - poorly sorted
stylolithes common
small articulated brachiopods present
Base: reworked

Top: large articulated brachiopods (p) & dm-scale intraclasts (p)
well sorted, fine shell-hash

black debris (p-c), poorly sorted

poorly sorted

poorly sorted, cm-scale intraclasts

poorly sorted

poorly sorted

poorly sorted

poorly sorted, brachio. partly articul.

poorly sorted

calcisiltitic laminae intercalated

poorly sorted

poorly sorted

Base: wavy laminated calcisiltit

Base: calcisiltit

argillaceous marl w/ micrit nodules

Top: wave ripples, Base: reworked

Depth 1:60 **Bettenfeld (Q 5)**

k (h) [mD] 0 50

GR [cps] 10 40

poro. [%] 20 0

k (v) [mD] 0 50

mb lmdthofaciLFT.thata bou a tr oo cg oein rf bi br sh

Remarks

p di Stru

lineral

special

rt. Si

0 11

GK

OT

HT + D(g)

D(ß)

D(a)

TH (z)

TH (e)

f-u

f-u

f-u

f-u

c-u

f-u

c-u

Fe

D

Fe

Fe

D

Fe

Fe

D

Fe

large brachiopods

very small skeletal + non-skel. grains
basis (40 cm) large shells

very small skeletal + non-skel. grains

much debris

large brachiopods, large well rounded intraclasts (beige)

Top coarse shell layer
partly interbedded coarser shell layers,
poorly sorted, w/ higher porosity
Basis (5 cm) well sorted pure ooid GS

poorly - medium sorted

medium - well sorted shell GS, brachiopods small - medium
basis fine debris

poorly sorted

50 cm bed of large, poorly sorted brachiopods and shells

small ooids dolomitized, poorly sorted

ooids small

well sorted ooid GS

medium sorted, top well sorted

poorly sorted, shells w/ micrit residue,
large ooids

poorly sorted, ooids increasing up

Top components very fine, well sorted,
coarser + finer beds alternating,
partly large intraclasts + brachiopods

medium grey MS, at 11.4 m Dolo - MS

partly black peloids

poorly sorted

basis well sorted ooid GS

poorly sorted

Top medium sorted,
ooids coarsening up,
partly thin interbeded shell layers,
medium - poorly sorted
basis pure ooid GS layer of
small, well sorted ooids

Top: fining up to pure, well sorted ooid GS

intercaleted poorly sorted coarse brachiopod - shell layer

intercaleted brachiopod - shell layer

coarser shell layers alternate with finer shell layers,
altogether poorly sorted

small components, filaments

skeletal debris PS

skeletal debris PS

tempestite ?

MS beds thickening up,
thin marl layers between

Top: very large, well rounded micrit intraclasts,
Middle: large brachiopods + shells
Basis: small bioclasts coarsening up

diagenesis ?

diagenesis ?

blue - medium grey MS

thin (10 cm), wavy laminated MS beds

Haltenmühle (Q 6)

Depth 1:60

GR [cps] 10 45

poro. [%] 20 0

k(h) [mD] 0 50

k(v) [mD] 0 50

p i. stru

pecial

d conta

ticle s

0 11

Ph

GB BT OT G(g) G(ß) HT D(g) ? D(ß) D(a) TH (z) TH (e)

f-u c-u f-u f-u f-u f-u

dolomitic marl with dolomite nodules

top + basis: debris, middle: shell hash, well sorted

fine-grained shell hash, well sorted

well sorted shell hash, FeC in interparticle space common

wide channel on top,

fine-grained dolo-packstone (?) with scattered large, double valved brachiopods

fine-grained dolo-packstone (?)

basis: channel filled with large brachiopods + bivalves

more shells on the basis

well rounded intraclasts + large shells

unit is composed of 3 tempestites

fine-grained shell hash, well sorted

basis: very large (several cm), rounded, micrit intraclasts

coarse-grained shell hash

very fine-grained shell hash

basis: angular intracl. + large shells

large shells

filaments common, large shells

large, double valved brachiopods

fine laminated calcisiltite

dark colored bed, black debris

very fine-grained debris + shells

black, arenitic debris

rounded micritic intraclasts

bonebed layer on top

coaly fragments

tempestites, poorly sorted,

basis: large, angular intraclasts

black grains available

black grains very common

black grains common

black grains common, large peloids

black grains, poorly sorted

poorly sorted

well sorted, channel (?), components decrease upwards

top: fine laminated debris

top: fine laminated debris

basis: bonebed

calcisiltite

Dürrenhof (Q 7)

Depth 1:60

GR [cps] 10 45

poro. [%] 20 0

k(h) [mD] 0 50

k(v) [mD] 0 50

mb lfd thofaci LFT th ineral a tr oo cg ein rf bi br sh

p conta

i. stru

pecial

rt. si

0 11

articl

0 11

remarks

remarks#2

0 1 2 3 4 5 6 7 8 9 10 11 12 13 14 15 16 17 18 19 20

GB GK ? BT OT G(ß) HT D(g) D(ß) D(a) TH (z) TH (e)

f-u f-u c-u f-u bs f-u f-u

bonebed

large micrit intraclasts poorly rounded

intercaleted layers with large brachiopods + shells, poorly sorted

large brachiopods

large brachiods, coarse shell hash w/ micrit residue

smaller brachiopods

intercaleted layers with large brachiopods

fine shell hash

debris P-GS (basis), shell hash GS (top)

Top: ichnofossils, large brachiopods

large brachiopods

Top: dark debris, black peloids

dark grey, black peloids

basis: partly large (dissolved) shells

top: cross bedding - trough, large shells, middle: thin shells, horizontal embedded

on bed surfaces large brachiopods, basis: micrit intraclasts, angular

top (10 cm): large longish intraclasts, angular altogether pure shell hash with rarely complete bivalve + brachiopod shells

basis: large brachiopods + bivalves

large brachiopods + shells turning up to fine shell hash

large complete brachiop. + bivalves, very large intraclasts, rounded

coarser layers: large shells, basis: large micrit intraclasts rounded

pure arenitic-debris GS

large brachiopods

top: well sorted ooid-coated grain-debris GS, altogether arenitic-debris GS

arenitic debris GS with filaments, large micritic intraclasts, rounded

pure arenitic-debris GS, disolved large brachiopods + bivalves

on bed surfaces large complete brachiopods

gutters filled with large brachiopods + shells

black peloids, large micrit intraclasts

top: beds thining up, filaments common

top: large, poorly rounded micrit intraclasts components dark / black, large black peloids common

top + basis medium - light grey MS between marly MS

black pebbles + ophiure ossicles common

HCS

ophiure ossicles, basis: coarse debris

top: fine laminated, basis: coarse

ophiure ossicles available

ophiure ossicles available

ophiure ossicles available

ophiure ossicles available

tempestite, basis: coarse, umbrella structures, top: fine shelly

double valved brachiopods

basis: large brachiopods and bivalves

large double valved brachiopods + oysters common

large brachiopods available

angular micritic intraclasts common

double valved brachiopods

tempestite, basis: intracl. top: coarse shells

basis: black debris, ophiure ossicles

channels filled with debris

Depth poro. [%] k(h) [mD] GR [cps] mb lfd thofaci LFT.th ineral a tr oo cg ein rf bi br sh remarks

1:60 20 0 0 50 10 45

k(v) [mD] p pecial remarks#2

0 50

Gattenhofen (Q 8)

i. stru

d conta

rt. si

0 11

articl

0 11

0 1 2 3 4 5 6 7 8 9 10 11 12 13 14 15 16 17 18 19 20

GB BT OT G(ß) G(a) HT D(g) D(ß) D(a) TH (z) TH(

f-u c-u f-u f-u

10-9b 9b-10 9b 1a 4 1a 4 1a 9b 1a 1b

very poorly sorted, gutter ?, large brachio.

large brachiopods

top: large brachiopods,

more shell debris

poorly sorted, intercaleted layers with very coarse components, between complete shells

medium sorted, set height: 5-10 cm

well sorted, set height: 5-10 cm, partly small brachiopods, much shell debris

partly large shells, shell debris common

small brachiopods

black peloids

black peloids

black peloids

black peloids

black peloids

black peloids rare

middle-top: fining-up to fine debris, altogether black peloids common, basis: black debris, angular, small brachiopods

large, rounded micrit intraclasts, altogether shell hash

common disolved and replaced by FeC

large brachiopods, common disolved + replaced by FeC, altogether shell hash

brachiopod-layer, complete brachiopods

from bottom to top increasing shells

large micrit intraclasts

complete brachiopods

pure debris GS with intercaleted brachiopod layers, brachiopods commonly replaced by FeC

large Coenothyris vulgaris

complete brachiopods

with intercaleted marl layers

through marl layers separeted MS beds

large bivalves replaced by sparite

black debris, ophiure ossicles

black debris, ophiure ossicles

well-rounded, micritic intrasclasts

middle: large shells, bottom: small shells

tempestite, basis: coarse debris, top: fine laminated calcisiltite

tempestite, basis: coarse debris, top: finer

ophiure ossicles

large brachiopods, partly double valved

poorly sorted

top: well sorted ooid-grainstone

middle: medium sorted

basis: coarse, poorly sorted

top: fragmented shells, bottom: small brachiopods, partly double valved

top: fine laminated, basis: large shells

basis: well rounded, micritic intraclasts

large double valved brachiopods

graded

Core Oesfeld (C 1)

Depth 1:60

poro. [%] 20 0

k(h) [mD] 0 50

k(v) [mD] 0 50

No GR 10 45

mb lfd thofaci LFT ith d conta dip tr oo cg ein rf bi br sh

por ec.lit a

d.struc

ineral

art.siz 0 11

remarks

0 1 2 3 4 5 6 7 8 9 10 11 12 13 14

GB GK BT OT G(g) G(ß) HT

13c - 9 | 9b | 4a | 7a-3 | 13a - 13c | 4a | 13a | 13c-x | 13c | 7a | 9 - 13c | 13c | 1 | 13c | 13a | 13c | 13a | 13c | 13a | 6a | 13a | 13c | 13a | 7a ? | 13c | 6a | 7a | 7b-13a | 13c | 13a | 13c | 13a | 4a | 15a-7b

fu fu fu fu fu fu fu fu

Py

partly dolomitized ?
marly intercalations (mm-scale)

limestone blueish grey

claystone greenish gray, partly black or light grey

shelly limestone,
grey
coarse grained

complete succession is composed of several stacked event sheets
Tops: dolomitic calcarenites of biocl. (c)
Bases: fine calciruditic shell-hash, shells w/ me + coated grains (c-a), biocl. (c), dolomitized ooids (p), moderately sorted

Base: large shells (c)

laminated by aligned shells w/ umbrella structures, dolomit. biocl. debris (c)

partly dolomitized, mottled, glauconite

moderately sorted, Base: bioturbated

complete succession composed of stacked event sheets
pure ooid-coated grain grainstones, well sorted intercalate with coarser, poorly sorted shelly beds = event sheets

large dolo-intracl. -> flat pebbles congl.

ooids are dolomitized
Top: moderately sorted, large shells and intraclasts
between: well sorted shelly-oolitic gs
Basis: poorly sorted
sporadic event sheets, reworking & edge-wise fabric of comp. + umbrella structures

dolo-marl, beige with calcite-streaks
Basis: horizontally aligned up to 5cm large intraclasts

Top: umbrella structures
upward increasing ooids
upward decreasing shells w/ me
altogether poorly sorted

shell-hash, moderately sorted

Top: reworked, edge-wise fabric
Basis: muddy, large shells, poorly sorted

poorly sorted, dolo-intraclasts, large shells, umbrella structures (c)

moderately sort., angular dolo-intracl., shells w/ me up to 5 cm large

large shells, umbrella struct. (c)

Top: poorly sorted, mottled -> bioturb.
below well- m. sorted shelly-oolitic ps
Mid.-basis: poorly sorted, large shells, umbrella structures (c), articulated br.

horizontal aligned shells
moderately sorted (Basis: mod. - poorly)

Top: well - moderately sorted
large shells w/ me (p-c)
upwards increasing level of sorting
Basis: poorly sorted

dolo-intraclasts (p)

micritic, grey limestone
intercalated with thin, beige
dolo-marlstone seams

grey marlstone
with few micritic limestone beds

marly claystone, greyish brown

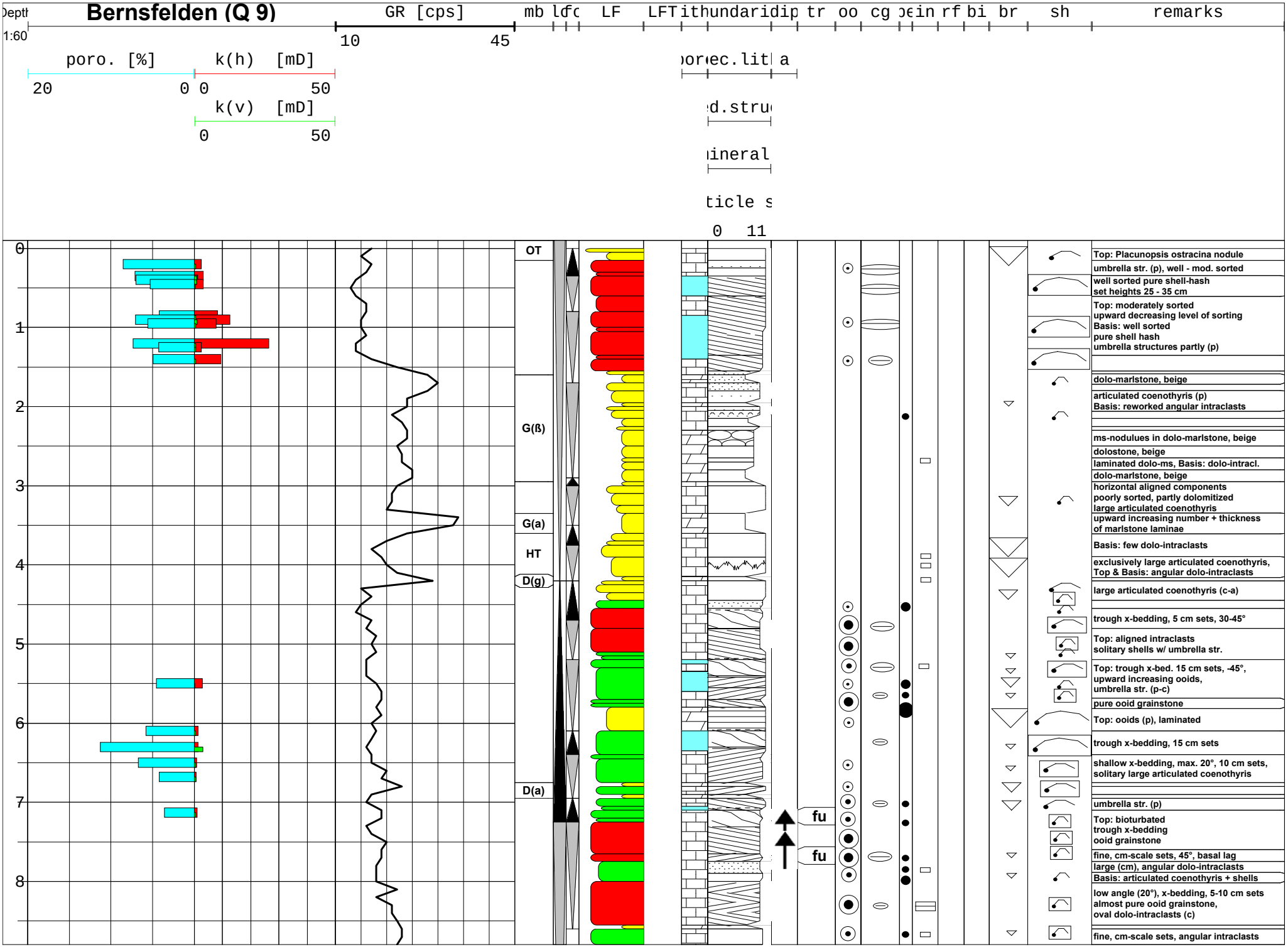
Bernsfelden (Q 9)
GR [cps]
10
45
poro. [%]
20
0
k(h) [mD]
0
50
k(v) [mD]
0
50
0
1
2
3
4
5
6
7
8
OT
G(ß)
G(a)
HT
D(g)
D(a)
fu
fu
Top: Placunopsis ostracina nodule
umbrella str. (p), well - mod. sorted
well sorted pure shell-hash
set heights 25 - 35 cm
Top: moderately sorted
upward decreasing level of sorting
Basis: well sorted
pure shell hash
umbrella structures partly (p)
dolo-marlstone, beige
articulated coenothyris (p)
Basis: reworked angular intraclasts
ms-nodulues in dolo-marlstone, beige
dolostone, beige
laminated dolo-ms, Basis: dolo-intracl.
dolo-marlstone, beige
horizontal aligned components
poorly sorted, partly dolomitized
large articulated coenothyris
upward increasing number + thickness
of marlstone laminae
Basis: few dolo-intraclasts
exclusively large articulated coenothyris,
Top & Basis: angular dolo-intraclasts
large articulated coenothyris (c-a)
trough x-bedding, 5 cm sets, 30-45°
Top: aligned intraclasts
solitary shells w/ umbrella str.
Top: trough x-bed. 15 cm sets, -45°,
upward increasing ooids,
umbrella str. (p-c)
pure ooid grainstone
Top: ooids (p), laminated
trough x-bedding, 15 cm sets
shallow x-bedding, max. 20°, 10 cm sets,
solitary large articulated coenothyris
umbrella str. (p)
Top: bioturbated
trough x-bedding
ooid grainstone
fine, cm-scale sets, 45°, basal lag
large (cm), angular dolo-intraclasts
Basis: articulated coenothyris + shells
low angle (20°), x-bedding, 5-10 cm sets
almost pure ooid grainstone,
oval dolo-intraclasts (c)
fine, cm-scale sets, angular intraclasts

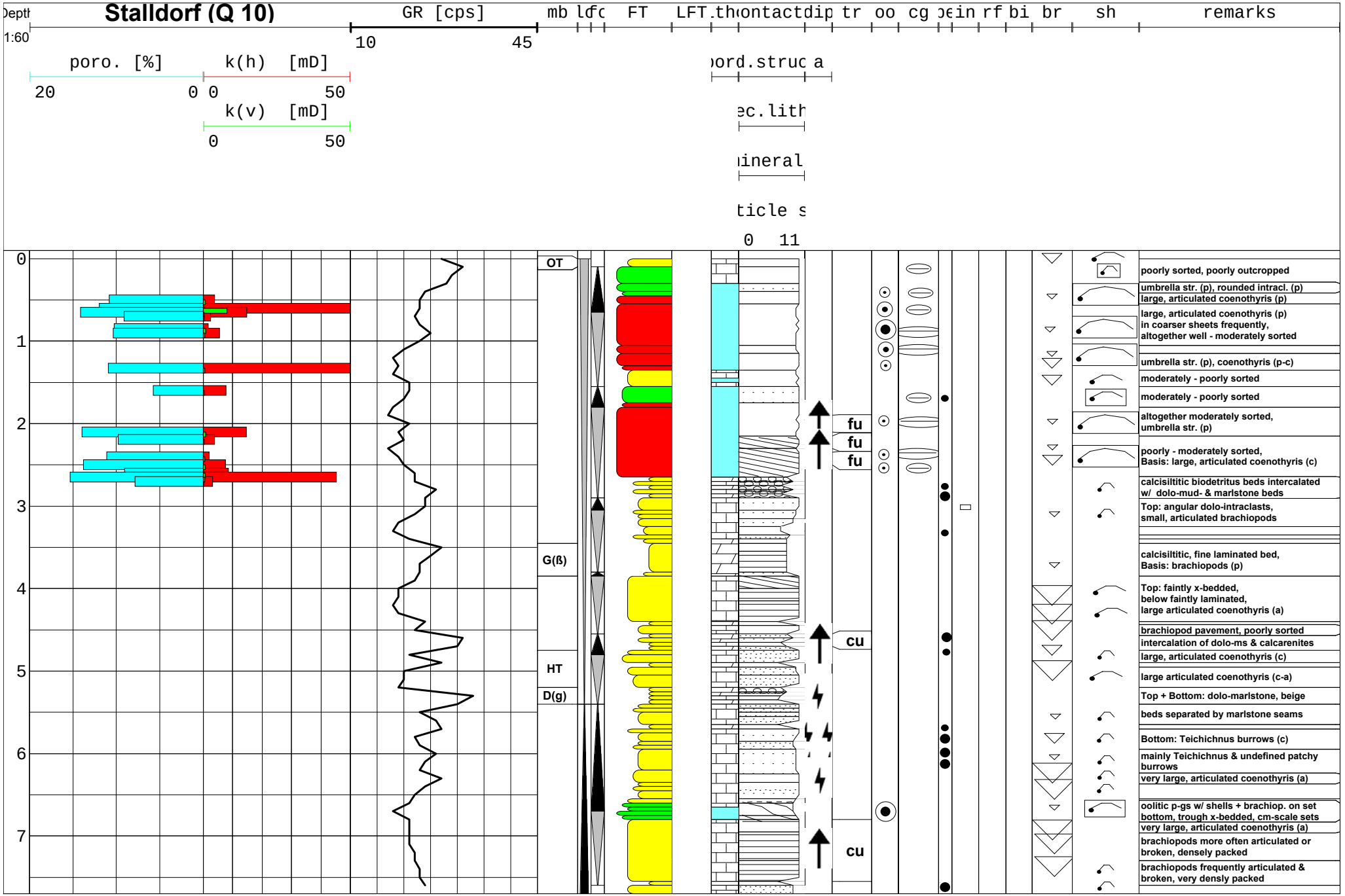
Stalldorf (Q 10)
Depth
1:60
GR [cps]
10
45
mb
lfc
FT
LFT.th
ontact
dip
tr
oo
cg
ein
rf
bi
br
sh
remarks
poro. [%]
20
0
k(h) [mD]
0
50
k(v) [mD]
0
50
ord.struc
a
ec.lith
ineral
ticle s
0
11
0
1
2
3
4
5
6
7
OT
G(ß)
HT
D(g)
fu
fu
fu
cu
cu
poorly sorted, poorly outcropped
umbrella str. (p), rounded intracl. (p)
large, articulated coenothyris (p)
large, articulated coenothyris (p)
in coarser sheets frequently,
altogether well - moderately sorted
umbrella str. (p), coenothyris (p-c)
moderately - poorly sorted
moderately - poorly sorted
altogether moderately sorted,
umbrella str. (p)
poorly - moderately sorted,
Basis: large, articulated coenothyris (c)
calcisiltitic biodetritus beds intercalated
w/ dolo-mud- & marlstone beds
Top: angular dolo-intraclasts,
small, articulated brachiopods
calcisiltitic, fine laminated bed,
Basis: brachiopods (p)
Top: faintly x-bedded,
below faintly laminated,
large articulated coenothyris (a)
brachiopod pavement, poorly sorted
intercalation of dolo-ms & calcarenites
large, articulated coenothyris (c)
large articulated coenothyris (c-a)
Top + Bottom: dolo-marlstone, beige
beds separated by marlstone seams
Bottom: Teichichnus burrows (c)
mainly Teichichnus & undefined patchy
burrows
very large, articulated coenothyris (a)
oolitic p-gs w/ shells + brachiop. on set
bottom, trough x-bedded, cm-scale sets
very large, articulated coenothyris (a)
brachiopods more often articulated or
broken, densely packed
brachiopods frequently articulated &
broken, very densly packed

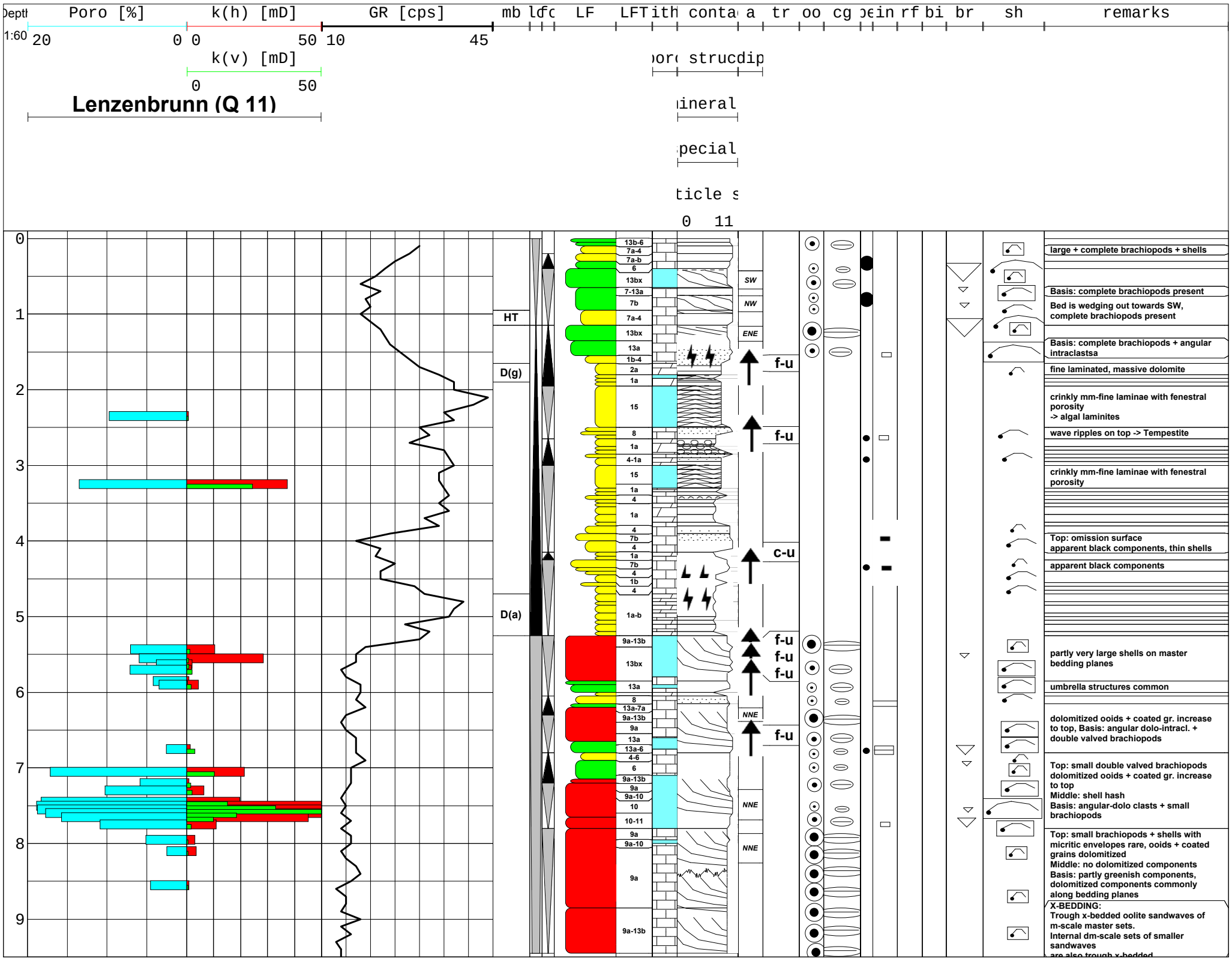
Depth
1:60
Poro [%]
20
0
k(h) [mD]
0
50
k(v) [mD]
0
50
GR [cps]
0
10
45
mb
LF
LFT
ith
conta
a
tr
oo
cg
in
rf
bi
br
sh
remarks
Lenzenbrunn (Q 11)
structdip
mineral
special
ticle s
0
11
HT
D(g)
D(a)
13b-6
7a-4
7a-b
6
13bx
7-13a
7b
7a-4
13bx
13a
1b-4
2a
1a
15
8
1a
4-1a
15
1a
4
1a
4
7b
4
1a
7b
4
1b
4
1a-b
9a-13b
13bx
13a
8
13a-7a
9a-13b
9a
13a
13a-6
4-6
6
9a-13b
9a
9a-10
10
10-11
9a
9a-10
9a
9a-13b
SW
NW
ENE
NNE
NNE
NNE
f-u
f-u
c-u
f-u
f-u
f-u
f-u
large + complete brachiopods + shells
Basis: complete brachiopods present
Bed is wedging out towards SW, complete brachiopods present
Basis: complete brachiopods + angular intraclastsa
fine laminated, massive dolomite
crinkly mm-fine laminae with fenestral porosity
-> algal laminites
wave ripples on top -> Tempestite
crinkly mm-fine laminae with fenestral porosity
Top: omission surface
apparent black components, thin shells
apparent black components
partly very large shells on master bedding planes
umbrella structures common
dolomitized ooids + coated gr. increase to top, Basis: angular dolo-intracl. + double valved brachiopods
Top: small double valved brachiopods
dolomitized ooids + coated gr. increase to top
Middle: shell hash
Basis: angular-dolo clasts + small brachiopods
Top: small brachiopods + shells with micritic envelopes rare, ooids + coated grains dolomitized
Middle: no dolomitized components
Basis: partly greenish components, dolomitized components commonly along bedding planes
X-BEDDING:
Trough x-bedded oolite sandwaves of m-scale master sets.
Internal dm-scale sets of smaller sandwaves
are also trough x-bedded
0
1
2
3
4
5
6
7
8
9

Core Röttingen (C 2)

Depth 1:60

poro [%] 20 0

k(h) [mD] 0 50

k(v) [mD] 0 50

No GR 0 10

mb lfd 45

thofaci

LFT.thd

contact

dip

tr

oo

cg

pein

rf

bi

br

sh

remarks

p i.stru a

ec.lith

ineral

art.siz 0 11

GB

GK

BT

OT ?

G(ß) ?

HTB ?

D(a)

TH (z)

Ph

Gl

4b

7b

7b - 4b

7b

7b-a - (4b)

7a

cu

cu

11-x

9 - 13c-x

13c - 9

6a

13c-9

13a-7a

7a

1a-4a

13c-x

13a-c-x

13c-6a

9-13c

7b-10

13c-7b

13c

7a-b

7a

1a-0

7a

1a

1a+9b

13c-10

10

10-13c

10

fu

fu

fu

partly dolomitized

fish scales

black-grey argillaceous marlstone
with intercalated shelly wackestones

phosphatic remains

marlstone, light brown - beige
intercalated beds with
phosphatic remains

shelly limestone
blueish-grey,
partly dolomitized

marly limestone, brownish yellow

dolostone
grey - brownish
fine crystaline dolomite

Basis: well sorted

wavy muddy top
aligned, angular intraclasts

bioturbated, mottled fabric

flaser bedded

large aligned shells (c)

large shells (c),
parallel laminated
Basis: large dolo-intraclasts

large shells
grey shelly Lst., partly dolomitized

shelly limestone
alternating porous & tight beds
repeatedly stylolithes

yellow Lst. -> dolomitized ?

upward increasing CaCO3 content

dark grey marlstone
with phosphatic remains
(fish scales)

mudstone interbedding

mudstone interbedding

marlstone
phosphatic remains (fish scales)

marlstone - mudstone intercalation

intercalation of micritic- & sparitic
limestone beds, blueish-grey,
lowermost 55 cm partly dolomitized

succession stacked of 5-10 cm thick
amalgamated "event-sheets"
umbrella str. (p), shelly bottom sets

succession composed of
well - moderately sorted oolitic-gs beds
and
stacked, amalgamated, poory sorted
shelly "event-sheets"
mm-scale stylolithes abundant

large articulated shells w/ me (p-c)

large ooids (c)

upward decreasing ooids & coated gr.,
black, articulated, bored shells (p),

succession composed of coarse, shelly
"event-sheets", typical features:
umbrella str. (c), dolomitized & original
ooids mixed together, reworked
components, grading, angular intracl.

angular cm-scale intracl. (p), large shells

Basis: well sort. ooid.coated grain gs

shells w/ me increasing upwards

large, articulated shells/brachiopods (c)
-> Placunopsis oysters Basis: reworked

hummocky cross stratification (HCS)

Top: HCS

tempestite succession w/ current ripples

Top: large cm-scale intraclasts, bioturb.

Top: light green ooids
altogether well sorted shell hash
aligned components
solitary large intraclasts

intense bioturbation ?

limestone micritic to sparitic, grey

argillaceous marlstone
dark grey
shale-like

limestone, upper bed sparitic
lower bed micritic

argillaceous marlstone

Frauental (Q 12)

Depth 1:60

GR [cps] 10 45

Poro [%] 20 0

k(h) [mD] 0 50

k(v) [mD] 0 50

mb lfd thofaci LFT ith D conta a tr oo cg p in rf bi br sh

por Struct

special

lineral

ticle s

0 11

remarks

OT

G(ß) ?

G(a) ?

HT + D(g)

D(a)

TH (z)

f-u

c-u

f-u

f-u

cu

f-u

f-u

poorly sorted, coarse sparitic, FeC+ dolomite common, large brachiopods

complete, large brachiopods only

completely dolomitized, contour of brachiopods recognizable

complete, large brachiopods
poorly sorted

components dolomitized, allochthonous

complete brachiopods
allochthonous components dolomitized
Top gs: small brachiopods common
dolo. ooids, coated grains etc. common
Basis gs: br + sh with me very common

dolomitized components increasing-up

Top: large, complete brachiopods and bivalves
medium - p. sorted, homogenous
coarse shell hash + umbrella structures

well sorted shell hash
Basis gs:
fine shell-calcarenite
Basis p-gs:
complete, large br. + intraclasts

calcarenite

large, complete brachiopods + bivalves (commonly dissolved)
Basis: large brachiopods sporadic

Top: large shells present
Middle: small shells
Basis: filaments

calcarenite-calcsiltite

mudstone, medium grey

Top + Basis: dark yellow-brown dolost.
Middle: dolostone, light yellow

turquoise claystone

mudstone, medium grey
solitary peloids & shells

upward increasing number of comp.:
mainly shells & peloids
and upward increasing level of bioturb.

light grey - greenish mud- to marlstone

wave rippled, fine lamin. calcisiltit

upward increasing number of comp.
& level of bioturbation

wave rippled, fine lam. calcisiltit

"event-sheet" with aligned comp.
Basis: well sort. Top: poorly sorted

greenish-brownish argillaceous marl.

Basis: more & larger shells (c)

Top: moderately sorted, dark grey
below: poorly sorted, light grey
Basis: large (cm-scale) brachiopods

very large shells w/ me, brachio. & intracl.
Basis: strongly recrystalized / cemented

large, rounded intracl. upward decreasing in size

components are very small, dolomitized ooids (c)

large shells, strongly recristalized
bed wedges out towards S

poorly sorted

poorly sorted

Basis: large shells

Top: pure calcarentite, Basis: comp.

mudstone, medium grey

intercalation of light-medium grey ms & dolo-marlstone beds

Basis: calcisiltite fine laminated

articulated brachiop., cm-scale intracl.

nodular peloid wackestone

intense bioturb. peloidal packstone

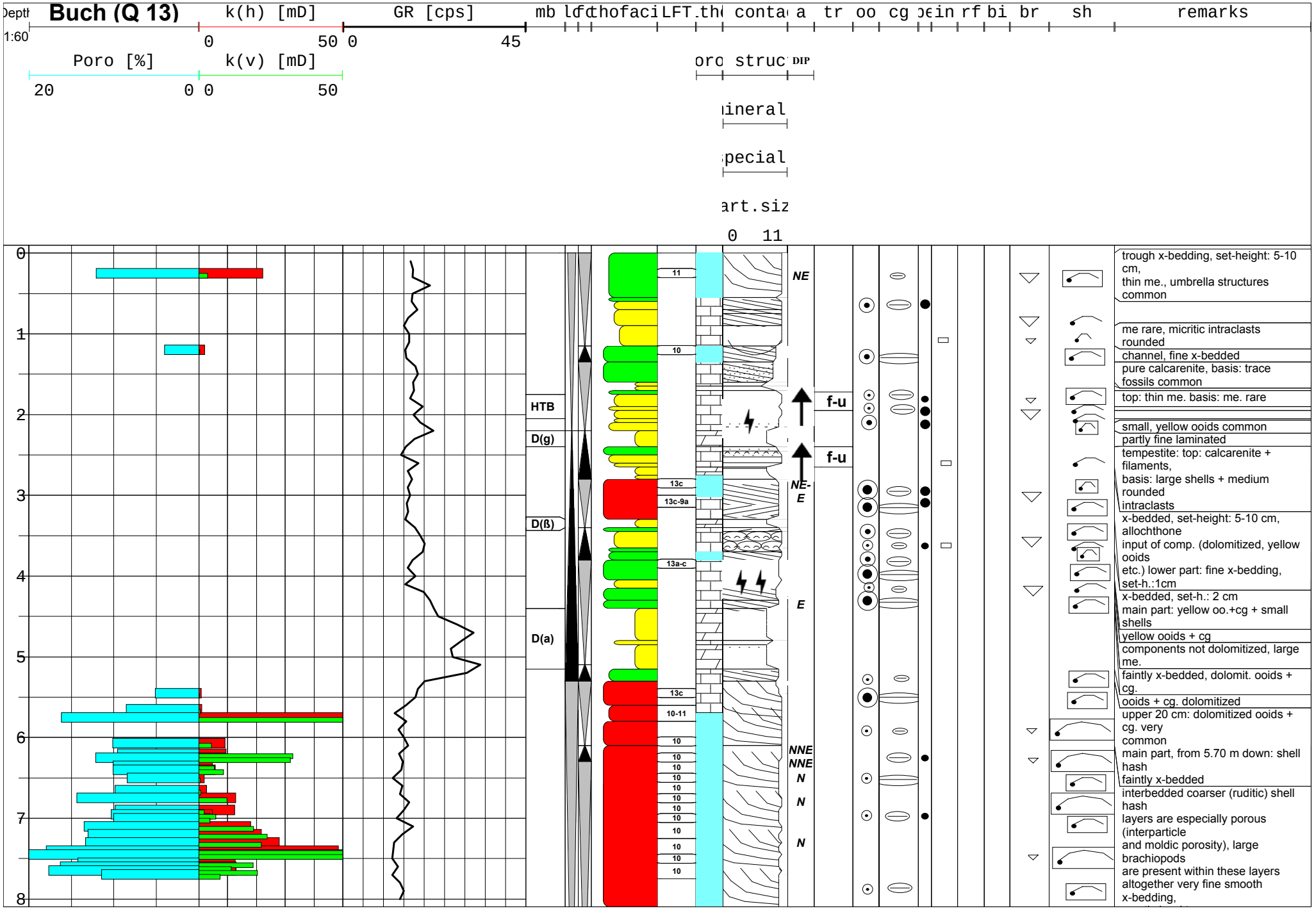
Buch (Q 13)
Depth
1:60
k(h) [mD]
0
50
GR [cps]
0
45
Poro [%]
20
0
k(v) [mD]
0
50
mb
lfd
thofaci
LFT.th
conta
a
tr
oo
cg
ein
rf
bi
br
sh
remarks
oro
struc
DIP
ineral
pecial
art.siz
0
11
HTB
D(g)
D(ß)
D(a)
NE
NE-E
E
NNE
NNE
N
N
N
f-u
f-u
11
10
13c
13c-9a
13a-c
13c
10-11
trough x-bedding, set-height: 5-10 cm,
thin me., umbrella structures common
me rare, micritic intraclasts rounded
channel, fine x-bedded
pure calcarenite, basis: trace fossils common
top: thin me. basis: me. rare
small, yellow ooids common
partly fine laminated
tempestite: top: calcarenite + filaments,
basis: large shells + medium rounded
intraclasts
x-bedded, set-height: 5-10 cm, allochthone
input of comp. (dolomitized, yellow ooids
etc.) lower part: fine x-bedding, set-h.:1cm
x-bedded, set-h.: 2 cm
main part: yellow oo.+cg + small shells
yellow ooids + cg
components not dolomitized, large me.
faintly x-bedded, dolomit. ooids + cg.
ooids + cg. dolomitized
upper 20 cm: dolomitized ooids + cg. very
common
main part, from 5.70 m down: shell hash
faintly x-bedded
interbedded coarser (ruditic) shell hash
layers are especially porous (interparticle
and moldic porosity), large brachiopods
are present within these layers
altogether very fine smooth x-bedding,

Depth
1:60

Aub (Q14)

k(h) [mD]
0 50

GR [cps]
10 45

poro. [%]
20 0

k(v) [mD]
0 50

mb lfdthofaciLFT.thd conta a tr oo cg pein rf bi br sh

remarks

p struc

ineral

pecial

art.siz
0 11

GK
BT
OT ?
G(ß)
HT
D(g) ?
D(a)
kl. T
TH (z)
TH (e)

f-u

basis: large sparit intraclasts, angular
large brachiopods

basis: large micrit intraclasts, angular, fining-up

micrit intraclasts especially at marly bedding planes

basis - middle : greenish-grey micrit lenses

top + basis GS: debris, between large brachiopods

large brachiopods

large brachiopods

large brachiopods

top: ooids very common

small intraclasts common, large micrit intraclasts present

filaments common

tempestites: finer shell top: debris shells with me, peloids + micrit intraclasts
coarse shell basis (brachiopods + bivalves without me + debris

top: peloids common
basis: micrit intraclasts common

top: debris, basis: shell layer

top: debris, basis: micrit intraclasts + large brachiopods

top: debris, basis: small brachiopods common

debris fine laminated

top: debris, basis: large intraclasts

basis: micrit intraclasts

small filaments

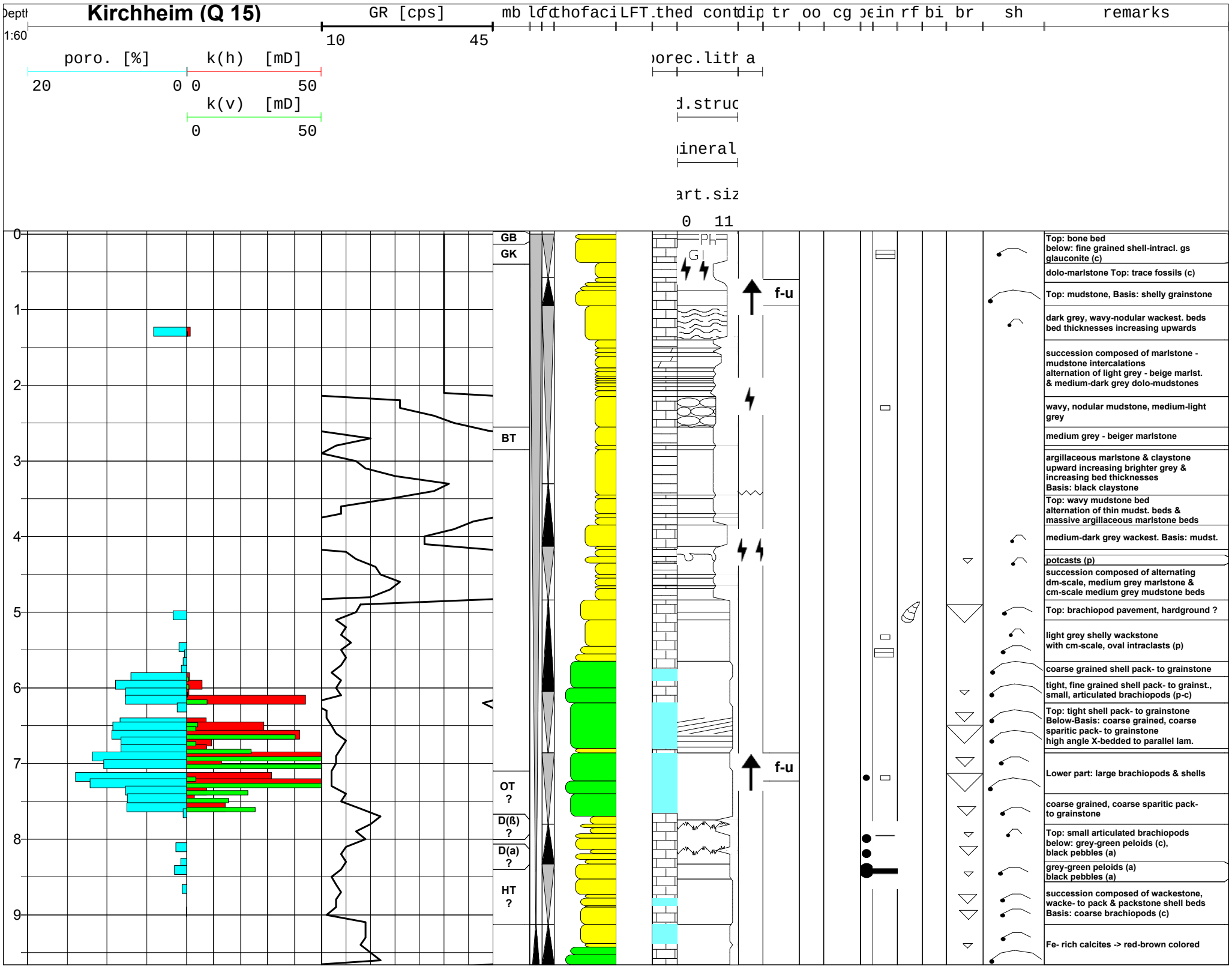
Kirchheim (Q 15)
Depth
1:60
GR [cps]
10
45
mb lfd thofaci LFT.thed cont dip tr oo cg ein rf bi br sh
remarks
poro. [%]
20
0
k(h) [mD]
0
50
k(v) [mD]
0
50
porec.lith a
d.struc
ineral
art.siz
0
11
0
1
2
3
4
5
6
7
8
9
GB
GK
BT
OT
?
D(ß)
?
D(a)
?
HT
?
f-u
f-u
Top: bone bed
below: fine grained shell-intracl. gs
glauconite (c)
dolo-marlstone Top: trace fossils (c)
Top: mudstone, Basis: shelly grainstone
dark grey, wavy-nodular wackest. beds
bed thicknesses increasing upwards
succession composed of marlstone -
mudstone intercalations
alternation of light grey - beige marlst.
& medium-dark grey dolo-mudstones
wavy, nodular mudstone, medium-light
grey
medium grey - beiger marlstone
argillaceous marlstone & claystone
upward increasing brighter grey &
increasing bed thicknesses
Basis: black claystone
Top: wavy mudstone bed
alternation of thin mudst. beds &
massive argillaceous marlstone beds
medium-dark grey wackest. Basis: mudst.
potcasts (p)
succession composed of alternating
dm-scale, medium grey marlstone &
cm-scale medium grey mudstone beds
Top: brachiopod pavement, hardground ?
light grey shelly wackstone
with cm-scale, oval intraclasts (p)
coarse grained shell pack- to grainstone
tight, fine grained shell pack- to grainst.,
small, articulated brachiopods (p-c)
Top: tight shell pack- to grainstone
Below-Basis: coarse grained, coarse
sparitic pack- to grainstone
high angle X-bedded to parallel lam.
Lower part: large brachiopods & shells
coarse grained, coarse sparitic pack-
to grainstone
Top: small articulated brachiopods
below: grey-green peloids (c),
black pebbles (a)
grey-green peloids (a)
black pebbles (a)
succession composed of wackestone,
wacke- to pack & packstone shell beds
Basis: coarse brachiopods (c)
Fe- rich calcites -> red-brown colored

Goßmannsdorf (Q 16)

Depth 1:60

GR 10 45

poro. [%] 20 0

k(h) [mD] 0 50

k(v) [mD] 0 50

hofacie

hofacie

ho pecial

p#1 struct

ineral

ticle s

0 11

0 1 2 3 4 5 6 7 8 9 10 11 12 13 14 15

GB+ GK

BT

OT

G(ß)

G(a)

HT

D(g)

D(ß)

D(a)

f-u

f-u

f-u

top: large ceratite

tempestite

brachiopods concentrated on bedding surface

dolomitized brachiopod layer + trace fossils on bedding planes, basis: placunopsis bioherms common

sporadic large brachiopods, well sorted ooid-gs basis: large (cm), rounded intraclasts, large shells fining-up, ooids increasing-up, x-bedding, set height 5 cm

placunopsis ostracina bioherm

x-bedding, set height 10 cm, scattered dolomitized ooids, large, thin shells common

tempestite, dolomitized ooids

upper part: poorly sorted, x-bed. set heights 5-10 cm

middle-top: well sorted ooid-grainstone, middle-basis: well sorted oolitic-shell-hash, altogether homogeneous

ooids, coated grains + micritic envelopes around shells increasing-up. x-bedding, set heights 30 cm

grain-sizes increasing-up, ooids decreasing-up

x-bedding set heights 5-10 cm

"

sparitic- recrystallised ?

ooids decreasing-up, shells increasing-up

well sorted

dissolved ooids

Depth
1:60

poro. [%] 20 0
k(h) [mD] 0 50
k(v) [mD] 0 50
GR [cps] 10 45

mb lfd thofaci LFT.th mineral a tr oo cg pein rf bi br sh

p.. str

special

conta

art.siz 0 11

articl 0 11

remarks

Sommerhausen (Q 17)

0 1 2 3 4 5 6 7 8 9 10 11 12 13 14 15 16 17 18

GB
GK
BT
OT
G(ß)
G(a)
HT
D(g)
D(ß)
D(a)
TH (z)

GI
c-u
f-u
Fe
D
Fe
f-u
f-u
Fe
f-u
f-u

Unknown
fine skeletal debris
fine skeletal debris, partly nodular layers
MS layers thickening up, dark grey - blue gray MS
marl dark grey - blue grey with partly intercaleted nodular MS beds
nodular MS, dark blue grey
MS layers thining up,
basis: small brachiopods
light beige marly Dolo - MS
dark green grey MS
small brachiopods common
nodular, medium grey MS with intercaleted thin marl layers, nodules thining up
Top: micrit intraclasts + small ooids (FeC) common, large brachiopods
poorly sorted, very large brachiopods
poorly sorted, umbrella struct. common
imbrication
pure ooid - shell GS
imbrication, large intraclasts
pure ooid - shell GS
PS basis: trace fossils very common
MS with intercaleted thin marl layers
Top: cross bedding - trough, set height 15-20 cm
nodular MS
Top: ooids common replaced by FeC, well sorted
medium-well sorted fine shell P-GS,
Basis: large micrit intraclasts
Top: 10 cm nearly pure ooid GS, large (- 50 cm) micrit intraclasts, well rounded, horizontal embedded
thin P-GS beds fining up to MS intercaleted by thin marl layers

Winterhausen (Q 18)

Depth 1:60

GR [cps] 10 45

poro. [%] 20 0

k(h) [mD] 0 50

k(v) [mD] 0 50

mb lfc lf LFT lith cont dip tr oo cg ein rf bi br sh remarks

hofacie

porec.lith a

r

d.struc

ineral

art.siz 0 11

0 1 2 3 4 5 6 7 8 9 10 11 12 13 14 15 16

GB + GK

BT

OT

G(ß)

G(a)

HT

D(g)

D(ß)

D(a)

cu

cu

fu

Top: bonebed layers, lower w/ glauconite

(dolo-) marlstone, beige

wavy-nodular intra- & bioclastic w-pst.

fine skeletal debris

fine laminated brownish claystone

grrenish - grey claystone
calcilutitic nodules intercalated

fine laminated, brown - grey argill. marlst.

calcisiltitic nodular mudstone

greenish-grey mudstone, small shell fragments & filaments (r-p)
poorly sorted, large shells
poorly sorted, umbrella str. (c)

Top & bottom: shallow channel-like bedforms, altogether moderately sorted large brachiopods (c)

well sorted shell hash

altogether moderately sorted,
Top: large brachiopods
high-angle x-bedding

Top: cm-scale quarz-rich layer,
angular intraclasts (p), mod.-poorly sort.

shale-like marlstone with intercalated limestone beds

nodular limestone

shelly limestone

argillaceous marlstone, greenish

marlstone, bright yellow

shell-dominated pack- to grain- & grainstone, coarse grained shell beds with intraclasts (top & basis)

Nodular Bank:
blueish grey sheet-like & nodular limestone beds with intercalated marlstone seams

Gravel Bank:
argillaceous marlstones & marlstones
yellow - greenish

brachiopod wacke- to packstone
with large coenothyris

Marlstone Markerbed:
6 limestone sheets separated by argillaceous marlstones

shelly limestone beds

7-8 limestone sheets intercalated with few argillaceous marlstone,
faintly wavy laminated

Top:
wave ripples
x-bedded
Basis:
wavy mud-dominated intercalations

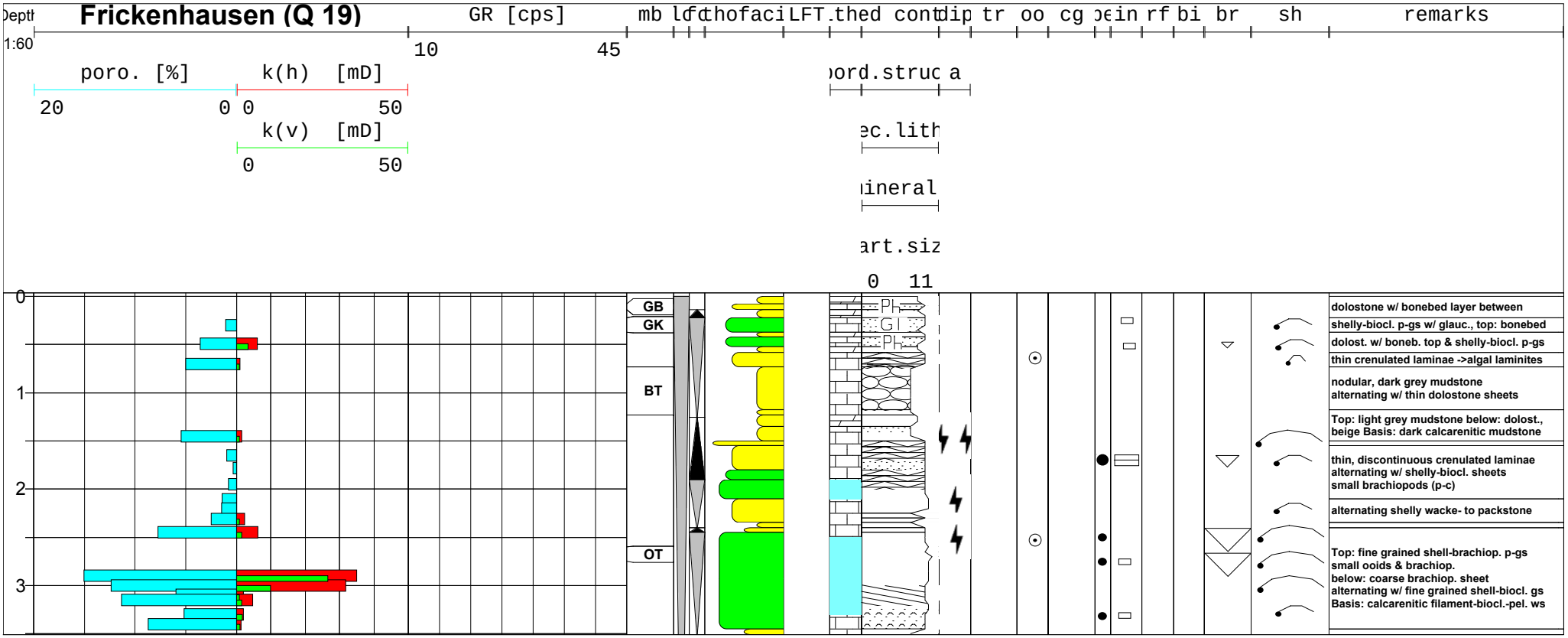
Frickenhausen (Q 19)
GR [cps]
10
45
poro. [%]
20
0
k(h) [mD]
0
50
k(v) [mD]
0
50
0
1
2
3
GB
GK
BT
OT
PH
GI
PH
dolostone w/ bonebed layer between
shelly-biocl. p-gs w/ glauc., top: bonebed
dolost. w/ boneb. top & shelly-biocl. p-gs
thin crenulated laminae ->algal laminites
nodular, dark grey mudstone
alternating w/ thin dolostone sheets
Top: light grey mudstone below: dolost.,
beige Basis: dark calcarenitic mudstone
thin, discontinuous crenulated laminae
alternating w/ shelly-biocl. sheets
small brachiopods (p-c)
alternating shelly wacke- to packstone
Top: fine grained shell-brachiop. p-gs
small ooids & brachiop.
below: coarse brachiop. sheet
alternating w/ fine grained shell-biocl. gs
Basis: calcarenitic filament-biocl.-pel. ws

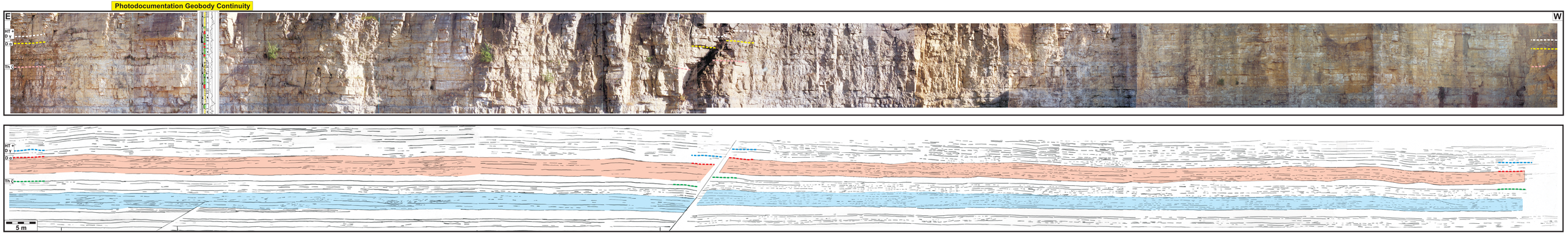

E 22: The mapped outcrop wall based on the photo-panel of quarry Bettenfeld illustrates almost constant thicknesses of carbonate sandbodies (red & blue stained) in the field scale.
This 265 m wide quarry wall represents the maximum observable lenght of continuous shoal bodies in outcrops in this study.

Table A & B Evaluation of Facies and Reservoir Characteristics of Cross Section 4

Cross Section 4 (Fig. 25)

	L i t h o l o g y & F a c i e s	
Cycle -Nr.	**Carbonates & texture**	**Lithofacies association & depositional processes**
1	Mud-and marlstones predominate, thin wacke- to packstones are intercalated	Offshoal (undifferentiated), quiet depositional setting with distal tempestites
2	Seawards: Intensely bioturbated, peloid-rich wacke- and nodular mudstones with intercalated thin marlstones and wacke- to packstones (Q 12) Landwards: Ruditic, skeletal-bioclastic pack- to grainstones, partly cross-bedded, including black pebbles and rarely oncoids (Q 8).	Seawards: Offshoal, quiet depositional setting, possibly lagoonal environment Landwards: Shoal transition, presumably backshoal flank of a shoal. Storm induced event sheets or spillover lobes.
3	Increasing amounts of graded bioclastic calcarenitic pack to grainstone sheets with skeletal basis between intense bioturbated, peloid-wackestones (at least landwards at Q 8)	Offshoal to proximal offshoal (landwards probably lagoonal). Medial to proximal tempestites and channels.
4	Mainly cross-bedded grainstones. They change from well sorted arenitic shell hash (seawards in C 2) to poorly sorted skeletal rudites (landwards in Q12). In Q 8 just nodular bioturbated mud-wackestones and wackestones with abundant peloids and black pebbles are deposited.	Shoal bodies appear in C 2 and Q 12 passing landwards into a lagoonal environment. Storm and wave induced high energetic banks seawards and event sheets landwards, followed by a quiet setting.
5	An enormous thickness increase of grainstones units is significant. Their composition changes from mainly cross-bedded oolite grainstones seawards (Q 11) to cross-bedded oolitic-skeletal grainstones (C 2) to pure cross-bedded shell hash grainstones in Q 13. Subordinate amounts of thin oolitic-skeletal grainstones occur landwards between marl-, mud-and dolo-mudstones and bioturbated bioclastic-peloidal wackestones, including black pebbles.	Shoal complex from Q 11, respectively assumed from Q 10 to Q 13. Q12 and Q8 are obviously backshoal, lagoonal areas. The thick carbonate sandbody accumulation is caused by storm- and wave action while behind shoal derived single storm-spillover events are documented in a quiet, sheltered area with low energetic deposition.
6	Maximum grainstone extension during this cycle. Their composition varies laterally from separated lower oolite grainstone to upper oolitic-skeletal grainstone beds, both cross-bedded (Q 9, Q 11) which amalgamate to mixed oolitic-skeletal grainstones in C 2, while cross-bedded shell hash predominate in Q 13. Mudstones and bioturbated peloidal wackestones are common in Q 12. The thick laminated to low angle cross-bedded grain-stone in Q 8 consists of pure bioclastic calc-arenite.	Largest shoal body from Q 9 to Q 13. Backshoal setting is again present in Q 12 while for Q 8 a shoal transition situation was interpreted. The same depositional processes as described before are responsible for the deposition of the shoal bar with the connected backshoal part. The very well sorted calcarenite unit in Q 8 is interpreted as beach ridge caused by wave action.

	R e s e r v o i r c h a r a c t e r i s t i c s		
	Reservoir facies	**Thickness & lateral continuity of reservoir units**	**Reservoir quality**
1	No reservoir facies	No reservoir units	No reservoir units
2	Seawards: No reservoir facies Landwards: Ruditic, medium- to poorly sorted skeletal pack- to grainstones (LFT: 13b, 11,10)	Seawards: No reservoir units Landwards: Marginal (backshoal ?) reservoir unit in Q 8 is 0,4 m and predicted to pinch out in short distance towards land- and a few km´s distance in seaward direction	Seawards: No reservoir Landwards: Good reservoir quality. Φ = 4 to 20 %, Kh(air) = 1,4 to 58,6 mD
3	No reservoir facies	Channels of few dm thickness may represent reservoir units, they wedge out laterally within a few meters.	The reservoir quality of channels is estimated as medium to poor.
4	Cross-bedded well sorted shell hash (LFT 10) change to poorly sorted skeletal rudites (LFT 11) No reservoir facies in Q 8 and landwards.	The reservoir unit in C 2 is 1m thick and 0,8 m in Q 12. The lateral continuity is approximately 10 km if they are connected and 4 km each if they are separated. They pinch out towards both sides.	The reservoir quality is medium in C 2. Φ = 3 to 8 %, Kh(air) = 0,4 to 10,8 mD and excellent in Q 12. Φ = 3 to 22 %, Kh(air) = 7,8 to 419 mD
5	Mainly cross bedded, well sorted shell hash (LFT 10) and sub-ordinate cross-bedded oolitic-skeletal grainstones (LFT 13b) and pure oolite grainstones (LFT 9a)	Reservoir unit is 2,25 m thick in Q 11, 0,9 m in C 2 and 2 m in Q 12. The lateral continuity amounts 10 to 12 km depending on the lengths of the sea- and landwards wedging –out parts of the reservoir. The single event sheets behind the shoal have little reservoir potential.	The reservoir quality is good in Q 11. Φ = 2 to 19 %, Kh(air) = 0,8 to 186 mD. Medium in C 2. Φ = 3 to 9 %, Kh(air) = 0,4 to 7,5 mD and very good in Q 13. Φ = 8 to 21 %, Kh(air) = 1,9 to 161 mD
6	Mainly cross bedded, well sorted shell hash (LFT 10) and sub-ordinate cross-bedded oolitic-skeletal grainstones (LFT 13b) and pure oolite grainstones (LFT 9a)	Reservoir units are both 0,5 m thick in Q 9, 0,5 and 0,6 m in Q 11 and 1,7 m in C 2, respectively 0,8 m in Q 13. The lateral continuity is 13 to 15 km.	The reservoir quality is poor in Q 9. Φ = up to 4 %, Kh(air) = up to 1 mD. Medium in Q 11. Φ = 3 to 7 %, Kh(air) = 0,8 to 28 mD. Medium to good in C 2. Φ = 5 to 15 %, Kh(air) = 0,6 to 207 mD. Also medium to good in Q 13. Φ = 5 to 16 %, Kh(air) = 0,8 to 186 mD

	Lithology & Facies	
Cycle -Nr.	**Carbonates & texture**	**Lithofacies-association & depositional processes**
7	Trough cross-bedded oolitic-skeletal pack-grainstone sheets in Q 9 and Q 13 are separated by a thick succession of laminated dolo-mudstones with fenestral fabric and intercalated bioturbated bioclastic wacke- to packstones including black pebbles in Q 11 respectively supposed in C 2. The landward sections Q 12 and Q 8 are dominated by laminated, relatively well sorted calcarenites (pack- to grainstones).	Dominant shoal transition facies land- and seawards is interrupted by lagoonal facies in Q 11 and C 2. In the most basinward section C 1 offshoal facies was presumed. Storm induced event sheets and current -derived sand dunes- and waves in Q 9 and Q 13 into sheltered lagoonal areas with algal-laminites in between and pass to wave-dominated beach ridges landwards.
8	Trough cross-bedded oolitic-skeletal pack-grainstone sheets increasing seawards (Q 11 to C 1) while laminated bioclastic packstones in Q 10 and laminated dolo-mudstones with fenestral fabric in Q 11 predominate. Mainly cross-bedded oolitic (-skeletal) grainstones in Q 13 pass to trough cross-bedded, well-sorted shell hash in Q 12 and Q 8. They were superimposed by nodular bioclastic-peloidal wackestones in Q 8.	A small-scale shoal geobody in Q 9 continues seawards into shoal transition facies (C 1), while Q 10 is dominated by undifferentiated offshoal-, respectively Q 11 and C 2 by lagoonal facies. Landwards again shoal geobodies occur that pass into shoal transition facies (Q 12) to lagoonal facies (Q 8) in the uppermost parts of the sedimentary successions.
9	Dolo-mud- and marlstones with intercalated poorly sorted bioclastic wacke- to packstones are commonly spread seawards. Oolitic-skeletal pack- to grainstone sheets (dm-scale), rarely cross-bedded, are present in certain cases (C 1, Q 11, Q 13, Q12) as well as cross-bedded poorly sorted bioclastic pack-grainstone sheets (Q 13, Q 12). Nodular, bioturbated, bioclastic wackestones only occur in Q 8.	Shoal transition facies by amalgamated storm-induced event sheets, spillover lobes, current-derived sandwaves-, dunes and channels are spread over the investigated area (C 1, Q 11, Q 13,Q12) while undifferentiated offshoal facies, essentially low energetic carbonates and dolomites are deposited behind and between them (Q 9, Q 10, Q 13), as well as lagoonal deposits (Q 8).
10	Massive well-sorted oolite grainstones to faintly cross bedded oolitic-skeletal grainstones in C 1 change landwards to pure cross-bedded shell hash grainstone in Q 9 and turn to poorer sorted mixed shell hash grainstones in Q 10. In opposition nodular to laminated dolo-mudstones with intercalated calcarenitic, bioclastic wackestones were deposited behind in C 2, Q 12 and Q 8).	A shoal geobody extends from C 1 over Q 9 to Q 10. Offshoal, respectively backshoal-lagoonal facies was deposited behind (C 2, Q 12 and largely Q 8). Beginning storm- and wave-induced calcarenitic beach and spillover sedimentation can be observed once again in most landward position of Q 8.

	Reservoir characteristics		
	Reservoir facies	**Thickness & lateral continuity of reservoir units**	**Reservoir quality**
7	Mainly trough cross-bedded medium- to well sorted oolitic-skeletal pack-grain- and grainstones (LFT 13 b / rarely13 a). Some laminated, fenestral-dolo-boundstones (LFT 15) and well-sorted calcarenites (LFT 9b)	Event-sheets, sanddunes and sandwaves are some dm´s thick (in Q 9 and decrease in thickness in Q 13) as well as the algal-laminites in Q 11 and C 2. Both tend to wedge out in few 100 m´s to km scale in both directions. The thickness of the calcarenites amounts to more than a meter while they pinch out in km to 10´s of km´s (Q 12 and Q 8).	Medium in Q 9. Φ = 4 to 11 %, Kh(air) = 0,6 to 1,4 mD and presumably similar in Q 13 (just 1 datapoint). Possibly medium in Q 11 and C 2. Only 1 datapoint with Φ = 13 %, Kh(air) = 37 mD. Medium in Q 12. Φ = 4 to 7 %, Kh(air) = 0,9 to 3,5 mD and medium in Q 8. Φ = 4 to 13 %, Kh(air) = 0,4 to 6,4 mD
8	Mainly trough cross-bedded shell hash landwards (LFT 10) and further basin-wards trough cross-bedded medium- to well sorted oolite (LFT 9a) and oolitic-skeletal pack-grain- and grain-stones (LFT 13b). Some laminated, fenestral-dolo-boundstones (LFT 15) and well-sorted calcarenites (LFT 9b)	Thicknesses of shoal complex bodies are 0,5 m in Q 9, Q13 and Q 8, respectively 0,9 m in Q 12. Their continuity is estimated between 2 km (Q 9) and 7 km (Q 13 and Q 12). Some dm´s thick event-sheets, (in C 1, Q 9 and Q 12) and channels (Q 10) rapidly decrease in thick-ness to both sides within a few 100 m´s to a km as well as the algal-laminites in Q 11.	Poor to medium in C 1. Φ = <1 to 12 %, Kh(air) = 0,2 to 13 mD and presumably similar in Q 9 (just 1 datapoint: Φ = 4 %, Kh(air) = 2,9 mD). Possibly medium in Q 11 and C 2. Just 1 datapoint with Φ = 10 %, Kh(air) = 0,6 mD. Medium to good in C 12. Φ = 9 to 13 %, Kh(air) = 1 to 17 mD and very good in Q 8. Φ = 11 to 23 %, Kh(air) = 10 to 110 mD
9	Cross bedded poorly sorted bioclastic pack-grainstones (LFT 11) Medium- to poorly sorted oolitic-skeletal pack-grain- and grainstones (LFT 13b and 13a). No reservoir units are present in Q 9, Q 10, C 2 and Q 8.	Possible reservoir units are generally thin during cycle 9, i.e. maximum 0,3 m in Q 12, 0,5 m in Q 13 and 0,4 m in C 1. They rapidly decrease in thickness to both sides within a few km.	Medium in C 1. Φ = 4 to 12 %, Kh(air) = 0,5 to 3,5 mD Medium to good in Q 13. Φ = 4 to 12 %, Kh(air) = 2 to 22 mD. Also medium to good in Q 12. Φ = 4 to 12 %, Kh(air) = 0,4 to 31 mD.
10	Shell hash grainstones (LFT 10) Medium- to well-sorted oolite- (LFT 9a) and oolitic-skeletal grainstones (LFT 13b), all cross-bedded.	The thickness of reservoir units are 1,3 m in C 1, 0,7 m in Q 9 and 1,1 m in Q 10. The lateral continuity is at least 10 km.	Medium to poor in C 1. Φ = 2 to 9 %, Kh(air) = 0,7 to 2,3 mD Medium in Q 9. Φ = 4 to 7 %, Kh(air) = 2,5 to 26 mD. Good in Q 10. Φ = 8 to 15 %, Kh(air) = 2 to 45 mD.

E N C L O S U R E S E 24

Poro-Perm Data Sheets

Abbreviations:

size:

f-a = fine arenite

m-a = medium arenite

c-a = coarse arenite

vc-a- = very coarse arenite

f-a = fine rudite

m-a = medium rudite

pore type:

t = tight / no pores

vs = separate-vug pores

vt = touching-vug pores

ip = interparticle pores

sorting:

ws = well sorted

w-ms = well to medium sorted

ms = medium sorted

m-ps = medium to poorly sorted

ps = poorly sorted

texture:

WS = wackestone

PS (md) = packstone (mud-dominated)

PS (gd) = packstone (grain-dominated)

GS = grainstone

Poroperm Weckelweiler (Q 1)

Sample #	Depth [m]	Poro. [%]	k(h) [mD]	k(v) [mD]	size	sorting	pore type	texture	LFT
11-1772	17,72	2,11	3,83	0,84	vc-a	w-ms	vs-t	GS	13b
11-1660	16,60	6,83	0,85	0,58	vc-a	ws	vs	GS	9a
11-1540	15,40	3,41	0,39	0,25	vc-a	m-ps	vs-t	GS	11-13a
11-1345	13,45	3,62	0,32	0,17	vc-a	w-ms	(vs)-t	GS	13b(-10)
11-1330	13,30	2,34	0,37	0,56	f-r	w-ms	t	GS	13b(-10)
11-1310	13,10	14,63	15,94	18,56	vc-a	m-ps	vs+ip	PS(gd)	7a-b
11-1300	13,00	18,98	16,34	21,58	vc-a	ps	vs+ip	PS(md)	7a-b
11-1270	12,70	3,73	0,50	0,89	f-r	m-ps	vs-t	PS(md)	7a
11-1260	12,60	11,27	11,59	7,07	vc-a	ms	vs+ip	PS(gd)	10-11
11-1250	12,50	8,68	1,17	0,74	f-r	m-ps	vs+ip	PS(gd)	10-11
11-980	9,80	2,47	0,57	0,23	f-r	ps	vs-t	PS(md)	5
11-890	8,90	12,89	188,41	48,45	m-r	ps	vs+ip	PS(gd)	11-7a
11-870	8,70	4,04	9,21	5,71	f-r	ps	vs	PS(gd)	11-7a
11-705	7,05	1,18			vc-a	m-ws	t	PS(gd)	13b
11-690	6,90	2,19	0,25	0,30	vc-a	ps	(vs)	PS(md)	7a-(4)
11-600	6,00	3,09	1,46	2,35	vc-a	ms	vs	PS(gd)	13b
11-575	5,75	0,00			vc-a	ps	t	PS(md)	7a-(4)
11-010	0,10	8,17	58,30	47,87	m-fr	ps	vs	PS(md)	8

Poroperm Gammesfeld (Q 3)

Sample #	Depth	Porosity (%)	k(h) [mD]	k(v) [mD]	size	sorting	pore type	texture	LFT
8-2060	0,00	1,73							4
8-2000	0,60	0,31							6
8-1890	1,70	2,31	0,34	0,16	vc-a	ms	t	PS(md)	4
8-1785	2,75	6,17	1,58	1,52	f-r	ms	vs	GS	13(a/b)
8-1760	3,00	9,92	1,45	1,33	m-r	ps	vs	W-(P)S	7a-6
8-1730	3,30	7,93	0,94	0,92	f-r	ps	vs	GS	13a-(9a)
8-1720	3,40	8,54	1,72	1,25	f-r	ps	vs	GS	13a-(9a)
8-1710	3,50	7,55	0,91	0,68	f-r	ms	vs	GS	13a-(9a)
8-1700	3,60	9,48	0,63	0,39	vc-a	ws	vs	GS	13a-(9a)
8-1680	3,80	11,41	0,73	1,47	c-a	ws	t	WS	4
8-1645	4,15	1,83							4
8-1625	4,35	1,59	3,26	1,36	vc-a	ps	t	PS(md)	6
8-1540	5,20	3,74	1,25	0,23	vc-a	ps	vt-t	W-PS	4
8-1530	5,30	1,97							4-5
8-1480	5,80	2,17	0,28	0,36	vc-a	ms	t	PS(md)	4
8-1400	6,60	4,84	0,49	0,26	vc-a	ms	t	PS(gd)	13a
8-1390	6,70	2,20	0,3	0,41	f-r	ps	t	PS(gd)	13a
8-1330	7,30	4,70	0,98	0,46	vc-a	ws	vs-t	PS(gd)	13b
8-1320	7,40	8,96	1,03	2,37	vc-a	ms	vs	GS	13b
8-1310	7,50	8,40	3,27	1,12	vc-a	ps	vs	GS	13b
8-1290	7,70	6,57	0,77	0,17	vc-a	ps	vs	GS	13b-9
8-1260	8,00	1,69							9a
8-1240	8,20	0.00							7a(-11)
8-1220	8,40	23,93	48,36	38,45	vc-a	ms	vs+ip	GS	11-(10)
8-1115	9,45	14,89	2,13	0,68	f-r	ps	vs	GS	11
8-990	10,70	3,54	1,1	0,67	vc-a	ws	vs	GS	9a
8-980	10,80	10,88	0,37	0,56	vc-a	ws	vs	GS	9a-(13)
8-965	10,95	9,38	0,61	0,95	vc-a	ws	vs	GS	9a
8-940	11,20	5,82	1,64	6,64	m-r	ps	vs	GS	11
8-930	11,30	5,95	4,6	1,5	f-r	ps	vs	GS	11
8-920	11,40	12,76	5,19	2,06	m-r	ps	vs (+ip)	GS	11
8-895	11,65	3,38	0,52	0,19	m-r	ps	vs	W-PS	7a
8-860	12,00	0,00			f-r	m-ps	t	PS(md)	6
8-815	12,45	0,85			f-r	ms	t	PS(md)	6-4
8-805	12,55	1,32			f-r	ps	z	WS	4-6
8-790	12,70	8,02	0,18	0,47	vc-a	ms	t-(vs)	GS	9a
8-775	12,85	7,40	1,13	0,92	vc-a	ws	vs	GS	9a
8-760	13,00	6,50	1,21	0,88	vc-a	ms	vs	PS(gd)	9a-(13b)
8-752	13,08	6,55	4,74	2,55	vc-a	w-ms	vs	GS	9a
8-740	13,20	6,17	3,36	1,57	f-r	ms	vs	GS	13b
8-725	13,35	8,40	9,42	6,80	vc-a	ws	vs+ip	GS	13b
8-710	13,50	6,08	1,12	0,71	vc-a	w-ms	vs	GS	9a
8-700	13,60	7,09	5,05	0,04	vc-a	ms	vs	GS	13b
8-690	13,70	15,83	67,63	122,71	m-r	ms	vs+ip	GS	11
8-680	13,80	5,66	2,47	2,24	f-r	ps	vs+ip	GS	11
8-665	13,95	3,54	0,45	0,14	vc-a	ps	t	WS	13a
8-660	14,00	2,05	3,29	0,81	f-r	ps	vs	PS(gd)	13a
8-650	14,10	5,15	1,26	0,89	vc-a	ms	vs	PS(gd)	13a-(b)
8-645	14,15	4,52	7,66	0,91	vc-a	ms	vs	PS(gd)	13a-6
8-630	14,30	2,41	0,39	0,07	m-r	(m)-ps	t-(vs)	PS(md)	(13a)-6
8-600	14,60	0,45			vc-a	ms	t	PS(gd)	13b
8-590	14,70	1,97			m-r	ps	t	PS(md)	6
8-575	14,85	4,66	0,73	0,78	(f)-m-r	ps	t-(vs)	WS	4
8-560	15,00	12,85	5,85	2,51	f-r	ms-ps	vs	GD	10-7b
8-550	15,10	12,77	21,98	3,38	m-r	ms-ps	vs+ip	PS(md)	7b-(10)
8-540	15,20	15,99	45,87	44,65	vc-a-fr	m-ws	vs+ip	PS(gd)	10-(6)
8-530	15,30	17,98	45,17	59,32	vc-a-fr	ms	vs+ip	GS	10
8-520	15,40	19,16	38,34	75,80	vc-a-fr	ws	vs+ip	GS	10
8-510	15,50	20,65	54,94	34,91	vc-a-fr	ws	vs+ip	GS	10
8-500	15,60	18,63	18,24	10,27	vc-a	ws	vs+ip	GS	10
8-465	15,95	1,61			vc-a	ps	t	PS(md)	6-7b
8-425	16,35	1,28			vc-a	m-ps	t	WS	4
8-270	17,90	1,29			f-r	m-ps	t	PS(md)	5b
8-225	18,35	3,36	0,77	1,81	vc-a	ms	t-(vs)	GS	7b-(10)
8-090	19,70	3,09	1,52	0,33	vc-a	ps	vs	W-PS	4

Poroperm Schmalfelden (Q 4)

Sample #	Depth [m]	Porosity [%]	k(h) [mD]	k(v) [mD]	size	sorting	pore type	texture	LFT
18-1960	1	8,63	12,71	3,83	vc-a	m-ps	vs	PS(md)	5a-(6)
18-1950	1,1	11,22	11,17	1,54	vc-a	m-ps	vs+ip/dolo	W-PS	5
18-1945	1,15	12,89	61,66	74,7	m-r	m-ps	vs+ip/dolo	W-PS	2-(5)
18-1935	1,25	9,28	3,68	3,56	vc-a	m-ps	vs/dolo	PS(md)	5
18-1710	3,5	1,76	0,73	0,82	f-r	ps	vs-t	PS(md)	7a
18-1643	4,17	7,19	4,22	4,66	f-r	m-ps	vs-t	GS	13b
18-1625	4,35	13,69	9,14	25,47	f-r	ms	vs	PS(gd)	13b
18-1622	4,38	14,53	40,47	18,09	vc-a	ws	vs+ip	GS	10
18-1450	6,1	8,40	0,61	0,82	vc-a	ms	t	PS(gd)	10-7b
18-1445	6,15	11,49	11,3	0,7	vc-a	ms	vs+ip	GS	10
18-1440	6,2	13,86	7,68	4,53	vc-a	m-ws	vs+(ip)	GS	10
18-1435	6,25	14,45	17,35	11,98	vc-a	m-ws	vs+ip	GS	10
18-1430	6,3	17,46	21,24	9,89	vc-a	m-ws	vs+ip	GS	10
18-1425	6,35	14,16	17,33	3,4	vc-a	m-ws	vs+ip	GS	10
18-590	14,7	0,40	0,31	0,03	f-r	ms	t	PS(m-gd)	11-7b
18-580	14,8	6,91	5,56	3,60	f-r	m-ps	vs	PS(gd)	11(-10)
18-570	14,9	13,54	102,54	237,21	m-r	ps	vs+ip	PS(gd)	11
18-568	14,92	11,39	25,90	75,48	f-r	m-ps	vs+ip	PS(gd)	11
18-535	15,25	7,48	20,50	14,52	vc-a	ws	vs+ip	GS	10
18-525	15,35	11,77	4,88	5,69	vc-a	ws	vs+(ip)	GS	10
18-520	15,4	17,90	49,30	1,23	vc-a	ws	vs+ip	GS	10
18-510	15,5	3,97	1,43	0,67	vc-a	w-ms	vs+(vt)	GS	10
18-505	15,55	9,79	8,17	4,05	f-r	ms	vs+ip	GS	10(-11)
18-495	15,65	8,67	5,39	3,30	f-r	ms	vs+ip	PS(gd)	11
18-490	15,7	8,25	1,83	12,85	f-r	ps	vs+(ip)	PS(gd)	11
18-480	15,8	8,20	3,98	21,02	f-r	ps	vs(+ip)	GS	11
18-470	15,9	8,95	7,66	0,52	f-r	ms	vs	GS	(11)-10
18-455	16,05	8,16	5,56	1,78	vc-a	ms	vs	GS	10
18-440	16,2	2,92	0,77	13,19	f-r	m-ps	vs	GS	10-(11)
18-425	16,35	9,40	3,02	5,13	vc-a	w-ms	vs(+ip)	GS	10
18-420	16,4	17,64	18,09	8,95	vc-a	w-ms	vs+ip	GS	10
18-410	16,5	12,27	20,14	4,41	f-r	ms	vs+ip	PS(gd)	(7b)-10

Poroperm Bettenfeld (Q 5)

Sample #	Depth [m]	Porosity [%[	k(h) [mD]	k(v) [mD]	size	sorting	pore type	texture	LFT
3-2175	0,95	2,63	0,1	0,19	f-r	ps	vs-t	ps(md)	7a
3-2145	1,25	6,39	1,94	0,4	c-a	ws	vs-t	gs	13b-9a
3-2095	1,75	9,42	19,91	16,15	c-vc-a	w-ms	t(dolo)	ps(md)	4-1b
3-2054	2,16	5,97	0,22	0,48	m-r	ps	(vs)t	ps(md)	5a-12
3-1942	3,28	4,85	0,34	0,4	vc-a	ws	t	ps(md)	4
3-1902	3,68	1,38	2,01	1,21	c-vc-a	ws	8t)-vs	gs	9b
3-1880	3,9	4,86	2,46	2,06	vc-a	m-(ws)	t	ps(md)	4-1b
3-1865	4,05	8,77	0,64	0,37	vc-a	ms	t	ws	3-4
3-1855	4,15	4,56	7,82	8,55	m-(f-r)	ps	vs-t	w-ps	7a
3-1825	4,45	17,41	45,52	106,61	m-r	ps	vs+ip	ps(gd)	11
3-1770	5	19,58	87,02	265,91	m-r	ps	vs+ip	gs	11
3-1745	5,25	2,98	4,42	0,51	c-vc-a	ws	vs-t	gs	13b
3-1740	5,3	1,01			vc-a	ms	t	w-ps	6
3-1725	5,45	8,74	6,31	4,79	vc-a	ms	vs	ps(gd)	13b
3-1715	5,55	5,82	1,15	1,02	f-r	ms	vs	ps(md)	7b-(13c)
3-1680	5,9	8,38	4,84	0,28	vc-a-f-r	ms	vs	ps(gd)	13a
3-1650	6,2	11,56	9,99	0,65	vc-a-f-r	ms	vs+ip	ps(gd)	13a-12
3-1640	6,3	12,75	8,34	4,7	vc-a	ps	vs+(ip)	gs	
3-1630	6,4	3,37	1,43		vc-a	ps	vs	ps(md)	8
3-1585	6,85	9,13							
3-1585	6,85	8,59	25,27	37,8	f-r	ms	vs+ip	ps(gd)	12-13b
3-1575	6,95	13,05	20,02	33,17	f-r	ms	vs+ip	gs	12
3-1500	7,7	5,83	12,96	12,89	f-r	ps	vs+ip	gs	13b
3-1445	8,25	5,51	0,29	0,41	vc-a	ws	vs	gs	9a
3-1432	8,38	0,28		0,94	vc-a-(f-r)	ms	t	gs	13a
3-1354	9,16	2,42	3,05	2,4	vc-a-(f-r)	ms	vs	gs	13a
3-1315	9,55	0,87	0,23	0,2	vc-c-a	ws	t	ps(md)	8-(2a)
3-1306	9,64	3,89	0,51	7,27	vc-a-(f-r)	ms	t-vs	ps(gd)	13a
3-1290	9,8	8,52	16,57	10,18	vc-a-(f-r)	ms	vs+ip	ps(gd)	13a
3-1260-2	10,01	14,04							
3-1260	10,1	16,46	50,55		f-(m)-r	m-ps	vs+ip	ps(gd)	11-10
3-1185	10,85	0,21			c-a	w-ms	t	w-ps	4
3-978	12,92	0,00			f-r	ps	t	ps(md)	6-(7)
3-973	12,97	3,42	0,65	0,51	vc-a	ws	t	gs	13b
3-965	13,05	0,78			vc-a	ps	t	w-ps	4
3-953	13,17	0,62			f-r	ps	t	w-ps	6-7a
3-940	13,3	8,00	0,85	0,11	vc-a-(f-r)	ms	t-(vs)	gs	13b
3-935	13,35	4,05	2,08	0,23	f-r	ms	vs	gs	13b
3-900	13,7	3,89	0,68	0,17	vc-a	ws	(vs)-t	ps(gd)	13a
3-882	13,88	4,09	2,44	0,39	vc-a	m-ps	vs	w-ps	6-(4)
3-877	13,93	11,28	2	0,53	vc-a	ws	vs	gs	13b-(9a)
3-847	14,23	10,30	4,32	1,22	c-a	vws	vs+(ip)	gs	13b-(9a)
8-840	14,3	4,21						gs	
3-840	14,3	4,79	5,4	1,71	vc-a	vws	vs	gs	13c-(9a)
3-750	15,2	16,38	14,37	4,47	vc-a	w-ms	vs+ip	gs	10
3-740	15,3	11,98	2,76	1,01	vc-a-(f-r)	(w)-ms	vs	gs	10
3-720	15,5	15,77	11,25	11,68	vc-a	ws	vs+ip	gs	10
3-710	15,6	15,67	12,57	7,61	f-r-(vc)-a	m-(ws)	vs+ip	gs	10
3-655	16,15	1,96	0,45	0,58	f-r	ms	t	ws	3
3-646	16,24	2,22	1,34	0,64	m-r	m-ps	t	(w)-ps	7a-3
3-633	16,37	0,64			vc-a	m-ps	t	w-ps	0b
3-620	16,5	0,90			vc-a	m-ps	t	w-ps	4
3-520	17,5	0,28			c-a	ms	t	(w)-ps	8
3-460	18,1	0,91			fr	m-ps	t	(w)-ps	5b(-4)
3-450	18,2	0,36			fr	m-ps	t	w-(ps)	5b
3-436	18,34	3,55	0,47	0,31	f-r	m-ps	vs	ps(md)	5b(-7b)
3-430	18,4	3,32	0,56	0,08	f-r	m-ps	vs	ps(gd)	13a
3-420	18,5	3,81	0,48	0,5	f-r	m-ps	vs	ps(gd)	13a
3-395	18,75	6,65	4,07	1,58	f-r-(vc-a)	ms	vs+vt	gs	13a
3-385	18,85	1,43	4,08	3,85	f-r-(vc-a)	ms	vs+vt	gs	13a

Poroperm Haltenmühle (Q 6)

Sample #	Depth [m]	Porosity [%]	k(h) [mD]	k(v) [mD]	size	sorting	pore type	texture	LFT
12-1065	10,65	2,64	2,66	1,93	f-r	m-ps	vs	PS(md)	7a
12-690	6,90	12,49	26,25	137,82	vc-a	m-ps	vs+ip	GS	10-(11)
12-650	6,50	17,27	201,06	290,34	f-r	ps	vs+ip	PS(gd)	11
12-640	6,40	15,39	215,33	239,17	f-r	ps	vs+ip	PS(md)	7a-(11)
12-635	6,35	13,75	57,75	64,08	f-r	ps	vs+ip	PS(gd)	11
12-630	6,30	20,72	17,84	65,66	vc-a	ws	vs+ip	GS	10
12-590	5,90	16,02	138,90	209,64	f-r	ms	vs+ip	PS(gd)	10-(11)
12-585	5,85	15,06	26,36	22,53	vc-a	ws	vs+ip	PS(gd)	10
12-570	5,70	15,35	27,60	21,58	vc-a	ws	vs+ip	GS	10
12-565	5,65	19,77	21,73	3,98	vc-a	ms	vs+ip	PS(gd)	10-(9b)
12-538	5,38	6,18	2,84	0,64	vc-a	ps	vs	PS(gd)	13a-(6a)
12-440	4,40	5,36	0,90	1,31	m-c-a	ms	vs	PS(gd)	15-4
12-220	2,20	23,90	74,67	56,39	vc-a	ps	vs+ip	GS	11-(9b)
12-195	1,95	11,71	3,11	1,93	f-r	m-ps	vs	GS	12-10
12-185	1,85	12,74	39,51	12,01	f-r	m-ps	vs+ip	GS	12-10

Poroperm Dürrenhof (Q 7)

Sample #	Depth [m]	Porosity [%]	k(h) [mD]	k(v) [mD]	size	sorting	pore type	texture	LFT
10-1340	0,45	2,14	0,94	0,49	f-r	ms	t- (vs)	WS	4b-3
10-1330	0,55	3,22	0,77	4,67	vc-a	ps	vs-vt	W-PS	4b
10-1320	0,65	12,47	77,11	2,27	f-r	m-ps	vs+ip	PS(gd)	13a-13b
10-1315	0,70	13,26	1,59	1,32	m-r	ps	vs+ip	GS	11
10-1300	0,85	12,71	4,56	4,7	f-r	ms	vs+(ip)	GS	13a-13b
10-1290	0,95	8,61	7,16	2,18	vc-a	ms	vs+ip	GS	13b
10-1283	1,02	6,29	4,2	3,29	vc-a	m-ps	vs	PS(gd)	13a
10-1260	1,25	4,79	1,45	1,94	f-r	ps	vs	PS(md)	7a
10-1250	1,35	13,64	0,97	0,73	m-r	ps	vs+ip	PS(md)	11-7a
10-1240	1,45	10,45	7,35	11,6	m-r	ps	vs+ip	PS(md)	11-7a
10-1230	1,55	7,46	8,97	1,31	f-r	m-ps	vs+ip	PS(gd)	11-(7a)
10-1220	1,65	9,18	22,4	10,88	f-r	m-ps	vs+ip	PS(md)	(7a)-11
10-1210	1,75	10,94	12,95	9,66	vc-a	m-ps	vs+ip	PS(gd)	13a-(11)
10-1200	1,85	9,88	1,05	1,55	f-r	ps	vs+ip	GS	11-(13a)
10-1190-2	1,95	10,42	63,04	1,58	vc-a	ps	vs+ip	GS	11
10-1190	1,95	11,57	243,43	47,91	m-r	ps	vs+ip	GS	11
10-1180	2,05	13,25	10,80	5,22	m-r	ps	vs+ip	GS	11
10-1170	2,15	7,91	3,55	1,76	vc-a	ms	vs	GS	13a
10-1152	2,33	5,25	4,26	0,62	c-a	ws	vs	GS	9a
10-1130	2,55	8,59	5,69	0,79	vc-a	ms	vs	PS(gd)	8
10-1100-2	2,85	10,84	20,99	7,09	vc-a	ms	vs+ip	GS	8-(10)
10-1100	2,85	10,12	8,45	60,23	vc-a	ms	vs+(ip)	GS	8-(10)
10-1095	2,90	17,61	103,94	80,71	vc-a	ws	vs+ip	GS	8-(10)
10-1090	2,95	9,55	3,59	16,91	c-vc-a	ws	vs	GS	8-(10)
10-830	5,55	3,28	0,67	0,41	m-r	ps	vs	WS	7a-4
10-805	5,80	4,95	1,64	0,58	vc-a	ws	vs	PS(md)	8-2a
10-785	6,00	4,63	24,80	1,49	c-a	ps	vs	PS(gd)	7a-11
10-760	6,25	12,13	83,59	42,54	f-r	ms	vs+ip	PS(gd)	11-(10)
10-750	6,35	11,57	21,78	2,91	vc-a	ms	vs+(ip)	PS(md)	8a-7b
10-740	6,45	16,02	37,65	6,66	vc-a	ms	vs+ip	PS(gd)	8a-7b
10-720	6,65	21,09	111,29	121,56	vc-a	ws	vs+ip	GS	10
10-710	6,75	18,25	76,13	101,34	vc-a	ws	vs+ip	PS(gd)	10
10-725	6,60	14,44	23,75	66,21	vc-a	ms	vs+ip	GS	10
10-700	6,85	22,63	237,56	248,32	f-r	m-ws	vs+ip	PS(gd)	10
10-690	6,95	23,66	136,81	194,29	f-r	ms	vs+ip	GS	10-(11)
10-670	7,15	19,48	152,60	227,62	f-r	ms	vs+ip	GS	10-(11)
10-660	7,25	18,40	89,17	121,55	f-r	ms	vs+ip	GS	10-(11)
10-635	7,50	18,19	91,97	337,03	vc-a	ms	vs+ip	GS	10
10-630	7,55	16,25	99,97	82,16	f-r	ps	vs+ip	GS	11-10
10-620	7,65	15,64	58,71	9,98	f-r	ms	vs+ip	GS	11
10-615	7,70	16,59	129,84	7,78	f-r	ms	vs+ip	GS	11-10
10-610-2	7,75	15,47					vs+ip	GS	11
10-610	7,75	16,52	241,62	300,61	m-r	ps	vs+ip	GS	11
10-600	7,85	11,96	4,57	4,57	vc-a	ws	vs+ip	GS	8-(9b)
10-590	7,95	11,60	33,33	26,01	m-a	ws	vs+ip	GS	9a-b
10-580	8,05	11,49	8,20	13,87	vc-a	ps	vs+ip	GS	9a-b
10-514	8,71	2,57	1,94	1,48	vc-a	ps	vs	PS(md)	9b-13
10-500	8,85	2,01	9,13	0,71	vc-a	ps	vs	GS	9b-(8)
10-477	9,08	5,90	0,99	0,77	m-a	ws	vs-t	GS	15
10-470	9,15	4,18	2,54	0,98	vc-a	ms	vs	GS	9b
10-445	9,40	8,60	2,65	2,71	vc-a	ms	vs	PS(md)	4-15
10-428	9,57	2,47	3,67	1,32	vc-a	ps	vs	PS(gd)	13a-(8)
10-418	9,67	3,83	3,00	1,51	c-a	ps	vs	PS(md)	8-13a
10-415	9,70	0,09							8-13a
10-340	10,45	3,13	0,48	0,38	m-a	ws	t	GS	9b

Poroperm Gattenhofen (Q 8)

Sample #	Depth [m]	Porosity [%]	k(h) [mD]	k(v) [mD]	size	sorting	pore type	texture	LFT
9-1460	0,25	15,05	44,08	289,86	f-m-r	ps	ip+vs	GS	11
9-1415	0,70	5,73	16,03	6,28	f-r	ps	ip+vs+vt	PS-1	11-10
9-1410	0,75	8,63	18,07	28,34	f-r	ps	ip+vs+vt	GS	11-10
9-1400	0,85	13,66	90,15	69,18	m-r	ps	ip+vs+vt	GS	11-(10)
9-1390	0,95	7,77	18,82	14,46	f-r	ms	vs+vt	GS	10-(11)
9-1375	1,10	4,47	2,17	1,41	m-r	ps	vs	PS (md)	7a
9-1360	1,25	6,88	3,21	18,08	vc-a	ps	vs+vt	PS-1	13a-(9a)
9-1345	1,40	2,18	0,08	0,10	m-a	ws	t (vs)	GS	9b
9-1325	1,60	7,82	0,52	1,78	vc-a	ms	vs	PS-2	4b
9-1310	1,75	7,84	8,30	3,81	vc-a	ps	ip+v	PS-1	11
9-1295	1,90	7,18	24,30	18,76	m-r	ps	vs+(vt)	PS-1	11
9-1287	1,98	12,52	5,91	1,85	m-r	ms	ip+v	GS	11-(10)
9-1275	2,10	14,39	7,13	30,31	m-r	ps	ip+v	GS	11-(10)
9-1260	2,25	8,00	13,14	7,96	f-r	ps	vs+(vt)	GS	13a
9-1250	2,35	6,01	1,74	0,22	f-r	ps	vs	GS	13a
9-1210	2,75	4,22	5,18	4,19	vc-a	ms	vs+vt+ip	GS	9b-a
9-1195	2,90	4,48	0,15	0,14	c-a	ms	ip+vs	PS-1	4
9-1180	3,05	9,27	2,27	0,82	c-a	ms	ip+vs+vt	PS-1	4
9-1170	3,15	9,62	5,92	3,34	vc-a	ws	vs+(ip)	PS (gd)	9b
9-1160	3,25	8,90	0,93	0,83	m-a	ws	ip+vs	GS	9b
9-1150	3,35	9,33	1,69	4,34	m-a	ws	ip+v	GS	9b
9-1030	4,55	3,10	1,78	3,05	c-vc-a	ms	ig	WS	4
9-790	6,95	5,66	2,00	2,00	vc-a	ms	vs	GS	9b-(10)
9-780	7,05	10,75	17,75	12,45	vc-a	ms	vs+ip	GS	10-(9b)
9-770	7,15	14,97	27,60	23,71	vc-a	ms	vs+ip	GS	10-(9b)
9-760	7,25	15,03	10,72	10,62	c-vc-a	ws	vs+ip	GS	9b
9-750	7,35	10,98	20,92	7,36	vc-a	ms	vs+ip	GS	10-(11)
9-730	7,55	22,75	110,79	102,62	vc-a	ws	vs+ip	GS	10
9-720	7,65	12,84	59,81	81,63	vc-a	ws	vs+ip	GS	10
9-715	7,70	17,91	76,93	29,81	vc-a	ws	vs+ip	GS	10
9-710	7,70	18,29	43,50	43,77	vc-a	ws	(vs)+ip	GS	10-(9b)
9-705	7,80	19,30	31,52	54,68	vc-a	ws	vs+ip	GS	9b-10
9-685	8,00	13,60	6,44	10,49	c-vc-a	ws	vs+ip	GS	9b
9-610	8,75	7,02	0,41	0,22	vc-a	ws	vs	GS	9b
9-603	8,82	4,92	0,72	0,21	vc-a	ws	vs	GS	9b
9-460+	17,50	4,24	1,38	0,04	f-r	ms	vs	PS (md)	5a-7b
9-455+	17,55	8,74	6,14	4,89	f-r	ms	vs+(ip?)	PS (gd)	13a-(10)
9-438+	17,72	6,13	6,73	4,73	m-r	ps	vs+ip	GS	13a
9-432+	17,78	10,77	19,70	6,38	m-r	ps	vs+(ip)	PS (gd)	13a-11
9-425+	17,85	20,08	58,57	48,12	f-r	ms	vs+ip	GS	10-11
9-415+	17,95	17,80	49,96	78,36	f-r	ms	vs+ip	GS	11-(10)
9-408+	18,02	6,76	5,37	5,47	f-r	ps	vs+(ip?)	PS (gd)	13a

Poroperm Oesfeld (Core 1)

Sample #	Depth [m]	Porosity [%]	k(h) [mD]	k(v) [m]	size	sorting	pore type	texture	LFT
15-1650	11,50	0,73							
15-1610	11,10	0,90							
15-1590	10,90	10,41	13,06	9,98	m-r	ps	vs+(ip)	PS(gd)	13a-7b
15-1580	10,80	12,50	4,57	4,32	f-r	m-ps	vs	PS(gd)	13a-7b
15-1570	10,70	12,06	23,47	4,02	m-r	ps	vs	PS(md)	7a
15-1560	10,60	5,57	0,48	1,77	m-r	ps	vs	PS(md)	7a
15-1540	10,40	5,38	0,45	1,21	f-r	m-ps	vs	PS(gd)	6
15-1490	9,90	5,30	0,60	0,24	m-r	m-ps	vs	PS(gd)	13a
15-1470	9,70	10,47	1,20	0,51	f-r	ms	vs	GS	13b
15-1460	9,60	10,96	3,54	3,58	m-r	ps	vs	GS	13a
15-1445	9,45	7,68	2,48	3,56	m-r	ps	vs	PS(gd)	13a
15-1437	9,37	9,24	2,38	1,31	f-r	m-ps	vs	PS(gd)	13a
15-1430	9,30	8,13	3,15	0,40	vc-a	m-ps	vs	GS	13a
15-1375	8,75	11,71	0,90	1,46	vc-a	m-ps	vs	GS	13a
15-1330	8,30	5,22	3,44	0,63	vc-a	ps	vs	GS	13a
15-1320	8,20	3,82	2,00	0,56	vc-a	ps	vs	PS(gd)	13a
15-1255	7,55	2,39	2,28	0,22	f-r	m-ps	vs	PS(gd)	13a
15-1190	6,90	8,58	0,97	1,45	c-vc-a	w-ms	t	GS	13b-9
15-1180	6,80	9,18	0,70	1,96	c-vc-a	w-ms	t	GS	13b-9
15-1105	6,05	5,37	0,32	0,25	f-r	m-(ps)	t	GS	13b
15-1085	5,85	9,90	9,42	0,89	m-r	ps	vs+(ip)	GS	13b
15-1065	5,65	11,35	45,41	3,13	m-r	ps	vs+(ip)	GS	13b
15-1060	5,60	7,37	3,51	0,60	vc-a	ms	vs+(ip)	GS	13b
15-1050	5,50	6,61	2,43	0,80	vc-a	ps	vs+(ip)	GS	13b
15-1030	5,30	6,05	5,37	0,38	vc-a	ms	vs+(ip)	GS	13b
15-1020	5,20	9,56	35,55	8,66	m-r	m-ps	vs+ip	PS(gd)	13a-(11)
15-1010	5,10	8,90	9,66	13,94	m-r	ps	vs	PS(gd)	13a-(11)
15-975	4,75	7,15	25,83	1,29	f-r	ms	vs	GS	13b-10
15-960	4,60	8,21	12,99	2,34	f-r	ms	vs	GS	13b-10
15-950	4,50	9,18	36,09	7,26	f-r	ms	vs	PS(gd)	13b
15-895	4,95	7,57	2,12	1,07	f-r	ms	vs	GS	13b-9
15-875	4,75	7,94	0,89	2,54	vc-a	w-ms	vs	GS	13b-9
15-865	4,65	8,21	0,89	1,29	vc-a	w-ms	vs	GS	13b-9
15-845	4,45	5,10	7,28	1,44	c-vc-a	ws	vs	GS	13b-9
15-835	4,35	5,98	2,64	0,81	vc-a	ws	vs	GS	13b-9
15-810	4,10	7,15	2,40	0,86	vc-a	m-ws	vs	GS	13b-9

Poroperm Bernsfelden (Q 9)

Sample #	Depth [m]	Porosity [%]	k(h) [mD]	k(v) [mD]	size	sorting	pore type	texture	LFT
19-860	0,20	8,52	2,58	0,45	vc-a	ws	vs	GS	10
19-845	0,35	7,12	3,23	0,84	f-r	ms	vs	GS	10
19-840	0,40	7,02	1,20	0,85	f-r	ms	vs	GS	10
19-835	0,45	5,32	3,12	0,41	vc-a	m-ws	vs	GS	10
19-795	0,85	4,19	8,29	0,49	vc-a	ws	vs+ip	GS	10
19-790	0,90	7,07	12,67	0,94	f-r	ws	vs+ip	GS	10
19-785	0,95	5,61	7,77	0,50	vc-a	ws	vs+(ip)	GS	10
19-760-2	1,20	5,59	15,05	0,45	f-r	ws	vs+ip	GS	10
19-760-1	1,20	7,33	26,42	0,45	f-r	ws	vs+ip	GS	10
19-755	1,25	4,27	2,54	0,53	vc-a	ws	vs	GS	10
19-740	1,40	4,96	9,47	0,43	m-r	m-ps	vs	PS(gd)	13a-7a
19-330	5,50	4,58	2,94	0,25	m-r	ps	vs	PS(md)	13a-7a
19-270	6,10	5,81	1,27	0,52	f-r	ms	vs	PS(gd)	10-11
19-250	6,30	11,30	1,39	2,98	f-r	ms	vs	PS(gd)	13b
19-230	6,50	6,72	0,92	0,45	vc-a	ms	t-(vs)	PS(gd)	13b
19-212	6,68	4,24	0,61	0,50	vc-a	ms	t-(vs)	PS(gd)	13a-b
19-167	7,13	3,57	1,02	0,49	vc-a	w-ms	vs	GS	13b

Poroperm Stalldorf (Q 10)

Sample #	Depth [m]	Porosity [%]	k(h) [mD]	k(v) [mD]	size	sorting	pore type	texture	LFT
20-720	0,50	10,82	3,82	0,67	m-r	m-ps	vs	GS	11
20-710	0,60	11,97	287,53	8,16	m-r	ps	vs+ip	PS(gd)	11-10
20-705	0,65	14,15	14,88	0,37	vc-a	w-ms	vs+ip	GS	10
20-703	0,67	9,13	2,57	0,35	f-r	m-ps	vs	GS	11-10
20-685	0,85	10,25	1,65	0,91	vc-a	w-ms	vs	GS	10-(13b)
20-680-2	0,90	7,84	5,53	0,55	vc-a	ws	vs	GS	10
20-680-1	0,90	10,39	5,53	0,55	vc-a	w-ms	vs	GS	10
20-637	1,33	10,92	64,22	0,49	vc-a	w-ms	vs+ip	GS	10
20-610	1,60	5,77	7,80	0,38	f-r	m-ps	vs/dolo	PS(md)	7b-7a
20-560	2,10	13,94	14,64	0,79	m-r	ms	vs+ip	GS	11-10
20-551	2,19	9,79	3,84	0,40	m-r	m-ps	vs	GS	11-10
20-530	2,40	11,11	2,08	0,45	f-r	m-ps	vs	GS	11-10
20-520	2,50	13,79	7,52	0,70	f-r	m-ps	vs+(ip)	GS	11-10
20-510	2,60	9,08	8,57	0,64	f-r	ms	vs+(ip)	GS	10
20-505	2,65	15,33	45,26	0,55	m-r	ps	vs+ip	GS	11
20-500	2,70	7,84	3,14	0,19	m-r	ps	vs	GS	11-10

Poroperm Lenzenbrunn (Q 11)

Sample #	Depth [m]	Porosity [%]	k(h) [mD]	k(v) [mD]	size	sorting	pore type	texture	LFT
21-710	2,35	9,76	0,59	0,56	f-a/dolo	ms	t-(vs)	Dolo-MS	15
21-620	3,25	13,48	37,39	24,49	f-a/dolo	ms	vs+vt+dol.	Dolo-MS	15
21-402	5,43	7,09	10,41	1,21	f-r	m-ps	vs+(ip)	GS	11-13b
21-390	5,55	5,98	28,43	0,63	vc-a	w-ms	vs+ip/dol.	GS	13b
21-382	5,63	3,80	2,01	0,85	vc-a	w-ms	vs	GS	13b
21-375	5,70	7,13	1,63	2,05	f-r	m-ps	vs	GS	13a-13b
21-360	5,85	4,21	0,79	0,41	vc-a	w-ms	t	GS	13a-b
21-355	5,90	3,46	4,31	1,71	f-r	ms	vs	GS	13a
21-270	6,75	2,59	1,32	3,01	m-r	ps	vs	PS(gd)	13a-6
21-240	7,05	17,13	21,30	10,25	vc-a	w-ms	vs+ip/dol.	PS(md)	6-9
21-225	7,20	5,85	0,85	1,53	vc-a	ms	t-(vs)	PS(gd)	13b-9a
21-215	7,30	10,25	6,48	1,98	vc-a	w-ms	vs	GS	9a-10
21-200	7,45	18,31	19,77	15,07	f-r	ms	vs+ip	GS	10-11
21-195	7,50	18,87	103,51	33,06	f-r	ms	vs+ip	GS	10-11
21-190	7,55	18,72	173,87	90,14	f-r	ms	vs+ip	GS	10-(11)
21-185	7,60	17,74	186,74	18,48	f-r	ms	vs+ip	GS	10
21-180	7,65	15,71	45,09	10,00	vc-a	w-ms	vs+ip	GS	10
21-170	7,75	10,89	10,89	1,69	vc-a	ms	vs+ip	GS	10
21-150	7,95	5,11	3,02	0,58	c-vc-a	ws	vs	GS	9a-(10)
21-135	8,10	2,48	0,58	0,58	c-vc-a	ws	t-(vs)	GS	9a
21-090	8,55	4,56	0,80	0,51	c-vc-a	ws	t	GS	9a

Poroperm Röttingen (Core 2)

Sample #	Depth [m]	Porosity [%]	k(h) [mD]	k(v) [mD]	size	sorting	pore type	texture	LFT
14-2455	17,40	3,12	0,36	0,89	vc-a	ws	t	GS	10
14-2445	17,30	4,15	1,86	0,96	vc-a	ws	vs	GS	10
14-2420	17,05	8,07	0,58	3,07	vc-a	ms	t	PS(gd)	10
14-2410	16,95	6,95	10,75	15,57	vc-a	ws	vs+vt	GS	10
14-2270	15,55	3,79	0,55	0,41	vc-a	ms	t	PS(md)	7b
14-2215	15,00	6,57	0,42	0,40	vc-a	ms	t	GS	13a-b
14-2205	14,90	6,85	7,47	16,16	f-r	ps	vs	PS(gd)	13a-b
14-2185	14,70	9,16	1,91	1,04	f-r	ms	vs	PS(gd)	13b
14-2175	14,60	2,82	1,91	0,93	f-r	ms	vs	PS(gd)	13b
14-2060	13,45	6,43	0,68	0,27	vc-a	ws	t	GS	9-13b
14-2035	13,20	1,00	0,33	0,21	vc-a	ms	t	PS(gd)	13b-9
14-2010	12,95	6,60	1,25	0,36	vc-a	ms	vs	GS	13b-9
14-2005	12,90	5,88	1,36	0,15	vc-a	m-ps	vs	GS	13b
14-1990	12,75	6,25	4,04	0,79	f-r	ps	vs	GS	13a
14-1970	12,55	7,57	2,12	1,35	f-r	ps	vs	GS	13a
14-1960	12,45	6,23	0,94	1,56	f-r	ps	vs	GS	13a
14-1950	12,35	5,24			vc-a	ms	t-(vs)	GS	13b
14-1940	12,25	6,28	0,58	0,52	vc-a	w-ms	t-(vs)	GS	13b-9
14-1920	12,15	10,26	2,23	1,03	f-r	ms	vs	GS	13b
14-1920	12,05	6,47	1,65	2,64	f-r	ms	vs	GS	13b
14-1910	11,95	7,92	127,25	57,77	m-r	ps	vs+ip	GS	11
14-1900	11,85	15,61	207,01	303,71	m-r	m-ps	vs+ip	GS	11
14-1230	5,15	6,68	1,35	0,50	vc-a	ms	vs	PS(md)	7b
14-1155	4,40	7,10	2,87		vc-a	ms	vs	PS(md)	7b

Poroperm Frauental (Q 12)

Sample #	Depth [m]	Porosity [%]	k(h) [mD]	k(v) [mD]	size	sorting	pore type	texture	LFT
17-1300	13,00		148,51	237,92	c-vc-a	ms	t	PS(gd)	8-(9b)
17-1050	10,50	18,74	419,17	384,95	m-r	ps	vs+ip	PS(gd)	11-7a
17-1040	10,40	3,29	98,73	0,12	f-r	ms	t-(vs)	PS(md)	7a
17-1030	10,30	20,04	408,43	524,94	m-r	m-ps	vs+ip	PS(gd)	11
17-1020	10,20	18,70	88,91	227,93	f-r	ms	vs+ip	PS(gd)	10
17-1015	10,15	16,13	376,38	185,90	f-r	ms	vs+ip	PS(gd)	10
17-1010	10,10	8,86	30,01	84,94	m-r	ps	vs+ip	GS	11-13a
17-1000	10,00	21,94	218,73	237,58	m-r	ps	vs+ip	PS(gd)	11
17-990	9,90	7,71	7,78	3,99	f-r	m-ps	vs+(ip)	GS	11-10
17-970	9,70	2,24	102,76	4,62	vc-a	m-ps	vs	GS	13a
17-490	4,90	6,24	3,02	0,82	vc-a	ms	vs	PS(gd)	7b-11
17-480	4,80	7,16	2,99	1,35	vc-a	ms	vs	PS(gd)	9b
17-460	4,60	4,24	0,88	2,33	c-vc-a	ws	vs	GS	9b
17-440	4,40	12,49	16,94	8,11	vc-a	ws	vs+ip	GS	10
17-400	4,00	8,45	1,26	1,88	vc-a	ws	vs	GS	10
17-390	3,90	10,39	2,99	1,14	vc-a	ws	vs+(ip)	GS	10
17-385	3,85	8,61	1,72	2,46	vc-a	ws	vs	GS	10
17-375	3,75	10,05	1,25	2,07	f-r	m-ws	vs	PS(gd)	10-13b
17-360	3,60	9,51	1,95	3,24	f-r	ms	vs	PS(gd)	13b-(10)
17-350	3,50	10,30	1,71	3,85	f-r	ms	vs	PS(gd)	13b-(10)
17-340	3,40	10,38	1,06	4,90	f-r	m-ps	vs	PS(gd)	13-(10)
17-325	3,25	12,62	96,96	7,10	f-r	m-ps	vs+ip	PS(gd)	13-(10)
17-320	3,20	13,29	4,42	6,46	f-r	m-ps	vs+(ip)	PS(gd)	13-(10)
17-310	3,10	12,96	2,16	7,01	f-r	ms	vs+(ip)	PS(gd)	13-(10)
17-220	2,20	12,21	4,18	4,08	f-r	ps	vs+(ip)	GS	11-13
17-210	2,10	5,25	31,79	1,91	vc-a	ms	vs+(ip)	GS	13-9a
17-200	2,00	4,06	0,43	0,88	vc-a	w-ms	vs	GS	13-9a

Poroperm Buch (Q 13)

Sample #	Depth [m]	Porosity [%]	k(h) [mD]	k(v) [mD]	size	sorting	pore type	texture	LFT
13-770	7,70	11,46	5,73	7,48	vc-a	ws	vs+(ip)	GS	10
13-765	7,65	17,65	12,73	20,39	vc-a	ws	vs+ip	GS	10
13-760	7,60	16,31	12,99	11,22	vc-a	ws	vs+ip	GS	10
13-755	7,55	14,22	12,70	18,89	vc-a	w-ms	vs+ip	GS	10
13-745	7,45	20,87	161,49	74,58	vc-a	w-ms	vs+ip	GS	10
13-740	7,40	17,94	48,51	68,04	vc-a	ws	vs+ip	GS	10
13-730	7,30	13,31	27,87	21,66	vc-a	ws	vs+ip	GS	10
13-720	7,20	13,05	21,74	23,80	vc-a	ws	vs+ip	GS	10
13-710	7,10	13,53	17,95	19,06	vc-a	ws	vs+ip	GS	10
13-700	7,00	10,04	3,89	3,81	vc-a	ws	vs	GS	10
13-695	6,95	10,31	4,75	5,84	vc-a	ws	vs	GS	10
13-690	6,90	9,84	12,44	1,78	vc-a	ws	vs+ip	GS	10
13-675	6,75	14,35	12,85	9,78	vc-a	ws	vs+ip	GS	10
13-665	6,65	9,85	2,75	0,69	vc-a	ws	vs	GS	10
13-650	6,50	8,44	1,90	0,49	vc-a	ws	vs	GS	10
13-640	6,40	10,07	5,70	8,57	vc-a	ws	vs+(ip)	GS	10
13-635	6,35	10,06	4,75	5,45	vc-a	ws	vs+(ip)	GS	10
13-625	6,25	12,13	9,29	31,77	f-r	ws	vs+(ip)	GS	10
13-620	6,20	9,59	9,38	32,66	f-r	ws	vs+(ip)	GS	10
13-607	6,07	10,15	9,06	4,39	f-r	ws	vs+(ip)	GS	10
13-575	5,75	16,20	186,12	108,18	m-r	w-ms	vs+ip	PS(gd)	11-10
13-565	5,65	8,56	0,94	0,57	f-r	m-ps	t-vs	PS(gd)	11-10
13-545	5,45	5,12	0,80	0,23	vc-a	w-ms	t	GS	13a-(9a)
13-380	3,80	0,00			f-r	ps	t	PS(gd)	13a
13-120	1,20	4,05	2,04	0,28	vc-a	w-ms	vs	GS	10
13-025	0,25	12,10	22,29	3,08	m-r	ps	vs+ip	PS(gd)	11-(7a)

Poroperm Aub-Baldersheim (Q 14)

Sample #	Depth [m]	Porosity [%]	k(h) [mD]	k(v) [mD]	size	sorting	pore type	texture	LFT
2-1755/1835	1,15	3,98	2,22	1,12	vc-a	ws	vs	gs	10
2-1715/1780	1,70	3,57			silit-lut.	ws	t	m-ws	1a-4
2-1465/1485	4,65	0,23			(f)-m-r	m-ps	t	ps(md)	8
2-1315	6,35	0,23			f-m-r	ps	t	w-ps	(4)-7a
2-1305	6,45	2,56	1,06		f-(m)-r	ps	vs	ws	(4)-7a
2-1210	7,40	0,40			m-r	ps	t	ws	4-7a
2-1195	7,55	2,11	1,58	0,79	m-r	ps	vs	w-ps	7a
2-1185	7,65	7,37	4,79		vc-a-(fr)	ms	vs	gs	13a
2-1175	7,75	1,34			vc-a-(fr)	m-(ps)	t	gs	13a
2-872	10,78	0,39	0,72	0,11	c-va-a	ws	t	ps(md)	15
2-745	12,05	2,51	0,80	0,88	f-r	m-(ps)	t	ps(gd)	8
2-575	13,75	0,65	0,90	0,47	c-vc-a	ps	t	w-ps	4
2-428	15,22	1,77	0,42	0,89	c-a	ms	t	ws	4
2-225	17,25	1,73	0,82	0,30	silit	ms	t	m-ws	1a-8
2-210	17,40	0,48	1,84	0,59	c-a	ws	t	gs	8-9
2-200	17,50	1,82	2,53	0,56	vc-a	m-(ws)	t-vs	gs	8-9
2-90	18,60	2,90	0,42	1,15	f-r	ms	vs	w-ps(md)	6-7a
2-66	18,84	8,50	1,80	0,37	f-r	m-ps	vs	ps(md)	6-13a
2-40	19,10	9,17	6,47	2,44	vc-a	m-ws	vs (ip)+vs	gs	10-(13b)
2-30	19,20	2,97	2,36	0,37	f-r	m-ps	t-(vs)	ps(md)	8
2-1025	9,25	13,44	9,77	7,63	fr	ms	vs+ip	gs	10-11

Poroperm Kirchheim (Q 15)

Sample #	Depth [m]	Porosity [%]	k (h) [mD]	k (v) [mD]	size	sorting	pore type	texture	LFT
4-837	1,29	4,14	1,41	0,30	f-r	ms	vt+vs	PS(md)	7a
4-462	5,04	1,69			f-r	m-(ps)	t	W-PS	7a-3
4-420	5,46	0,98			m-r	m-(ps)	t	WS	3
4-410	5,56	0,29			m-r	ms	t	W-PS	7a-(3)
4-400	5,66	0,43			f-r	m-(ps)	t	PS(md)	7a-(3)
4-390	5,76	0,70			f-r	ps	t	PS(md)	7a
4-380	5,86	7,02	0,95	0,67	m-r	ps	vs-t	PS(md)	7a
4-370	5,96	8,95	5,80	0,79	f-r	ms	vs-t	PS(gd)	13a
4-360	6,06	7,72	0,80	0,42	f-r	m-ps	t-(vs)	GS	13a
4-350	6,16	7,67	44,15	7,53	vc-a	ms	vs+ip	GS	13b
4-340	6,26	1,18			f-r	ms	t-(vs)	GS	13a
4-320	6,46	8,35	7,29	4,10	f-r	ps	vs+ip	PS(gd)	13a-11
4-315	6,51	9,26	28,63	3,44	f-r	ms	vs+ip	PS(gd)	13a-11
4-304	6,62	9,43	41,91	40,20	m-r	m-ps	vs+ip	PS(gd)	13a-11
4-295	6,71	8,25	9,32	3,42	m-r	m-ps	vs	PS(md)	13a-7a
4-285	6,81	8,25	7,48	23,96	m-r	ms-(ps)	vs	PS(md)	7a
4-275	6,91	11,84	93,52	175,72	f-r	ms	vs+ip	PS(gd)	13a-b
4-265	7,01	10,44	13,04	84,25	f-r	ms	vs+ip	PS(gd)	13a
4-248	7,18	13,96	31,50	3,31	f-r	ps	vs+ip	GS	11-13a
4-240	7,26	12,13	114,81	141,90	f-r	ps	vs+ip	GS	13a-11
4-230	7,36	7,68	7,48	22,68	f-r	m-(ps)	vs+ip	PS(gd)	13b
4-220	7,46	7,48	2,92	15,56	f-r	m-ps	vs+ip	PS(gd)	11-(13a)
4-208	7,58	7,51	14,32	25,43	f-r	m-(ps)	vs+ip	PS(gd)	13a-(11)
4-200	7,66	0,43			f-r	ps	t	PS(gd)	7a
4-155	8,11	1,35			vc-a	ps	t	PS(md)	5b
4-135	8,31	0,73			f-r	ms	t	PS(md)	5b-(7b)
4-125	8,41	1,51			f-r	ms	t	PS(md)	5b-(7b)
4-100	8,66	0,57			f-r	ms-(ps)	t	PS(md)	7a
4-70	8,96	0,08			m-r	ms-(ps)	t	W-PS	7a-(3)

Poroperm Goßmannsdorf / Hasenleite (Q 16)

Sample #	Depth [m]	Porosity [%]	k(h) [mD]	k(v) [mD]	size	sorting	pore type	texture	LFT
7-780	5,66	0,89							7a
7-733	6,13	3,64	1,18	0,07	m-r	ps	vs-t	WS	3
7-670	6,76	2,74	2,30	0,52	vc-a	ms	vs-t	PS(gd)	
7-640	7,06	0,96			vc-a	ws	t	GS	13b-9a
7-630	7,16	0,59			vc-a	ws	t	GS	13b-9a
7-615	7,31	2,32	0,20	1,04	vc-a	m-(ps)	t	GS	13b
7-605	7,41	1,28			vc-a	m-ps	t	PS(gd)	13b-9a
7-590	7,56	2,58	0,16	0,10	vc-a	ms	t-(vs)	GS	13b-9a
7-570	7,76	1,73			f-r	ps	t	PS(gd)	13b-9a
7-560	7,86	0,70			vc-a	ms	t	PS(gd)	13b-9a
7-550	7,96	2,35	2,56	0,13	f-r	m-ps	vs	PS(md)	13a
7-530	8,16	0,36			f-r	vps	t	W-PS	3-7a
7-471	8,75	0,37			m-r	ps	t	WS	3
7-435	9,11	0,99			f-r	ms	t	WS	3
7-408	9,38	0,75			f-r	ps	t	PS(md)	7a
7-383	9,63	1,79			vc-a	(m)-ps	t	PS(md)	6-13a
7-373	9,73	0,48			vc-a	ms	t	PS(gd)	13a-6
7-365	9,81	3,06	1,23	1,54	vc-a	ms	vs	(gd)	13a
7-355	9,91	3,32	0,16	0,50	f-r	m-ps	t-(vs)	W-PS	7a-7b
7-345	10,01	6,80	0,11	0,25	vc-a	ws	t-(vs)	GS	10-9a
7-335	10,11	11,30	1,91	4,97	vc-a	ms	vs	PS(gd)	10
7-325	10,21	13,51	4,29	1,25	vc-a	ws	vs	GS	10
7-315	10,31	11,81	2,14	1,45	vc-a	ws	vs	GS	10
7-305	10,41	13,76	2,83	1,01	vc-a	ws	vs	GS	10
7-295	10,51	13,72	2,60	1,27	vc-a	ws	vs	GS	10
7-285	10,61	16,39	11,42	6,07	vc-a	ws	vs-+ip	GS	10
7-275	10,71	12,94	4,05	0,95	vc-a	ws	vs	GS	10
7-265	10,81	16,21	8,41	7,37	vc-a	ws	vs+ip	GS	10
7-250	10,96	12,63	1,95	2,77	vc-a	ws	vs	GS	10
7-230	11,16	4,08	1,43	2,99	vc-a	ms	vs	GS	9a
7-220	11,26	12,40	4,39	3,35	vc-a	ms	vs	GS	10
7-210	11,36	11,14	12,47	11,84	vc-a	ms	vs+ip	GS	10
7-200	11,46	14,51	13,88	1,05	vc-a	ms	vs+vt+ip	GS	10
7-193	11,53	9,34	1,51	0,56	vc-a	ms	vs	GS	10(-13a)
7-180	11,66	9,55	1,72	2,00	f-r	m-ps	vs	GS	11
7-170	11,76	6,54	0,61	0,92	f-r	ws	t-(vs)	GS	13a
7-160	11,86	3,36	0,28	0,23	f-r	ms	t-(vs)	PS(md)	7b-3
7-150-2	11,96	6,15	3,26	0,74	f-r	ms	vs+vt	PS(md)	7b
7-150	11,96	5,01	3,26	0,74	f-r	ms	vs+vt	(md)	7b
7-143	12,03	3,86	0,27	0,89	f-r	m-ws	t-(vs)	(md)	7b
7-131	12,15	5,58	13,95	16,19	vc-a	ms	vs+vt	(gd)	6-13a
7-127	12,19	3,09	0,53	0,97	vc-a	ms	t-(vs)	(gd)	13a
7-105	12,41	4,09	0,58	0,02	f-r	ms	t-(vs)	PS(md)	7b

Poroperm Sommerhausen (Q 17)

Sample #	Depth [m]	Porosity [%]	k(h) [mD]	k(v) [mD]	size	sorting	pore-type	texture	LFT
1-1208	3,32	0,61	0,25	0,11	c-a	ws	t	ws-(ps)	4
1-1099	4,41	1,62	13,09	0,14	c-a	ms	t	ws-(ps)	4
1-1085	4,55	2,47	1,87	0,64	f-r	ps	vs	ps(md)	8-2a
1-908	6,32	0,52	0,46	0,46	f-r	ps	t	ps(md)	7a-(13a)
1-900	6,40	9,35	2,52	0,17	f-r	ps	vs	ps(md)	7a-13a
1-869	6,71	11,85	19,77	4,61	m-r	ps	vs+vt	w-ps	3-7a
1-837	7,03	0,29			f-m-r	ps	t	ps	7a
1-760	7,80	0,83			c-vc-a	ms	t	ps(gd)	13b
1-750	7,90	0,46	2,77	0,80	f-m-r	v	vs	ps(md)	7a
1-717	8,23	0,94	1,51	0,50	c-vc-a	ms	t	ps(gd)	13b
1-675	8,65	1,17	0,37	0,56	f-r	ms	t	ps(gd)	13b
1-610	9,30	0,36	0,72	0,32	f-r	m-ws	t	ps(md)	7b
1-539	10,01	4,46	1,99	2,04	vc-a	w-ms	vs (+ip)	gs	10
1-526	10,14	8,40	7,17	4,08	f-r	w-ms	ip+vs	gs	10
1-515	10,25	14,60			f-r	ms-ws	vs (+ip)	ps(gd)	10
1-514	10,26	6,31	2,97	0,68	vc-a	ws	vs (+ip)	gs	10
1-505	10,35	2,58	1,01	0,79	vc-a	ms	vs	ps-1	10
1-491	10,49	3,27	1,06	0,44	vc-a	ms	vs	gs	10
1-416	11,24	14,19	9,49	36,01	vc-a	ws	ip+vs	ps(gd)	10
1-408	11,32	19,83	25,25		c-vc-a	ws	ip+vs	ps(gd)	10
1-400	11,40	15,47	20,23	5,36	c-vc-a	ws	ip+vs	ps(gd)	10- (9a)
1-390	11,50	12,99	3,56	7,00	c-a	ws	ip+vs	ps(gd)	10
1-380	11,60	19,71	41,79	65,16	vc-a	ws	ip+vs	ps(gd)	10
1-369	11,71	16,81	33,17	2,65	vc-a-(f-r)	ms	ip+vs	gs	10
1-351	11,89	11,32	0,47	0,15	vc-a	m-ws	vs	ps(gd)	9a-10
1-330	12,10	0,89	0,26	0,34	vc-a	ms	t	gs	13b-8
1-284	12,56	8,12	1,8	1,04	c-vc-a	ws	vs	ps(gd)	9a-10
1-275	12,65	9,94	0,89	1,45	c-vc-a	ws	vs	gs	9a-10
1-239	13,01	1,59	1,08	0,83	vc-a	m-ws	vs	gs	10
1-60	14,80	13,07	14,65	11,38	f-r	ms	ip+vs	gs	10
1-50	14,90	8,48	1,07	1,23	f-r	ms	vs	gs	10
1-35	15,05	0,22	0,56	1,01	vc-a	ms	t	ps(gd)	8-(13b)

Poroperm Winterhausen (Q 18)

Sample #	Depth [m]	Porosity (%)	k(h) [mD]	k(v) [mD]	size	sorting	pore type	texture	LFT
16-160	4,25	3,95	3,98	1,10	f-(m)-r	ps	vs+vt	PS(gd)	7a-13a
16-140	4,45	7,56	15,80	9,83	m-r	ps	vs+ip	GS	11
16-130	4,55	10,06	70,81	178,41	f-r	ps	vs+ip	GS	11
16-120	4,65	8,66	85,08	13,28	f-r	m-(ps)	vs+ip	GS	13a-11
16-110	4,75	9,48	370,85	65,00	f-r	m-(ps)	vs+ip	GS	13b-13a
16-100	4,85	8,11	94,93	14,44	vc-a	ms	vs+ip	GS	13b
16-095	4,90	11,21	5,71	29,93	vc-a	ms	vs+ip	GS	13b
16-085	5,00	8,61	4,14	4,30	vc-a	m-ps	vs+ip	GS	11-13a
16-070	5,15	11,05	80,70	3,17	f-r	ps	vs+ip	GS	11
16-060	5,25	11,52	9,41	22,93	f-r	ps	vs+ip	PS(gd)	11
16-050	5,35	10,26	13,45	10,28	f-r	ps	vs+ip	PS(gd)	11
16-040	5,45	2,89	0,22	0,19	f-r	ps	vs+ip	GS	11

Poroperm Frickenhausen (Q 19)

Sample #	Depth [m]	Porosity [%]	k(h) [mD]	k(v) [mD]	size	sorting	pore type	texture	LFT
6-320,5	0,30	1,09			vc-a	m-ps	t	PS(gd)	13a
6-301	0,49	3,60	5,99	3,29	vc-a	ps	t-ig	PS(gd)-GS	13a
6-280	0,70	5,04	0,94	0,92	f-(m)-r	ms	t-ig	PS(md)	7a-b
6-205	1,45	5,46	1,44	0,78	c-a	ws	t-ig	PS(gd)-GS	15
6-185,5	1,65	0,95			f-r	ms	t	PS(md)	7a-b
6-172,5	1,78	0,34			m-r	ps	t	PS(md)	7a-b
6-155	1,95	0,82			vc-a	ms	t-vs	GS	13b-10
6-139,5	2,11	1,44			f-r	ms	t-vs	PS(md)	7a-b
6-130	2,20	1,46			m-r	ps	t	(W)-PS(md)	7a-b
6-119	2,31	2,50	2,35	0,85	m-r	ps	vs-t	PS(md)	7a-b
6-105	2,45	7,73	6,27	1,52	f-r	m-(ps)	vs	PS(gd)	13a-7a
6-60	2,90	15,05	35,00	26,53	f-r	ws	vs+ip	GS	10-13b
6-50	3,00	12,36	31,74	9,99	vc-a f-r	ms	vs+ip	GS	13b-(10)
6-40	3,10	6,00	2,00	0,90	vc-a fr	(m)-ws	vs	GS	13b-(10)
6-35	3,15	11,35	4,74	1,44	vc-a	(m)-ws	vs+(ip)	GS	13b-10
6-20	3,30	5,18	2,08	1,70	f-r	ws	vs	GS	13b
6-10	3,40	8,69	1,41	1,04	f-r	ms	vs	PS(md)	7b